Reconstructing R-regular Objects from Trinary Digital Images

Helene Matilde Svane

PhD Dissertation
July 2019

Supervisor: Andrew du Plessis

Institut for Matematik
Aarhus Universitet

Abstract

This paper deals with reconstructing an object from its digital 2- or 3-dimensional image. Inspired by similar work in the field, we restrict ourselves to consider images of objects of a certain regularity called r-regularity, which is why we start by deriving some results on the geometric properties of such sets.

The images that we focus on are constructed by placing the r-regular object in a grid, and then colouring grid squares (or cubes, when we work in three dimensions) black if they are completely inside the object, white if they are completely outside the object, and grey if they contain a boundary point of the object. In this way, we obtain a digital image with just the three colours black, white and grey; we call such an image a *trinary* image.

We then develop some results on possible pixel configurations in trinary images of 2-dimensional r-regular objects and use these configurations to propose a reconstruction algorithm that takes an image of an r-regular object as input, and outputs a reconstructed object. We proceed to obtain some results on the similarity between the original and reconstructed object in order to quantify how well the reconstruction algorithm works.

Our digitisation model is rather idealised, so we also try to adapt our reconstruction algorithm to noisy images. In a noisy image, the pixel intensities have been distorted, meaning that our digitisation model no longer fit such images. We try to use our knowledge about ideal images to spot which pixels have changed colours due to noise, and propose an algorithm to try to find the original colours of the pixels that have changed colours due to noise. We also construct another algorithm to try to find a noise-free image from a noisy one.

Finally we return to digital images without noise, but this time in three dimensions. Inspired by earlier work in the field we show that given the black voxels in a digital image of an r-regular object at a reasonable resolution, it is possible to reconstruct the topology of the original object in the sense that we can construct an object with smooth boundary that has the same topological features as the original one.

Resumé

Denne afhandling handler om at rekonstruere 2- og 3-dimensionelle objekter fra digitale billeder af dem. Inspireret af tidligere arbejde på området fokuserer vi på objekter der opfylder en særlig regularitetsbetingelse kaldet r-regularitet, hvorfor vi også vil udlede nogle resultater om de geometriske egenskaber for sådanne mængder.

De billeder, vi har fokus på, er lavet ved at placere et r-regulært objekt i et gitter, og så farve hvert gitterkvadrat (eller gitterkube, når vi arbejder i tre dimensioner) sort hvis det er helt indeholdt i objektet, hvidt hvis det er helt indeholdt i komplementet til objektet, og gråt hvis det indeholder noget af objektets rand. Derved opnår vi et digitalt billede med de tre farver sort, hvid og grå - vi kalder et sådant billede for et trinært digitalt billede.

Vi udleder diverse resultater om mulige pixelkonfigurationer i et trinært billede af et 2-dimensionalt r-regulært objekt og bruger disse til at bygge en rekonstruktionsalgoritme, som tager et trinært billede af et r-regulært objekt som input og leverer et rekonstrueret object som output. Derefter viser vi nogle resultater om ligheden mellem det oprindelige og rekonstruerede objekt for at kvantificere præcisionen af rekonstruktionsalgoritmen.

Da de billeder, vi arbejder med, er temmelig idealiserede, forsøger vi også at tilpasse vores rekonstruktionsalgoritme til billeder med støj. I billeder med støj er pixelintensiteterne blevet forvrænget, således at vores digitaliseringsmodel ikke længere passer på det observerede billede. Vi forsøger at bruge vores viden om de idealiserede billeder til at spotte, hvilke pixels der har ændret farve på grund af støj, og foreslår en algoritme til at prøve at finde de oprindelige farver på de pixels, som har ændret farve på grund af støj. Vi udvikler også en anden algoritme til at forsøge at genfinde det ideale billede ud fra det støjede.

Til sidst koncentrerer vi os igen om digitale billeder uden støj, men denne gang i tre dimensioner. Inspireret af tidligere arbejde på området viser vi, at givet de sorte voxels i et digitalt billede af et r-regulært objekt med passende billedopløsning kan man rekonstruere topologien af det oprindelige objekt i den forstand, at man kan konstruere et objekt med glat rand, som har de samme topologiske egenskaber som det oprindelige objekt.

Contents

Preface

This thesis consists of one paper, three paper drafts, one of which is also on arXiv, and a supplement to the paper draft on arXiv. We have included a short background chapter where we introduce the field, along with the important definitions related to the work in this thesis. The thesis is the result of three years of PhD studies at Department of Mathematics, Aarhus University, supervised by Andrew du Plessis, also from Department of Mathematics, Aarhus University. Furthermore, one of the papers, *Reconstructing Objects from Noisy Images at Low Resolution* has been made in collaboration with Prof. Aasa Feragen, who was then at the Department of Computer Science at University of Copenhagen, Denmark.

The papers included in this thesis are

- du Plessis, Andrew and Svane, Helene: *On r-regularity*. Paper draft, 2019
- Svane, Helene and du Plessis, Andrew: *Reconstruction of r-regular Objects from Trinary Images*. arXiv:1903.10942
- Svane, Helene: *A Stronger Result on the Similarity between an r-regular Object and Its Reconstruction from a Trinary Image*. Paper draft. 2019
- Svane, Helene and Feragen, Aasa: *Reconstruction of Objects from Noisy Images at Low Resolution*, Graph-based Representations in Pattern Recognition, 2019.
- Svane, Helene and du Plessis, Andrew: *Preservation of Topology during Digitisation of a 3-dimensional r-regular Object*. Paper draft, 2017

Of these three papers, I have contributed comprehensively to both the research and the writing of the second, third and fourth. The main work and writing of the first paper, *On r-regularity*, has mainly been carried out by Andrew du Plessis, and some of it dates back to before the beginning of my Ph.D. studies. My contribution has been to some of the calculations, along with proof-reading and illustrations. The research in the paper *Preservation of Topology during Digitisation of a 3-dimensional r-regular Object* has been carried out by both Andrew du Plessis and myself in collaboration, and I have done the writing. This paper and large parts of the paper *Reconstruction of r-regular Objects from Trinary Images* were also included as a part of my progress report. Furthermore, parts of the paper *On r-regularity* has earlier been included in the appendix of the Ph.D. thesis of Sabrina Tang Christensen.

The papers *Reconstruction of Objects from Noisy Images at Low Resolution* and partly *Reconstruction of r-regular Objects from Trinary Images* were finished for submission during my research stay at the Department of Computer Science, Hunter College, City University of New York, USA, and I would like to thank Prof. Katherine St. John, who I visited there, for valuable discussions in this process, as well as

for great hospitality. The work in this thesis has been presented at the following workshops:

- 19th Workshop on Stochastic Geometry, Stereology, and Image Analysis, Marseille, France, May 2017
- Internal CSGB Workshop, Denmark, November 2017
- Conference on Stereology, Spatial Statistics and Stochastic Geometry (S4G), Prague, Czech Republic, June 2018
- 20th Workshop on Stochastic Geometry, Stereology and Image Analysis, Sandbjerg, Denmark, 2019
- 12th International Workshop on Graph-based Representations in Pattern Recognition, Tours, France, June 2019

The results in the paper *Topological Reconstruction of r-regular Sets* that is also available on arXiv, appears in this thesis with minor changes.

Acknowledgements

My Ph.D. studies were funded by the Centre for Stochastic Geometry and Bioimaging (CSGB) at Aarhus University, who in turn is funded by the Villum Foundation. I would like to thank my supervisor, Andrew du Plessis, for valuable discussions, guidance and patience throughout my Ph.D, and my co-author Aasa Feragen, for helping me venture deeper into the field of computer science and applied mathematics. The CSGB have all been both helpful and supportive - I thank them all for our collaboration. A special thanks should be given to Katherine St. John at Hunter College, City University of New York. Aside for dedicating large amounts of her time to supervising my work, she and her family did a great job at making me feel at home during my research stay in New York.

I should also like to thank my brother, Kristian Svane, for correcting my grammar in this thesis even though its subject is not his area of expertise – any errors that lingers on are completely my own. And finally, I would like to thank my Thomas Schmidt very much for years of supporting and encouraging me in everything I do, and for keeping me fed during the completion of my thesis.

Chapter 1

Introduction

Understanding digital images and the information they contain is a subject of growing interest. This thesis deals with several aspects of analysis and reconstruction of objects from their digitisations, i.e. their images. The overall goal is to use digital images of objects to come up with a good reconstruction of the objects, according to some reconstruction criteria. What is precisely meant by a 'good' reconstruction may differ between different situations and for different images, depending on what features of the original object one is interested in knowing, and what quality the input image has. The task is thus to take a discrete representation, i.e. an image, of a continuous object, and then infer as much as possible about the object from the information stored in the discrete representation.

In this thesis, we build a model to describe the discretisation process that takes a continuous object and outputs a discrete representation (the image) of it. We work with two different classes of images. The first class consists of ideal images, which are images that exactly fit the image model that we have built. For this class of images we may reconstruct an object quite accurately since the entire set-up is idealised. The second class consists of noisy images, which are images where technical issues in the camera, dust on the lens or similar real-world interference distorts the signal from the object of interest, so that the resulting image no longer fit out model of the digitisation process. For noisy images a good reconstruction of the original object may not be a easily obtained, but the treatment of such images holds much more relevance to real-world applications.

We will give a summary of the results obtained in this thesis, but before we start doing that, we give a small introduction to the important notions and models used in the thesis, along with some basic notation. We then give an overview of the content of each of the chapters in the thesis, including the main results and ideas. Finally, we relate the work in this thesis to related work done in the field.

1.1 Background

We consider objects in Euclidean space $\mathbb{R}^n$, equipped with the usual Euclidean distance, which will be denoted by $d(\,\cdot\,,\,\cdot\,)$ or $\|\,\cdot\,-\,\cdot\,\|$. The corresponding inner product will be denoted $\langle\,\cdot\,,\,\cdot\,\rangle$. An open ball in $\mathbb{R}^n$ of radius r and centre c will be denoted by $B_r(c)$. In most of our applications, we will put $n = 2$ or $n = 3$.

Let X be a subset of $\mathbb{R}^n$. We will denote the interior of X by $\mathrm{Int}(X)$, the closure

by $\overline{X}$ and the boundary by ∂X. The distance from a point y to the set X is denoted by $\delta_X(y)$, or someimes simply $d(X, y)$. We measure the distance between two sets $A, B \in \mathbb{R}^n$ by means of the Hausdorff distance d_H, which is defined by

$$d_H(A, B) = \max\big(\sup_{x\in A}\inf_{y\in B} d(x, y), \sup_{y\in B}\inf_{x\in A} d(x, y)\big).$$

We will work with images of objects constructed in the following way:

Definition 1.1. Let μ denote the n-dimensional Lebesgue-measure. Let $X \subseteq \mathbb{R}^n$ be a Lebesgue-measurable set and $d > 0$ a number. Then $d\mathbb{Z}^n$ is a lattice and to each point p of this lattice, there is an n-square $C = C(p)$ of side length d whose centre lies at p. We associate an intensity

$$\lambda_C = \frac{\mu(C \cap X)}{d^n}$$

to each such n-dimensional square, calculating the fraction of the square that is covered by the object.

The *(ideal) digital image* I of X by the lattice $d\mathbb{Z}^n$ is the collection of grid points and associated intensities, and may be thought of (or visualised as) the collection of lattice squares $C(p)$, $p \in d\mathbb{Z}^n$, each coloured a shade of grey corresponding to the associated intensity, see Figure 1.1.

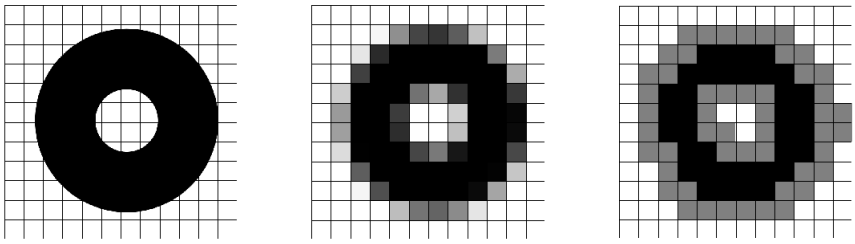

Figure 1.1: Example of a digital image. Left: Original object, Middle: Digital image of the object, Right: Trinary digital image of the object.

A discrete representation of a continuous object, such as an image, is known as a *discretisation* of the object. We will sometimes omit the term *ideal* when it is obvious which kind of digitisation we are dealing with. The squares $C(p)$, $p \in d\mathbb{Z}^n$ are called pixels when $n = 2$, and voxels when $n = 3$. In the following, we will assume that X is a black object on a white background, so that pixels (respectively voxels) of intensity 1 are black, pixels (respectively voxels) with intensity 0 are white, and the remaining pixels will be a shade of grey, corresponding to their associated intensities λ_C.

The motivation behind this model for digital images is that such images are made from the measurements of a collection of sensors sitting in a grid, each at a distance d from its nearest neighbour, and each of these sensors is measuring the amount of light coming from a square of side length d around it, and colours a square in the same position of the image accordingly.

In this thesis, we will mainly be dealing with what we call *trinary images*:

Definition 1.2. Let $X \subseteq \mathbb{R}^n$ be a Lebesgue-measurable set and $d > 0$. The *(ideal) trinary digital image* J of X is the ideal digital image I of X by the lattice $d\mathbb{Z}^n$ with all grey intensities set to 0.5.

In this way, the visualisation of trinary images will only consist of black, white and grey pixels, so we will only see three colours in a trinary digital image – hence the term *trinary*. An example of a trinary image is shown in Figure 1.1, right. Although ideal digital images in general contain a lot more information than trinary digital images do, the trinary images have turned out to be easier to work with in pratice. Note also that with the above definition, a trinary image J will remain the same, even when the intensities of the underlying ideal image I are calculated as

$$\lambda_C = \varphi\left(\frac{\mu(C \cap X)}{d^n}\right)$$

for each $C(p)$, $p \in d\mathbb{Z}^n$ and some function $\varphi : [0,1] \to [0,1]$ such that $\varphi(x) = 0$ if and only if $x = 0$, and $\varphi(x) = 1$ if and only if $x = 1$. Hence when we are only considering trinary images, we will often introduce the underlying ideal images with this more general intensity notion than the one we used in Definition 1.1.

In Paper C, we will also be considering noisy images. We think of these as ideal images where some of pixel intensities have been altered, so that the intensities of the pixels no longer match what we would expect to see in an ideal digital image.

When trying to infer anything about an object from its digital image, it is necessary to impose some regularity constraint on the object. We hence assume the objects that we are working with to be r-regular, as has been done in many other places in the literature on digital geometry:

Definition 1.3. Let $X \subseteq \mathbb{R}^n$ be closed and $r > 0$. X is said to be *r-regular* if for any point $x \in \partial X$, there exists two r-balls $B_r(x_b) \subseteq X$ and $B_r(x_w) \subseteq X^C$ such that

$$\overline{B_r(x_b)} \cap \overline{B_r(x_w)} = \{x\}.$$

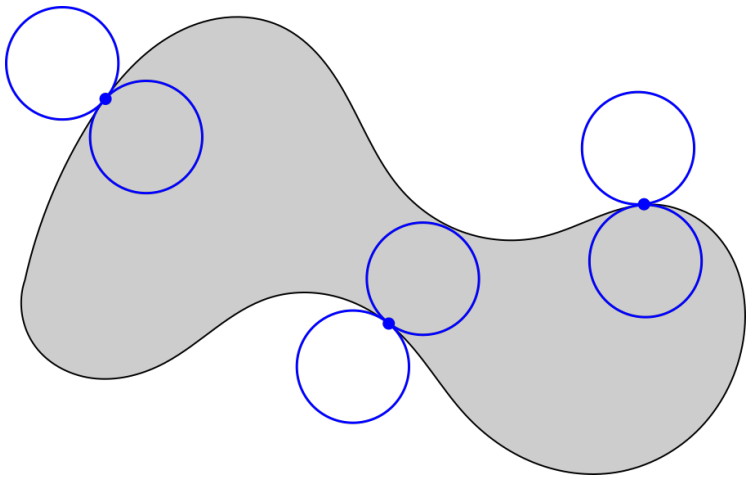

Figure 1.2: A set X is r-regular if there at each boundary point p of X are an r-ball inside X and an r-ball outside X whose boundaries meet in exactly at p - here such balls are shown for three different boundary points.

Intuitively, the notion of r-regularity ensures that the r-regular object cannot have a boundary with too many curlicues, or have sections with too narrow necks, see Figure 1.2. When the size of the ball r compared to the grid size d is reasonable,

this in particular means that all important features of the r-regular X object is caught by the ideal image of X by the lattice $d\mathbb{Z}^n$. This is the case when r is greater that the pixel or voxel diameter, so that in dimension 2, we assume that $d\sqrt{2} < r$, and in dimension 3, we assume that $d\sqrt{3} < r$. Hence we will assume that r is greater that the pixel or voxel diameter in this thesis.

Furthermore, we assume that the r-regular sets that we are working with are bounded (and hence compact), and that the boundary ∂X does not intersect a pixel corner anywhere. The latter assumption is not unreasonable: Indeed, given a curve in $\mathbb{R}^2$ (or a manifold in $\mathbb{R}^3$), the probability of hitting that curve (or manifold) by a randomly placed lattice $d\mathbb{Z}^2$ (or $d\mathbb{Z}^3$) is zero.

Before we give a summary of each of the papers in this thesis, we need to introduce the notion of *isotopy*:

Definition 1.4. Let M, N be manifolds and I an interval. An *isotopy* from N to M is a smooth map $F : N \times I \to M$ such that for each $t \in I$ the map

$$F_t : N \to M, \qquad x \mapsto F(x, t)$$

is an embedding. When such a map exists, the maps F_0 and F_1 are called *isotopic*.

When $N = M$, the map F_t is a diffeomorphism for each $t \in I$ and $F_0 = \mathrm{Id}_M$, F is called an *ambient isotopy*. Two smooth embeddings $f_0, f_1 : N \to M$ are called *ambiently isotopic* if there exists an ambient isotopy $F : M \times I \to M$ such that $f_1 = F_1 \circ f_0$.

1.2 The papers

1.2.1 r-regularity

When working with reconstruction from digital images it is necessary to put some constraint on the sets that are being considered, because the digitisation process wipes away features that are small compared to the pixel size. It is therefore useful to assume that no such features exist in the sets of interest. Within the field, it is thus standard custom to impose some regularity constraint on the sets considered, such that sets subject to this constraint exhibit useful properties, such as ensuring that their boundaries only has a controllable amount of curlicues, and that they always have a minimal thickness. Authors (e.g. [5, 6, 12, 15]) have formulated such regularity criterions in slightly different ways. The first part of this paper aims to prove that many of these regularity notions are actually equivalent, or almost equivalent, so that we may denote them all by r-regularity, as stated in Definition 1.3.

We show the following:

Theorem 1.5. *Let $X \subseteq \mathbb{R}^n$ be a closed set and $r > 0$. The following are equivalent:*

(i) *X and $\overline{\mathbb{R}^n \setminus X}$ are both unions of closed r-balls,*

(ii) *X is r-regular,*

(iii) *X is r-regular and its boundary ∂X is a C^1 manifold,*

(iv) *X and $\overline{\mathbb{R}^n \setminus X}$ are C^1 submanifolds-with-boundary of $\mathbb{R}^n$, and the unit normal vector field pointing out of X on the common boundary of X and $\overline{\mathbb{R}^n \setminus X}$ is Lipschitz with Lipschitz constant $\frac{1}{r}$,*

(v) *X and $\overline{\mathbb{R}^n \setminus X}$ have reach r.*

Here, *reach* is the notion introduced by Federer [6], defined by

Definition 1.6. Let A be a closed subset of $\mathbb{R}^n$, $r > 0$ and $\delta_A : \mathbb{R}^n \to \mathbb{R}_+$ the function measuring the distance from a point to A. Then A has reach r if every point $x \in \mathbb{R}^n$ with $\delta_A(x) < r$ has a unique nearest point in A

The above result does not only unify the regularity constraints from several authors who have been working in the field, it also provides a toolbox for working with r-regular sets, since different formulations of the definition of r-regularity may be preferred for different applications.

Note that in the paper, we will define a set to be r-regular if it satisfy condition (i) of this theorem, but the theorem shows that either definition may be used. We also remark that since item (ii) and (iii) are equivalent, the boundary of an r-regular set is a C^1 manifold - a result that was also proven in [4].

The next part of the paper develops a toolbox for working with r-regular set. Much of this part of the paper was also included as an appendix in the PhD thesis of Tang Christensen [2], who needed them in order to prove some of her main work.

The third part of the paper is devoted to showing the following:

Theorem 1.7. *Let $X \subseteq \mathbb{R}^n$ be an r-regular set for some $r > 0$, and let $0 < \varepsilon < r$. Then X can be approximated arbitrarily close by smooth $(r - \varepsilon)$-regular set, which is ambiently isotopic to X.*

Note that r-regular sets are C^1-manifolds but may not in general be smooth or even C^2 (See e.g. [4] for a counterexample), so this sort of smoothing may be interesting if one wants to use differential geometry on an r-regular set.

The final part of the paper deals with smooth curves of curvature $\frac{1}{r}$ and their relations to geodesics on smooth r-regular sets. We show that geodesics on smooth r-regular sets have curvature at most $\frac{1}{r}$, and then go on to consider curves with a so-called r-spindle property:

Definition 1.8. Let $x, y \in \mathbb{R}^n$ and ℓ be the line segment between them. The *r-spindle* generated by ℓ is the intersection of all r-balls whose boundaries intersect both x and y.

A closed smooth arc $\alpha \subseteq \mathbb{R}^n$ is said to have *r-spindle property* if every closed sub-arc α' of α is contained in the r-spindle with endpoints the endpoints of α'.

In particular, geodesics on r-regular sets satisfy this property. We show that a smooth closed curve α satisfying the r-spindle property has a Lipschitz condition on its unit tangent vector field, and that it have curvature at most $\frac{1}{r}$. We also show that such a curve have reach r, and that the angle between a tangent vector to α and the line ℓ joining the endpoints of α is at most the spindle angle of the spindle generated by ℓ.

1.2.2 Reconstruction of r-regular Objects from Trinary Images

This paper deals with the reconstruction of 2-dimensional r-regular objects from their trinary images. It was originally written in connection with the work presented

in Paper C, *Reconstructing Objects from Noisy Images at Low Resolution*, and was therefore put on arXiv, see [16]. The version in this thesis has some minor changes from the current version on arXiv. Most of the technical results in this paper were also presented in connection with the qualifying exam.

With inspiration from a paper by Stelldinger and Köthe [15], we adopt the notion of *weak s-similarity*:

Definition 1.9. Let $A, B \subseteq \mathbb{R}^2$ be bounded sets and $s > 0$. We call A and B weakly s-similar if there exists a homeomorphism $f : \mathbb{R}^2 \to \mathbb{R}^2$ such that $x \in A \iff f(x) \in B$ and the Hausdorff distance between the two set boundaries satisfies $d_H(\partial A, \partial B) < s$.

The main result of the paper is to show the following:

Theorem 1.10. *Given a trinary image of an r-regular object X by a lattice $d\mathbb{Z}^2$ with $d\sqrt{2} < r$, it is possible to construct an object Γ that is weakly d-similar to X, where d is the pixel side length.*

The reconstructed object is constructed from the image in the following way: Whenever two grey pixels share an edge, we place an auxiliary point on that edge (its exact position depends on the exact configuration), see Figure 1.3, left. We then argue that this endows the auxiliary points with a natural ordering, so that we may speak of 'consecutive auxiliary points'. Then through each three consecutive auxiliary points, we may fit a unique circle arc, see Figure 1.3, right. This means that each two consecutive auxiliary points are connected by two circle arcs, one starting in one of the points, the other one ending at the other point. Interpolating between these two curves for every two consecutive auxiliary points using a bump function we get a continuous curve, forming the boundary of the reconstructed set, see Figure 1.4.

From here on out, the result relies for a large part on the characterisation of trinary pixel configurations admitted in an image of an r-regular set. Using several results from the article on r-regularity described above, we among other things arrive at a complete characterisation of trinary 3×3 pixel configurations, as well as a list of trinary 4×4 pixel configurations with 2×2 grey pixels in the middle. In this way, we are able to characterize all building blocks present in an image of an r-regular object by a lattice $d\mathbb{Z}^2$ with $d\sqrt{2} < r$. Considering the original and reconstructed boundary in each of these building blocks separately, we find upper bounds on the Hausdorff distance between the original and reconstructed set in each of these configurations, thus eventually arriving at the conclusion that the original and reconstructed set boundaries are closer than d apart in Hausdorff distance. Finally, we find a homeomorphism of $\mathbb{R}^2$ taking X to the reconstructed set by using the Annulus Theorem and the fact that both ∂X and the reconstructed curve separate white pixels from black ones.

Already when this paper was first being written, the authors suspected that the main result could be improved, either by considering a stronger notion of similarity than that of weak similarity, or by proving weak s-similarity between reconstruction and original for an $s < d$. Both of these improvements to the main statement were later obtained, and they are the topic of the next paper, *A Stronger Result on the Similarity Between an r-regular Object and its Reconstruction from a Trinary Image*, which is written as a supplement to this paper.

The reconstruction algorithm itself also leaves room for improvement. In this paper, the main focus has been on constructing a set that is weakly d-similar to

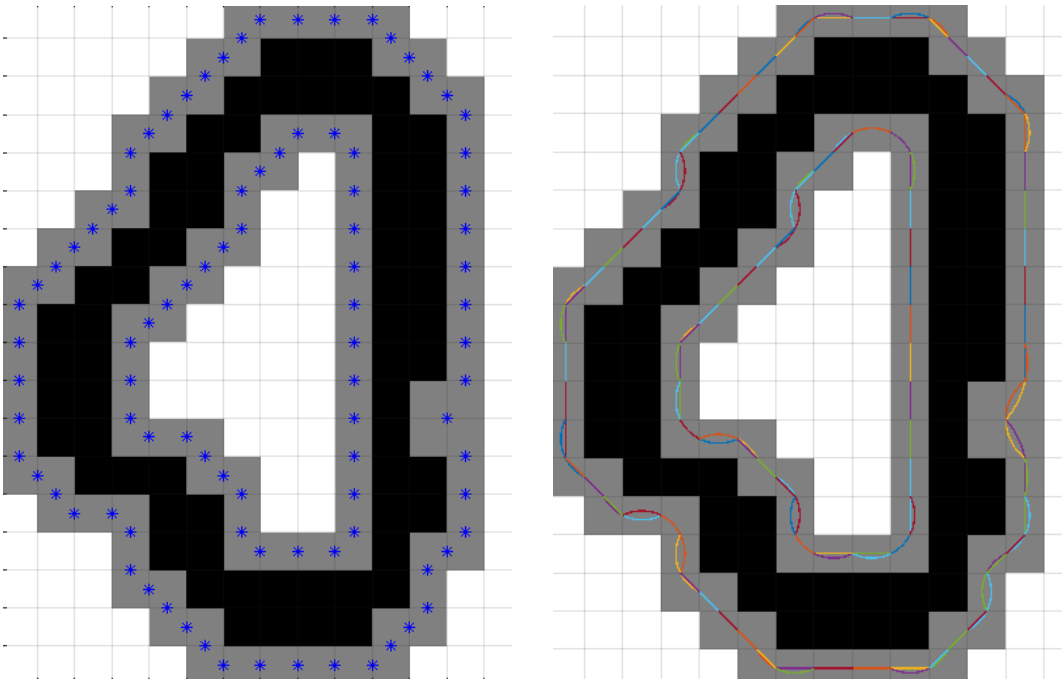

Figure 1.3: We make a reconstruction from a trinary image by first plotting auxiliary points on the boundaries of the grey pixels (left), and thereafter then connecting three consecutive auxiliary points by circle arcs (right).

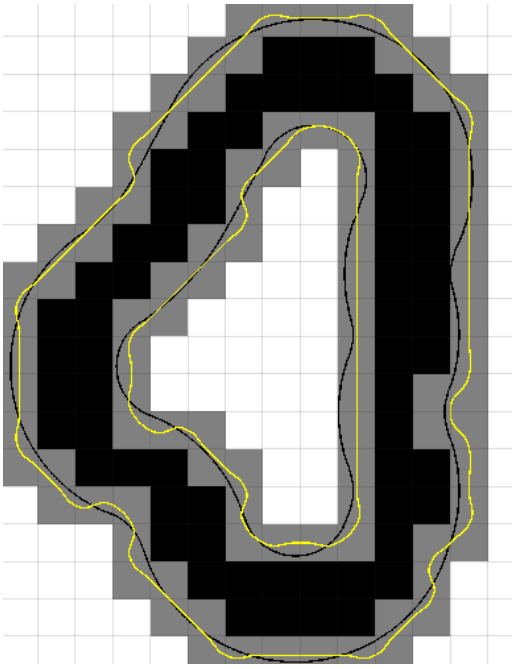

Figure 1.4: Interpolating these arcs to get a smooth curve (the yellow one in the right figure). The black curve in the right figure is the boundary of the original object.

the original, meaning that the reconstructed set is close to the original in Hausdorff distance, and that the two sets have the same topological properties. Apart from these, there may also be other properties than one wishes a good reconstruction to have. For instance, since the original set was assumed to be r-regular, one might wish the reconstructed set to be $(r-\varepsilon)$-regular for some small $\varepsilon > 0$. This article does not investigate what regularity the reconstructed set has, or discuss if the regularity can be improved.

This paper works exclusively with trinary images made from ideal digital images, but one may argue that in disregarding the exact intensities of each grey pixel when moving from digital images to trinary images, we are throwing a lot of information away. Another interesting topic for research could therefore be to study if a more precise reconstruction algorithm could be made from the ideal digital image than from its trinary version. If a reconstruction algorithm was proposed for ideal digital images, another interesting topic for study could be if such a reconstructed set would have the same digital image as the original one. The advantage of working with trinary images is, however, that there are only finitely many pixel configurations of a given size, enabling us to break up the problem f estimating Hausdorff distance into finitely many cases. This is partly the motivation for studying trinary images in this paper. Another part of the motivation for working with trinary images comes from our work on removing noise from images, as introduced in the paper *Reconstructing Objects from their Noisy Images at Low Resolution*: We try to remove noise from images by removing spurious grey (or black, or white) pixels appearing in places where they could not have been in an ideal image of an r-regular object. But if a grey pixel, after the addition of noise, is still grey, it is not possible to know how much noise were added to it using our method. We therefore wanted a result about reconstructing objects from images where the exact intensities of the grey pixels were unknown, leading to the work presented in this paper.

The proofs of some of the technical results in this paper have been moved to an appendix. This protocol is quite normal in computer science papers, but less so in mathematics papers. The paper is unpublished, but has been put on arXiv for reference (see [16]) in connection with the acceptance of the paper *Reconstructing Objects from their Noisy Images at Low Resolution.*

1.2.3 A Stronger Result on the Similarity Between an r-regular Object and its Reconstruction from a Trinary Image

This paper draft is written as a continuation of the previous paper, *Reconstruction of r-regular Objects from their Trinary Images.* Again, we are working with 2-dimensional trinary images of r-regular objects constructed using a lattice $d\mathbb{Z}^2$ with $d\sqrt{2} < r$. The paper uses parts of the results regarding configurations in trinary images of r-regular objects by lattices obtained in *Reconstruction of r-regular Objects from their Trinary Images*, and the reconstructed set is constructed in the same way as in the previous paper, but we fix the bump function used. The main result is a strengthening of the result in *Reconstruction of r-regular Objects from their Trinary Images*, since we instead of weak s-similarity now will consider the stronger notion *strong s-similarity* of capturing similarity between sets:

Definition 1.11. Let $A, B \subseteq \mathbb{R}^2$ be bounded sets and $s > 0$. The sets A and B are

called *strongly s-similar* if there exists a homeomorphism $f : \mathbb{R}^2 \to \mathbb{R}^2$ such that $f(A) = B$ and for all $x \in \partial A$ we have $d(x, f(x)) < s$.

The main theorem of this paper will be to show the following:

Theorem 1.12. *Let I be a trinary digital image of an r-regular object by a lattice $d\mathbb{Z}^2$ with $d\sqrt{2} < r$, and let Γ be the set reconstructed from I as explained in Paper B. Then the reconstructed set Γ and original set X are strongly $\frac{d}{\sqrt{2}}$-similar, where d again is the pixel side length.*

Note that this result does not only strengthen the previous result because weak similarity is replaced by strong similarity, but also because the similarity parameter is improved from d to $\frac{d}{\sqrt{2}}$.

Like in the previous paper, we have a collection of trinary pixel configurations that may be found in the trinary image of r-regular objects by lattices $d\mathbb{Z}^2$ with $d\sqrt{2} < r$. In the grey pixels of each of these configurations, we put what we call a *line covering* – a partition of the grey pixels into a set of disjoint lines, each with one endpoint in a black pixel and one endpoint in a white pixel. The idea is to show that we may push the reconstructed boundary along the lines of the line field until we hit the boundary of the original set, and then extend the map defining this push to a map of the entire plane. For this to work, we need to establish that such a map is actually well defined and carries the boundary of the reconstructed set to the boundary of the original set homeomorphically. This amounts to showing that each line of the line covering intersects both set boundaries in exactly one point. For the reconstructed set it is shown quite easily, since its boundary is a composition of known circle arcs. The real work lies in determining the behaviour of the boundary of the original set, since the only information available to us is that it is the boundary of an r-regular set, and that it passes through the grey pixels. We find subsets of the grey pixels where all boundary points of the original set is contained. This also enables us to estimate the Hausdorff distance between the point of the reconstructed set and the points of the boundary ∂X of the original set on each line of the line covering.

The upper bound $\frac{d}{\sqrt{2}}$ on the similarity between the original and reconstructed set is not necessarily the optimal one, but we believe that improving this bound significantly requires a large amount of extra work. With the existing reconstruction algorithm, it will be hard to get the similarity accuracy below $\frac{d}{2}$ (it is easy to come up with pixel configurations where the suggested homeomorphism moves points at least this distance. So before venturing out to improve the bound $\frac{d}{\sqrt{2}}$ for the similarity between the proposed reconstruction and the original object, one should consider if it is worth the trouble.

Another option could be to change the reconstructed set. Other than possibly improving the similarity parameter between the reconstructed set and the original, one could hope to be able to obtain interesting properties on the set boundary, such as $(r-\varepsilon)$-regularity for some suitably small ε. Likewise, like in the case of the previous paper, we believe that it should be possible to make a more precise reconstruction algorithm by taking exact pixel intensities into account, i.e. by considering ideal digital images rather than trinary images. However, such work is beyond the scope of this thesis.

1.2.4 Reconstructing Objects from their Noisy Images at Low Resolution

The work presented in this paper has been published in the proceedings for the 12th International Workshop on Graph-based Representations in Pattern Recognition [17], where the results were also presented in a talk. The work started out as an attempt to accommodate the theory presented in the two previous articles, *Reconstructioon of r-regular Objects from Trinary Images* and *A Stronger Result on the Similarity between an r-regular Object and Its Reconstruction from a Trinary Image*, to images that are more realistic to encounter in the real world. The basic idea behind the work is that even though real-world images are not necessarily as nice as the digital images of our model, we can regard an observed image as a slightly altered version of the ideal digital image, and try to spot the alterations in pixel intensities by comparing the observed image to the pixel configurations that we would expect to see in an ideal trinary image of an r-regular object.

Again, we work with 2-dimensional images of r-regular objects by a lattice $d\mathbb{Z}^2$ with $d\sqrt{2} < r$. But instead of working with the digital images from Definition 1.1, we now consider digital images with noise. Different types of noise are modelled in different ways, but common to them all is that the pixel intensities may have changed from what they were in the ideal, digital image. We thus regard the observed image as a pertubation of the ideal digital image.

From the paper *Reconstruction of r-regular Objects from Trinary Images* we get a list of all the 3×3 trinary configurations that may occur in an ideal digital image of an r-regular object. We propose a method for removing noise from a noisy image by comparing the observed 3×3 pixel configurations in the noisy image to the 3×3 trinary image configurations in the list. Loosely formulated, the idea is to replace each of the observed, noisy configurations with one from the list that looks the most like the observed one while also matching with the replacement configurations for the neighbouring 3×3 configurations. Thus we end up with a collection of trinary 3×3 configurations that all can occur in the digital image of an r-regular object, and which match on their overlaps. From these configurations we may then piece a trinary image together, containing only 3×3 configurations which can occur in the trinary image of an r-regular object – i.e. we attempt to recover the trinary, noise-free image from the noisy one by replacing illegal 3×3 configurations with ones from the list of possible 3×3 configurations. We formulate this as a linear integer programming problem, which is solvable, but computationally NP-hard.

The solution provided by this technique outputs a globally optimal algorithm (which is why we name the algorithm 'The global algorithm') with respect to a certain optimality criterion, depending on the similarity between the output image and the original one, see Figure 1.5. However, the computationality of this solution makes it inconvenient to work with in real applications, so we also propose a local approach for reconstructing the trinary image. Here, the idea is to start with a trinary image and then improve it in steps, one configuration at a time, making the trinary image look more like the observed, noisy one with each step. While doing this, however, we have to be careful not no introduce configurations that does not occur in any trinary image of an r-regular object. This algorithm is terminated when we cannot change the trinary image in the proposed way without either making the resulting reconstructed image differ more from the observed one than in the previous

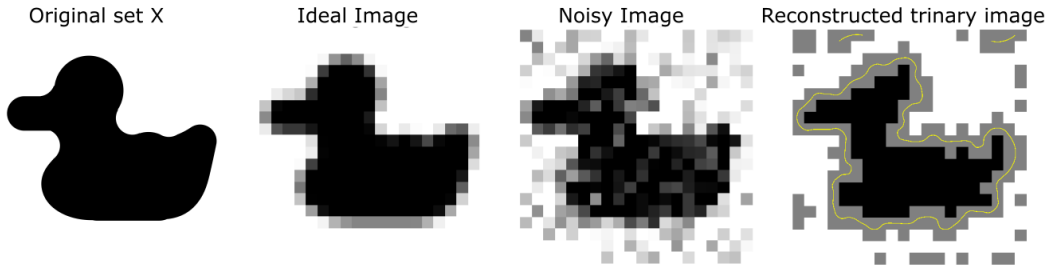

Figure 1.5: An example of the output of the global algorithm: The noisy image is the input for the algorithm, and the output is shown on the right, together with a yellow curve showing the boundary of the set that is reconstructed from the algorithm output. Compare to the original set on the left.

step, or introducing trinary configurations that cannot occur in a trinary image of an r-regular object. Hence this procedure produces a trinary image that is locally optimal in the sense that its output cannot be refined further without performing illegal steps.

The output of this algorithm depend greatly on how the algorithm is initiated, and it turns out that the requirement about not introducing configurations that cannot occur in trinary images of r-regular images is quite strict – for instance, it makes it impossible to reconstruct loops. The output from this local algorithm is therefore rather unstable, and a single output in general gives a rather poor result. We therefore suggest using a combination of several outputs with different initiations to reconstruct the trinary image. However, such a combination may in contain 3×3 trinary configurations which do not occur in trinary images of r-regular objects by a lattice $d\mathbb{Z}^2$ with $d\sqrt{2} < r$ – which was not what we wanted. We may then either choose to use the output anyway – accepting that it is not a correct reconstruction – or we may patch it up using the global algorithm that we mentioned first (sending us back to an NP-hard algorithm). As it turns out, the combination of several outputs from this local algorithm, used as an input for the global algorithm, gives pretty good output. On the downside, it is still very computationally heavy.

It would be interesting to have some result on the precision of the global algorithm. However, it is not clear how such precision should be measured. One idea could be to calculate the probability that a pixel that was supposed to be black is reconstructed as a white pixel or vice versa. However, our attempts on achieving such a result has hitherto been fruitless, since the seemingly local problem – the question of whether one pixel is reconstructed correctly – turns out to be a global problem, as the action of changing the colour of one pixel implies that an entire 3×3 has to be change, which in turn means that the neighbouring configurations are changed accordingly, and so on. Nonetheless, we hope that it is at least possible to put a bound on the precision of the algorithm by looking at the configurations locally.

More work could also be put into bringing down the computation time for the global algorithm. Since the problem is an integer linear programming problem, any solution will remain NP-hard, but the graph for the underlying problem contains a lot of structure which may be exploited in the implementation of the solution algorithm.

Another interesting thing to consider in relation to this paper could be to

investigate if the graph problem can be reformulated in another way. More specifically, in the paper presented in this thesis, we look at all 3×3 configurations in an image, but one could imagine only looking at some of them, so that two pixel configurations share at most 3 pixels (and not at most 6, as is the case in the proposed algorithm).

Also the local algorithm leaves a lot of room for improvement. As mentioned earlier, the requirement that we only add configurations that can occur in trinary digital images of r-regular objects in *all* steps of the algorithm is rather strict, and since we only care about the configurations in the final step of the algorithm, it may be possible to obtain better output by loosening the requirements on the images in the intermediate steps.

In this way, the work presented in this paper is a presentation of an idea, but there is still a lot of work that could be put into investigating its properties and improving its weaknesses.

1.2.5 Topological Reconstruction of r-regular Sets

In this paper, we work in three dimensions and consider digital images like the ones defined in Definition 1.1 of an r-regular object X by a lattice $d\mathbb{Z}^3$ with $d\sqrt{3} < r$. We let $V(X)$ denote the black pixels of the image (called the *inner Jordan Digitisation* of X by e.g. [8]) and prove the following:

Theorem 1.13. *Let X be an r-regular set and $d > 0$ satisfy $d\sqrt{3} < r$. Let $V(X)$ denote the set of black pixels in a digital image of X by a lattice $d\mathbb{Z}^3$. Then it is possible to construct a set Z from $V(X)$ such that Z is ambiently isotopic to X.*

The ambient isotopy between Z and X implies that the reconstructed set Z has the same topological properties as the original set. The work in this paper was also presented in connection with the qualifying exam for the PhD.

The procedure for proving this statement copies the approach of Tang Christensen [2], who proved an equivalent statement for another digitisation model called *Gauss digitisation* of r-regular objects by a lattice $d\mathbb{Z}^3$ with $0.95571d < r$. However, since we use a different digitisation model, we need the stronger assumption $d\sqrt{3} < r$ on our regularity parameter r and voxel side length d in order to prove an equivalent statement. The steps of the proof are the same as in Tang Christensen's thesis, but since we work with a different digitisation model, we need to adapt the model-specific proofs to our situation or, in some cases, change the proofs altogether.

The steps of the proof are the following: Let $V(X)$ denote the set of black voxels in the digital image of an r-regular object X by a lattice $d\mathbb{Z}^3$ with $d\sqrt{3} < r$. We first prove that there is a $1:1$-correspondence between connected components of X and connected components of $V(X)$, and also a $1:1$-correspondence between connected components of X^C and of $V(X)^C$. Note that if $r < d\sqrt{3}$, this would not be true in general, hence $d\sqrt{3} < r$ is the best possible bound on d and r that we can hope for in order to obtain the result. We then proceed to find a complete list of all possible $2 \times 2 \times 2$ configurations of black and non-black voxels, and prove that some of these do not occur in the digital image of an r-regular object by a lattice $d\mathbb{Z}^3$ with $d\sqrt{3} < r$. We may then prove that our reconstructed set Z is contained in a set homeomorphic to $\partial X \times [-1, 1]$ in such a way that it separates the sides $\partial X \times \{-1\}$ and $\partial X \times \{1\}$. For sets with this property, we may copy the approach of Tang Christensen [2] to show first that ∂Z and ∂X are homeomorphic, then that

they are isotopic. Extending this isotopy to an ambient isotopy, we finally arrive at the result.

The largest part of the work in this paper was put into proving that certain voxel configurations do not occur. The toolbox for these arguments comes from the paper *On r-regularity*. However, much of the heavy footwork on constructing the set Z was done in [2] and is not specific to her digitisation model, so we may use these parts of her work directly.

1.3 Related work

The task of reconstructing sets from their digital images is the task of deriving as much information about an object as possible from a discrete representation of it. One usually starts with a model for the digitisation process, and then investigates what information is kept during a digitisation under that model. Not all objects are well-suited for reconstruction from digital images at a given resolution. For example, object features on a sub-pixelar scale may easily be wiped away in a digitisation process. Therefore, many authors have dealt with the class of r-regular sets, see for instance [2, 9, 11–15]. These sets cover a wide range of shapes and objects and they have turned out to produce well-behaved digital images, which justifies that such sets are of interest in their own right and motivates investigating their properties further.

The precise definition of r-regularity differs a little from author to author. In [4, 5], an open set X is said to be r-regular if and only if both X and $\overline{X}^C$ are unions of open balls. However, in these papers, it is implicitly assumed that $\partial X = \partial \overline{X}^C$, which is not necessarily true for r-regular sets defined this way. This motivates our introduction of r-regular sets in Paper A as *closed* sets X where X and $\overline{X^C}$ are both unions of *closed* r-balls, because then $\partial X = \partial \overline{X^C}$ follows automatically. However, we show that our definition is equivalent to the definition in [4, 5] if we incorporate the extra assumption that $\partial X = \partial \overline{X}^C$.

In [5], an alternative characterisation of r-regular sets is given in terms of a Lipschitz condition on the boundary, plus an extra technical assumption. We show that the extra assumption may be replaced by the assumption that X and $\overline{X^C}$ are both manifolds with boundary.

In [12], Serra introduces the *regular model* as the class of compact sets that are morphologically open and closed with respect to a closed ball of radius r, and then remarks that this implies that each boundary point is contained in two closed r-balls included in X and $\overline{X^C}$, respectively. This is in accordance with our Definition 1.1, and with the definition in [11], where Pavlidis states that a square grid $d\mathbb{Z}^2$ and a set X are *compatible* if X is r-regular in the sense of Definition 1.1, and $\frac{d\sqrt{2}}{2} < r$. Our definition of r-regularity is also used in [9, 13, 15], though r-regularity is called $par(r)$-regularity in [9].

Since r-regularity of a set X implies the existence of a unique nearest point in ∂X for all points in $\mathbb{R}^n$ with $\delta_{\partial X}(x) < r$, we have also related the notion of r-regularity to the notion of *reach* defined in Definition 1.6, and first introduced by Federer in [6].

Since different definitions of r-regularity may be preferred in different situations, showing equivalence between these different notions of r-regularity is a strong result that allows us to attack problems concerning r-regular sets from many different

angles.

The process of obtaining a digitisation, i.e. of representing a continuous object in a discrete way, may be modelled in different ways. Many authors (see [2, 8, 12–15]) consider *Gauss digitisation* (also called *subset digitisation*), which makes a discrete representation of a continuous object X by placing X in a grid and colouring the Voronoi cells around each grid point black if the grid point is contained in X, and white otherwise. Serra [12] considers a 2-dimensional hexagonal grid, which gives him hexagonal Voronoi-cells. Pavlidis [11] considers a 2-dimensional square grid, giving him square pixels. Stelldinger and Köthe consider any 2-dimensional grid in [14, 15], and both Stelldinger et al. [13] and Tang Christensen [2] consider 3-dimensional square grids. We, too, consider square grids in first 2 and later 3 dimensions in this thesis, but we model images differently from the Gauss digitisation model. When creating images using Gauss digitisation, the resulting image is black-and-white, and corresponds to a doing a sampling of X by a grid. We, however, will think of images as created by a collection of sensors, each of which detects the light intensity of the object in a small area near the sensor. If the sensors are placed in a square grid and they each measure the light intensity of the object in a small square with the sensor as its midpoint, we will assume that the intensity that they measure is equal to the fraction of the square that is covered by the object. Colouring the squares corresponding to the sensor measurements, we thus obtain a grey-scale digital image where the intensity of each pixel is equal to the fraction of that pixel covered by the object. This way of modelling a digital image seeks to mimic the way real-world images are obtained. Our way of modelling images as defined in Definition 1.1 is a special case of the model introduced in [9], where Latecki et al. model the intensity of pixels as a monotonic function of the fraction of a pixel covered by a square. Latecki et al. goes on to thresholding their images, thus ending up with black and white images again. In this thesis, we will try to use the information contained in the pixel intensities, or at least in the knowledge that pixels can be either black, grey or white – therefore we, too, end up simplifying our obtained images further before we start reconstructing the objects.

Reconstructing objects from their images has been studied by many other authors, obtaining various reconstruction results for various models of digital images. Pavlidis [11], Serra [12], Stelldinger and Köthe [14, 15], Tang Christensen [2] and Latecki et al. [9] all reconstructed an object from its image that resembled the original one. They had different notions of what 'resemble' should mean, and for all except the latter one, they start with a Gauss digitisation of their object, as opposed to our approach. The exception is Latecki et al., who show that given a grey-scale digitisation of an r-regular object by a lattice of a certain size, the union of black pixels after applying any threshold to the image is homotopy equivalent and even homeomorphic to the original one (the homeomorphism is proved under the assumption that the r-regular object in question is a manifold with boundary, and they conjecture this to be true for all r-regular sets. This was later proved in [4]). All the above mentioned approaches used a union of pixels as their reconstructed object. This means, however, that the boundary of their reconstructed sets had corners. In contrast to this, we obtain reconstructions with smooth boundaries.

In our method for reconstructing objects from noisy images we do not make many assumptions on the nature of the noise on the image. This is in contrast to some of the other approaches to reconstructing images from suboptimal images. For instance,

in [15], Stelldinger and Köthe deals with reconstructing objects from blurred images. The problem of noise removal has also been tackled with more practical approaches, including deep convolutional neural networks [10]. Such approaches usually also deal with pixel classification (and hence not sub-pixelar reconstruction). The usual problems with neural networks are, however, that the need large training sets to function, which may not always be available.

Other standard algorithms for finding the boundaries of a digitised set from its image are Active Shape Models, [1, 3, 7]. In these models, the idea is to start with a curve representing a guess for the boundary of the digitised object, and then let the curve flow guided by some forces arising from edges in the image, curve smoothness and similar. Active shape models rely on some initial guess for the shape that one wishes to find in the image, and they require a lot of parameters that must be chosen wisely to obtain a good result - two problems that we try to work around in Paper C.

In Paper D we return to the idealised, noise-free images, but take the whole framework of images of r-regular sets to the next dimension, literally speaking. We prove that in 3 dimensions, the set of black voxels in a three-dimensional image of an r-regular set under certain restrictions on the image resolution gives rise to a set with the same topological features as the original one. This work is heavily inspired by the work started by Stelldinger et al. [13] and completed by Tang Christensen [2], who proved a corresponding result for Gauss digitisations of r-regular objects in $\mathbb{R}^3$.

References

[1] T. Chan and L. Vese. Active contours without edges. *IEEE TIP*, 10(2):266–277, 2001.

[2] Sabrina Tang Christensen. *Reconstruction of topology and geometry from digitisations*. PhD thesis, Aarhus University, 2016.

[3] T. F. Cootes and C. J. Taylor. Active shape models – "smart snakes". In *BMVC*, 1992.

[4] Pedro Duarte and Maria Joana Torres. Smoothness of boundaries of regular sets. *J. Math. Imaging Vis.*, 48(1):106–113, January 2014. ISSN 0924-9907. doi: 10.1007/s10851-012-0397-0. URL http://dx.doi.org/10.1007/s10851-012-0397-0.

[5] Pedro Duarte and Maria Joana Torres. r-regularity. *Journal of Mathematical Imaging and Vision*, 51(3):451–464, Mar 2015. ISSN 1573-7683. doi: 10.1007/s10851-014-0535-y. URL https://doi.org/10.1007/s10851-014-0535-y.

[6] Herbert Federer. Curvature measures. *Trans. Amer. Math. Soc.*, 93:418–491, 1959. ISSN 0002-9947. doi: 10.2307/1993504. URL https://doi.org/10.2307/1993504.

[7] M. Kass, A. Witkin, and D. Terzopoulos. Snakes: Active Contour Models. *IJCV*, 1(4):321–331, 1988.

[8] Reinhard Klette and Azriel Rosenfeld. *Digital Geometry: Geometric Methods for Digital Picture Analysis*. Morgan Kaufmann Publishers Inc., San Francisco, CA, USA, 2004. ISBN 1558608613.

[9] L.J. Latecki, C Conrad, and A Gross. Preserving topology by a digitization process. *Journal of Mathematical Imaging and Vision*, 8, 01 1998.

[10] G. et.al. Litjens. A survey on deep learning in medical image analysis. *MedIA*, 42:60–88, 2017.

[11] T. Pavlidis. *Algorithms for graphics and image processing*. Digital system design series. Computer Science Press, 1982. ISBN 9780914894650.

[12] Jean Serra. *Image Analysis and Mathematical Morphology*. Academic Press, Inc., Orlando, FL, USA, 1983. ISBN 0126372403.

[13] P. Stelldinger, L. J. Latecki, and M. Siqueira. Topological equivalence between a 3d object and the reconstruction of its digital image. *IEEE Transactions on Pattern Analysis and Machine Intelligence*, 29(1):126–140, Jan 2007. ISSN 0162-8828. doi: 10.1109/TPAMI.2007.250604.

[14] Peer Stelldinger and Ullrich Köthe. Shape preservation during digitization: Tight bounds based on the morphing distance. In Bernd Michaelis and Gerald Krell, editors, *Pattern Recognition*, pages 108–115, Berlin, Heidelberg, 2003. Springer Berlin Heidelberg. ISBN 978-3-540-45243-0.

[15] Peer Stelldinger and Ullrich Köthe. Towards a general sampling theory for shape preservation. *Image Vision Comput.*, 23(2):237–248, 2005.

[16] Helene Svane and Andrew du Plessis. Reconstruction of r-regular objects from trinary images. *CoRR*, abs/1903.10942, 2019. URL http://arxiv.org/abs/1903.10942.

[17] Helene Svane and Aasa Feragen. Reconstructing objects from noisy images at low resolution. In *Graph-Based Representations in Pattern Recognition*, pages 204–214, Cham, 2019. Springer International Publishing. ISBN 978-3-030-20081-7.

Paper A

On r-regularity

By Andrew du Plessis and Helene Svane

A.1 Definitions and basic results

The notion of r-regularity was originally developed independently by Serra [] and Pavlidis []. The object was to describe a classes of objects for which reconstruction from digital images preserved certain topological and/or geometrical features. Various versions of the definition have since been used by many authors ([],[],[]). Here is yet another version:

Definition A.1. Let X be a closed subset of $\mathbb{R}^n$, and let $r \in (0, \infty)$. X is r-regular if X and $\overline{\mathbb{R}^n \setminus X}$ are both unions of closed r-balls.

The first section of the paper will show that this definition is equivalent, or at least very closely related, to many of the alternative definitions which have been used previously. The remainder of the paper will discuss some geometry of r-regular sets and their boundaries which will be useful in applications.

Theorem A.2. *Let $r \in (0, \infty)$ and let X be a closed subset of $\mathbb{R}^n$. Then following are equivalent:*

(i) *X is r-regular;*

(ii) *For each $z \in \partial X$ there exist closed r-balls $A \subset X$, $B \subset \overline{\mathbb{R}^n \setminus X}$ such that $A \cap B = \{z\}$;*

(iii) *∂X is a C^1 $(n-1)$-submanifold of $\mathbb{R}^n$ and for each $z \in \partial X$ there exist closed r-balls $A \subset X$, $B \subset \overline{\mathbb{R}^n \setminus X}$ such that $A \cap B = \{z\}$;*

(iv) *X and $\overline{\mathbb{R}^n \setminus X}$ are C^1 n-dimensional submanifolds-with-boundary of $\mathbb{R}^n$, and the unit normal vector field $\{N(z) | z \in \partial X\}$ on their common boundary pointing out of X satisfies the Lipschitz condition*

$$\|N(z_1) - N(z_2)\| \leq \tfrac{1}{r}\|z_1 - z_2\| \quad \text{for all } z_1, z_2 \in \partial X;$$

(v) *X and $\overline{\mathbb{R}^n \setminus X}$ are of reach r.*

The notion of reach in Theorem A.2, (v) was introduced by Federer in his classic paper from 1959 [4].

Definition A.3. Let A be a closed subset of $\mathbb{R}^n$, $r \in (0, \infty)$ and $\delta_A : \mathbb{R}^n \to \mathbb{R}_+$ denote the distance to the set A. Then A has *reach* r if, for all $x \in \mathbb{R}^n$ such that $\delta_A(x) < r$, x has a *unique* nearest point in A.

This is a much more general notion than r-regularity. For example, if A has non-empty interior it does not imply that ∂A is a C^1-submanifold of $\mathbb{R}^n$: for example, it is a classical theorem that any closed convex set in $\mathbb{R}^n$ has reach r for any $r \in (0, \infty)$.

Definition A.4. Let $x \in \mathbb{R}^n$, $A \subset \mathbb{R}^n$. Then the *distance* from x to A is

$$\delta_A(x) = \inf\{\|x - a\| \mid a \in A\}.$$

It is well-known, and easy to see, that:

(i) if A is closed, then there exists $a \in A$ such that $\delta_A(x) = \|x - a\|$,

(ii) $|\delta_A(x) - \delta_A(y)| \leq \|x - y\|$ for all $x, y \in \mathbb{R}^n$.

Proposition A.5. *Let X be a closed subset of $\mathbb{R}^n$, and let $r \in (0, \infty)$. Then the following are equivalent:*

(i) *X is r-regular*

(ii) *for each $z \in \partial X$ there exist closed r-balls $A \subset X$, $B \subset \overline{\mathbb{R}^n \setminus X}$ such that $A \cap B = \{z\}$.*

Proof.

(i) ⇒ (ii): Let $z \in \partial X$. Since X is closed, $\partial X = X \cap \overline{\mathbb{R}^n \setminus X}$, and thus there exist closed r-balls $A \subset X$ and $B \subset \overline{\mathbb{R}^n \setminus X}$ such that $z \in A \cap B$. If A and B meet in more than one point then $\operatorname{Int} A \cap \operatorname{Int} B$ is not empty. But

$$\operatorname{Int} A \cap \operatorname{Int} B \subset A \cap B \subset X \cap \overline{\mathbb{R}^n \setminus X} = \partial X,$$

and thus ∂X contains a non-empty open set. But this is not possible because X is closed. So $A \cap B = \{z\}$.

(ii)⇒(i): It is immediate that $\partial X \subset X$, so X is closed.

Let $x \in X$. If $\delta_{\partial X}(x) \geq r$, then $x \subset B_r(x) \subset X$, where $B_r(x)$ is the closed r-ball with centre x. Otherwise, $\delta_{\partial X}(x) = s < r$. Since ∂X is closed, there exists $z \in \partial X$ with $\|x - z\| = s$. Let C be the closed s-ball with centre x; then $z \in C \subset X$. Let $A \subset X$, $B \subset \overline{\mathbb{R}^n \setminus X}$ be closed r-balls with $A \cap B = \{z\}$. Now $z \in C \cap B$. Arguing as in the first half of the proof, we have $C \cap B = \{z\}$. It follows that A, B, C share a common tangent hyperplane at z, and that $C \subset A$. In particular, x is contained in a closed r-ball contained in A.

Thus X is a union of closed r-balls. A similar argument, with the roles of X and $\overline{\mathbb{R}^n \setminus X}$ interchanged, shows this also holds for $\overline{\mathbb{R}^n \setminus X}$, completing the proof. □

Definition A.6. X is *r-regular* if one of the two equivalent statements (i), (ii) of Proposition A.5 holds. Notice that X is r-regular if, and only if, $\overline{\mathbb{R}^n \setminus X}$ is r-regular.

Proposition A.7. *Let X be r-regular. Let $z \in \partial X$ and let $s \in (0, r]$. Then there is a unique closed s-ball $\alpha(z, s)$ with $z \in \alpha(z, s) \subset X$, and a unique closed s-ball $\beta(z, s)$ with $z \in \beta(z, s) \subset \overline{\mathbb{R}^n \setminus X}$.*

Proof. Let $\alpha \subset X$, $\beta \subset \overline{\mathbb{R}^n \setminus X}$ be closed r-balls such that $\alpha \cap \beta = \{z\}$.

Let C be a closed s-ball, with $s \in (0, r]$, in X such that $z \in C$. Arguing as in the first half of the proof of Proposition A.5, $C \cap \beta = \{z\}$. It follows that α, β, C share a common tangent hyperplane at z, and that $C \subset \alpha$. If $s = r$, this shows that $\alpha = C$, so $\alpha = \alpha(z, r)$ is the unique closed r-ball in X containing z. If $s < r$, $C = \alpha(z, s)$ is the unique closed s-ball contained in $\alpha(z, r)$ which is tangent to $\alpha(z, r)$ at z.

Now let C be a closed s-ball, with $s \in (0, r]$, in $\overline{\mathbb{R}^n \setminus X}$ such that $z \in C$. Arguing as above, if $s = r$ then $\beta = C$ so $\beta = \beta(z, r)$ is the unique closed r-ball in $\overline{\mathbb{R}^n \setminus X}$ containing z, and if $s < r$, $C = \beta(z, s)$ is the unique closed s-ball contained in $\beta(z, r)$ which is tangent to $\beta(z, r)$ at z. □

Corollary A.8. *Let X be r-regular. Then ∂X is of reach r.*

Proof. We must show that for any $y \in \mathbb{R}^n$ such that $\delta_{\partial X}(y) < r$, there is a *unique* point $z \in \partial X$ such that $\|y - z\| = \delta_{\partial X}(y)$.

Let $y \in X$ be such that $\delta_{\partial X}(y) = s < r$. Since ∂X is closed, there exists $z \in \partial X$ such that $\|y - z\| = s$. The closed s-ball with centre y is contained in X, and contains z; thus it is $\alpha(z, s)$. Since $s < r$, $\alpha(z, s) \setminus \{z\} \subset \operatorname{Int} \alpha(z, r) \subset \operatorname{Int}(X)$. Thus $\alpha(z, s) \cap \partial X = \{z\}$, and z is the *unique* point in ∂X such that $\|y - z\| = s$.

Now let $y \in \overline{\mathbb{R}^n \setminus X}$ be such that $\delta_{\partial X}(y) = s < r$, and let $z \in \partial X$ be such that $\|y - z\| = s$. Arguing as above, the closed s-ball with centre y is $\beta(z, s)$, and z is the *unique* point in ∂X such that $\|y - z\| = s$. □

Definition A.9.

(i) For $s \in [0, r]$, let

$$U_s = \{x \in \mathbb{R}^n \mid \delta_{\partial X}(x) < s\},$$

and let $\pi : U_r \to \partial X$ be defined by setting $\pi(x)$ to be the nearest point in ∂X to x, for every $x \in U_r$.

(ii) For each $z \in \partial X$ let $N(z)$ be the outward-pointing unit normal at z to the boundary of the closed r-ball $\alpha(z, r) \subset X$; notice that $-N(z)$ is then the outward-pointing unit normal to the boundary of the closed r-ball $\beta(z, r) \subset \overline{\mathbb{R}^n \setminus X}$.

Remark A.10. It follows from Corollary A.8 that

(i) if $z \in \partial X$ and $s \in (-r, r)$ then $\pi(z + sN(z)) = z$; here $z + sN(z) \in X$ if $s \leq 0$, $z + sN(z) \in \overline{\mathbb{R}^n \setminus X}$ if $s \geq 0$.

(ii) if $x \in X$ is such that $\delta_{\partial X}(x) = s < r$ then $x = \pi(x) - sN(\pi(x))$; similarly, if $x \in \overline{\mathbb{R}^n \setminus X}$ is such that $\delta_{\partial X}(x) = s < r$ then $x = \pi(x) + sN(\pi(x))$.

Remark A.11. Duarte and Torres adopt a different approach to r-regularity in [2]; they define a subset $U \subset \mathbb{R}^n$ to be r-regular if both U and $\mathbb{R}^n \setminus \overline{U}$ are connected unions of open r-balls. (The connectedness assumption seems irrelevant; it is not used anywhere in [2].)

The statement of Proposition 5 of their paper [2] is essentially that for such U, Proposition A.5, (ii) holds for $\overline{U}$. The proof of that proposition contains an error, however; there is an implicit assumption that $\partial U = \partial(\mathbb{R}^n \setminus \overline{U})$, but this is not necessarily true. For example, consider $U = \mathbb{R}^n \setminus (B \cup L)$, where B is a closed r-ball, and L is either a point or a closed bounded line segment with $\delta_B(L) \geq 2r$. Then U is a connected union of open r-balls, as is $\mathbb{R}^n \setminus \overline{U} = \mathrm{Int}(B)$, an open r-ball, but $\partial U = \partial B \cup L$ whilst $\partial(\mathbb{R}^n \setminus \overline{U}) = \partial B$. The difficulty is resolved by the following proposition:

Proposition A.12. *Let $U \subset \mathbb{R}^n$ be an open set with $\partial U = \partial(\mathbb{R}^n \setminus \overline{U})$. Then the following are equivalent:*

(i) *$\overline{U}$ is r-regular,*

(ii) *U and $\mathbb{R}^n \setminus \overline{U}$ are both unions of open r-balls.*

Proof.

(i) ⇒ (ii): We suppose that $\overline{U}$ is r-regular. Observe that $\partial\overline{U} = \partial(\mathbb{R}^n \setminus \overline{U}); = \partial U$ by assumption. For any $x \in U$, we will exhibit an open r-ball containing x which avoids ∂U. Since the ball is connected, this will in fact show that it is contained in U.

Suppose first $\delta_{\partial\overline{U}}(x) \geq r$. Then the open r-ball with centre x avoids $\partial\overline{U} = \partial U$.

Otherwise, suppose $\delta_{\partial\overline{U}}(x) \in (0, r]$. Then x is contained in $\mathrm{Int}(\alpha(\pi(x), r))$, an open r-ball avoiding $\partial\overline{U} = \partial U$.

Thus U is a union of open r-balls. A similar argument, replacing $\overline{U}$ with $\overline{\mathbb{R}^n \setminus \overline{U}}$, shows that $\mathbb{R}^n \setminus \overline{U}$ is also a union of open r-balls.

(ii) ⇒ (i): Suppose U and $\mathbb{R}^n \setminus \overline{U}$ are unions of open r-balls. Let $z \in \partial U$, and let $\{x_i\} \subset U$ be a sequence converging to z. For $i = 1, 2, \ldots$ let A_i be an open r-ball containing x_i and contained in U, and let a_i be the centre of A_i. We have

$$\|a_i - z\| \leq \|a_i - x_i\| + \|x_i - x\| < r + \|x_i - z\| \qquad (*)$$

Since $\|x_i - z\| \xrightarrow{i\to\infty} 0$, $\{a_i\}$ is bounded, and thus has a convergent subsequence, with limit a, say. Replacing $\{a_i\}$ with this subsequence, and $\{x_i\}$ with its corresponding subsequence, we can suppose $x_i \to x$ and $a_i \to a$. Letting $i \to \infty$ in $(*)$ gives $\|a - z\| \leq r$.

Since $A_i \cap \partial U$ is empty, we have $\delta_{\partial U}(a_i) \geq r$; letting $i \to \infty$ gives $\delta_{\partial U}(a) \geq r$. Combining this with the previous inequality gives

$$\|a - z\| = r = \delta_{\partial U}(a),$$

so the closed r-ball A with centre a contains z and is contained in $\overline{U}$.

We have $z \in \partial U = \partial(\mathbb{R}^n \setminus \overline{U}) = \partial\overline{U}$. Arguing as above with U replaced by $\mathbb{R}^n \setminus \overline{U}$ yields a closed r-ball B with $z \in B$ and $B \subset \overline{\mathbb{R}^n \setminus \overline{U}}$.

It now follows from Proposition A.5 that $\overline{U}$ is r-regular. □

Theorem A.13. *Let X be r-regular. Then:*

(i) *The map* $N : \partial X \to \mathbb{R}^n$ *is Lipschitz continuous with Lipschitz constant* $1/r$, *i.e.* $\|N(y) - N(z)\| \leq (1/r)\|y - z\|$ *for all* $y, z \in \partial X$.

(ii) *Let* $s \in [0, r)$, *and let* $U_s = \{x \in X \mid \delta_{\partial X}(x) < s\}$. *Then the restriction* $\pi|U_s$ *is Lipschitz continuous with Lipschitz constant* $\frac{r}{r-s}$, *i.e.* $\|\pi(x) - \pi(y)\| \leq \frac{r}{r-s}\|x - y\|$ *for all* $x, y \in U_s$.

(iii) *Let* $f : U_r \to \mathbb{R}$ *be given by* $f(x) = \langle x - \pi(x), N(\pi(x)\rangle$. *Then* f *is continuously differentiable, with gradient function given by* $\operatorname{grad} f(x) = N(\pi(x))$ *for all* $x \in U_r$.

(iv) $\partial X = f^{-1}(0)$ *is a* C^1 $(n-1)$*-dimensional submanifold of* $\mathbb{R}^n$ *and* X *is a* C^1 n*-dimensional submanifold-with-boundary of* $\mathbb{R}^n$.

Remark A.14. This theorem is a slight sharpening of results of Duarte and Torres, see in particular Propositions 6, 7 and 8 of [2]. Our proof will also follow theirs quite closely, but with a few improvements and a correction.

We begin with two technical lemmas which are slight improvements of Lemmas 3 and 4 of [2].

Lemma A.15. *Let* $r > 0$, *let* $u, v, w \in \mathbb{R}^n$, *and suppose*

(a) $\|v\|, \|w\| = r$

(b) $\|u + (v + w)\| \geq 2r$, $\|u - (v + w)\| \geq 2r$

Then

(i) $\|v - w\| \leq \|u\|$

(ii) $|\langle v + w, u\rangle| \leq \frac{1}{2}(\|u\|^2 - \|v - w\|^2)$

(iii) $|\langle u, v\rangle| \leq \frac{1}{2}\|u\|^2$, $|\langle u, w\rangle| \leq \frac{1}{2}\|u\|^2$

(iv) $|\langle v - w, u\rangle| \leq \|u\|^2$

(v) $\langle v, v - w\rangle = \frac{1}{2}\|v - w\|^2 \leq \frac{1}{2}\|u\|^2$, $\langle , w - v\rangle = \frac{1}{2}\|w - v\|^2 \leq \frac{1}{2}\|u\|^2$.

Proof.

(i): Using the parallelogram identity and the hypothesis (a), we have

$$\|v + w\|^2 + \|v - w\|^2 = 2\|v\|^2 + 2\|w\|^2 = 4r^2,$$

so that $\|v + w\|^2 = 4r^2 - \|v - w\|^2$.

Using the parallelogram identity and the hypothesis (b), we have

$$2\|u\|^2 + 2\|v + w\|^2 = \|u + (v + w)\|^2 + \|u - (v + w)\|^2 \geq 8r^2,$$

so that $\|v + w\|^2 \geq 4r^2 - \|u\|^2$.

Hence $4r^2 - \|v - w\|^2 \geq 4r^2 - \|u\|^2$, so $\|v - w\|^2 \leq \|u\|^2$ and $\|v - w\| \leq \|u\|$.

(ii): Using hypothesis (b),

$$4r^2 \leq \|u \pm (v+w)\|^2 = \|u\|^2 \pm \langle 2u, v+w\rangle + \|v+w\|^2.$$

Substituting for $\|v+w\|^2$ as in the proof of (i), we have

$$4r^2 \leq \|u\|^2 + 4r^2 - \|v-w\|^2 \pm 2\langle u, v+w\rangle,$$

so $\mp 2\langle u, v+w\rangle \leq \|u\|^2 - \|v-w\|^2$ and $|\langle u, v+w\rangle| \leq \frac{1}{2}(\|u\|^2 - \|v-w\|^2)$.

(iii): We have

$$|\langle u, v\rangle| = |\tfrac{1}{2}(\langle u, v+w\rangle - \langle u, v-w\rangle)| \leq \tfrac{1}{2}(|\langle u, v+w\rangle| + |\langle u, v-w\rangle|).$$

Using (ii) and the Cauchy-Schwary inequality gives

$$|\langle u, v\rangle| \leq \tfrac{1}{2}(\tfrac{1}{2}(\|u\|^2 - \|v-w\|^2) + \|u\|\|v-w\|).$$

Write $t = \|v-w\|/\|u\|$, so, using (i), $0 \leq t \leq 1$. The inequality above may be rewritten

$$|\langle u, v\rangle| \leq (\tfrac{1}{4}(1-t^2) + \tfrac{1}{2}t)\|u\|^2.$$

The function $t \mapsto \frac{1}{4}(1-t^2) + \frac{1}{2}t$ has derivative $\frac{1}{2}(1-t)$, so is monotone increasing on $[0,1]$, and thus takes its maximum value on $[0,1]$, $\frac{1}{2}$, when $t = 1$. It follows that

$$|\langle u, v\rangle| \leq \tfrac{1}{2}\|u\|^2.$$

Interchanging the roles of v, w gives

$$|\langle u, w\rangle| \leq \tfrac{1}{2}\|u\|^2.$$

(iv): Applying the Cauchy-Schwarz inequality and (i) gives

$$|\langle v-w, u\rangle| \leq \|v-w\|\|u\| \leq \|u\|^2.$$

(v): We have, using hypothesis (a),

$$\begin{aligned}\|v-w\|^2 = \langle v-w, v-w\rangle &= 2\langle v, v-w\rangle - \langle v+w, v-w\rangle \\ &= 2\langle v, v-w\rangle - (\|v\|^2 - \|w\|^2) = 2\langle v, v-w\rangle,\end{aligned}$$

so, using (i),

$$\langle v, v-w\rangle = \tfrac{1}{2}\|v-w\|^2 \leq \tfrac{1}{2}\|u\|^2.$$

Interchanging the roles of v, w gives

$$\langle w, w-v\rangle = \tfrac{1}{2}\|w-v\|^2 \leq \tfrac{1}{2}\|u\|^2.$$

□

Lemma A.16. *With $u, v, w \in \mathbb{R}^n$ as in Lemma A.15, let $s \in (0, r)$, let $s_v, s_w \in \mathbb{R}$ be such that $|s_v|, |s_w| \leq s$, and let $v' = \frac{s_v}{r}v$, $w' = \frac{s_w}{r}w$.*

Then $\|u\| \leq \frac{r}{r-s}\|u + w' - v'\|$.

Proof. By the Cauchy-Schwarz inequality, we have

$$\|x\| \geq \frac{|\langle x, u\rangle|}{\|u\|}.$$

Applying this with $x = u + w' - v'$ gives, applying Lemma A.15,(iii),

$$\begin{aligned}\|u\|\|u + w' - v'\| &\geq |\langle u + w' - v', u\rangle| \\ &= |\|u\|^2 + \tfrac{s_w}{r}\langle w, u\rangle - \tfrac{s_v}{r}\langle v, u\rangle| \\ &\geq \|u\|^2(1 - \tfrac{1}{2}|\tfrac{s_w}{r}| - \tfrac{1}{2}|\tfrac{s_v}{r}|) \\ &\geq \|u\|^2(1 - \tfrac{s}{r}).\end{aligned}$$

It follows at once that

$$\|u\| \leq \frac{1}{1 - \frac{s}{r}}\|u + w' - v'\| = \frac{r}{r - s}\|u + w' - v'\|.$$

□

Proof of Theorem A.13.

(i): We must prove that the unit normal vector field $N : \partial X \to \mathbb{R}^n$ satisfies $\|N(x) - N(y)\| \leq \frac{1}{r}\|x - y\|$ for any $x, y \in \partial X$. It is clear that this holds when $x = y$; so suppose $x \neq y$. According to Proposition A.7 there are unique closed r-balls $A_x, A_y \subset X$ and $B_x, B_y \subset \overline{\mathbb{R}^n \setminus X}$ such that $A_x \cap B_x = \{x\}$, $A_y \cap B_y = \{y\}$. It follows that

$$\mathrm{Int}(A_x) \cap \mathrm{Int}(B_y) = \emptyset,\ \mathrm{Int}(A_y) \cap \mathrm{Int}(B_x) = \emptyset. \qquad (*)$$

Write a_x, b_x, a_y, b_y for the centres of A_x, B_x, A_y, B_y respectively. Then $(*)$ is equivalent to

$$\|a_x - b_y\| \geq 2r,\ \|b_x - a_y\| \geq 2r. \qquad (**)$$

It follows from the Definition A.9, (ii) that

$$a_x = x + rN(x),\ b_x = x - rN(x),\ a_y = y + rN(y),\ b_y = y - rN(y),$$

so $(**)$ is equivalent to

$$\|x - y + rN(x) + rN(y)\| \geq 2r,\ \|x - y - (rN(x) + rN(y))\| \geq 2r.$$

Applying Lemma A.15, (i), with $v = rN(x)$, $w = rN(y)$, and $u = x - y$ gives $\|rN(x) - rN(y)\| \leq \|x - y\|$, whence $\|N(x) - N(y)\| \leq \frac{1}{r}\|x - y\|$, as claimed.

(ii): Let $x, y \in U_s$. We have, following Remark A.10, (ii), that

$$x - \pi(x) = s_x N(\pi(x)),\ y - \pi(y) = s_y N(y),$$

for some $|s_x|, |s_y| < s$. Applying Lemma A.16 with

$$u = \pi(x) - \pi(y),\ v = rN(x),\ w = rN(y),\ v' = x - \pi(x),\ w' = y - \pi(y),$$

gives

$$\begin{aligned}\|\pi(x) - \pi(y)\| &\leq \tfrac{r}{r-s}\|\pi(x) - \pi(y) + (x - \pi(x)) - (y - \pi(y)\| \\ &= \tfrac{r}{r-s}\|x - y\|,\end{aligned}$$

as claimed.

(iii): It is enough to prove that, for any $s \in (0, r)$, there exists $C > 0$ such that

$$|f(y) - f(x) - \langle y - x, N(\pi(x))\rangle| \leq C\|x - y\|^2$$

for all $x, y \in U_s$. We will apply Lemma A.15, (iii) and (v), with

$$u = \pi(x) - \pi(y),\ v = rN(\pi(x)),\ w = rN(\pi(y)).$$

Notice that $y - \pi(y) = s_y N(\pi(y))$ for some $s_y \in (-s, s)$.

A direct calculation shows

$$\begin{aligned}
&|f(y) - f(x) - \langle y - x, N(\pi(x))\rangle| \\
&\quad = |\langle y - \pi(y), N(\pi(y))\rangle - \langle x - \pi(x), N(\pi(x))\rangle - \langle y - x, N(\pi(x))\rangle| \\
&\quad = |\langle y - \pi(y), N(\pi(y)) - N(\pi(x))\rangle + \langle \pi(x) - \pi(y), N(\pi(x))\rangle| \\
&\quad = |\tfrac{s_y}{r^2}\langle w, w - v\rangle + \tfrac{1}{r}\langle u, v\rangle| \\
&\quad \leq \tfrac{s}{r^2}|\langle w, w - v\rangle| + \tfrac{1}{r}|\langle u, v\rangle| \\
&\quad \leq \tfrac{s+r}{2r^2}\|u\|^2.
\end{aligned}$$

Now, by (ii), $\|u\| = \|\pi(y) - \pi(x)\| \leq \frac{r}{r-s}\|y - x\|$, so

$$|f(y) - f(x) - \langle y - x, N(\pi(x))\rangle| \leq \tfrac{s+r}{2(r-s)^2}\|y - x\|^2,$$

completing the proof.

(iv): Since $x - \pi(x)$ is parallel to $N(\pi(x))$ for all $x \in U_r$, it is immediate that $\partial X = f^{-1}(0)$. Since f is C^1 and $\operatorname{grad} f(x) = N(\pi(x)) \neq 0$ for all $x \in U_r$, $\partial X = f^{-1}(0)$ is a C^1 $(n-1)$-dimensional submanifold of U_r, so of $\mathbb{R}^n$. Since $f^{-1}(-r, 0]$ is a collar neighbourhood of ∂X in X, X is a C^1 n-dimensional submanifold-with-boundary of $\mathbb{R}^n$. □

Proposition A.17. *Let $r \in (0, \infty)$ and let X be a closed C^1 n-dimensional submanifold with boundary of $\mathbb{R}^n$. Suppose that the outward-pointing unit normal vector field $\{N(z) \mid z \in \partial X\}$ of its boundary ∂X satisfies*

$$\|N(z_1) - N(z_2)\| \leq \tfrac{1}{r}\|z_1 - z_2\| \text{ for all } z_1, z_2 \in \partial X.$$

Then X has reach r.

Proof. Let $y_0 \in \mathbb{R}^n$ be such that there are two distinct points $x_1, x_2 \in X$ with

$$\|x_1 - y_0\| = \|x_2 - y_0\| = \delta_X(y_0).$$

Then $y_0 \notin X$; and $x_1, x_2 \in \partial X$.

Thus the distance-squared function $\delta^2_{y_0}$ from y_0, given by $\delta^2_{y_0}(x) = \|y - y_0\|^2$ for $y \in \mathbb{R}^n$ has, when restricted to ∂X, minima at both x_1 and x_2. Since ∂X is a C^1-submanifold and $\delta^2_{y_0}$ is smooth, it follows that $\operatorname{grad} \delta^2_{y_0}$ is orthogonal to ∂X at both y_1 and y_2. Since $\operatorname{grad} \delta^2_{y_0}(y) = 2(y - y_0)^2$ for all $y \in \mathbb{R}^n$, we thus have $x_1 - y_0$ is parallel to $N(x_1)$ and $x_2 - y_0$ is parallel to $N(x_2)$, whence

$$x_1 - y_0 = tN(x_1), \quad x_2 - y_0 = tN(x_2),$$

where $t = \|x_1 - y_0\| = \|x_2 - y_0\|$ and . Subtracting these equations gives $x_1 - x_2 = t\,(N(x_1) - N(x_2))$, so

$$\|N(x_1) - N(x_2)\| = \tfrac{1}{t}\|x_1 - x_2\|.$$

But we have $\|N(x_1) - N(x_2)\| \leq \frac{1}{r}\|x_1 - x_2\|$, so $\frac{1}{t} \leq \frac{1}{r}$, or $r \leq t = \delta_X(y_0)$. Thus if $y \in \mathbb{R}^n$ has distance less than r from X, there is a unique nearest point in X to y; that is, X has reach r, as claimed. □

We have now proved most of Theorem A.2. Proposition A.5 proves A.2 (i) $\iff$ A.2 (ii), Theorem A.13 proves these are equivalent to A.2 (iii) and imply A.2 (iv), and Proposition A.17 applied to both X and $\overline{\mathbb{R}^n \setminus X}$ proves A.2 (iv) $\implies$ A.2 (v). It thus remains to prove that A.2 (v) $\implies$ A.2 (ii). We require some results on reach.

Proposition A.18. *Let $r > 0$ and let $A \subset \mathbb{R}^n$ be a closed set of reach r. Then $\mathbb{R}^n \setminus A$ is a union of open balls of radius r.*

The proof relies on a result of Federer from [4]:

Lemma A.19. *Let $A \subset \mathbb{R}^n$ be a closed set, let*

$$\mathrm{Unp} = \{x \in \mathbb{R}^n \mid x \text{ has a unique nearest point in } A\},$$

and, for $x \in \mathrm{Unp}$, write $\pi(x)$ for the nearest point in A to x.

Let $a \in A$, $v \in \mathbb{R}^n$, and suppose

$$\tau = \sup\{t \geq 0 \mid a + tv \in \mathrm{Unp} \text{ and } \pi(a + tv) = a\} \in (0, \infty).$$

Then $a + \tau v \notin \mathrm{Int}(\mathrm{Unp})$.

Proof. See [4, Theorem 4.8 (6)]. The argument is rather subtle; it requires [4, Theorem 4.7 (6)], and [4, Theorem 4.8 (3), (4) and (5)]. □

Lemma A.20. *With the notation of Lemma A.19, if $a+tv \in \mathrm{Unp}$ and $\pi(a+tv) = a$ for some $t \geq 0$ then $a + t'v \in \mathrm{Unp}$ and $\pi(a + t'v) = a$ for all $t' \in [0, t]$.*

Proof. The closed ball $B(t)$ with centre $a + tv$ and radius $t\|v\|$ meets A only at a. If $t' \in [0, t]$, then the closed ball $B(t')$ with centre $a + t'v$ and radius $t'\|v\|$ is contained in $B(t)$; so $B(t')$ meets A only at a. Thus a is the unique nearest point in A to $a+t'v$, so $a + t'v \in \mathrm{Unp}$ and $\pi(a + t'v) = a$. □

Proof of Proposition A.18. We will use the notation of Lemma A.19. Let $x \in \mathbb{R}^n \setminus A$. We must find an open r-ball in $\mathbb{R}^n \setminus A$ containing x.

Suppose $\delta_A(x) \geq r$. Then the open r-ball with centre x is contained in $\mathbb{R}^n \setminus A$.

Now suppose $\delta_A(x) < r$. Then $x \in V_r = \{z \in \mathbb{R}^n \mid \delta_A(z) < r\}$, an open neighbourhood A; since A has reach r, $V_r \subset \mathrm{Int}(\mathrm{Unp})$. Let $a = \pi(x)$ and $v = x - a$. Notice that $\|v\| = \delta_A(x) < r$. Let

$$\tau = \sup\{t \in [0, r/\|v\|) \mid a + tv \in \mathrm{Unp} \text{ and } \pi(a + tv) = a\}.$$

We claim that $\tau = r/\|v\|$. For suppose $\tau < r/\|v\|$. Then

$$\tau = \sup\{t \geq 0 \mid a + tv \in \mathrm{Unp} \text{ and } \pi(a + tv) = a\}$$

and Lemma A.19 implies $a + \tau v \notin \mathrm{Int}(\mathrm{Unp})$. Since $V_r \subset \mathrm{Int}(\mathrm{Unp})$, it follows that $a + \tau v \notin V_r$, so $\delta_A(a + \tau v) \geq r$. However,

$$\delta_A(a + \tau v) \leq \|(a + \tau v) - a\| = \tau \|v\| < r,$$

a contradiction. So $\tau = r/\|v\|$, as claimed.

It thus follows from Lemma A.20 that $a + tv \in \mathrm{Unp}$ and $\pi(a + tv) = a$ for all $t \in [0, r/\|v\|)$. Equivalently, the closed ball $B(t)$ with centre $a + tv$ and radius $t\|v\|$ meets A only at a, for all $t \in [0, r/\|v\|)$. It follows that $W \subset \mathbb{R}^n \setminus A$, where

$$W = \bigcup_{t \in [0, r/\|v\|)} B(t) \setminus \{a\}.$$

Now it is easy to see that W is the open ball with centre $a + (r/\|v\|)v$ and radius $(r/\|v\|)\|v\| = r$. Also, since $\|v\| < r$, W contains the centre of $B(1)$, which is x. So there is an open ball of radius r in $\mathbb{R}^n \setminus A$ which contains x, as required. This completes the proof. □

We can, finally, prove Theorem A.2 (v) $\implies$ (ii):

Proposition A.21. *Let X be closed, and suppose that X and $\overline{\mathbb{R}^n \setminus X}$ are of reach r. Then X is r-regular.*

Proof. We have, by Proposition A.18, that $\mathbb{R}^n \setminus X$ and $\mathbb{R}^n \setminus (\overline{\mathbb{R}^n \setminus X}) = \mathrm{Int}(X)$ are unions of open r-balls.

Let $U = \mathrm{Int}(X)$. Then $\partial U = \partial X = \partial(\mathbb{R}^n \setminus \overline{U})$, and it follows from Proposition A.12 that $\overline{U} = X$ is r-regular. □

Remark A.22. Duarte and Torres claim, in [3],§5, that the implication Theorem A.2 (iv) $\implies$ (i) does not hold in general. They claim that the C^1 2-dimensional submanifold-with-boundary whose interior is the bounded region of the complement of the curve sketched in Figure A.1 is a counter-example for r greater than half the width of the central narrow connection, apparently because the unit normal vectors along the boundary of the connection (the two blue normal vectors) are parallel.

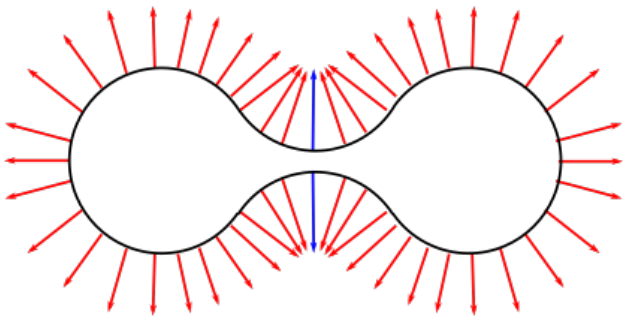

Figure A.1: The above 2-dimensional submanifold with boundary is *not* a counter-example to the implication *iv*) ⇒ *i*) from Theorem ...,

However, this does *not* imply that the distance between these vectors is zero – we are considering outward-pointing normals, so the distance between those on the upper and lower parts of the boundary of the connection is 2. So this is not a counter-example.

A.2 Some geometry of r-regular sets

Proposition A.23. *Let $X \in \mathbb{R}^n$ be r-regular, let $a \in (0, r)$, and let*

$$X' = \{x \in X \mid \delta_{\partial X}(x) \geq a\}.$$

The X' is $(r-a)$-regular.

Proof. It is immediate that X' is closed.

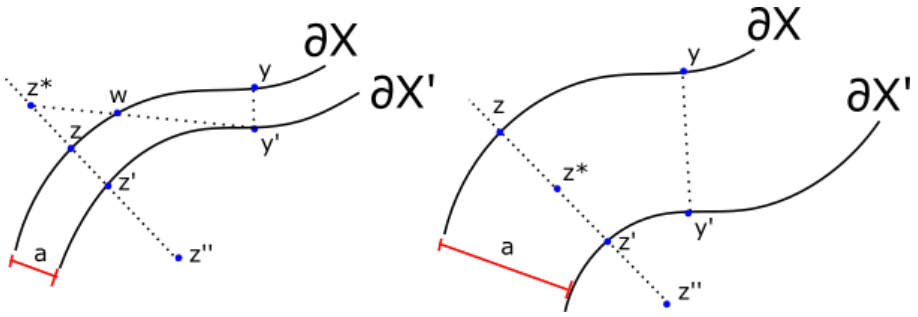

Figure A.2: Left: The position of the points in the lemma in the case where $2a < r$. Right: The position of the points i the lemma in the case where $2a \geq r$.

Let $\{N(z) \mid z \in \partial X\}$ be the outward-pointing unit normal bundle for ∂X. Then

$$\partial X' = \{x \in X \mid \delta_{\partial X}(x) = a\} = \bigcup_{z \in \partial X} \{z - aN(z)\}.$$

For $z \in \partial X$, let $z' = z - aN(z) \in \partial X'$, and let $z'' = z - rN(z) = z' - (r-a)N(z)$, see Figure A.2.

Let $y' \in \partial X'$, $y' \neq z'$; so $y' = y - aN(y)$ for some $y \in \partial X$, $y \neq z$.

We have $\|z'' - y\| \leq \|z'' - y'\| + \|y' - y\| = \|z'' - y'\| + a$. Now z'' is the centre of the closed r-ball $\alpha = \alpha(z, r)$ with $z \in \alpha \subset X$ which meets ∂X at z; so $r \leq \|z'' - y\|$. Thus $r < \|z'' - y'\| + a$, whence $r - a < \|z'' - y'\|$.

Thus the closed $(r-a)$-ball with centre z'' meets $\partial X'$ only at z'; it also follows that it is is contained in X'.

Now let $z^* = z' + (r-a)N(z) = z - (2a - r)N(z)$; so $z^* \neq X'$.

Consider first the case where $2a < r$, so that $z^* \in \mathbb{R}^n \setminus X$ – this case is shown on the left in Figure A.2. Let $y' \in \partial X'$, $y' \neq z'$; so $y' = y - aN(y)$ for some $y \in \partial X$, $y \neq z$. Let w be a point of intersection of ∂X and the line segment joining y' to z^*, and notice that w cannot be equal to z. We have $\|z^* - y'\| = \|z^* - w\| + \|w - y'\|$. Also, $\|y' - w\| \geq a$, since $\delta_{\partial X}(y') = \|y' - y\| = a$, and $\|z^* - w\| \geq r - 2a$, since $\delta_{\partial X}(z^*) = \|z^* - z\| = r - 2a$. So $\|z^* - y'\| \geq a + (r - 2a) = r - a$, and thus the closed $(r-a)$-ball with centre z^* meets $\partial X'$ at z', and is contained in $\overline{\mathbb{R}^n \setminus X'}$.

Now consider the case $2a \geq r$ (shown on the right in Figure A.2); here $z^* \in X$. Let $y \in \partial X'$, $y' \neq z'$; so $y' = y - aN(y)$ for some $y \in \partial X$, $y \neq z$. Since $\delta_{\partial X}(y') = a$, we have

$$a \leq \|y' - z\| \leq \|y' - z^*\| + \|z^* - z\| = \|y' - z^*\| + 2a - r,$$

so that $\|y' - z^*\| \geq a - (2a - r) = r - a$. Thus again the closed $(r-a)$-ball with centre z^* meets $\partial X'$ at z', and is contained in $\overline{\mathbb{R}^n \setminus X'}$.

It now follows from the arguments of Proposition A.5 that X' is $(r-a)$-regular, as claimed. □

Corollary A.24. *Let X be r-regular, let $a \in (-r, r)$, and define*

$$X_a = \begin{cases} X \cup \overline{U_a} & a \geq 0 \\ X \setminus U_{|a|} & a < 0 \end{cases}$$

Then X_a is $(r - |a|)$-regular.

Proof. For $a \leq 0$, notice that $X_a = \{x \in X \mid \delta_{\partial X}(x) \geq -a\}$ is of the same form as X' in Proposition A.23, hence X_a is $(r + a)$-regular in this case.

For $a \geq 0$, remember that $\overline{\mathbb{R}^n \setminus X}$ is also r-regular. Thus since

$$\overline{\mathbb{R}^n \setminus X_a} = \{x \in \overline{\mathbb{R}^n \setminus X} \mid \delta_{\partial X}(x) \geq a\},$$

the set $\overline{\mathbb{R}^n \setminus X_a}$ is again of the same form as in Proposition A.23, implying that $\overline{\mathbb{R}^n \setminus X_a}$ is $(r-a)$-regular. But if this is true for $\overline{\mathbb{R}^n \setminus X_a}$, it is also true for the closure of its complement which is X_a, by Remark A.6. □

Remark A.25. We may note that the ∂X_a are C^1 submanifolds of $\mathbb{R}^n$, by Theorem A.13, (iv), and that they share a common normal bundle, in the sense that if $z' \in \partial X_a$, then $z' = z - aN(z)$ for some unique $z \in \partial X$, and the normal for ∂X_a at z' is $N(z)$. This allows us to extend the domain of the normal vector field N to all of U_r.

Remark A.26. For $a \leq 0$, the set X_a of Corollary A.24 can also be written in terms of the function f from Theorem A.13 as $X_a = X \setminus f^{-1}((a, r))$. Likewise, for $a \geq 0$, we may write $X_a = X \cup f^{-1}((r, a])$.

Proposition A.27. *Let X be r-regular, and let a_1, $a_2 \in (-r, r)$, $a_1 < a_2$.*

(i) *$f^{-1}[a_1, a_2]$ has C^1 boundary $\partial X_{a_1} \cup \partial X_{a_2}$.*

(ii) *$f^{-1}[a_1, a_2]$ is C^1-diffeomorphic to $\partial X \times [0, 1]$.*

Proof.

(i): Clearly $f^{-1}[a_1, a_2]$ has boundary $f^{-1}(\{a_1, a_2\})$, which is C^1 by the remark above, and equal to $\partial X_{a_1} \cup \partial X_{a_2}$ by the preceding corollary.

(ii): We observe that $f^{-1}[a_1, a_2] = \{x + sN(x) \mid x \in \partial X, s \in [a_1, a_2]\}$, so that $\varphi : X \times [0, 1] \to f^{-1}[a_1, a_2]$ given by $\varphi(x, t) = x + ((1 - t)a_1 + ta_2)N(x)$ is a homeomorphism. It is not, however, a C^1-diffeomorphism when N is not continuously differentiable. Instead, we consider $\eta : U_r \to \mathbb{R}^n$, a close C^1 approximation to $N : U_r \to \mathbb{R}^n$, where N is extended to all of U_r as explained in Remark A.25. Let γ be an integral curve of η. We note that

$$\frac{d}{dt}(f \circ \gamma)(t) = \operatorname{grad} f_{\gamma(t)} \gamma'(t) = \langle N(\gamma(t)), \eta(\gamma(t)) \rangle,$$

which we can suppose is uniformly close to 1. It now follows from general theory that there is an open neighbourhood W of $f^{-1}(a_1) \times \{0\}$ in $f^{-1}(a_1) \times \mathbb{R}$ and a C^1-diffeomorphism $\Gamma : W \to U_r$ such that $t \mapsto \Gamma(x, t)$ is the complete integral curve

through x, for each $x \in f^{-1}(a_1)$. In particular, $\Gamma^{-1}(f^{-1}(a_2))$ is a C^1-submanifold of W, indeed a graph manifold over $f^{-1}(a_1)$,

$$\Gamma^{-1}(f^{-1}(a_2)) = \{(x, T(x)) \mid x \in f^{-1}(a_1)\},$$

where $T : f^{-1}(a_1) \to (0, \infty)$ is a C^1-function. Define now $\psi : f^{-1}(a_1) \times [0,1] \to f^{-1}[a_1, a_2]$ by

$$\psi(x,t) = \Gamma(x, \frac{t(a_2 - a - 1)}{T(x)});$$

this gives the required C^1-diffeomorphism. □

Definition A.28. Let $X \subset \mathbb{R}^n$ be an r-regular set; and let U_r and $\pi : U_r \to \partial X$ be as defined in Definition A.9.

A retraction $\rho : X \cup U_r \to X$ is then defined by

$$\rho(y) = \begin{cases} \pi(y) & y \in U_r \setminus X, \\ y & y \in X. \end{cases}$$

Since $\pi(y) = y$ for $y \in \partial X$, ρ is continuous.

Proposition A.29. *(Stelldinger* et al.*) Let $X \subset \mathbb{R}^n$ be an r-regular set, let $x, y \in X$ with $\|x - y\| < 2r$, and let $L \subset \mathbb{R}^n$ be the line-segment from x to y. Then:*

(i) *$L \in X \cup U_r$ and $\rho|L$ is injective, so that $\rho(L)$ is a simple curve in X joining x to y.*

(ii) *Let B be an s-ball, $s \leq r$, with $x, y \in B$. Then $\rho(L) \subset B$.*

Proof.

(i): Let $z \in L \setminus X$. We have$\|x - z\| + \|y - z\| = \|x - y\| < 2r$, so at least one of $\|x - z\|, \|y - z\| < r$, and thus $\delta_{\partial X}(z) = \delta_X(z) < r$, so $z \in U_r$. It follows that $L \subset X \cup U_r$.

Suppose now $z_1, z_2 \in L$ with $z_1 \neq z_2$ and $\rho(z_1) = \rho(z_2); = w$, say. Thus $z_1, z_2 \in \rho^{-1}(w) = \{w + sN(w) \mid s \in [0, r)\}$. In particular, at least one of z_1, z_2 – let us say z_1 for definiteness – is contained in the open line segment $\ell = \{w + sN(w) \mid s \in (0, 2r)\}$, which, in the notation of Proposition A.7, is contained in the interior of $\beta(w, r)$, so in $\mathbb{R}^n \setminus X$.

The unique affine line containing x and y also contains z_1 and z_2 between them. ℓ is a connected open subset of this line which intersects L (at z_1) but does not meet its end-points x and y (which are contained in X). It follows that $\ell \subset L$. This gives a contradiction, since ℓ has length $2r$, while L has length $< 2r$. Thus our supposition was false, and ρ is injective.

(ii): Let $z \in L \setminus X$, and write $w = \rho(z)$, so that $z = w + tN(w)$ for some $t \in (0, r)$. Let P be the affine plane containing L and w. Then $C = P \cap B$ is an s'-disc, for some $s' \in (0, s]$ containing L, whilst $A = P \cap \beta(w, r)$ (using the notation of Proposition A.7) is an r-disc, because P contains the centre $w + rN(w)$ of $\beta(w, r)$. $M = A \cap L$ is line segment whose interior is contained in $\mathbb{R}^n \setminus X$, and so avoids x and y; since $z \in M$ we conclude that $M \subset L$, see Figure A.3.

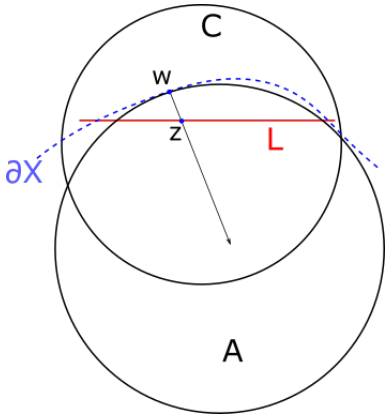

Figure A.3: The circle C contains L, while $M = A \cap L$ is contained in L.

Let $S(A)$ be the intersection of A with its mirror image across the affine line ℓ containing L; similarly let $S(C)$ be the intersection of C with its mirror image across ℓ. Clearly $M = \ell \cap S(A)$, and $M \subset L \subset S(C)$. The lemma immediately following this proof will show that $S(A) \subset S(C)$; thus $z \in S(A) \subset S(C) \subset C$, and we can conclude that $\rho(L) \subset C$. □

Definition A.30. Let L be a closed line-segment in $\mathbb{R}^n$ of length $|L| \leq 2r$; then the *r-spindle* $S(L, r)$ generated by L is the intersection of all r-balls whose boundaries each contain both end-points of L.

When L has length $2r$, there is just one r-ball containing L (with L as a diameter), so in this case $S(L, r)$ is this ball.

When L has length less than $2r$ and $n = 2$ there are just two closed r-balls (or, since $n = 2$, r-discs) whose boundaries contain both end-points of L, each the mirror-image of the other in the affine line containing L; and $S(L, r)$ is the intersection of these two discs, see Figure A.4, left.

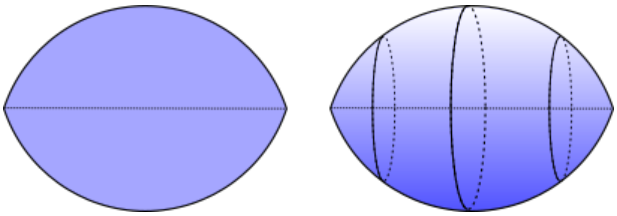

Figure A.4: Examples of spindles in two (left) and three (right) dimensions.

When L has length less than $2r$ and $n \geq 3$ we consider restriction to an affine plane P containing L. Any r-ball containing the end-points of L in its boundary intersects P in an s-disc, for $s \leq r$, the case $s = r$ being attained by the two such r-balls with centres in P. It follows from the $n = 2$ case of the following lemma that the intersection of all these discs is the r-spindle $S_P(L, r)$ generated by L in P. Since distinct affine planes containing L intersecting only in L, we see that $S(L, r)$ is the union of the $S_P(L, r)$ for all affine planes P containing L, see Figure A.4, right.

Lemma A.31.

(i) *Let $0 < s \leq r$, and let $M \subseteq N \subseteq \mathbb{R}^n$ be closed line segments of length less than $2s$. Then $S(M,r) \subseteq S(N,s)$.*

(ii) *Let M be a closed line segment of length $|M| < 2r$ in $\mathbb{R}^n$. Then $S(M,r)$ is the intersection of all closed balls of radius at most r which contain M.*

Proof.

(i): We begin with the case $n = 2$, and let a, b be the end-points of M. Then

$$S(M,r) = \{x \in \mathbb{R}^2 \mid \text{the angle } \angle axb \text{ is obtuse, with } \sin(\angle axb) \leq \frac{|M|}{2r}\}.$$

This follows easily from the fact, already known to Euclid, that the angle subtended by a chord at points of a circle is constant in the corresponding major arc and minor arc, together with a calculation of the sine of this angle. If the circle has radius r and the chord has length l, then this sine is $l/2r$, for both the major and the minor arc.

We also have, of course,

$$S(N,s) = \{x \in \mathbb{R}^2 \mid \text{the angle } \angle cxd \text{ is obtuse, with } \sin(\angle cxd) \leq \frac{|N|}{2s}\},$$

where c, d are the end-points of N.

Now let $x \in S(M,r)$. Then $\angle axb$ is obtuse, so the larger angle $\angle cxd$ is too. Also, $|M| \leq |N|$ and $r \geq s$, so

$$\frac{|M|}{2r} \leq \frac{|N|}{2s},$$

and $x \in S(N,s)$, as required.

Now consider the general case, and intersect with affine planes P containing M. By the observations in the definition above, $S(M,r) \cap P = S_P(M,r)$ and $S(M,r)$ is the union of the $S_P(M,r)$. Similarly, $S(N,s)$ is the union of the $S_P(N,s)$. By what we have just proved in the two-dimensional case, $S_P(M,r) \subset S_P(N,s)$ for all P; so $S(M,r) \subset S(N,s)$, as claimed.

(ii): Write S for the intersection of all closed balls of radius at most r which contain M. By definition, $S \subset S(M,r)$.

Let C be a closed s-ball containing M, where $s \leq r$. Then the intersection of C with the affine line containing M is a closed line-segment N containing M. By the first part of the proof, $S(M,r) \subset S(N,s) \subset C$. Thus $S(M,r) \subset S$. □

Addendum A.32. *Let M be a closed line segment of length $|M| < 2r$ in $\mathbb{R}^n$. Then $S(M,r)$ is the intersection of all closed balls of radius strictly less than r which contain M.*

Proof. Let S be the intersection of all closed balls of radius strictly less than r which contain M. Then clearly $S(M,r) \subset S$.

Let $x \in S$. Clearly $x \in S(M,s)$ for all $s \in (\frac{1}{2}|M|, r)$. We must show $x \in S(M,r)$. Intersecting with the affine plane containing M and x allows us to reduce to the case $n = 2$. Let a, b be the end-points of M. The characterisation of spindles in the case $n = 2$ in Lemma A.31, (i) shows that $\angle axb$ is obtuse, with

$$\sin(\angle axb) \leq \frac{|M|}{2s}$$

for all $s \in (\frac{1}{2}|M|, r)$. Taking the limit as $s \to r$ gives

$$\sin(\angle axb) \leq \frac{|M|}{2r},$$

and the spindle characterisation from the proof of Lemma A.31, (i) gives $x \in S(M, r)$, completing the proof. □

Corollary A.33. *Let $X \subset \mathbb{R}^n$ be an r-regular set, let $x, y \in X$ with $\|x - y\| < 2r$, and let $L \subset \mathbb{R}^n$ be the line-segment from x to y. Then $\rho(L) \subset S(L, r)$.*

Proof. This is immediate from Proposition A.29, (ii) and the definition of spindles. □

Remark A.34. For the approach of Stelldinger *et al* to Proposition A.29 and Corollary A.33, see [7], Theorem 6 and Lemma 8.

Addendum A.35. *Let $X \subset \mathbb{R}^n$ be an r-regular set, let $x, y \in X$ with $\|x - y\| < 2r$, and let $L \subset \mathbb{R}^n$ be the line-segment from x to y. Then orthogonal projection Π of $\mathbb{R}^n$ onto the affine line ℓ containing L gives a homeomorphism $\rho(L) \to L$.*

Proof. Let v, $w \in \rho(L)$ be such that $\Pi(v) = \Pi(w) = z$. Assume without loss of generality that $\|v - z\| \geq \|w - z\|$, see Figure A.5

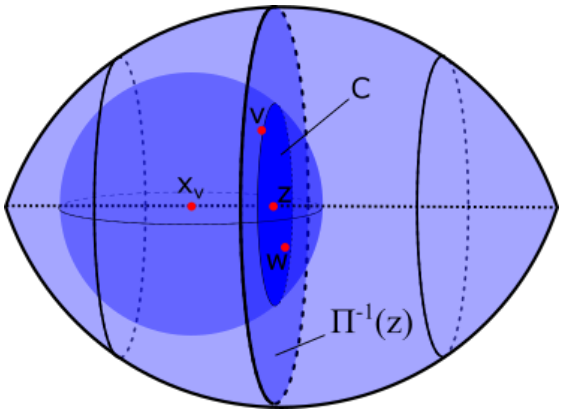

Figure A.5: if two points v and w both lie in $\Pi^{-1}(\{z\})$ with $\|v - z\| \geq \|w - z\|$ for some $z \in L$, then the point x_v that is mapped to v by ρ is not mapped to its unique nearest point, yielding a contradiction.

Let $x_v \in L$ be such that $\rho(x_v) = v$, i.e. v is the unique nearest point to x_v. Then the closed ball $\overline{B_{\|v-x_v\|}(x_v)}$ meets $\Pi^{-1}(\{z\})$ in a closed $(n-1)$-dimensional ball C of radius $\|v - z\|$, centered at z, and $v \in \partial C$. Since $\|v - z\| \geq \|w - z\|$, we must have that w lies in C, and hence $w \in \overline{B_{\|v-v\|}(x_v)}$. But then w is a point in X that is as not further from x_v than v – a contradiction, since v was the unique nearest point to x_v. □

Definition A.36. The *spindle angle* of a two-dimensional spindle $S(L, r)$ is the acute angle φ between L and the boundary arcs of $S(L, r)$. An easy calculation shows $\sin\varphi = \frac{|L|}{2r}$, where $|L|$ is the length of L.

The *spindle angle* of a higher dimensional spindle $S(L, r)$ is the spindle angle of $S_P(L, r)$ for any affine plane P containing L.

Lemma A.37. *Let $X \subset \mathbb{R}^n$ be r-regular, and let $x, y \in \partial X$, with $0 < \|x - y\| < 2r$; write L for the line segment joining x and y. Then the angles between L and the tangent spaces to ∂X at x and y and are at most the spindle angle of $S(L, r)$.*

Proof. It is enough to show this holds at x. Let T be the tangent space to ∂X at x, N its orthogonal complement. We observe first that $y \notin N$.
(For suppose otherwise. Then L is be contained in the interior an an r-ball tangent to ∂X at x, so that y is contained either in $\mathrm{Int}(X)$ or $\mathbb{R}^n \setminus X$, contradicting $y \in \partial X$.)
Let P be the affine plane through x containing L and N, so that the angle between L and T is the angle between L and $T \cap P$. Choose orthonormal coordinates in P so that $x = (0, 0)$, $y = (|L|, 0)$ and let θ be the anticlockwise angle between L and $T \cap P$. Reflecting in the x-axis if necessary, we can suppose that $\theta \in (0, \frac{\pi}{2})$. The two closed r-balls tangent to ∂X at x have centres on N at $(-r\sin\theta, r\cos\theta)$ and $(r\sin\theta, -r\cos\theta)$. Since $y \in \partial X$, neither of these balls has y in its interior, so we must have

$$(-r\sin\theta - |L|)^2 + (r\cos\theta)^2 \geq r^2, \quad (r\sin\theta - |L|)^2 + (-r\cos\theta)^2 \geq r^2.$$

Since $\theta \in (0, \frac{\pi}{2})$, the first of these is always satisfied. The second expands to $|L|^2 - 2r|L|\sin\theta + r^2 \geq r^2$, so is equivalent to $|L| \geq 2r\sin\theta$, so to $\sin\theta \leq \frac{|L|}{2r}$; so θ is at most the spindle angle of $S(L, r)$, as claimed. □

Proposition A.38. *Let $X \subset \mathbb{R}^n$ be an r-regular set. Let x, y, z be three non-collinear points in X, and suppose that $x, y, z \in C$, where $C \subset \mathbb{R}^n$ is a closed s-ball, for some $s \in (0, r)$. Let T be the plane triangle in $\mathbb{R}^n$ with vertices x, y, z, and write L_x, L_y, L_z for the three sides of T, respectively opposite x, y, z.*

Then there exists a continuous map $\sigma : T \to X$ such that

(i) $\sigma(T) \subset C$,

(ii) $\sigma = \rho$ *on* $L_x \cup L_y \cup L_z$,

Proof. Let Δ be the plane triangle in $\mathbb{R}^3$ with vertices $(1, 0, 0), (0, 1, 0), (0, 0, 1)$, so that

$$\Delta = \{(s, t, u) \in \mathbb{R}^3 \mid s, t, u \in [0, 1] \text{ and } s + t + u = 1\}.$$

The map $\varphi : \Delta \to T$ defined by $\varphi(s, t, u) = sx + ty + uz$ for $(s, t, u) \in \Delta$ is continuous and bijective (because of the non-collinearity of x, y, z), so is a homeomorphism, and the points of T are uniquely and continuously parametrised by φ.

We will define $\sigma : T \to X$ via this parametrisation:

$$\sigma(sx + ty + uz) = \begin{cases} \rho\big[(1-u)\rho\Big(\frac{1}{s+t}(sx+ty)\Big) + uz\big] & \text{for } (s,t,u) \in \Delta \setminus \{(0,0,1)\}, \\ z & \text{for } (s,t,u) = (0,0,1). \end{cases}$$

We must see that σ is well-defined.

This is clear when $(s, t, u) = (0, 0, 1)$, where $\sigma(z) = z \in X \cap C$. Now suppose $(s, t, u) \in \Delta \setminus \{(0, 0, 1)\}$. Observe first that $w_{s,t} = \frac{1}{s+t}(sx + ty) \in L_z$. Since C is convex $L_z \subset C$, so is of length at most $2s$, the diameter of C. Since $s < r$, it follows from Proposition A.29 that $\rho|L_z$ exists and that $\rho(L_z) \subset C$. Thus $\rho(w_{s,t})$ is defined and contained in C.

Next, observe that $v_{s,t,u} = (1-u)\rho(w_{s,t}) + uz$ is contained in the line-segment $K_{s,t}$ from $\rho(w_{s,t})$ to z. These end-points are both in C, so applying Proposition A.29 again, $\rho|K_{s,t}$ is defined and $\rho(K_{s,t}) \subset C$. Thus $\sigma(sx+ty+uz) = \rho(v_{s,t,u})$ is defined and contained in C; so σ is well-defined, and $\sigma(T) \subset C$.

We must also see that σ is continuous. This is clear from the definition on $T \setminus \{z\}$, since ρ is continuous. To study continuity at z, let $\{(s_n, t_n, u_n) \,|\, n \in \mathbb{N}\}$ be a sequence in $\Delta \setminus \{(0,0,1)\}$ converging to $(0,0,1)$. We must show that $\sigma(s_n x + t_n y + u_n z) \to z$ as $n \to \infty$.

For all $n \in \mathbb{N}$, $w_{s_n,t_n} = \frac{1}{s_n+t_n}(s_n x + t_n y) \in L_z$, so $\rho(w_{s_n,t_n}) \in \rho(L_z)$. Since L_z is compact, so is $\rho(L_z)$, so $\|\rho(w_{s_n,t_n}) - z\|$ is bounded.

Now consider $v_{s_n,t_n,u_n} = (1-u_n)\rho(w_{s_n,t_n}) + u_n z$. We have

$$\begin{aligned}\|v_{s_n,t_n,u_n} - z\| &= \|(1-u_n)\rho(w_{s_n,t_n}) + u_n z - z\| = \|(1-u_n)(\rho(w_{s_n,t_n}) - z)\| \\ &= (1-u_n)\|\rho(w_{s_n,t_n}) - z\|,\end{aligned}$$

which converges to 0 as $n \to \infty$, because $\|\rho(w_{s_n,t_n}) - z\|$ is bounded and $1 - u_n \to 0$ as $n \to \infty$. Thus $v_{s_n,t_n,u_n} \to z$ as $n \to \infty$, whence, since ρ is continuous,

$$\sigma(s_n x + t_n y + u_n z) = \rho(v_{s_n,t_n,u_n}) \to \rho(z) = z$$

as $n \to \infty$, as required.

Finally, we compute σ on the edges of T. We note first that $\sigma(z) = z = \rho(z)$.

L_z is parametrised by $t \mapsto (1-t)x + ty, t \in [0,1]$, and

$$\sigma((1-t)x + ty) = \rho(\rho((1-t)x + ty)) = \rho((1-t)x + ty),$$

so $\sigma|L_z = \rho|L_z$.

$L_y \setminus \{z\}$ is parametrised by $u \mapsto (1-u)x + uz, u \in [0,1)$ and

$$\sigma((1-u)x + uz) = \rho((1-u)\rho(x) + uz)) = \rho((1-u)x + uz),$$

so $\sigma|L_y = \rho|L_y$.

Similarly, $L_x \setminus \{z\}$ is parametrised by $u \mapsto (1-u)y + uz, u \in [0,1)$ and

$$\sigma((1-u)y + uz) = \rho((1-u)\rho(y) + uz)) = \rho((1-u)y + uz),$$

so $\sigma|L_y = \rho|L_y$, completing the proof. □

Remark A.39. With the notation of the preceding proposition, it is immediate that $\sigma(T)$ is contained in the intersection $P_r(T)$ of all closed balls of radius less than r which contain T. This set is a little difficult to describe in general, but can often be usefully approximated. As an example, and for later use, consider the case $n = 3$, and suppose that the circumcircle C for T (that is, the unique circle containing x, y and z) has radius $s < r$. Then $P_r(T)$ is contained in the intersection of all closed balls of radius less than r which contain C in their boundaries, which is in fact the intersection of the two closed r-balls containing C in their boundaries, the *r-lens* $L_r(C)$ associated with the circle C. Intersecting with the three closed r-balls containing T with centres in the plane spanned by T and whose boundaries pass through two of vertices of T yields the *reduced* r-lens $R_r(C)$.

Remark A.40. Stelldinger *et al.* claim a stronger result in the case $n = 3$ in [7], Lemma 11:

Let $X \subset \mathbb{R}^3$ be an r-regular set, let $x, y, z \in X$ be such that $\|x-y\|, \|y-z\|, \|z-x\| < 2r$, and let T be the plane triangle with vertices x, y, z. Then Stelldinger *et al.* claim

(i) $\rho|T : T \to X$ is well-defined,

(ii) $\rho(T) \subset P_r(T)$,

(iii) $\rho(T)$ is homeomorphic to a closed disc.

All three of these are false in the generality claimed. Consider

$$X = \{x \in \mathbb{R}^3 \mid \|x\| \geq r\};$$

it is easy to see that X is r-regular.

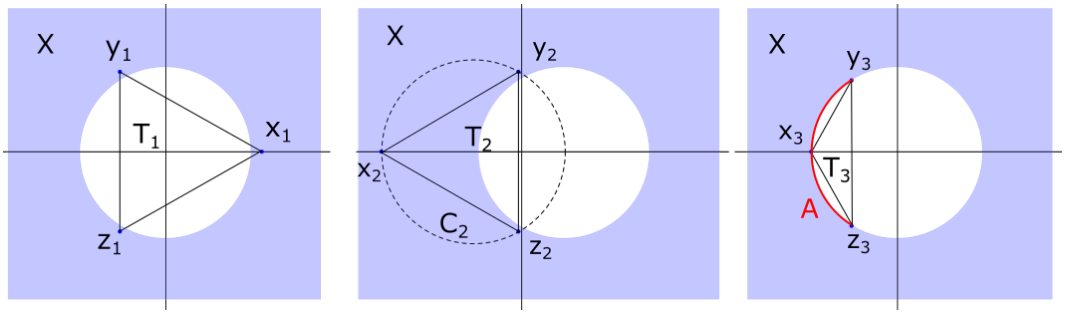

Figure A.6: None of the three claims in Remark A.40 are true. Indeed, consider an r-regular set like the blue one in the above figure (all our counter-examples are drawn in 2D, although they are actually 3-dimensional). The first figure is a counter-example to the first claim, the second figure is a counter-example to the second claim, and the third figure is a counter-example to the third claim.

(i): Suppose $x_1 = d(1,0,0), y_1 = d(-\frac{1}{2}, \frac{\sqrt{3}}{2}, 0), z_1 = d(-\frac{1}{2}, -\frac{\sqrt{3}}{2}, 0)$, where $d \in (r, \frac{2}{\sqrt{3}}r)$. Then T_1, the triangle with vertices x_1, y_1 and z_1, is an equilateral triangle with side-length $d\sqrt{3} \in (r\sqrt{3}, 2r)$, see Figure A.6, left. We observe $\mathbf{0} \in T_1$ and $\mathbf{0} \notin X$, but ρ cannot be defined there, because there is not a unique nearest point to $\mathbf{0}$ in ∂X – which is the sphere of radius r and centre $\mathbf{0}$. Thus $\rho|T_1 : T_1 \to X$ is not well-defined.

(ii): Consider the equilateral triangle T_2 with vertices $x_2 = -\frac{3}{2}d(1,0,0), y_2 = y_1, z_2 = z_1$, see Figure A.6, middle. These vertices are all contained in X. Then T_2 is also an equilateral triangle with side-length $d\sqrt{3} \in (r\sqrt{3}, 2r)$, and its circumcircle C_2 has centre $(-d, 0, 0)$ and radius d. We note that $\mathbf{0} \notin T_2$, so $\rho|T_2$ is well-defined, with $\rho(T_2) \subset X$; indeed, it is easy to see that $\rho(T_2) = T_2 \setminus \{x \in \mathbb{R}^3 \mid \|x\| < r\}$.

We claim that T_2 is not contained in any closed ball of radius less than d. For suppose $T_2 \subset B$, where $B \subset \mathbb{R}^3$ is a closed ball of radius $e \in (d\frac{\sqrt{3}}{2}, d)$. Let L_1, L_2, L_3 be the sides of T_2 opposite x_2, y_2, z_2, respectively. Observe that $T \cup \bigcup_{i=1}^{3} S(L_i, d) = D$, the plane disc with boundary C_2. By Lemma A.31 $S(L_i, d) \subset S(L_i, e) \subset B$; so $D \subset B$. But this is impossible, since D has diameter $2d$, while B has diameter $2e < 2d$. So no such B exists, proving the claim.

It follows that $P_r(T_2)$ is empty; so $\rho(T_2) \not\subset P_r(T_2)$.

(iii): Let x_3, z_3 be the end-points of a closed minor arc A of a circle C of radius r centered at $\mathbf{0}$; and let y_3 lie in the interior of A, see Figure A.6, right. Since $C \subset \partial X$, $x_3, y_3, z_3 \in \partial X \subset X$. Let T_3 be the triangle with vertices x_3, y_3, z_3; it is a genuine triangle, since x_3, y_3, z_3 are not collinear. Notice that $T_3 \setminus \{x_3, y_3, z_3\} \not\subseteq X$. Since its vertices lie in a minor arc of C, T_3 does not contain the centre of C, which is $\mathbf{0}$; so $\rho|T_3$ is well-defined. Since ρ is given by radial projection to ∂X away from $\mathbf{0}$ on $\mathbb{R}^n \setminus (X \cup \{\mathbf{0}\})$, we have $\rho(T_3) = A$. Certainly, then, T_3 is not homeomorphic to $\rho(T_3)$.

It is also possible to give examples with the triangle vertices in $X \setminus \partial X$. Let a, b be the midpoints of the sides of T_3 opposite x_3, y_3, respectively. Then $\|a\|, \|b\| < r$. Let

$$\epsilon = \frac{1}{2}\min\{\frac{r}{\|a\|} - 1, \frac{r}{\|b\|} - 1\},$$

let $x_3' = (1+\epsilon)x_3, y_3' = (1+\epsilon)y_3, z_3' = (1+\epsilon)z_3$, and let T_3' be the triangle with vertices x_3', y_3', z_3'. Then $\rho|T_3'$ is well-defined, and $\rho(T_3') = T_3' \setminus \{x \in \mathbb{R}^3 \mid \|x\| < r\}$, which is the union of the arc A with three disjoint sets D_1, D_2, D_3 each homeomorphic to a closed disc; so $\rho(T_3')$ is not homeomorphic to T_3'.

It turns out that (i) and (ii) are correct if it is also assumed that the three points $x, y, z \in X$ lie in a closed ball of radius strictly less than r, as in Proposition A.38, but we will not prove this here, since the map σ of Proposition A.38 will suffice for our purposes.

However, even with this extra condition, (iii) does not hold in general, as the examples T_3 and T_3' show – since the vertices involved there can be chosen arbitrarily close together.

A.3 Smoothing r-regular sets

We will show that, given any $r' < r$, any r-regular set in $\mathbb{R}^n$ can be arbitrarily closely approximated by r'-regular sets with smooth boundary. The arguments will make use of convolution. We recall some definitions (see e.g. [5]). Let $\varphi : \mathbb{R}^n \to \mathbb{R}$ be continuous, with compact support. The *support radius* of φ is $\sigma := \inf\{s \mid \operatorname{supp}\varphi \subset B(s, 0)\}$.

Let $V \subset \mathbb{R}^n$ be open, and let $g : V \to \mathbb{R}^m$ be a continuous map. The *convolution* of g by φ is the map

$$\varphi * g : V_\sigma \to \mathbb{R}^m$$

given by

$$\varphi * g(x) = \int_{B_\sigma(0)} \varphi(y)g(x-y)dy$$

for $x \in V_\sigma$; here $V_\sigma = \{x \in V \mid B_\sigma(x) \subset V\}$. For fixed $x \in V_\sigma$ we can make the change of variables $z = x - y$, giving the useful alternative formulation

$$\varphi * g(x) = \int_{B_\sigma(x)} \varphi(x-z)g(z)dz.$$

Definition A.41. A *mollifier* is a smooth map $\varphi : \mathbb{R}^n \to [0, \infty)$ with compact support such that $\int_{\mathbb{R}^n} \varphi(y)dy = 1$.

Remark A.42. It is well-known that mollifiers exist: for example, let $\psi : \mathbb{R}^n \to [0, \infty)$ be given by

$$\psi(x) = \begin{cases} \exp(\frac{1}{\|x\|^2 - 1}) & \text{if } \|x\| < 1, \\ 0 & \text{otherwise;} \end{cases}$$

then $\psi : \mathbb{R}^n \to [0, \infty)$ given by $\psi(x) = \psi(x)/\int_{\mathbb{R}^n} \psi(y)dy$ for $x \in \mathbb{R}^n$ is a mollifier with support radius 1, and $\psi_\epsilon : \mathbb{R}^n \to [0, \infty)$ given by $\psi_\epsilon(x) = \frac{1}{\epsilon^n}\psi(\frac{x}{\epsilon})$ for $x \in \mathbb{R}^n$ is a mollifier with support radius ϵ, for any $\epsilon > 0$.

Convolution with mollifiers leads to smooth approximations:

Theorem A.43. *Let $V \subset \mathbb{R}^n$ be open, and let $g : V \to \mathbb{R}^m$ be a continuous map, φ a mollifier with support radius σ. Then:*

(i) *$\varphi * g$ is smooth, and $D^k(\varphi * g) = (D^k\varphi) * g$ for $k \in \mathbb{N}$;*

(ii) *If g is C^k, then $D^k(\varphi * g) = \varphi * (D^k g)$;*

(iii) *If g satisfies a Lipschitz condition with constant κ, then so does $\varphi * g$.*

(iv) *If g satisfies a Lipschitz condition with constant κ, then*

$$\|\varphi * g(x) - g(x)\| < \kappa\sigma \text{ for all } x \in U_\sigma.$$

Proof.

(i): See [5], (2.3) (i).

(ii): See [5], (2.3) (ii).

(iii): Let x, $x' \in V_\sigma$. Then

$$\begin{aligned} \|\varphi * g(x) - \varphi * g(x')\| &= \left\| \int_{B_\sigma(0)} \varphi(y)(g(x-y) - g(x'-y))dy \right\| \\ &\leq \int_{B_\sigma(0)} \varphi(y)\|g(x-y) - g(x'-y)\|dy \\ &\leq \int_{B_\sigma(0)} \varphi(y)\kappa\|x - x'\|dy \\ &= \kappa\|x - x'\|. \end{aligned}$$

(iv): Let $x \in V_\sigma$. Then

$$\begin{aligned}\|\varphi * g(x) - g(x)| &= \left\| \int_{B_\sigma(x)} \varphi(x-z)(g(z)-g(x))dz \right\| \\ &\leq \int_{B_\sigma(x)} \varphi(x-z)\|g(z)-g(x)\|dz \\ &\leq \int_{B_\sigma(x)} \varphi(x-z)\kappa\|z-x\|dz \\ &< \int_{B_\sigma(x)} \varphi(x-z)\kappa\sigma dz \\ &= \kappa\sigma.\end{aligned}$$

□

Now let $X \subset \mathbb{R}^n$ be an r-regular set, and let U_s for $0 < s < r$, $\pi : U_r \to \partial X$, $N : \partial X \to \mathbb{R}^n$, and $f : U_r \to \mathbb{R}$ be as defined in Definition A.9 and Theorem A.13.

Lemma A.44.
(i) *f satisfies a Lipschitz condition with constant* 1*, i.e.*

$$|f(x) - f(y)| \leq \|x-y\| \text{forall} x, y \in U_r,$$

(ii) $\operatorname{grad} f|U_s$ *satisfies a Lipschitz condition with constant* $\frac{1}{r-s}$*, i.e.*

$$\|\operatorname{grad} f(x) - \operatorname{grad} f(y)\| \leq \tfrac{1}{r-s}\|x-y\| \text{forall} x, y \in U_s.$$

Proof. Let us prove the claims separately.

(i): Without loss of generality we can suppose $f(x) \geq f(y)$. We then have

$$|f(x) - f(y)| = f(x) - f(y) = \delta_{X_{f(y)}}(x); \leq \|x-y\|$$

since $y \in X_{f(y)}$, where $X_{f(y)}$ is the set introduced in Corollary A.24.

(ii): By Theorem A.13, (iii), $\operatorname{grad} f|U_s = N \circ \pi|U_s$. By Theorem A.13, (i) and (ii), N and $\pi|U_s$ satisfy Lipschitz conditions with constants $\frac{1}{r}$, $\frac{r}{r-s}$, respectively. It follows that $\operatorname{grad} f|U_s$ satisfies a Lipschitz condition with constant the product of these, $\frac{1}{r} \cdot \frac{r}{r-s} = \frac{1}{r-s}$, as claimed. □

Proposition A.45. *Let $\varphi : \mathbb{R}^n \to [0, \infty)$ be a mollifier with support radius σ, and suppose $\sigma < s < r$.*

(i) $|\varphi * f(x) - f(x)| < \sigma$ *for all* $x \in U_{r-\sigma}$,
(ii) $\|\operatorname{grad}(\varphi * f)(x) - \operatorname{grad} f(x)\| < \frac{\sigma}{r-s}$ *for all* $x \in U_{s-\sigma}$,

Proof. We prove the claims separately.

(i): This follows at once from Theorem A.43, (iv) and Lemma A.44, (i).

(ii): It follows from Theorem A.43, (ii) that $\operatorname{grad}(\varphi * f) = \varphi * \operatorname{grad} f$, so the result follows from Theorem A.43, (iv) and Lemma A.44, (ii). □

Lemma A.46. *Suppose $s < r - \sigma$; and define $M : U_s \to \mathbb{R}^n$ by*

$$M(x) = \frac{\operatorname{grad}(\varphi * f)(x)}{\|\operatorname{grad}(\varphi * f)(x)\|}.$$

Then

$$\|M(x) - M(y)\| \leq \tfrac{1}{r-s-\sigma}\|x - y\| \text{ forall} x,\, y \in U_s.$$

Proof. Let x, $y \in U_s$. Write $a = \|\operatorname{grad}(\varphi * f)(x)\|$, $b = \|\operatorname{grad}(\varphi * f)(y)\|$ and $c = \|\operatorname{grad}(\varphi * f)(x) - \operatorname{grad}(\varphi * f)(y)\|$. Let θ be the angle between $\operatorname{grad}(\varphi * f)(x)$ and $\operatorname{grad}(\varphi * f)(y)$. By the cosine rule, $c^2 = a^2 + b^2 - 2ab\cos\theta$; so

$$\cos\theta = \frac{a^2 + b^2 - c^2}{2ab}.$$

Since θ is also the angle between the unit vectors $M(x)$ and $M(y)$, we have

$$\|M(x) - M(y)\|^2 = 2 - 2\cos\theta = 2 - 2\left(\frac{a^2 + b^2 - c^2}{2ab}\right) = \frac{c^2 - (a-b)^2}{ab} \leq \frac{c^2}{ab}.$$

Now $\|\operatorname{grad} f(x)\| = \|\operatorname{grad} f(y)\| = 1$, so by Proposition A.45, (ii) a, $b \geq 1 - \frac{\sigma}{r-s}$, whence, applying also Lemma A.44, (ii) and Theorem A.43, (iii),

$$\begin{aligned}\|M(x) - M(y)\| &\leq \frac{1}{1 - \frac{\sigma}{r-s}}c = \frac{1}{1 - \frac{\sigma}{r-s}}\|\operatorname{grad}(\varphi * f)(x) - \operatorname{grad}(\varphi * f)(y)\|;\\ &\leq \frac{1}{1 - \frac{\sigma}{r-s}}\frac{1}{r-s}\|x - y\| = \frac{1}{r-s-\sigma}\|x - y\|.\end{aligned}$$

□

Theorem A.47. *Let $X \subset \mathbb{R}^n$ be an r-regular set. Let $\epsilon \subset (0, \frac{r}{4})$. Then there exists an $(r-\epsilon)$-regular set $\tilde{X}$ with C^∞ boundary and a C^1 isotopy Ψ_s, $s \in [0,1]$ of $\mathbb{R}^n$ to itself such that Ψ_0 is the identity, $\Psi_1(\tilde{X}) = X$ and such that $\|\Psi_s(x) - x\| < \frac{\epsilon}{2}$ for all $x \in \mathbb{R}^n$ and $s \in [0,1]$.*

Proof. Let U_s for $0 < s < r$, $\pi : U_r \to \partial X$, $N : \partial X \to \mathbb{R}^n$, and $f : U_r \to \mathbb{R}$ be as defined in Definition A.9 and Theorem A.13.

Let $\varphi : \mathbb{R}^n \to [0, \infty)$ be a mollifier with support radius $\sigma \leq \frac{\epsilon}{2}$. Write g for the smooth function $\varphi * f : U_{r-\sigma} \to \mathbb{R}$, and let $Z = g^{-1}(0)$. It follows from Proposition A.45, (i) with $s = r - \sigma$ that $Z \subset U_\sigma$, and from Proposition A.45, (ii) that $\operatorname{grad} g$ is non-zero on U_σ, so on Z. Thus 0 is a regular value for g; so Z is a smooth $(n-1)$-submanifold of U_σ. Note that Z separates $f^{-1}([-\sigma, \sigma])$, since $g(x) > 0$ if $f(x) \geq \sigma$ and $g(x) < 0$ if $f(x) \leq -\sigma$. Thus Z is the boundary $\partial\tilde{X}$ of the closed set

$$\tilde{X} = (g^{-1}(-\infty, 0] \cap f^{-1}([-\sigma, \sigma]) \cup X_{-\sigma}.$$

Note also that the unit normal vector field $\tilde{N} : \partial\tilde{X} \to \mathbb{R}^n$ on $\partial\tilde{X}$ pointing out of $\tilde{X}$ is the restriction to Z of the map M defined in Lemma A.46; thus, since $\partial\tilde{X} = Z \subset U_\sigma$, $\tilde{N}$ satisfies the Lipschitz condition

$$\|\tilde{N}(z) - \tilde{N}(z')\| \leq \frac{1}{r - 2\sigma}\|z - z'\| \text{for} z, z' \in \partial\tilde{X}.$$

Since $\sigma \leq \frac{\epsilon}{2}$, it follows from Theorem A.2, (iv) $\implies$ (i), that $\tilde{X}$ is $(r - \epsilon)$-regular.

Let $\tilde{r} = r - \epsilon$, and, as in Definition A.9 let $\tilde{U}_s = \{x \in \mathbb{R}^n \mid \delta_{\partial\tilde{X}} < s\}$ for $0 < s \leq \tilde{r}$, and define $\tilde{\pi} : U_{\tilde{r}} \to \partial\tilde{X}$ so that, for any $x \in \tilde{U}_{\tilde{r}}$, $\tilde{\pi}(x)$ is the unique nearest point in $\partial\tilde{X}$ to x. As in Theorem A.13, (ii), $\tilde{\pi}$ is continuous. As in Theorem A.13, (iii), define $\tilde{f} : \tilde{U}_{\tilde{r}} \to (-\tilde{r}, \tilde{r})$ so that $\tilde{f}(x) = (x - \tilde{\pi}(x)) \cdot \tilde{N}(\tilde{\pi}(x))$ for all $x \in \tilde{U}_{\tilde{r}}$; as there, $\tilde{f}$ is also continuous.

Define $\Phi : \partial\tilde{X} \times (-\tilde{r}, \tilde{r}) \to \tilde{U}_{\tilde{r}}$ by

$$\Phi(z, s) = z + s\tilde{N}(z) \text{forall}(z, s) \in \partial\tilde{X} \times (-\tilde{r}, \tilde{r}).$$

Since $\tilde{N}$ is smooth, so in Φ. We claim that Φ is a smooth diffeomorphism.

To see this, note first that Φ is a homemorphism, since its inverse is the continuous map $(\tilde{\pi}, \tilde{f}) : \tilde{U}_{\tilde{r}} \to \partial\tilde{X} \times (-\tilde{r}, \tilde{r})$. Thus, by the inverse function theorem, to see that Φ is a diffeomorphism it suffices to show that $D\Phi$ is nowhere singular, that is, we must show, for any $(z_0, t_0) \in Z \times (-\tilde{r}, \tilde{r})$ and $(u, v) \in T(Z \times (-\tilde{r}, \tilde{r})_{(z_0,t_0)} = TZ_{z_0} \times \mathbb{R}$, that

$$D\Phi_{(z_0,t_0)}(u, v) = 0 \text{implies}(u, v) = (0, 0).$$

Differentiating gives

$$D\Phi_{(z_0,t_0)}(u, v) = u + v\tilde{N}(z_0) + t_0 D\tilde{N}_{(z_0)}(u).$$

Since$\|\tilde{N}(z)\| = 1$ for all $z \in Z$, $D\tilde{N}_{z_0}(v)$ is orthogonal to $\tilde{N}(z_0)$, so, since also $u \in TZ_{z_0}$ is orthogonal to $\tilde{N}(z_0)$, $D\Phi_{(z_0,t_0)}(u, v) = 0$ implies $v\tilde{N}(z_0) = 0$ and $u + t_0 D\tilde{N}_{z_0}(u) = 0$. The first of these conditions implies $v = 0$. As to the second, we note that, since $\tilde{N}$ satisfies a Lipschitz condition with constant $\frac{1}{\tilde{r}}$, we have$\|D\tilde{N}_{z_0}\| \leq \frac{1}{\tilde{r}}$, and thus

$$\begin{aligned}\|u + t_0 D\tilde{N}_{z_0}(u)\| &\geq \|u\| - \|t_0 D\tilde{N}_{z_0}(u)\| \\ &\geq \|u\| - |t_0|\|D\tilde{N}\|\|u\| \\ &\geq \left(1 - \frac{|t_0|}{\tilde{r}}\right)\|u\|.\end{aligned}$$

Since $|t_0| < \tilde{r}$, it follows that the second condition implies $u = 0$.

Thus Φ is indeed a diffeomorphism. In particular, its inverse is smooth, so $\tilde{\pi}$ is smooth. It follows that $\tilde{\pi}|\partial X : \partial X \to Z$ is C^1. We claim that it is a C^1-diffeomorphism.

We begin by showing it is bijective:

Surjectivity: We have seen that Z separates $U_{\frac{\epsilon}{2}}$, so that for any $y \in U_{\frac{\epsilon}{2}}$ the line-segment $\{\pi(y)+sN(\pi(y))|s \in (-\frac{\epsilon}{2}, \frac{\epsilon}{2})\}$ meets Z, at z, say. Since this line segment also meets y, $\delta_Z(y) < \epsilon$. Thus if $\delta_Z(y') \geq \epsilon$ then $y' \notin U_{\frac{\epsilon}{2}}$. It follows that ∂X is contained in and separates $\tilde{U}_\epsilon$. Thus for any $z \in Z$, the line-segment $\{z + s\tilde{N}(z) \mid s \in (-\epsilon, \epsilon)\}$ meets ∂X, at x, say. Thus $z = \tilde{\pi}(x)$; and we have shown that $\tilde{\pi}|\partial X : \partial X \to Z$ is surjective.

Injectivity: Suppose that it is not injective, so there exist y_1, $y_2 \in \partial X$ and $z \in Z$ with $y_1 \neq y_2$ such that $\tilde{\pi}(y_1) = \tilde{\pi}(y_2) = z$. Since Z separates $U_{\frac{\epsilon}{2}}$, any point in ∂X has distance less that $\frac{\epsilon}{2}$ from Z, and thus y_1, $y_2 \in \tilde{U}_{\frac{\epsilon}{2}}$. Thus y_1, y_2 lie on the line-segment $\{z + s\tilde{N}(z) \mid \|s\| < \frac{\epsilon}{2}\}$, so $\|y_1 - y_2\| \leq \epsilon$. The r-spindle with end-points y_1, y_2 thus has spindle angle α with $\sin\alpha \leq \frac{\epsilon}{2r}$; by A.37, the angle between the line L joining y_1 and y_2 and the tangent spaces to ∂X at y_1 and y_2 is at most α. Of course L is parallel to $\tilde{N}(z)$. We calculate, for $i = 1, 2$,

$$\begin{aligned}
\|\tilde{N}(z) - N(y_i)\| &= \left\| \frac{\operatorname{grad} g(z)}{\|\operatorname{grad} g(z)\|} - \operatorname{grad} f(y_i) \right\| \\
&\leq \| \frac{\operatorname{grad} g(z)}{\|\operatorname{grad} g(z)\|} - \operatorname{grad} g(z))\| + \|\operatorname{grad} g(z) - \operatorname{grad} f(y_i)\| \\
&= |\|\operatorname{grad} g(z)\| - 1| + \|\operatorname{grad} g(z) - \operatorname{grad} f(y_i)\| \\
&= |\|\operatorname{grad} g(z)\| - \|\operatorname{grad} f(z)\|| + \|\operatorname{grad} g(z) - \operatorname{grad} f(y_i)\| \\
&\leq 2\|\operatorname{grad} g(z) - \operatorname{grad} f(z)\| + \|\operatorname{grad} f(z) - \operatorname{grad} f(y_i)\|; \\
&\leq \frac{2\epsilon}{r - \epsilon},
\end{aligned}$$

by Proposition A.45, (ii) and Lemma A.44, (ii), since $z \in U_\sigma$ and $\sigma < \frac{\epsilon}{2}$. If β is the angle between $\tilde{N}(z)$ and $T(\partial X)_{y_i}$, then $\frac{\pi}{2} - \beta$ is the angle between $\tilde{N}(z)$ and $N(y_i)$, and the cosine rule gives

$$\sin\beta = \cos\left(\frac{\pi}{2} - \beta\right) = 1 - \frac{1}{2}\|\tilde{N}(z) - N(y_i)\|^2; \geq 1 - \frac{1}{2}\left(\frac{2\epsilon}{r - \epsilon}\right)^2.$$

But $\beta \leq \alpha$, so $\sin\beta \leq \sin\alpha$, whence

$$1 - \frac{1}{2}\left(\frac{2\epsilon}{r - \epsilon}\right)^2 \leq \frac{\epsilon}{2r}.$$

Write $\epsilon = ar$; then the inequality above becomes

$$1 - \frac{2a^2}{(1 - a)^2} \leq \frac{a}{2}.$$

An easy calculation shows this inequality does not hold for $a \in (0, 0.388)$, so does not hold under our hypothesis $\epsilon \in (0, \frac{r}{4})$. This contradiction shows that $\tilde{\pi}|\partial X : \partial X \to Z$ is injective.

Thus $\tilde{\pi}|\partial X : \partial X \to Z$ is bijective.

We remark that a similar calculation to that in the surjectivity argument above the above shows that $\tilde{N}(\pi(y))$ cannot be parallel $T(\partial X)_y$ for any $y \in \partial X$.

Consider $\tilde{\pi} \circ \Phi| : \Phi^{-1}\partial X \to Z$. Since $\tilde{\pi}|\partial X : \partial X \to Z$ is bijective, as is Φ, $\tilde{\pi} \circ \Phi| : \Phi^{-1}\partial X \to Z$ is bijective. Since, for any $z \in Z$, Φ^{-1} maps the line $\{z + sN(z) \mid s \in (-\tilde{r}, \tilde{r})\}$ to the line $z \times (-\tilde{r}, \tilde{r})$, it follows from the remark above that the lines $z \times (-\tilde{r}, \tilde{r})$ are nowhere tangent to $\Phi^{-1}\partial X$. Thus the projection $p : Z \times (-\tilde{r}, \tilde{r}) \to Z$ maps tangent spaces to $\Phi^{-1}\partial X$ isomorphically to tangent spaces to Z, and thus, since p is its own differential everywhere, it is an immersion when restricted to $\Phi^{-1}\partial X$. But $p = \tilde{\pi} \circ \Phi$, since $\Phi^{-1} = (\tilde{\pi}, \tilde{f})$. So $p| = \tilde{\pi} \circ \Phi| : \Phi^{-1}\partial X \to Z$ is a bijective C^1

immersion, so, via the inverse function theorem, is a C^1 diffeomorphism, whence, composing with Φ^{-1}, $\tilde{\pi}|\partial X : \partial X \to Z$ is a C^1 diffeomorphism.

The inverse to $p| : \Phi^{-1}\partial X \to Z$ is necessarily of form $z \mapsto (z, q(z))$ for $z \in Z$, where $q : Z \to (-\tilde{r}, \tilde{r})$ is a C^1 function; so $\psi = (\tilde{\pi}|\partial X)^{-1} : Z \to \partial X$ is given by $z \mapsto z + q(z)\tilde{N}(z)$ for $z \in Z$. We note that since $\partial X \subset \tilde{U}_{\frac{\epsilon}{2}}$, $q(z) \in (-\frac{\epsilon}{2}, \frac{\epsilon}{2})$ for all $z \in Z$.

Consider now real numbers $a > 0$ and b, and the function $\eta : \mathbb{R} \to \mathbb{R}$ given by

$$\eta_{a,b}(t) = \begin{cases} b\exp(1 + \frac{a^2}{t^2 - a^2}) & \text{if} |t| < a, \\ 0 & \text{otherwise;} \end{cases}$$

$\eta_{a,b}$ is a smooth function. Calculation of its first two derivatives shows that $|\eta_{a,b}|$ has maximum $|b|$, attained when $t = 0$, and that $|\eta'_{a,b}|$ has, to seven significant figures, maximum $2.170357\frac{|b|}{a}$ attained when $t^2 = \sqrt{3}a^2$. Let $\chi_{a,b} : \mathbb{R} \to \mathbb{R}$ be given by $\chi_{a,b}(t) = t + \eta_{a,b}(t)$ for $t \in \mathbb{R}$. It is clear that $\chi_{a,b}$ is smooth, and varies smoothly with a and b. If the maximum value of $|\eta'_{a,b}|$ is strictly less than 1 then $\chi'(t) > 0$ for all t; it follows that χ is a smooth diffeomorphism such that $\chi_{a,b}(t) = t$ for $|t| \geq a$, $|\chi_{a,b}(t) - t| \leq |b|$ for all $t \in \mathbb{R}$, and $\chi_{a,b}(0) = b$.

Define now $X_s : Z \times (-\tilde{r}, \tilde{r}) - Z \times (-\tilde{r}, \tilde{r})$ by

$$X_s(z, t, s) = \left(z, \chi_{\frac{\tilde{r}}{2}, sq(z)}(t)\right)$$

for $(z, t) \in Z \times (-\tilde{r}, \tilde{r})$ and $s \in [0, 1]$. Since $|sq(z)| \leq \frac{\epsilon}{2}$ for all $z \in Z$ and $s \in [0, 1]$, we have

$$\frac{|sq(z)|}{\tilde{r}/2} \leq \frac{\epsilon}{\tilde{r}} = \frac{\epsilon}{r - \epsilon}; \leq \frac{1}{3}$$

by our hypothesis $\epsilon \in (0, \frac{r}{4})$; so $\chi_{\frac{\tilde{r}}{2}, sq(z)}$ is a smooth diffeomorphism for all $z \in Z$ and $s \in [0, 1]$. It follows that, for $s \in [0, 1]$, X_s is a C^1 isotopy of $Z \times (-\tilde{r}, \tilde{r})$ such that $X_s(z, t) = (z, t)$ for $|t| \geq \frac{\tilde{r}}{2}$ and $\|X(z, t) - (z, t)\| \leq \frac{\epsilon}{2}$ for all $(z, t) \in Z \times (-\tilde{r}, \tilde{r})$, and such that X_0 is the identity and X_1 maps $Z \times \{0\}$ to $\Phi^{-1}\partial X$. It now follows that, for $s \in [0, 1]$, $\Psi_s = \Phi \circ X_s \circ \Phi^{-1} : \tilde{U}_{\tilde{r}} \to \tilde{U}_{\tilde{r}}$ is a C^1 isotopy such that Ψ_s is the identity on $\tilde{U}_{\tilde{r}} \setminus \tilde{U}_{\frac{\tilde{r}}{2}}$, $\|\Psi(x) - x\| \leq \frac{\epsilon}{2}$ for all $x \in \tilde{U}_{\tilde{r}}$, and such that Ψ_0 is the identity and Ψ_1 maps $Z = \partial\tilde{X}$ to ∂X. Extending by the identity on $\mathbb{R}^n \setminus \tilde{U}_{\tilde{r}}$ gives the isotopy claimed, completing the proof. □

A.4 Schur's Theorem and applications

Theorem A.48 (Schur's Theorem). *Let α be a closed C^2 arc in $\mathbb{R}^n$, $\overline{\alpha}$ a closed C^2 arc in $\mathbb{R}^2$, both of length L; we suppose the arcs both parametrized by arc length $s \in [0, L]$. Suppose also that the curvature $\overline{\kappa}$ of $\overline{\alpha}$ is everywhere positive, and that $\overline{\alpha}$ and the line segment ℓ joining its end-points together form the boundary of a convex set. Suppose further that the curvature κ of α satisfies $\kappa(s) \leq \overline{\kappa}(s)$ for all $s \in [0, L]$.*

Then

$$\|\alpha(L) - \alpha(0)\| \geq \|\overline{\alpha}(L) - \overline{\alpha}(0)\|.$$

Moreover, if $\|\alpha(L) - \alpha(0)\| = \|\overline{\alpha}(L) - \overline{\alpha}(0)\|$, then $\kappa = \overline{\kappa}$ and there exists a regular motion M of $\mathbb{R}^n$ such that $M \circ \alpha(s) = \overline{\alpha}(s) \times 0 \subset \mathbb{R}^2 \times \mathbb{R}^{n-2} \equiv \mathbb{R}^n$.

Proof. See [1], pp. 36-7. □

Addendum A.49. *Under the hypotheses of the theorem α is a simple arc.*

Proof. It is clear from the hypotheses of Theorem A.48 that $\overline{\alpha}$ is simple.

Let $x, y \in \alpha$ be distinct points, and let $\overline{x}, \overline{y} \in \overline{\alpha}$ be the corresponding points in $\overline{\alpha}$ with respect to the joint arc-length parameter; $\overline{x}, \overline{y}$ are clearly distinct. Let $\beta \subset \alpha$ be the arc with end-points x, y, $\overline{\beta} \subset \overline{\alpha}$ the arc with end-points $\overline{x}$, $\overline{y}$. Applying the result of Theorem A.48 to β and $\overline{\beta}$ gives $\|x - y\| \geq \|\overline{x} - \overline{y}\|$. Thus, since $\overline{x}$ and $\overline{y}$ are distinct, so are x and y. □

Corollary A.50 (Schwarz' Theorem). *Let α be a closed C^2 arc in $\mathbb{R}^n$ with curvature everywhere $\leq \frac{1}{r}$, and suppose that the distance between its end-points x, y is $\leq 2r$. Write L_α for the length of α. Let C be a circle of radius r containing x and y; let A_0, A_1 be the two arcs of C with end-points x and y. Write L_0 and L_1 for the lengths of A_0 and A_1, respectively; we may suppose $L_1 \geq L_2$. Then either $L_\alpha \geq L_1$ or else $L_\alpha \leq L_2$.*

Proof. See [1], p. 38. □

We relate these results with spindles:

Proposition A.51. *Let α be a closed C^2 arc in $\mathbb{R}^n$ of length L_α, with curvature everywhere $\leq \frac{1}{r}$. Suppose that the distance between its end-points x, y is $\leq 2r$. Then α is contained in the r-spindle with end-points x, y if, and only if, $L_\alpha \leq r\pi$.*

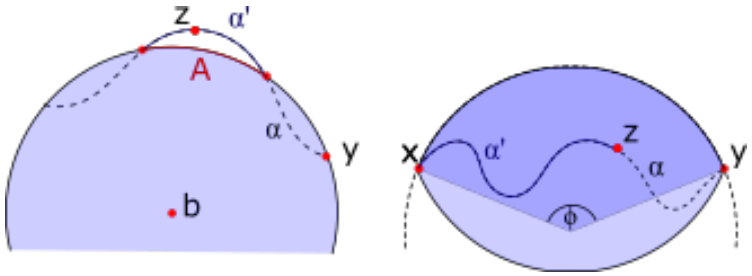

Figure A.7: We name the curve segments, points and angles as in this figure.

Proof. We show the two directions.

'If': We suppose $L_\alpha \leq r\pi$. Let B be any closed ball of radius r with x and y contained in its boundary ∂B. It follows from the definition of r-spindles (Definition A.30) that it is enough to show that $\alpha \subset B$.

Suppose otherwise, so that there is a point $z \in \alpha$ with $z \notin B$, see Figure A.7. Let $\gamma : [0, 1] \to \mathbb{R}^n$ be a parametrization of α with $\gamma(0) = x$, $\gamma(1) = y$; then $z = \gamma(s_0)$ for some $s_0 \in [0, 1]$. Let

$$s_1 = \max\{\in [0, s_0] \mid \gamma(s) \in B\},\ s_2 = \min\{s \in [s_0, 1] \mid \gamma(s) \in B\}.$$

Since γ is continuous, B is closed, and $\gamma(s_0) \notin B$, we have $s_1 < s_0 < s_2$, and $\alpha' = \gamma([s_1, s_2])$ is a closed arc meeting B only at its end-points, which lie in ∂B. Let b be the centre of B. The radial projection $p : \mathbb{R}^n \setminus \{b\} \to \partial B$ has partial derivatives with absolute value less than 1 at any point outside B, so the length of $\pi(\alpha')$ is less than the length $L_{\alpha'}$ of α'. Since the shorter great circle arc A in ∂B joining the end-points of α' is the shortest path between these points, it has length L_A at most the length of $\pi(\alpha')$, so $L_A < L_{\alpha'}$. However, $L_{\alpha'} \leq L_\alpha; \leq r\pi$ by hypothesis; so by Corollary A.50 $L_{\alpha'} \leq L_A$. This contradiction shows that our supposition was false, completing the proof.

'Only if': We suppose that α is contained in the r-spindle S with end-points x, y. Let $\varphi \in (0, \pi]$ be the angle subtended at the centre of a circle C of radius r through x and y. We claim that $L_\alpha \leq r\varphi$ - which will of course complete the proof. We argue by contradiction. So suppose that $L_\alpha > r\varphi$. Let $z \in \alpha$ be such that the subarc α' of α between x and z has length $r\varphi$. Clearly $z \in S \setminus \{y\}$, so $\|z - x\| < \|y - x\|$ - because the sphere of radius $\|y - x\|$ centred at x meets S only at y. But, by Theorem A.48, $\|z - x\| \geq \|y - x\|$, since α' and the minor arc of C with end-points x, y have the same length, and C has curvature $\frac{1}{r}$. This contradiction shows our supposition to be false, concluding the proof. □

This result is relevant to the study of smooth r-regular sets in $\mathbb{R}^n$:

Lemma A.52. *Let $X \subset \mathbb{R}^n$ be r-regular with smooth boundary ∂X. Then any geodesic arc in ∂X has curvature everywhere $\leq \frac{1}{r}$.*

Proof. Since ∂X is smooth, so is the outward-pointing unit normal vector field $N : \partial X \to \mathbb{R}^n$.

Let $J \subset \mathbb{R}$ be an interval, $\gamma : J \to \partial X$ an arc-length-parametrized geodesic curve. Thus, for any $s \in J$, $\gamma''(s)$ is parallel to $N(\gamma(s))$ for all $s \in J$. Now for all $s \in J$, $\gamma'(s) \in T(\partial X)_{\gamma(s)}$, so $\gamma'(s) \cdot N(\gamma(s)) = 0$. Differentiating with respect to s gives

$$\gamma''(s) \cdot N(\gamma(s)) + \gamma'(s) \cdot (N \circ \gamma)'(s) = 0 \text{forall} s \in J.$$

Thus, since $\|\gamma'(s)\| = 1$ for all $s \in J$, the curvature $\kappa(s)$ of γ at s is given by

$$\kappa(s) = \|\gamma''(s)\| = \|\gamma''(s) \cdot N(\gamma(s))\| = \| - \gamma'(s) \cdot (N \circ \gamma)'(s)\| \leq \|(N \circ \gamma)'(s)\|.$$

Now $N : \partial X \to \mathbb{R}^n$ satisfies a Lipschitz condition with constant $\frac{1}{r}$, by Theorem A.2 (iv), so

$$\|N(\gamma(s + h)) - N(\gamma(s)\| \leq \frac{1}{r}\|\gamma(s + h) - \gamma(s)\| \text{forall} s, s + h \in J.$$

Dividing the inequality above by $|h|$ and letting $h \to \infty$ gives

$$\|(N \circ \gamma)'(s)\| \leq \frac{1}{r}\|\gamma'(s)\| = \frac{1}{r};$$

so $\kappa(s) \leq \frac{1}{r}$ for all $s \in J$, completing the proof. □

Remark A.53. In the case $n = 2$, ∂X is a disjoint union of smooth curves, which are therefore geodesic; it follows that these boundary curves have curvature everywhere $\leq \frac{1}{r}$.

Lemma A.54. *Let $X \subset \mathbb{R}^n$ be a smooth r-regular set, and let $x, y \in \partial X$ be such that $\|x - y\| < 2r$. Then there is a geodesic arc joining x and y.*

Proof. Let $\pi : U_r \to \partial X$ be as defined in Definition A.9. Each point on the line ℓ joining x and y has distance less than r from either x or y, so is contained in U_r. Since π is continuous, $\pi(\ell)$ is connected, so x and y lie in the same connected component of ∂X. So by the Hopf-Rinow theorem [6], there exists a shortest path joining x and y, which is a smooth geodesic. □

Definition A.55. A closed smooth arc $\alpha \subset \mathbb{R}^n$ has the *r-spindle property* if every closed sub-arc α' of α is contained in the r-spindle with end-points the end-points of α'.

Proposition A.56. *Let $\alpha \subset \mathbb{R}^n$ be a smooth closed arc with the r-spindle property, and let $\boldsymbol{t} : \alpha \to \mathbb{R}^n$ be a smooth unit tangent vector field for α. Then*

(i)
$$\|\boldsymbol{t}(z_1) - \boldsymbol{t}(z_2)\| \leq \|z_1 - z_2\| \text{forall} z_1, z_2 \in \alpha,$$

(ii) *the curvature of α is everywhere $\leq \frac{1}{r}$.*

Proof. We prove each claim separately.

Ad (i): Let z_1, $z_2 \in \alpha$, let β be the sub-arc of α with end-points z_1, z_2, and let S be the r-spindle with end-points z_1, z_2. Then $\beta \subset S$, and thus the angles between $\mathbf{t}(z_1), \mathbf{t}(z_2)$ and the line joining z_1 to z_2 are $\leq$ the spindle angle φ (Lemma A.37) of S. It follows that the angle θ between $\mathbf{t}(z_1)$ and $\mathbf{t}(z_2)$ is $\leq 2\varphi$.

Thus, using the cosine rule, a double-angle formula, and the spindle angle calculation of Lemma A.37,

$$\begin{aligned}\|\mathbf{t}(z_1) - \mathbf{t}(z_2)\|^2 &= 2 - 2\cos\theta \\ &\leq 2 - 2\cos(2\varphi) \\ &= 2 - 2(1 - 2(\sin\varphi)^2) = (2\sin\varphi)^2 \\ &= \left(\frac{1}{r}\|z_1 - z_2\|\right)^2,\end{aligned}$$

so

$$\|\mathbf{t}(z_1) - \mathbf{t}(z_2)\| \leq \frac{1}{r}\|z_1 - z_2\|,$$

as claimed.

Ad (ii): Let $\gamma : [0, L] \to \mathbb{R}^n$ be an arc-length parametrization of α such that $\gamma'(s) = \mathbf{t}(\gamma(s))$ for $s \in [0, L]$. Thus, by (i), for s, $s + h \in [0, L]$,

$$\|\gamma'(s + h) - \gamma'(s)\| \leq \frac{1}{r}\|\gamma(s + h) - \gamma(s)\|.$$

We suppose $h \neq 0$. Then dividing by $|h|$ and letting $h \to 0$ gives

$$\|\gamma''(s)\| \leq \frac{1}{r}\|\gamma'(s)\|; = \frac{1}{r}.$$

Since $\|\gamma''(s)\|$ is the curvature of α at $\gamma(s)$, this completes the proof. □

Corollary A.57. *A smooth arc $\alpha \subset \mathbb{R}^n$ has the r-spindle property if, and only if,*

(i) *the distance between the end-points of α is $\leq 2r$,*

(ii) *α has curvature $\leq \frac{1}{r}$ everywhere,*

(iii) *α has length $\leq r\pi$.*

Proof. This follows at once from Propositions A.51 and A.56 (ii). □

We conclude with two further consequences of the r-spindle property.

Proposition A.58. *Let $\alpha \subset \mathbb{R}^n$ be a smooth closed arc with the r-spindle property. Let ℓ be the line-segment joining the end-points of α, and let φ be the spindle angle of the r-spindle S generated by ℓ. Then the angle between ℓ and any tangent vector to α is at most φ.*

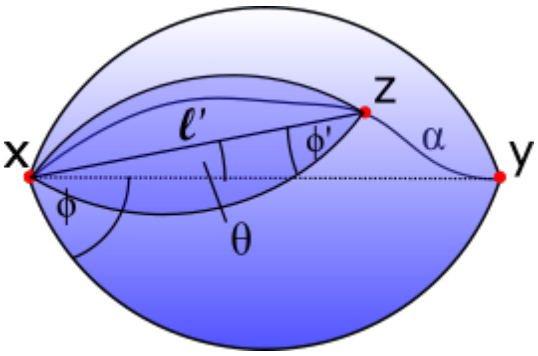

Figure A.8: We name the points, angles and curve as in this figure.

Proof. This is clear for the tangent vectors at the end-points x and y of α. Let z be any other point in α, let ℓ' be the line segment joining x and z, and let S' be the r-spindle with end-points x and z, see Figure A.8. Then $S' \subset S$, by A.31, (ii). The angle between a tangent vector $\mathbf{t}$ to α at z and ℓ' is at most the spindle angle φ' of S', and thus the angle between $\mathbf{t}$ and ℓ is at most φ' plus the angle θ between ℓ and ℓ'. But $\theta + \varphi'$ is also the maximum angle between ℓ and tangent vectors to S' at x; since $S' \subset S$, it follows that $\theta + \varphi' \leq \varphi$, completing the proof. □

Proposition A.59. *Let $\alpha \subset \mathbb{R}^n$ be a smooth closed arc with the r-spindle property. The α has reach r.*

Proof. Let $x \in \mathbb{R}^n$ be such that there exist distinct points z_1, $z_2 \in \alpha$ such that$\|x - z_1\| = \|x - z_2\| = \delta_\alpha(x)$. Write $d = \delta_\alpha(x)$. We claim that $d \geq r$. Suppose the contrary, that $d < r$. The ball B with centre x and radius d is such that z_1, $z_2 \in \partial B$. Since $d < r$, the r-spindle S with end-points z_1, z_2 exists, and is contained in B, by A.31, (ii). Indeed, $S \cap \partial B = \{z_1, z_2\}$. Now the sub-arc α' of α with end-points z_1, z_2 is contained S, so there are points of α' in the interior of B; so there exists $z_3 \in \alpha$ such that $\|x - z_3\| < d$. This contradicts the assumption $d = \delta_\alpha(x)$, so our supposition was false, and $d \geq r$. Thus if $x \in \mathbb{R}^n$ is such that $\delta_\alpha(x) < r$, then x has a unique nearest point in α, and α is of reach r. □

References

[1] S. S. Chern. Curves and surfaces in Euclidean space. In *Studies in Global Geometry and Analysis*, pages 16–56. Math. Assoc. Amer. (distributed by Prentice-Hall, Englewood Cliffs, N.J.), 1967.

[2] Pedro Duarte and Maria Joana Torres. Smoothness of boundaries of regular sets. *J. Math. Imaging Vis.*, 48(1):106–113, January 2014. ISSN 0924-9907. doi: 10.1007/s10851-012-0397-0. URL http://dx.doi.org/10.1007/s10851-012-0397-0.

[3] Pedro Duarte and Maria Joana Torres. r-regularity. *Journal of Mathematical Imaging and Vision*, 51(3):451–464, 2015. doi: 10.1007/s10851-014-0535-y. URL https://doi.org/10.1007/s10851-014-0535-y.

[4] Herbert Federer. Curvature measures. *Trans. Amer. Math. Soc.*, 93:418–491, 1959. ISSN 0002-9947. doi: 10.2307/1993504. URL https://doi.org/10.2307/1993504.

[5] M.W. Hirsch. *Differential Topology*. Graduate Texts in Mathematics. Springer New York, 1997. ISBN 9780387901480. URL https://books.google.dk/books?id=iSvnvOodWl8C.

[6] H. Hopf and W. Rinow. Ueber den Begriff der vollständigen differentialgeometrischen Fläche. *Comment. Math. Helv.*, 3(1):209–225, 1931. ISSN 0010-2571. doi: 10.1007/BF01601813. URL https://doi.org/10.1007/BF01601813.

[7] P. Stelldinger, L. J. Latecki, and M. Siqueira. Topological equivalence between a 3d object and the reconstruction of its digital image. *IEEE Transactions on Pattern Analysis and Machine Intelligence*, 29(1):126–140, Jan 2007. ISSN 0162-8828. doi: 10.1109/TPAMI.2007.250604.

Paper B

Reconstruction of r-regular Objects from Trinary Images

By Helene Svane and Andrew du Plessis

Abstract

We study digital images of r-regular objects where a pixel is black if it is completely inside the object, white if it is completely inside the complement of the object, and grey otherwise. We call such images *trinary*. We discuss possible configurations of pixels in trinary images of r-regular objects at certain resolutions and propose a method for reconstructing objects from such images. We show that the reconstructed object is close to the original object in Hausdorff norm, and that there is a homeomorphism of $\mathbb{R}^2$ taking the reconstructed set to the original.

B.1 Introduction

The purpose of this paper will be to introduce a way to reconstruct objects from their grey-scale digital images. More specifically, we focus on objects that are small compared to the image resolution and satisfy a certain regularity constraint called *r-regularity*. The notion of r-regularity was developed independently by Serra [5] and Pavlidis [4] to describe a class of objects for which reconstruction from digital images preserved certain topological features. They both consider *subset digitisation*, that is, digitisation formed by placing a grid on top of an object and then colouring an cell black if its midpoint is inside the object, and white if the cell midpoint is outside the complement of the object. This way a binary image is produced, and Pavidis and Serra consider the set of black cells as the reconstructed set. Serra showed that if the grid is hexagonal and the object satisfies certain constraints related to r-regularity, the original and reconstructed sets have the same homotopy, and Pavlidis showed that for a square grid and for certain r-regular sets, the set and its reconstruction are homeomorphic. Later on, Stelldinger and Köthe [7, 8] argued that the concepts of homotopy or homeomorphism were not strong enough to fully capture human perception of shape similarity. Instead they proposed two new similarity criterions called *weak* and *strong r-similarity*, and showed that under certain conditions, an

r-regular set and its subset digitisation by a square grid are both weakly and strongly r-similar. We, too, will consider the notion of weak r-similarity in this paper.

However, Serra, Pavlidis, Stelldinger and Köthe were modelling images using subset digitisation, which outputs a binary image. In contrast to this approach, Latecki et al. [3] modelled an image by requiring the intensity in each pixel to be a monotonic function of the fraction of the pixel covered by the object. This way they seek to model a pixel intensity as the light intensity measured by a sensor in the middle of the pixel, and the result is a grey-level image much like the ones obtained in real situations. They show that after applying any threshold to such an image of an r-regular object with certain constraints, the set of black pixels has the same homotopy type as the original object and, in the case where the original object is a manifold with boundary, the two are even homeomorphic. They also conjecture that all r-regular objects are manifolds with boundary. This was later proven by Duarte and Torres in [2].

We will model our images in the same way as Latecki et al. did, namely by requiring each pixel intensity to be a monotonic function of the fraction of the pixel covered by the object. In contrast to the above reconstruction approaches, we do not wish to use a set of pixels as our reconstructed set, but rather to construct a new set with smooth boundary that we may then use as the reconstruction. Also in contrast to the above, we will not consider binary images, but keep the information stored in the grey pixels in our endeavour to make a more precise reconstruction.

When working with reconstruction, one should decide which properties one wishes the reconstructed object to share with the original one. Should the reconstructed set have the same topological features as the original one? Should the reconstructed set be close to the original one? Should a digitisation of the reconstructed set yield the same image as the original set? Should the reconstructed set be r'-regular for some r' close to r? Though all of these comparison criteria may be justified and an ideal reconstruction should satisfy them all, it is hard to construct such a set. In this paper, we will therefore focus on constructing a set that is close to the original one in Hausdorff norm (which will be introduced in the following), has a smooth boundary, and is homeomorphic to the original set. This means that we show that our reconstructed set and the original are weakly r-similar in the sense of [8].

B.2 Basic definitions and theorems about r-regular sets

Let us start by establishing some terminology. Let $X \subset \mathbb{R}^2$ be a set. We will denote the closure of X by $\overline{X}$, the interior of X by $\mathrm{Int}(X)$ and the boundary of X by ∂X. The complement $\mathbb{R}^2 \setminus X$ will be denoted by X^C. The set X is compact if and only if X is closed and bounded.

The Euclidean distance between two points x and y in $\mathbb{R}^2$ will be denoted by $d(x, y)$ or, occasionally, by $\|x - y\|$.

For an $s > 0$, we let $B_s(x) = \{y \in \mathbb{R}^2 \mid d(x, y) < s\}$ be the open ball with centre x and radius s. For a line segment L we will denote the length of L by $|L|$.

A part of the goal will be to construct a set Γ from a digital image, such that the boundary of Γ is close to the boundary of the original set. The intuitive concept of closeness between two sets is captured by the Hausdorff distance: For $X, Y \subseteq \mathbb{R}^2$,

the Hausdorff distance d_H between X and Y is given by

$$d_H(X,Y) = \max\{\sup_{x\in X}\inf_{y\in Y} d(x,y), \sup_{y\in Y}\inf_{x\in X} d(x,y)\}.$$

The set of compact sets of $\mathbb{R}^2$ equipped with the Hausdorff metric is a complete metric space.

The digital images that we will be working with in this paper are formed in the following way:

Definition B.1. Let $X \subseteq \mathbb{R}^2$ be a set and $d\mathbb{Z}^2 \subseteq \mathbb{R}^2$ a grid with side length d. To each grid square C, we assign an *intensity* λ given by

$$\lambda = \varphi\left(\frac{\text{area}(X \cap C)}{d^2}\right) \in [0,1],$$

where $\varphi : [0,1] \to [0,1]$ is a function with $\varphi(0) = 0$, $\varphi(1) = 1$ and $\varphi((0,1)) \subseteq (0,1)$.

The *digitisation* of X is the matrix of intensities. We will visualise it as the collection of pixels of side length d, each coloured a shade of grey corresponding to the value of λ.

Let $V(X)$ denote *the black pixels* of this digitisation of X. We will sometimes refer to $V(X)$ as the black digitisation pixels of X.

To make sure that the objects in the images we are considering are not arbitrarily strange, we will follow in the footsteps of previous approaches and only consider r-regular sets:

Definition B.2. Let $r > 0$. A closed set $X \subseteq \mathbb{R}^n$ is said to be *r-regular* if for each $x \in \partial X$ there exists two r-balls $B_r(x_b) \subseteq X$ and $B_r(x_w) \subseteq X^C$ such that $\overline{B_r(x_b)} \cap \overline{B_r(x_w)} = \{x\}$, see Figure B.1.

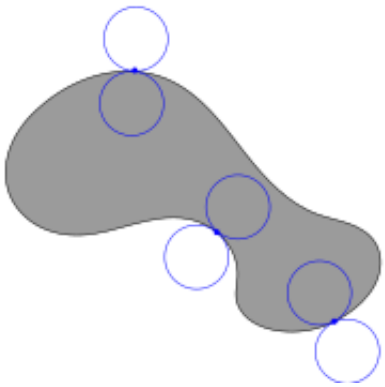

Figure B.1: An r-regular set X is a set where each boundary point belongs to both the boundary of an open r-ball contained in X and the boundary of an open r-ball contained in X^C

In general, we believe that a reconstruction from a digital image can be made more accurately by taking the intensities of the grey pixels into account, and we are currently working on this idea. However, in this paper we restrict ourselves to

looking at images where each pixel is considered to be either black, grey or white, without taking the exact intensities of the grey pixels into account. This leads to the notion of *trinary images*:

Definition B.3. A *trinary* digital image is a digital image where the intensities of all grey pixels are set to 0.5.

These trinary images will be our main interest in this paper. Note that the colour of a pixel (black, grey or white) does not depend on the monotonic function φ used for calculating the pixel intensities – in fact, a pixel in a trinary image of an object X is black if it is contained in X, white if it is contained in X^C and grey if ∂X passes through it.

When we make the digital image of an r-regular object by a lattice $d\mathbb{Z}^2$, we can in general not be certain that there are any black or white pixels in the image – for instance, if d is large compared to r, all pixels could contain an r-ball, which would mean that the image would be all grey. Since we cannot hope to make a very good reconstruction in this case, we will put a restriction on the relationship between the r and d:

Convention B.4. Throughout the following, we assume that X is a bounded r-regular set and that $d\sqrt{2} < r$. We also assume that ∂X does not pass through a pixel corner.

Note that the boundedness condition on X implies that X is compact.

Pavlidis [4] defines a grid $d\mathbb{Z}^2$ and a set X to be *compatible* if X is r-regular with $d\sqrt{2} < r$. With this restriction, since $d\sqrt{2}$ is the diameter of a pixel, each black r-ball contains the pixel that its centre belongs to, meaning that each black r-ball is centered in a black pixel. Similarly the centre of each white r-ball is contained in a white pixel. This means that for each component of X yields at least one black pixel, and each component of X^C yields at least one white pixel. Latecki et al. showed that for a compatible grid $d\mathbb{Z}^2$ and set X, the set $V(X)$ of black pixels is homeomorphic to X. Hence X and $V(X)$ have the same topological features. Furthermore, the above conditions ensure that we do not get too large grey areas, as will be clear in the following section. We will only concern ourselves with images that capture all of the objects photographed, and not just a part of them.

Let us introduce the notion of *weak r-similarity*, as introduced in [6, 8].

Definition B.5. Let $A, B \subseteq \mathbb{R}^2$ be bounded sets and $r > 0$. We call A and B weakly r-similar if there exists a homeomorphism $f : \mathbb{R}^2 \to \mathbb{R}^2$ such that $x \in A \iff f(x) \in B$ and the Hausdorff distance between the set boundaries satisfies $d_H(\partial A, \partial B) < r$.

The overall purpose of this paper will be to show the following:

Theorem B.6. *Let I be a digital image of an r-regular set X by a lattice $d\mathbb{Z}^2$ with $d\sqrt{2} < r$. We may construct an object Γ from I such that Γ and X are weakly d-similar, where d is the pixel side length.*

We believe that the above result may be strengthened to prove strong $d + \varepsilon$-similarity between the two for a suitable ε, but such a result is beyond the scope of this paper.

A large part of the proof of Theorem B.6 will be to prove the following:

Theorem B.7. *Let I be a digital image of an r-regular set by a lattice $d\mathbb{Z}^2$ with $d\sqrt{2} < r$. We may construct an object Γ from I such that $d_H(\partial\Gamma, \partial X) < d$, where d_H is the Hausdorff distance.*

To start working with r-regular sets, we first sum up some basic statements about them:

Proposition B.8 (Proposition A.5). *Let $A \subseteq \mathbb{R}^n$ be a closed set and $r > 0$. Then the following are equivalent:*

(i) *At any point $x \in \partial X$ there exist two closed r-balls $B_r \subseteq A$ and $B'_r \subseteq \overline{A^C}$ such that $B_r \cap B'_r = \{x\}$.*

(ii) *The sets A and $\overline{A^C}$ are equal to unions of closed r-balls.*

Definition B.9. For $\delta > 0$, we denote the δ-tubular neighbourhood of ∂X in $\mathbb{R}^2$ by $N_\delta = \{x \in \mathbb{R}^2 \mid d(x, \partial X) < \delta\}$.

Lemma B.10 (Duarte & Torres, [2], Lemma 5). *Let X be an r-regular set. For each $x \in N_r$ there is a unique point $\pi(x) \in \partial X$ satisfying $d(x, \partial X) = d(\pi(x), x)$. Hence there is a well-defined projection $\pi : N_r \to \partial X$.*

Theorem B.11 (Theorem A.13, (ii)). *The projection map $\pi : N_r \to \partial X$ is continuous.*

Another important fact that we will be using heavily is the following:

There is a retraction $\rho_{X^C} : N_r \to X^C \cup \partial X$ (that we will sometimes just denote by ρ) defined by

$$\rho_{X^C}(x) = \begin{cases} x & \text{if } x \in X^C \cup \partial X, \\ \pi(x) & \text{otherwise,} \end{cases}$$

and likewise a retraction $\rho_X : N_r \to X$ defined by

$$\rho_X(x) = \begin{cases} x & \text{if } x \in X, \\ \pi(x) & \text{otherwise.} \end{cases}$$

These retractions will prove to be crucial in later arguments, since they have some useful properties.

We now state some results about $\rho := \rho_{X^C}$. However, the similar results for ρ_X also hold.

Proposition B.12 (Stelldinger et al., [6]). *Let $x, y \in X^C$ with $d(x, y) < 2r$ and let $L \subseteq \mathbb{R}^n$ be the line segment between them. Then*

(i) *The line segment L is a subset of $X^C \cup N_r$, and $\rho|_L$ is injective,*

(ii) *For $s < r$ and B_s any s-ball containing x and y, $\rho(L)$ is a subset of B_s.*

Definition B.13. Let $L \subseteq \mathbb{R}^n$ be a closed line segment of length $|L| < 2r$. Then the r-spindle $S(L, r)$ around L is the intersection of all closed balls of radius r whose boundaries contain both endpoints of L. If x and y are the endpoints of L, we will sometimes write $S(x, y, r)$ in stead of $S(L, r)$.

Lemma B.14 (du Plessis and Tang Christensen, A.20 [1]). *Let L be a closed line segment in $\mathbb{R}^2$ of length $|L| < 2r$. Then the maximal distance from a point in the r-spindle $S(L,r)$ to L is $r - \sqrt{r^2 - \frac{L^2}{4}}$.*

Lemma B.15 (Lemma A.31,(ii)). *Let $L \subseteq \mathbb{R}^n$ be a closed line segment of length $|L| < 2r$. Then the r-spindle $S(L,r)$ is the intersection of all closed balls of radius at most r that contain L.*

Corollary B.16 (Corollary A.33). *Let $x, y \in X^C$ with $d(x,y) < 2r$ and let $L \subseteq \mathbb{R}^n$ be the line segment between them. Then $\rho(L)$ is a subset of the r-spindle $S(L,r)$.*

Remark B.17. Since the projection π satisfy $\pi = \rho_X \circ \rho_{X^C} = \rho_{X^C} \circ \rho_X$, the above corollary is also true for π. Hence, we will in the following repeatedly be using that whenever $x, y \in \partial X$ are two boundary points with $d(x,y) < 2r$ and L is the line between them, there is a path $\pi(L)$ in ∂X joining them such that $\pi(L) \subseteq S(L,r)$.

B.3 Impossible configurations at a resolution satisfying $d\sqrt{2} < r$

Before we start reconstructing the original r-regular object, we need some results on which configurations of 3×3 pixels of grey, black and white pixels can occur in the digital image of an r-regular object by a lattice $d\mathbb{Z}^2$ where $d\sqrt{2} < r$. We can put together all possible configurations of 3×3 pixels with a computer programme that takes the possible configurations of 2×2 pixels as input. All possible configurations of 2×2 pixels are shown in Figure B.2, up to rotation and interchanging of black and white. We have made a MatLab programme that combines these configurations in all possible ways. If we do this, we get (up to rotation, mirroring and switching of black and white pixels) the configurations in Figure B.3.

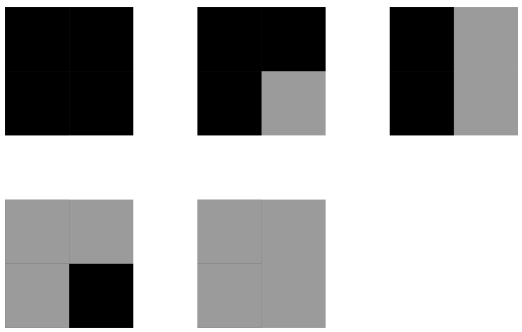

Figure B.2: The only possible configurations of 2×2 pixels, up to rotation and switching of black and white. Note that we have used Lemma B.24, part (ii), which is stated below.

Note that not all the configurations in Figure B.3 can occur in the image of some r-regular object by a lattice $(d\mathbb{Z})^2$ with $d\sqrt{2} < r$. We would like to remove configurations that do not occur from the list in the Figure. To do so, we need to prove a series of lemmas. Their proofs are mainly geometric and rather technical, so we will put them in an appendix instead of presenting them here.

First of all, let us start with a definition, borrowed from Pavlidis' book [4].

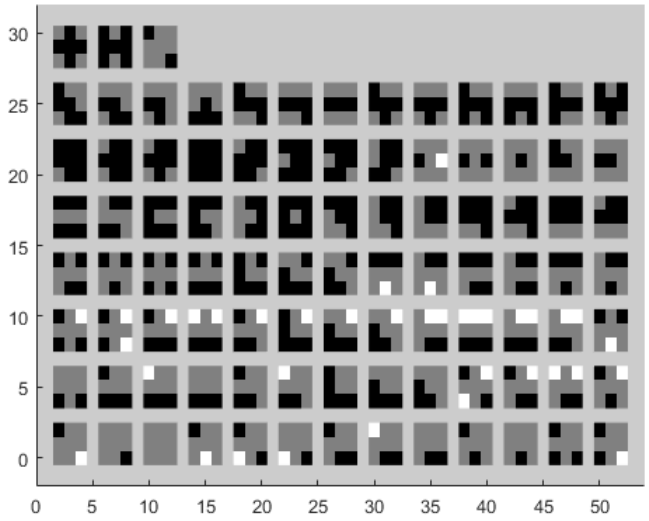

Figure B.3: All possible combinations of the allowed 3×3 pixel configurations, up to rotation, mirroring and interchanging of black and white pixels.

Definition B.18. Two pixels are *direct neighbours* (abbreviated *d-neighbours*) if the respective cells share a side. Two pixels are *indirect neighbours* (abbreviated *i-neighbours*) if those cells touch only at a corner. The term *neighbour* denotes either type.

In the following lemmas, we will only be considering pixel configurations in images of r-regular objects by lattices $d\mathbb{Z}^2$ with $d\sqrt{2} < r$ according to our convention, but for brevity we will omit this requirement from the lemma statements. We remark that any result stated in the following also holds if the roles of black and white are switched.

Lemma B.19. *Consider four pixels as in Figure B.4, left. Suppose ∂X intersects the edge l between the two pixels B and C more than once. Then one of the pixels A and D is black, and the other one is white. The same result is true if l is tangent to ∂X in a point.*

Similarly, consider eight pixels as in Figure B.4, right. Suppose ∂X intersects the line l between the pixels $B_1 \cup B_2$ and $C_1 \cup C_2$ more than once. Then for either $i = 1$ or $i = 2$, one of the pixels A_i and D_i is black, and the other one is white. The same result is true if l is tangent to ∂X in a point.

Lemma B.20. *Consider a configuration as the one in Figure B.5. The pixel named A in the figure must be black, and the the pixel named D must be white.*

Lemma B.21. *Consider a configuration of 3×3 pixels, where the middle one is grey. Then at least one of its 8 neighbour pixels is not grey.*

Lemma B.22. *Consider a configuration of 3×3 pixels as in Figure B.6, where the centre pixel is grey and has centre c. Let $p = \pi(c)$ be the point of ∂X that is nearest*

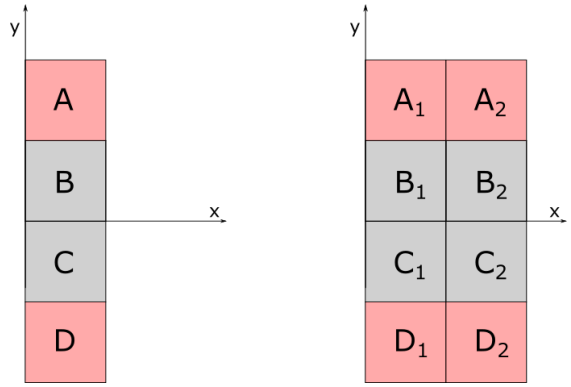

Figure B.4: Left: If the boundary ∂X intersects the edge between the pixels B and C twice, then one of pixels A and D is black, and the other is white. Right: If ∂X intersects the line between $B_1 \cup B_2$ and $C_1 \cup C_2$, the for either $i = 1$ or $i = 2$, one of A_i, D_i is black, and the other one is white.

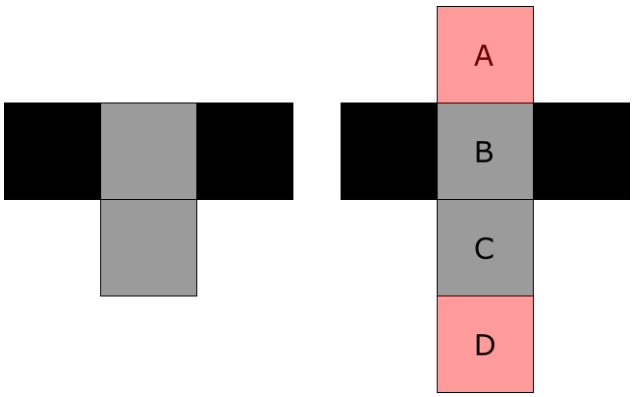

Figure B.5: Consider a configuration as the left one, and name the pixels in this configuration as in the right figure. If a configuration as the left one occurs in a digital image of an r-regular object with $d\sqrt{2} < r$, then pixel A must be black, and pixel D must be white.

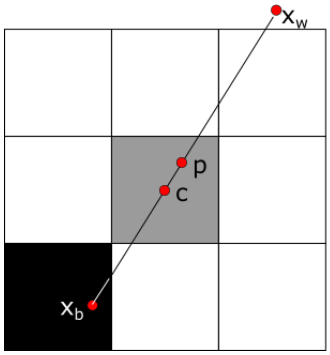

Figure B.6: In Theorem B.22, we consider 3×3 pixels, where the middle one is grey.

to c, and let $B_r(x_b) \subseteq X$, $B_r(x_w) \subseteq X^C$ be the black and white r-balls tangent to ∂X at p. Suppose $\|c - x_b\| \leq \|c - w_w\|$, and that x_b belongs to the lower left pixel (which is hence black).

Then the upper right pixel is white.

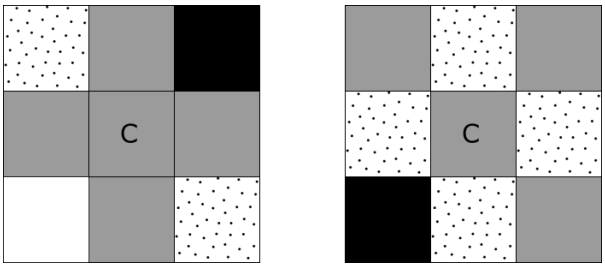

Figure B.7: If a grey pixel has four grey d-neighbours as in the left figure, it must have a black and a white i-neighbour sitting diagonally across from each other. Equivalently, if a grey pixel does not have a black and a white i-neighbour sitting across from each other as in the right figure, it cannot have four grey d-neighbours.

Remark B.23. Theorem B.22 and Lemma B.21 combined tell us that a grey pixel C with four grey d-neighbours must always have a black and a white i-neighbour whose common vertices with C sit diagonally across from each other, see Figure B.7, left. Equivalently, if a grey pixel C does not have a black and a white neighbour sitting opposite of each other, then at least one of its d-neighbours is not grey.

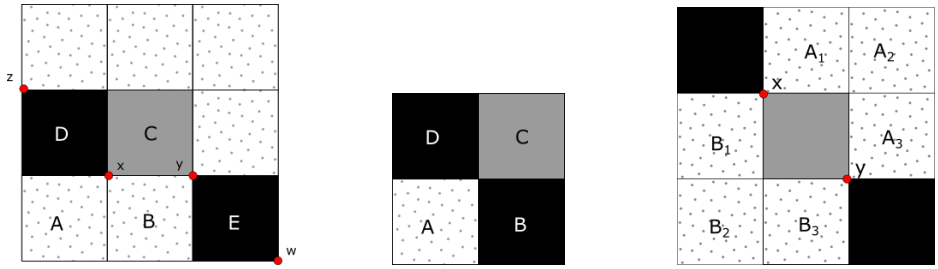

(a) **(b)** **(c)**

Figure B.8: Consider configurations of two black and a grey pixel (we do not assume anything about the colour of the dotted pixels). If a grey and two black pixels sit in a configuration as in (a) or (b), then the pixels A and B must also be black. If a grey and two black (or two white) pixels sit in a configuration as in (c), then either the pixels A_1, A_2, A_3 are all black, or the pixels B_1, B_2, B_3 are all black.

Lemma B.24. *The following holds:*

(i) *Consider 2×3 pixels as in Figure B.8(a) with the grey and black pixels placed relative to each other as in the figure. Then pixels A and B must necessarily be black.*

(ii) *Consider 2×2 pixels as in Figure B.8(b), with the grey and black pixels placed relative to each other as in the figure. Then A must necessarily be black.*

(iii) *Consider 3×3 pixels as in Figure B.8(c), with the grey and black pixels placed relative to each other as in the figure. Then either the pixels A_1, A_2, A_3 are all black, or the pixels B_1, B_2, B_3 are all black.*

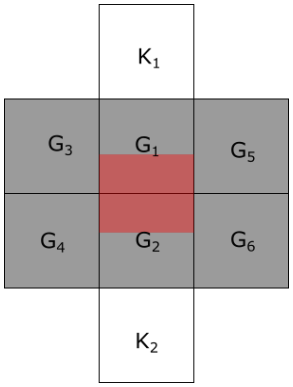

Figure B.9: We consider 6 grey pixels in a 2×3 configuration and show that $\partial X \cap (G_1 \cup G_2)$ belongs to the red set in the figure, and that one of the pixels K_1, K_2 must be black, and the other one white.

Lemma B.25. *Consider a configuration of 6 grey pixels as in Figure B.9, with pixels G_i, $i = 1, \ldots, 6$, and K_1 and K_2 as in the figure. Then the following holds:*

(i) *One of the pixels K_1, K_2 must be black, and the other one white,*

(ii) *The set $\partial X \cap (G_1 \cup G_2)$ belongs to the set of points in $G_1 \cup G_2$ that are no further than $(\sqrt{2} - 1)d$ from the common edge of $G_1 \cup G_2$ (i.e. the red set in the figure).*

(iii) *The boundary ∂X intersects the common boundary of pixel G_i and G_{i+1} at least once for $i = 1, 3, 5$.*

Lemma B.26. *A configuration as the one in Figure B.10 left cannot occur.*

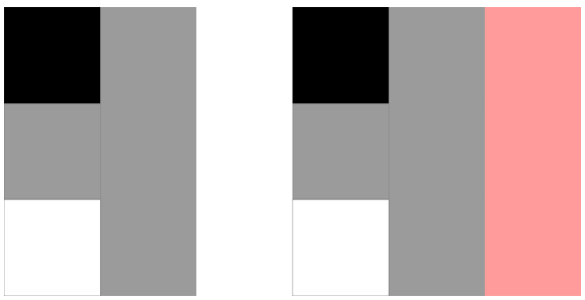

Figure B.10: The configuration to the left cannot occur in the digital image of an r-regular object with $d\sqrt{2} < r$, for if it did, one of the pixels that are coloured red in the figure on the right would have a colour that is incompatible with any legal configuration.

Lemma B.27. *A configuration as the one in Figure B.11 cannot occur.*

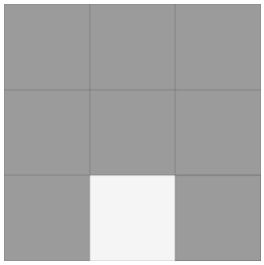

Figure B.11: The configuration in this figure cannot occur in the image of an r-regular object with $d\sqrt{2} < r$.

Theorem B.28. *Up to rotation, mirroring and interchanging of black and white, any* 3×3 *configuration of pixels is one of those shown in Figure B.12.*

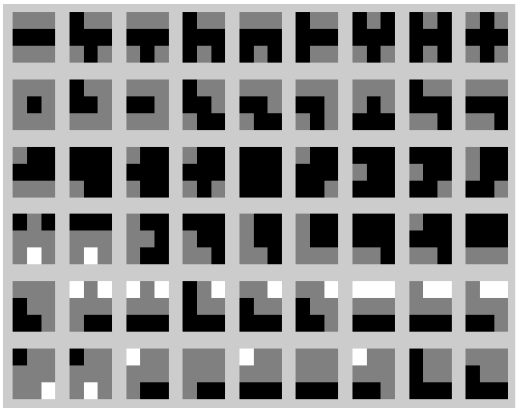

Figure B.12: Up to rotation, mirroring and interchanging of black and white colours, these are the only 3×3-configurations that can occur in the digital image of an r-regular object by a lattice $(d\mathbb{Z})^2$ with $d\sqrt{2} < r$.

For the following, it is also useful to know which 4×4-configurations with a 2×2 centre of grey pixels may occur in a digital image of an r-regular object by a lattice $d\mathbb{Z}^2$. We may have a computer find these by combining all possible 3×3-configurations from Figure B.12, along with rotations, mirror images and inverses of these configurations (where we by 'inverse' of a configuration mean the configuration where the roles of black and white have been exchanged). After removing configurations that violate Lemma B.25, this yields the configurations in Figure B.13 (up to rotations, mirroring and interchanging of black and white). We aim to remove configurations from the list if they cannot occur in a digital image like the ones we are considering.

Lemma B.29. *The configuration in Figure B.14 cannot occur.*

Lemma B.30. *The left configuration in Figure B.15 cannot occur.*

Lemma B.31. *The boundary* ∂X *cannot intersect all four boundary edges of a configuration of* 2×2 *grey pixels.*

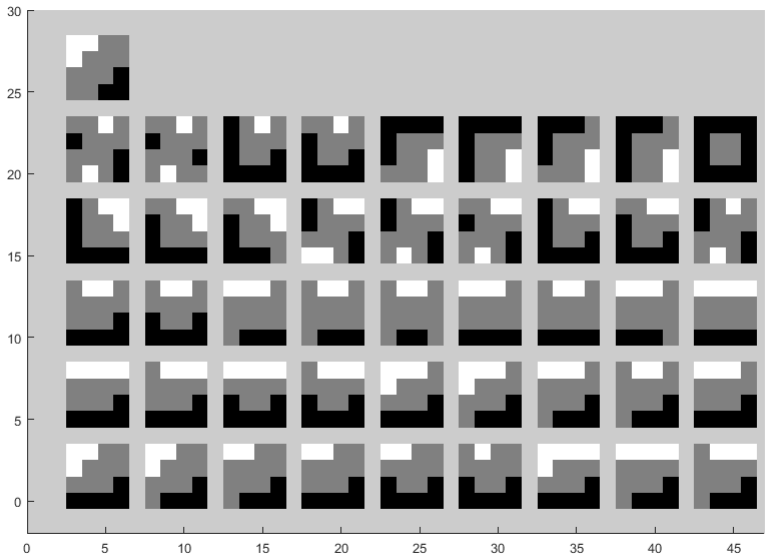

Figure B.13: These are all possible combinations of the configurations in Figure B.12, their inverses, rotations and mirror images.

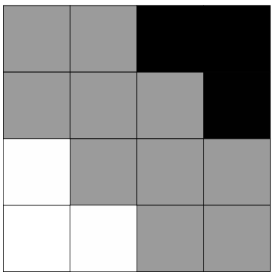

Figure B.14: We show that this configuration cannot occur in the digitisation of an r-regular object.

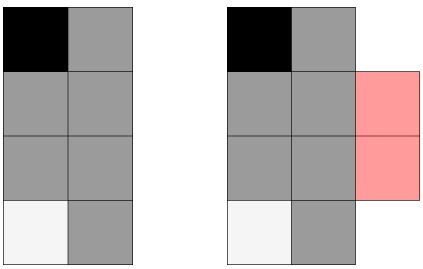

Figure B.15: The right configuration does not occur in the digitisation. If it did, one of the red pixels in the figure on the right would have to be non-grey by Theorem B.25.

Theorem B.32. *The only possible configurations of* 4×4*-configurations that have* 2×2 *grey pixels in the middle are the ones shown in Figure B.16.*

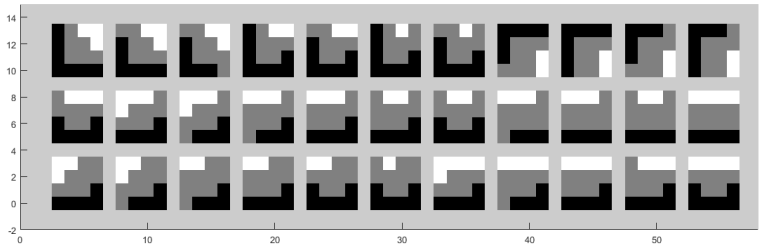

Figure B.16: The 33 possible configurations of 4×4 pixels with the centre pixels grey, up to rotation, reflection and interchanging of black and white.

Note that the converse is not true: There are configurations in Figure B.16 that does not occur in any image of an r-regular object by a lattice $d\mathbb{Z}^2$ with $d\sqrt{2} < r$. But since the proofs of this are rather technical and their results are not relevant to our further progress, we will not discuss them here.

B.4 Reconstruction of the boundary of the set

All the work done in the previous section was leading up to the development of a reconstruction algorithm, which we will introduce in this section. The idea is to use circle arcs to approximate the boundary of the original object. The reconstructed set will not in general be r-regular.

Before we start, we will introduce some points, called auxiliary points, that our reconstructed boundary must pass through. These are defined differently for different grey pixels. Thus we proceed to define

Definition B.33. A grey pixel sitting in a 2×2 configuration of grey pixels is called complex. A grey pixel that is not sitting in a 2×2 configuration of grey pixels is called simple.

We now introduce the auxiliary points needed for the constructing a reconstruction algorithm for an image.

Consider a pixel edge shared by two grey pixels A and B. If $A \cup B$ belongs to a configuration of 2×2 grey pixels, we introduce an auxiliary point at the midpoint of this configuration. If they do not, we introduce a point on the midpoint of their common edge, see Figure B.17. (Note that $A \cup B$ may be part of two different 2×2 configurations of grey pixels at the same time. In that case, we introduce two auxiliary points, one at the centre of each of the two 2×2 configurations).

Lemma B.34. *All simple grey pixels have between one and three auxiliary points on their boundary. All complex grey pixels have either one or two grey auxiliary points on their boundary.*

Proof. For the simple pixels, consider all possible configurations in Figure B.12. For the complex pixels, consider all possible configurations in Figure B.16. □

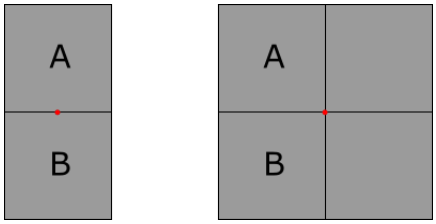

Figure B.17: Left: If two grey pixels share an edge and are not part of a 2×2 configuration of grey pixels, we introduce an auxiliary point (red) at the midpoint of their common edge. Right: If on the other hand the two pixels are part of the same 2×2 configuration of grey pixels, we introduce an auxiliary point at the centre of this 2×2 configuration.

Lemma B.35. *A simple pixel with just one auxiliary point on its boundary must share this point with a simple pixel that has three auxiliary points on its boundary. On the other hand, a simple pixel with three auxiliary points on its boundary must share exactly one of these points with a simple pixel that has just one auxiliary point on its boundary.*

Proof. Consider all cases as presented in Figure B.12, and use Lemma B.20. □

We will now remove the auxiliary point of all simple pixels that have only one auxiliary point. By the above lemmas, this now means that all simple pixels have zero or two auxiliary points on their boundary, and all complex pixels have one or two auxiliary points on their boundary.

Lemma B.36. *In each 2×2 configuration of grey pixels there are exactly 3 auxiliary points – one at the centre and two on the configuration boundary.*

Proof. Each 2×2-configuration of grey pixels sits in one of the configurations in Figure B.16 (up to rotation, mirroring and interchanging of colours). Hence we get the above theorem by checking all possible cases. □

Definition B.37. Two auxiliary points p, q are called *neighbours* if there exists a grey pixel having both p and q on its boundary.

Theorem B.38. *Each auxiliary point p has exactly two neighbours.*

Proof. Consider an auxiliary point p, sitting on the boundary of pixel C. If p is the centre of some 2×2 configuration of black pixels, then by Lemma B.36 there are only two auxiliary points on the boundary of this configuration as claimed.

Suppose instead that p is the midpoint of the edge between some pixels C, C'. Then C is either simple (and hence has two auxiliary points on its boundary), or it is complex and hence has another auxiliary point in a corner of C. In both cases, p has a neighbour on the boundary of C, and by a similar argument, it also has a neighbour on the boundary of C'. So p has two neighbouring auxiliary points. □

The next step is to approximate the boundary of X with curve segments: Consider an auxiliary point and its two neighbouring auxiliary points. We approximate ∂X by circle arc segments through these three points (or, if the points are collinear, by line segments). This means that there are two curve segments through each two neighbouring auxiliary points sitting on the boundary of the same pixel C, one

starting in one of the points, the other ending in the other point. Each of these curve segments are graphs over the straight line L through the points, so we may write them as $\gamma_1 : [0, |L|] \to \mathbb{R}$ and $\gamma_2 : [0, |L|] \to \mathbb{R}$. Then choosing a bump function $\varphi : [0, |L|] \to [0, 1]$ with $\varphi(0) = 1$ and $\varphi(|L|) = 0$, we may patch a connected curve γ together by putting $\gamma_C(t) = (1 - \varphi(t))\gamma_1(t) + \varphi(t)\gamma_2(t)$ in each pixel C, see Figure B.18. The resulting curve γ_C is then also a graph over L, and the curve γ is a smooth embedded submanifold of $\mathbb{R}^2$.

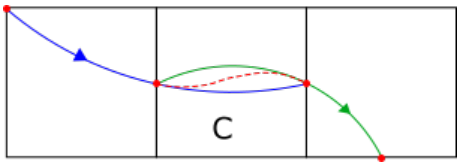

Figure B.18: The curve γ_1 (blue) and the curve γ_2 (green) are patched together inside C using a bump function. This produces the curve γ_C (dashed red curve).

Lemma B.39. *The path γ_C is contained in the area bounded by γ_1 and γ_2.*

Proof. Since γ_C is a graph over a line L and it is a convex combination of a point on γ_1 and a point on γ_2, the curve γ_C must lie between these two points, and hence also between the curves γ_1 and γ_2. □

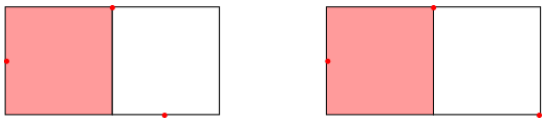

Figure B.19: Auxiliary points sitting in one of these configurations around the red pixel are exemptions to Lemma B.40.

Lemma B.40. *Consider two neighbouring auxiliary points on the boundary of some pixel C not sitting in a configuration like the ones in Figure B.19.*

(i) *If the two neighbouring auxiliary points are the endpoints of the edge shared by C and some other pixel C', then the curve γ_C is contained in $C \cup C'$.*

(ii) *If the two neighbouring auxiliary points are not the endpoints of some edge of C, then the curve γ_C is contained in C.*

Proof. We start by proving the lemma for the arc segments γ_1 and γ_2: We can consider all possible positions of three neighbouring auxiliary points, see Figure B.20. Consider auxiliary points p_1, p_2 sitting in configurations around a red pixel as in any of the five figures to the left. A calculation (or a look at the figures!) then shows that save for auxiliary points in configurations as the ones shown in Figure B.19, all possible circle arcs through two auxiliary points sitting on a red pixel are contained in that red pixel.

Now, lets argue that γ_C is contained in C: By Lemma B.39, γ_C is contained in the area A_C bounded by γ_1 and γ_2. Since γ_1 and γ_2 are both contained in C which is convex, A_C is also contained in C. Hence γ_C must also be contained in C. This

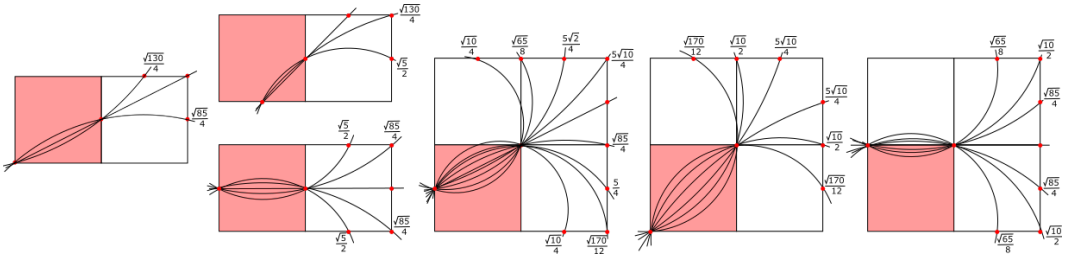

Figure B.20: The figure shows all possible positions of two auxiliary points on the boundary of some pixel C (the red ones in the figure), and all circle arcs through these two and a third auxiliary point. The radii of the circle arcs are also calculated.

proves (ii). Part (i) is proved in the same way, but now considering the rightmost figure in Figure B.20. □

Proposition B.41. *The curves γ_C have no self-intersections, and do not intersect each other. Hence each component of γ is a simple closed curve.*

Proof. Since each segment γ_C is a graph over some straight line L, we only need to show that two segments γ_C and $\gamma_{C'}$ do not intersect. By Lemma B.39 it suffices to show that the area A_C bounded by two arcs γ_1 and γ_2 in a pixel C does not intersect the area $A_{C'}$ bounded by two arcs γ_1' and γ_2' in another pixel C'.

Consider the possible circle arcs shown in Figure B.20. With the exception of auxiliary points sitting in configurations like the ones in Figure B.19, all arc segments stay inside the pixel(s) containing both of the auxiliary points they join. Since no pixel can have more than two auxiliary points on their boundary, the only possible way that two curve segments can intersect is if one of them, say γ_C, is made using a curve γ_1 connecting points in a configuration like the one in Figure B.19. But by going through all possible configurations where such a γ_1 could occur one can conclude that γ cannot intersect itself in this case either.

That each segment of γ is a simple closed curve follows from the fact that the segments γ_C always connect two neighbouring auxiliary points, and that all auxiliary points have two neighbours. If a component of γ were not a closed curve, it would have an endpoint (since all components of γ are bounded) – but γ is the merge of curve segments between neighbouring auxiliary points, meaning that such an endpoint only can occur in one of the auxiliary points. But since all auxiliary points have two neighbouring auxiliary points, this is impossible. □

Theorem B.42. *For each component of ∂X, there is exactly one component of γ. Each component of γ separates the boundary components of a connected component A of the set of grey pixels.*

Proof. Let $\partial X'$ be a component of ∂X, and let A be the set of grey pixels containing points of $\partial X'$. Note that A cannot have any grey neighbour pixel B, since this would imply that B contained a point from another component of ∂X, which would further imply that two points on different components of ∂X lay closer than $2d\sqrt{2}$ – a contradiction by Corollary B.16 applied to π. Therefore A is a connected component of the set of grey pixels.

Consider any chain of grey pixels in A, where each pixel in the chain is a neighbour of both the previous and the next pixel in the chain, and each pixel appears in the

chain no more than once. Assume that the first pixel and last pixel of the chain have at least two grey d-neighbours. We aim to show that the first and last pixel in such a chain are connected by a segment of γ.

By construction, each pixel in such a chain has at least two grey d-neighbours, hence at least one auxiliary point on its boundary. If a pixel C in the chain has only one auxiliary point on its boundary, its two grey d-neighbours must sit in a 2×2 configuration including C, and hence one of its grey d-neighbours must have two auxiliary points on its boundary. Hence if we replace C by its d-neighbours with two auxiliary points on their boundary, we still get a chain of pixels in A. Repeating this, we end up with a chain of pixels where all pixels in the chain have two auxiliary points on their boundary. The construction of γ then yields a segment of γ through this pixel chain.

Now by r-regularity of X, A must be larger than 2 pixels and therefore have at least one pixel with two grey d-neighbours. Hence A contains at least one component of γ. If A contained two components γ', γ'' of γ, we could pick a chain of grey pixels connecting two pixels containing a point of γ' and a point of γ'', respectively. Then by the above, the auxiliary points on the first pixel would be connected to the auxiliary points on the last pixel by a segment of γ. But then, γ' and γ'' would be connected – a contradiction, since they were assumed to be distinct components. In conclusion, for any component of ∂X, there is exactly one component of γ.

For the second part of the statement, consider a chain of pixels following a boundary component $\partial A'$ of A. By the first part, this chain yields a segment of γ' which is a closed curve containing $\partial A'$, but not containing any other component of the boundary of A. Hence γ' separates any component of ∂A from the others – in particular, there can be at most two boundary components of A, and γ separates them. In fact, there are always two components of ∂A: Any point $x \in \partial X'$ has a black and a white $\sqrt{2}d$-ball osculating at x, and these balls contain the pixels in which they are centred. Since $\partial X'$ separates the two balls and hence the two pixels where they are centred, so does A. But then A must have two different boundary components, and both $\partial X'$ and γ' separates these two components. □

Since the set of grey pixels separates the white pixels from the black, the above theorem actually implies that γ also separates the white pixels from the black (in the sense that any curve from a black to a white pixel must intersect γ). We may conclude (via the Jordan Curve Theorem) that each component of γ separates $\mathbb{R}^2$ into two sets, a bounded and an unbounded. From now on, γ is the boundary of the reconstructed set, which we define as follows:

Definition B.43. We define *the reconstructed set* Γ to be the bounded set having γ as boundary.

B.5 Hausdorff distance between the boundaries of the original set and the reconstruction

We are now ready to look at the Hausdorff distance between our reconstruction and the original object. Let us start by proving a lemma:

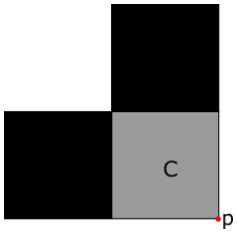

Figure B.21: A point $q \in \partial X$ that belongs to a pixel with two black neighbouring pixels that share an edge must belong to the ball $B_d(p)$.

Lemma B.44. *Consider a grey pixel C as the one in Figure B.21, with two black (or two white) neighbouring pixels sharing a vertex. Let p be the vertex of C which does not belong to the two black (or white) neighbouring pixels. If $q \in \partial X \cap C$, then $q \in B_d(p)$.*

Proof. Let q be as above. Then q belongs to a component of ∂X that must enter and leave C in two places, say in points x_1 and x_2. These points belong to one of the edges of C having p as a corner. Let L be the line segment between x_1 and x_2.

Now q must belong to $\pi(L)$, which in turn must belong to $S(L, r)$ by Corollary B.16, which again is contained in any ball of radius less than r containing L by Lemma B.15. The ball $B_d(p)$ contains both of the edges of C that have p as an endpoint, meaning that it also contains x_1 and x_2 and consequently L, $S(L, r)$ and q. □

Now that we have a suggestion for a reconstruction of the boundary of the original set, we aim to show how good this approximation is. The first step will be to prove the following:

Theorem B.45. *Any point of ∂X has a distance of at most d to the curve γ consisting of curve segments γ_C. Hence* $\sup_{y \in \partial X} \inf_{x \in \gamma} d(x, y) \leq d$.

This theorem, however, requires some additional lemmas:

Lemma B.46. *If two neighbouring auxiliary points sit on the common boundary edge of two grey pixels C_1 and C_2, then the curve $\gamma_{C_1} = \gamma_{C_2}$ is contained in the set C' of points in $C_1 \cup C_2$ that lie at a distance of $0.133d$ from the common edge of C.*

Proof. If two auxiliary points sit at the common boundary edge e of pixels C_1 and C_2, then they must sit on the ends of e, i.e. be the two common vertices of C_1 and C_2.

By Lemma B.40, part (i), $\gamma_{C_1} = \gamma_{C_2}$ belongs to $C_1 \cup C_2$. Let γ_1 and γ_2 be the two arc segments whose merge is γ_{C_1}. Then both are circle arcs of radius no smaller than $s = \frac{\sqrt{65}}{8}$ (see Figure B.20), hence they are contained in the spindle $S(e, s)$ whose height is $(s - \sqrt{s^2 - \frac{1}{4}})d \approx 0.133d$. Thus, no point on γ_1 or γ_2 is further away than $0.133d$ from e. Since the curve γ_{C_1} belongs to he area bounded by γ_1 and γ_2 by Lemma B.39, we must also have that γ_{C_1} belongs to C'. □

Lemma B.47. *If two auxiliary points sit on two edges of a pixel C sharing a corner p, then γ_C is contained in $B_d(p) \cap C$.*

Proof. We know from Lemma B.40 that γ_C belongs to C. Therefore we only need to show that γ_C belongs to $B_d(p)$. By Lemma B.39 it suffices to show that the area A between the two curves γ_1 and γ_2 belongs to $B_d(p)$. In fact, since $B_d(p)$ is convex, it is even enough to show that γ_1 and γ_2 both belong to $B_d(p)$. This can be done by a calculation for all possible cases, or by looking at Figure B.22. □

Lemma B.48. *If two neighbouring auxiliary points on the boundary of some pixel C neither sit on the same edge of C, nor in a configuration as the ones shown in Figure B.19, then the distance between any point of ∂X in C and the curve γ_C is less than d.*

Proof. Consider two auxiliary points on the boundary of pixel C. Suppose they sit on two opposite edges e_1, e_2 of C. If furthermore the two points do not sit in one of the configurations in Figure B.19, then by Lemma B.40, the curve γ_C belongs to C. Hence the curve γ_C must run from one side of C to the other side without crossing the boundary of C, see Figure B.22 left. Thus, projecting any point in C to γ_C along a line parallel to e_1 moves it no further than a distance d. Hence all points of C is closer than d to γ_C.

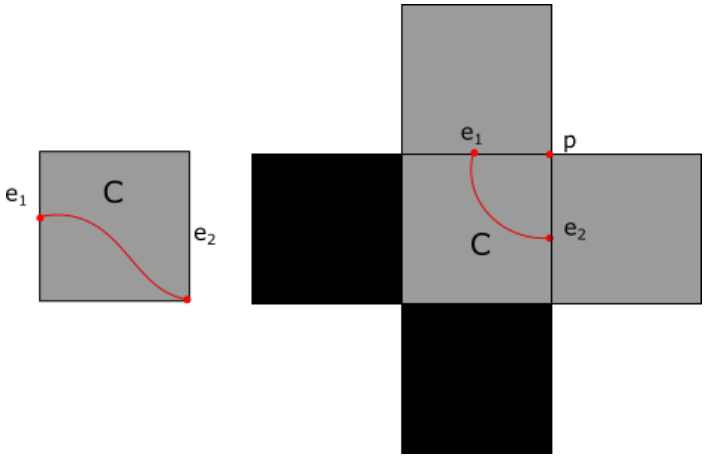

Figure B.22: Two different ways that a curve γ can pass through a pixel C with two auxiliary points on its boundary.

On the other hand, suppose the two auxiliary points on the boundary of C sit on the midpoints of two edges e_1, e_2 sharing a vertex p, see Figure B.22, right. Then C is a simple pixel, and since its auxiliary points do not sit on opposite edges, it cannot be one of the simple pixels that we removed auxiliary points from (by the proof of Lemma B.35). So C must have two grey d-neighbour pixels sharing the vertex p, and two non-grey d-neighbour pixels sharing the vertex opposite of p, as in Figure B.22 right. Let us assume these two non-grey pixels to be black.

Consider a point $q \in C \cap \partial X$. By Lemma B.44, q must belong to the ball $B_d(p)$. Then, since the path γ_C is also contained in this ball by Lemma B.47, and since γ_C runs from e_1 to e_2, we hit γ_C somewhere if we move a point in $B_d(p) \cap C$ along a radius of $B_d(p)$. Such a movement displaces the point a distance of at most $d - \frac{1}{2\sqrt{2}}d$, since this is the maximal distance between a point on γ_C and a point on $\partial B_d(p)$ on the same radius of $B_d(p)$. Hence a point of $\partial X \cap C$ is at most a distance d from γ_C. □

Proof of Theorem B.45. By Lemma B.48, the theorem holds for any point of ∂X contained in a pixel with two auxiliary points not sitting on the same edge, and not sitting in one of the configurations of Figure B.19. We therefore need to show the result for points on ∂X contained in i) grey pixels with two auxiliary points sitting on the same edge, ii) the special cases in Figure B.19, iii) grey pixels with one auxiliary point on their boundary and iv) grey pixels with zero auxiliary points on their boundaries.

Ad i): By Lemma B.46, γ_{C_1} must belong to the set C' of points in $C_1 \cup C_2$ closer than $0.133d$ to e, and by Lemma B.25, all points of ∂X in $C_1 \cup C_2$ must be closer than $(\sqrt{2}-1)d$ to e. Since the curve γ_{C_1} runs from one side of C' to the other, then pushing a point $p \in \partial X \cap C'$ orthogonally to e inside $C_1 \cup C_2$, we must hit γ_{C_1} at some point. The displacement made in this manner can be no larger than $(\sqrt{2}-1+0.133)d \approx 0.55d$, hence any point of $(C_1 \cup C_2) \cap \partial X$ is closer than $0.55d$ to $\gamma_{C_1} = \gamma_{C_2}$.

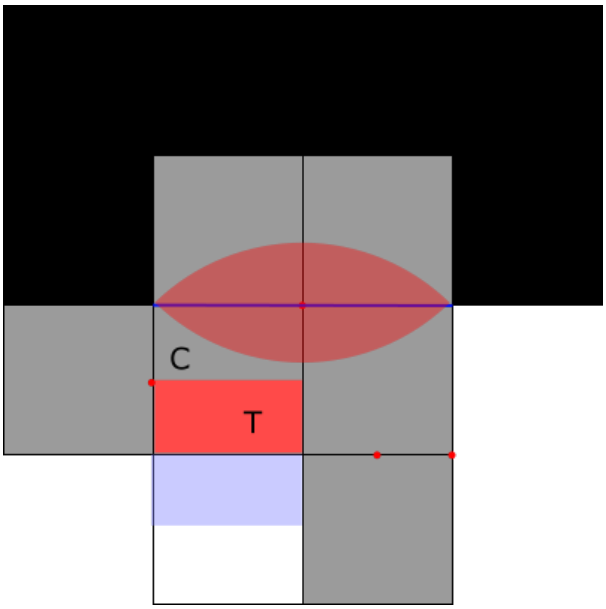

Figure B.23: Both of the configurations excepted from Lemma B.40 must sit in a configuration like the one shown above. We aim to show that the red rectangle cannot contain any points of ∂X.

Ad ii): Now consider instead either of the cases from Figure B.19. Such a configuration must necessarily sit in a configuration like in Figure B.23, by considering the possible configurations involving 2×2 grey pixels in Figure B.16. We will aim to show that the rectangle T in the figure, which shares two vertices with pixel C and has the other two vertices at the midpoints of the vertical pixel edges of C, does not contain any points of ∂X.

Look at the blue line L separating the two upper grey pixels from the lower. Since there are grey pixels on both sides of L, ∂X must pass it somewhere, and since both endpoints of L are black, ∂X must pass L at least twice. Then there must be some point p in one of the two upper pixels where ∂X has a horisontal tangent, which

means that the centres of the black and white $\sqrt{2}d$-balls meeting at this point sit on the vertical line through p. Since the pixels above the 2×2 grey pixels are black in the figure, the upper ball osculating ∂X at p must be black, and the lower must be white.

By Corollary B.16 applied to π, the part of ∂X which lies between two points in $\partial X \cap L$ must be contained in the spindle $S(L, r)$ (shown in the figure), which contains points no further from L than $(\sqrt{2} - 1)d$. So p cannot be further above L than $(\sqrt{2} - 1)d$.

Now, if p belonged to the right upper grey pixel, the centre of the white ball osculating ∂X at p would belong to a grey pixel and hence colour that pixel white. So p belonging to the upper left grey pixel is not possible. Therefore p must belong to the upper left pixel, and be no further from L than $(\sqrt{2} - 1)d$. The centre of the white $\sqrt{2}d$-ball osculating ∂X at p must therefore lie in the white pixel, no further than $\sqrt{2}d$ from p and hence no further from the common edge between the white pixel and pixel C than $(\sqrt{2} - 1)d$ (i.e. somewhere in the light blue rectangle of the white pixel in the figure). But any $\sqrt{2}d$-ball centred centred in the top half of the white pixel must contain T, i.e. the bottom half of pixel C. This means that the white ball osculating ∂X at p must contain all of T, and therefore T cannot contain any points of ∂X.

A calculation shows that no point of γ_C lies further above L than $0.041d$. Hence if we take any point q in $C \setminus T$ and push it along a vertical line towards γ_C, we can do this without moving q more than a distance $0.541d$. In conclusion, any point of $\partial X \cap C$ is closer than d to γ_C.

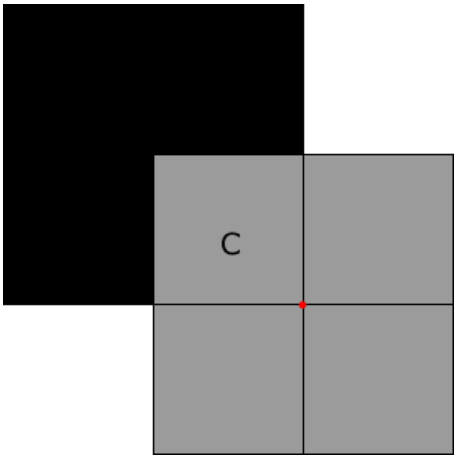

Figure B.24: A pixel C with just one auxiliary point on its boundary must sit in a configuration as the above.

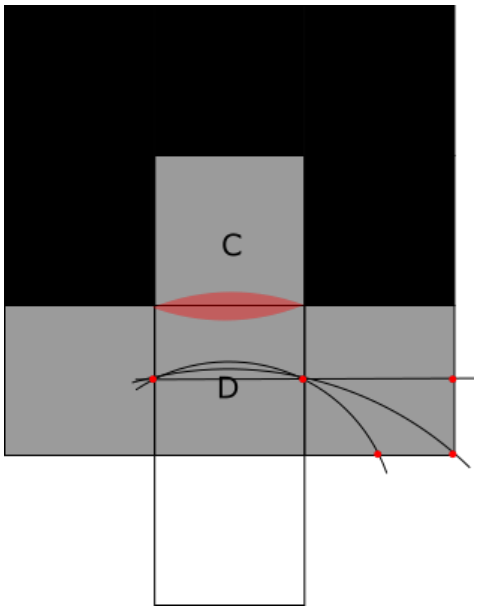

Figure B.25: A grey pixel with zero auxiliary points on its boundary must sit in this configuration of pixels. Then any circle arc through the auxiliary points of D and one of its neighbours must look like one of the above

Ad iii): Consider a grey pixel C with only one auxiliary point p on its boundary. By construction, C must be complex and have two grey neighbouring pixels, and two non-grey neighbouring pixels, see Figure B.24. By Lemma B.44, all points of $\partial X \cap C$ must belong to the ball $B_d(p)$. Hence the distance from a point in $\partial X \cap C$ to p is less than d. Since p belongs to γ, this proves the claim in this case.

Ad iv): Consider a grey pixel C without any auxiliary points on its boundary. By construction, it means that C is a simple grey pixel with one grey d-neighbour pixel D, and three non-grey d-neighbour pixels, see Figure B.25.

Now, the boundary ∂X must pass the common edge e of C and D in order to pass into and out of pixel C. Hence the part of ∂X that is inside C must be contained in $S(e, r)$.But $S(e, r)$ contains no points in C that are further from e than $\sqrt{2}d - \sqrt{2d^2 - \frac{d^2}{4}} < 0.1d$, since this is the height of the spindle.

Furthermore, D must have one auxiliary point on the midpoint of each vertical edge – let us call these p_1 and p_2. Then, an arc segment γ_1 through p_1 and p_2 and a third auxiliary point of one of the grey pixels neighbouring C must lie above the straight line connecting p_1 and p_2 (one need only consider all possible cases, as is done in Figure B.25).

Concludingly, any point p in $C \cap \partial X$ is closer than $0.1d$ to e, and any point in e is closer than $\frac{d}{2}$ to γ_D. This means that the distance from p to γ is less than $0.6d < d$. This finishes the proof that any point of ∂X is closer than d to γ.

For any point x in ∂X, there is a point y' in γ that is no further than a distance d from x, meaning that

$$\inf_{y \in \gamma} d(x, y) \leq d(x, y') \leq d.$$

Thus we get

$$\sup_{y \in \partial X} \inf_{x \in \gamma} d(x, y) \leq d.$$

□

This proof is the first step on our way towards showing that ∂X and γ are close to each other in Hausdorff distance. The second step is taken when we prove the following:

Theorem B.49. *Any point of γ has at most distance d to the boundary ∂X of the original set X. Hence* $\sup_{y \in \gamma} \inf_{x \in \partial X} d(x, y) \leq d$.

The proof of this theorem is very similar to the proof of Theorem B.45. Again, we split the proof into a couple of lemmas.

Lemma B.50. *Consider a simple pixel C with two auxiliary points on either of two opposing edges. Then any point of γ_C is closer than d to some point of ∂X.*

Proof. Notice that C must sit in one of the two configurations of Figure B.26. For the first configuration, pick a point $p \in \gamma_C \subseteq C$. The horisontal line in C through p has a black and a white endpoint, meaning that it must contain a point of ∂X. Since p is no further than $0.62d$ from the endpoints of this line, there must be a point in ∂X that is closer than $0.62d < d$ to p.

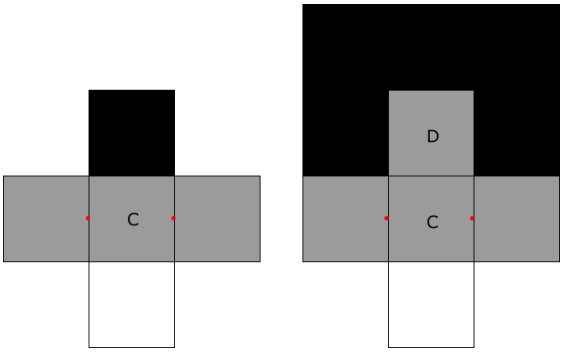

Figure B.26: A simple pixel C with auxiliary points on opposite edges must sit in one of the configurations above.

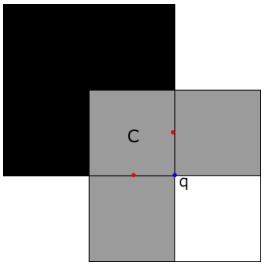

Figure B.27: A simple pixel C with auxiliary points on vertex-adjacent edges must sit in the configuration above.

For the second configuration, pick again a point p in $\gamma_C \subseteq C$. Let D be the pixel above C. Notice that ∂X must enter and leave D by crossing e in order for D to be grey and both endpoints of e to be black. Then by Corollary B.16 with ρ replaced by π, any point of ∂X in D must belong to the spindle $S(e, r)$ which contains points no further from e than $\sqrt{2}d - \sqrt{2d^2 - \frac{d^2}{4}} < 0.1d$, by Lemma B.14. So, any point of $\partial X \cap (C \cup D)$ must either belong to C or be no further from e than $0.1d$. On the other hand, a calculation shows that the path γ_C is closer than $0.5d$ to e.

Consider a vertical line in $C \cup D$ through p. There has to be a point on this line belonging to ∂X, since its endpoints have different colours. Either this particular point belongs to C (in which case they can be no further apart than $0.62d$ by the first part of the proof), or it belongs to D. If it belongs to D, it is no further from e than $0.1d$, and since p is in turn no further than $0.5d$ from e, the point in question belonging to ∂X must be closer than d to p. □

Lemma B.51. *Consider a simple pixel C with two auxiliary points located at the midpoint of two vertex-adjacent edges of C. Then no point of γ_C is further away from ∂X than d.*

Proof. A pixel C as described above must sit in a configuration as the one in Figure B.27. Let q denote the vertex of C where the two edges containing auxiliary points meet. Let $p \in \gamma_C \subseteq C$.

Consider the line in C through p and q. Since it has endpoints of different colours, it must contain a point s in ∂X. By Lemma B.44, any point of $\partial X \cap C$ must belong to the ball $B_d(q)$, and by Lemma B.47, so must p. Hence p and s both sit on a radius of the ball $B_d(q)$. By looking at the possible curves γ_C, such two points cannot be further apart than a distance $d - \frac{1}{2\sqrt{2}}d$. So any point $p \in \gamma_C$ is closer than d to ∂X. □

Lemma B.52. *Consider a complex pixel C with two auxiliary points located at the endpoints of some edge e of C. Then no point of γ_C is further away from ∂X than d.*

Proof. The pixel C must sit in a configuration as the one in Figure B.28, by means of Lemma B.25. By Lemma B.40, part (i) γ_C must belong to $C \cup D$.

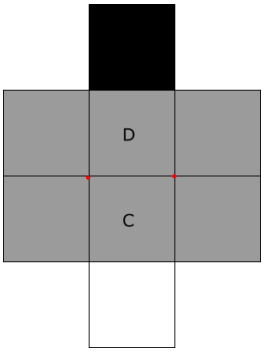

Figure B.28: A complex pixel C with auxiliary points at the endpoints of one of its edges e must sit in a configuration as the one above.

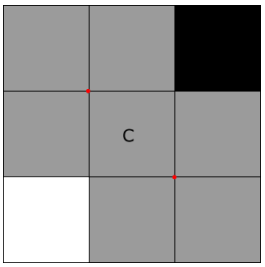

Figure B.29: A complex pixel C with auxiliary points at two vertices of C located opposite of one another must sit in a configuration as the one above.

Now pick a point $p \in \gamma_C$, and look at the vertical line in $C \cup D$ through p. Since this line has endpoints of different colours, it must contain a point $q \in \partial X$. By Lemma B.25 again, q must belong to the set of points in $C \cup D$ that are no further than $\frac{d}{2}$ from the common edge e of C and D, and by Lemma B.46 p is no further than $0.133d$ from e. Hence p and q cannot be further than $0.55d < d$ from each other. □

Lemma B.53. *Consider a complex pixel C with two auxiliary points located at vertices of C diagonally opposite each other. Then no point of γ_C is further away from ∂X than d.*

Proof. A pixel C as in this lemma must sit in a configuration as the one in Figure B.29, by means of Lemma B.22. Let p_1 and p_2 denote the two auxiliary points on the boundary of C.

A calculation shows that any circle arc through p_1, p_2 and an auxiliary point neighbouring p_2 has radius greater than d. Hence any such circle arc is contained in the spindle $S(L, d)$ where L is the line segment between p_1 and p_2, by Lemma B.15. By the same lemma, this means that any such circle arc γ_1 is contained in any ball of radius d containing L. The same holds for the area bounded by the two circle arcs γ_1 and γ_2 (since $S(L, d)$ is also convex), and hence also for γ_C. Thus, if we can find some point q in ∂X such that the d-ball around q contains L and hence $S(L, d)$ as well as γ_C, then any point of γ_C must be closer than d to ∂X.

Consider the line M connecting the black and white vertex of C. Since its endpoints have different colours, it must contain some point $q \in \partial X$. Since the distance between any point in M and p_1, p_2 is less than d everywhere, the ball $B_d(q)$ contains p_1 and p_2 and hence the spindle $S(L, d)$ between them, and we are done. □

Lemma B.54. *Suppose C is a complex pixel with an auxiliary point on one of its edge midpoints and another auxiliary point at one of the vertices of C. Then any point of γ_C is closer than d to ∂X.*

Proof. A pixel as the one in this lemma must sit in a configuration as the one shown in Figure B.30.

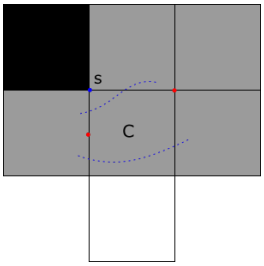

Figure B.30: A complex pixel as the one in Lemma B.54 must sit in a configuration as the one above. Then ∂X must either intersect the upper edge of C (the upper blue dashed line), or it must intersect the right vertical edge of C (the lower blue line).

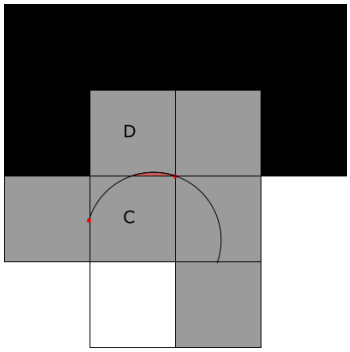

Figure B.31: The only case where γ_C may not stay inside C is when C sit in a configuration as the one above. In this case, the part of γ_C inside D must belong to the red set.

There are two cases: Either γ_C is contained in C or it is not.

Suppose first that $\gamma_C \subseteq C$. Note that ∂X must intersect the left vertical edge of C once, since the endpoints of this edge has different colours. It cannot intersect the edge multiple times by Lemma B.19. Let q_1 be the intersection between the left vertical edge of C and ∂X.

Now, ∂X must intersect the boundary of C in at least two points, one of which is q_1. Suppose that ∂X intersects C somewhere on the upper edge of C, say in a point q_2. Let L be the line between q_1 and q_2. Then by Corollary B.16 there is a path $\pi(L)$ in ∂X from q_1 to q_2 contained in $S(L, r)$, and by changing q_2 if necessary, we may assume that $\pi(L)$ does not intersect the upper edge of C except at q_2, hence it stays inside C. Let s be the upper left vertex of C.

Since $B_d(s)$ contains the left and upper edge of C, it contains both q_1, q_2 and hence L. Since $d < r$, this also means that it contains $S(L, r)$ by Lemma B.15, hence it contains the path $\pi(L)$. It also contains γ_C, which can be seen by considering the possible cases in Figure B.20.

Now, take any point p on γ_C. Then it belongs to a radius of $B_d(s)$. Since $\pi(L)$ runs from one side of C to another inside $C \cap B_d(s)$, there must also be a point q on $\pi(L)$ lying on the same radius of $B_d(s)$ as p. But then q and p can be no further than d apart, so the lemma is true in this case.

If on the other hand γ_C belongs to C, but there are no points of ∂X on the upper edge of C, then there must be a point $q_2 \in \partial X$ on the right edge of C. Let L be the line between q_1 and q_2. By Corollary B.16, there must be a path $\pi(L)$ in ∂X connecting q_1 and q_2, and this path can nowhere intersect other edges of C.

Again pick a point p in γ_C, and look at the vertical line in C containing p. This line must be intersected by $\pi(L)$ in some point q, since $\pi(L)$ connects the two sides of C. But then $p \in \gamma_C$ and $q \in \partial X$ both lie on the same line of length d, hence they can be no further than d apart, as claimed. This concludes the proof in the case where γ_C is contained in C.

Finally, assume γ_C is not contained in C. Then one of the curve segments γ_1 and γ_2 are not contained in C - let us say it is γ_1. Copying the results from before, we see that all points of γ_C inside C are closer than d to some point of ∂X, so it remains to

show this for points of γ_C outside C. Such points must lie in the set A bounded by γ_1 and one of the edges of C (the red set in Figure B.31).

Notice that the only case where the curve segment γ_1 is not contained in C is when C sit in a configuration as the one in Figure B.31. Let D be the pixel above C in this configuration.

The boundary ∂X must intersect the boundary of D at least twice in order for D to be grey. By Lemma B.19, ∂X cannot intersect the right boundary of D twice. Hence it must intersect the common edge e of C and D at least once, say in a point q.

Now, a calculation shows for any point $q' \in e$, the ball $B_d(q')$ contains all of A. In particular, the ball $B_d(q)$ contains all of A and hence any point of γ_C in D, so any such point can be no further away from ∂X than d. This concludes the proof. □

Proof of Theorem B.49. The curve γ consists of a curve segments γ_C for each pixel C with two auxiliary points on its boundary. Hence the theorem follows from the Lemmas B.50, B.51, B.52, B.53 and B.54.

Furthermore, for any point x in γ, there is a point y' in ∂X that is no further than a distance d from x, meaning that

$$\inf_{y \in \partial X} d(x, y) \leq d(x, y') \leq d.$$

Thus we get

$$\sup_{y \in \gamma} \inf_{x \in \partial X} d(x, y) \leq d.$$

□

Corollary B.55. *The reconstructed boundary γ is closer than d to the boundary of X.*

Proof. Combining Theorems B.45 and B.49, we get that

$$\sup_{y \in \gamma} \inf_{x \in \partial X} d(x, y) \leq d \text{ and } \sup_{x \in \partial X} \inf_{y \in \gamma} d(x, y) \leq d,$$

hence

$$d_H(\gamma, \partial X) = \max\big(\sup_{y \in \gamma} \inf_{x \in \partial X} d(x, y), \sup_{x \in \partial X} \inf_{y \in \gamma} d(x, y)\big) \leq d.$$

□

B.6 Homeomorphism between Object and Reconstruction

Let us now finish the proof of Theorem B.6. We need to show that there is homeomorphism taking the reconstructed set Γ to the original set X. To do so, let us start with a lemma:

Lemma B.56. *Let $M \subseteq \mathbb{R}^2$ be a set homeomorphic to $S^1 \times [-1, 1]$, and let $m \subseteq M$ be the subset homeomorphic to $S^1 \times \{0\}$. Let $\gamma : S^1 \to M$ be a closed curve. Then there is a homeomorphism $f : \mathbb{R}^2 \to \mathbb{R}^2$ taking γ to m fixing points in the unbounded component of $\mathbb{R}^2 \setminus M$.*

Proof. Since there exists a homeomorphism of $\mathbb{R}^2$ taking the outer boundary component M_o of M to the unit circle by Schoenflies' Theorem, we may assume that M_o is the unit circle. By the Annulus Theorem, the set A between M_o and γ is homeomorphic to the annulus $S^1 \times [\frac{1}{2}, 1]$ – let g denote this homeomorphism. We may assume that g is the identity on M_o – if this is not the case, then after reversing the orientation of the map $g|_{M_o}$ if necessary there is an isotopy from $g(M_o)$ to M_o which we may extend to an ambient isotopy of A in a small tubular neighbourhood of $g(M_o)$ in M, and composing the result of this isotopy with g we get a homeomorphism that is the identity on M_o.

We may continuously extend g to a map g_1 of all of $\mathbb{R}^2$ by extending it by the identity on the unbounded component of M_o^C (since the map $g|_\gamma \to g(\gamma)$ may be extended to a map of the disc bounded by γ) . Thus we get a map $g_1 : \mathbb{R}^2 \to \mathbb{R}^2$ taking γ to $\frac{1}{2}S^1$ and fixing points in the unbounded component of $\mathbb{R}^2 \setminus M_o$.

Repeating the above with γ replaced by m, we also get a map $g_2 : \mathbb{R}^2 \to \mathbb{R}^2$ taking $S^1 \times \{0\}$ to $\frac{1}{2}S^1$. Hence the composition $g_1^{-1} \circ g_2 : \mathbb{R}^2 \to \mathbb{R}^2$ takes $S^1 \times \{0\}$ to γ and fixes points in the unbounded component of M_o. □

Theorem B.57. *There is a homeomorphism $H : \mathbb{R}^2 \to \mathbb{R}^2$ taking X to Γ. Hence X and Γ are weakly d-similar.*

Proof. Note that by Theorem B.42 γ separates black pixels from white ones, and there is a 1-1 correspondence between components of ∂X and components of γ.

Consider an outermost component $\partial X'$ of ∂X. Since $\partial X'$ is a manifold of dimension 1, it is homeomorphic to S^1. Thus its tubular neighbourhood $N_{d\sqrt{2}}(\partial X')$ is homeomorphic to $S^1 \times [-1, 1]$ (see [1], Proposition A.10) via a map h that takes the points of each normal line of length $2\sqrt{2}$ to a fiber $\{x\} \times [-1, 1]$ in $S^1 \times [-1, 1]$, and takes $\partial X'$ to $S^1 \times \{0\}$. Moreover, $h^{-1}(S^1 \times \{-1\})$ is a subset of the set of white pixels, and $h^{-1}(S^1 \times \{-1\})$ is a subset of the black pixels. Since the boundary γ of the reconstructed set Γ separates black and white pixels, this means that there is a component γ' of γ in $N_{d\sqrt{2}}(\partial X')$.

Then by Lemma B.56 there is a homeomorphism $f_1 : \mathbb{R}^2 \to R^2$ taking γ' to $\partial X'$ and fixing points in the unbounded component of $h^{-1}(S^1 \times \{1\})$. Since $\partial X'$ and γ' both separates black pixels from white, any component of ∂X inside $\partial X'$ also lies inside γ'. Hence f_1 also takes any component of ∂X inside $\partial X'$ to the inside of γ'.

Applying the above technique to the other components of ∂X, we thus get a series of homeomorphisms $f_1, f_2, \ldots, f_n$ that each takes one component ∂X_i of ∂X to a component γ_i of γ. Since each homeomorphism fixes the points of the unbounded component of ∂X_i^C, the composition $f_n \circ \cdots \circ f_1 : \mathbb{R}^2 \to \mathbb{R}^2$ that starts by mapping the outer component(s) of ∂X to γ and then works its way in, sends ∂X to γ. Since it also sends bounded sets to bounded sets and Γ was the bounded set bounded by γ and X was compact, this means that $H := f_n \circ \cdots \circ f_1$ takes X to Γ.

Since there is a map of $\mathbb{R}^2$ taking X to Γ, and since $d_H(\partial X, \gamma) \leq d$ by Corollary B.55, they are weakly d-similar. □

B.7 Example of the reconstruction algorithm

Example B.58. An example of this algorithm is shown in Figure B.32. In this figure, we used the bump function

$$\varphi(t) = \begin{cases} 1 & \text{if } x = 0, \\ 0 & \text{if } x = 1, \\ 1 - \dfrac{1}{1 + \exp(\frac{6}{7x} - \frac{6}{7-7x})} & \text{otherwise.} \end{cases}$$

It seems from our example that the curves ∂X and γ may be even closer than d.

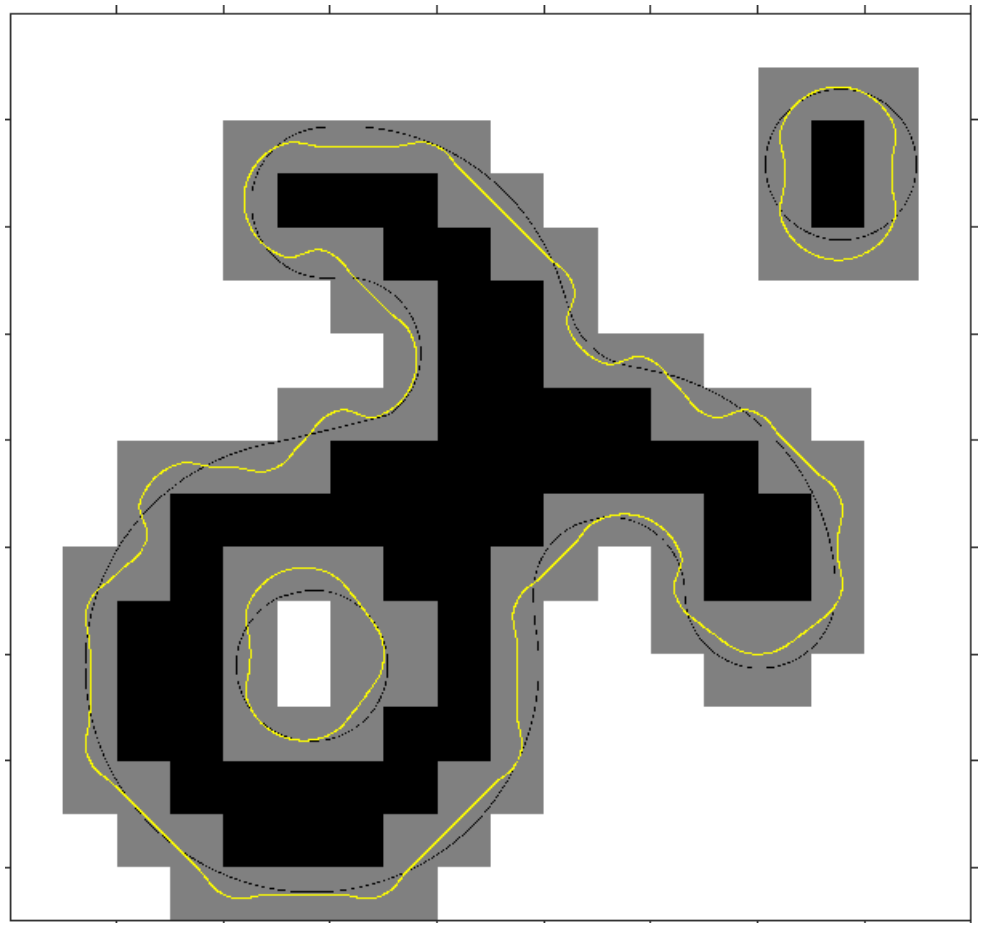

Figure B.32: Example of the algorithm: The thin black line is the outline of the original r-regular set, from which the image came. The yellow line is the reconstructed boundary of the original set.

B.8 Conclusion

In this paper we have presented restrictions on pixel configurations in digital images of r-regular objects at a reasonable resolution. We have used these restrictions to reconstruct the original object by constructing an object with smooth boundary that

is weakly d-similar to the original object (where d is the side length of each pixel). This tells us that our reconstruction is not far from the original object and has the right topology, and though that ensures that the sets are not fundamentally different, sadly it is not quite enough to cover all aspects of human perception of similarity, as discussed in [8], [6].Ongoing work is aiming at showing that the reconstructed object is in fact strongly s-similar to the original one for a suitable s.

We do by no means believe that a Hausdorff distance of d between the original object and our reconstructed object is the optimal – in fact, we are working on obtaining even stronger bounds on their Hausdorff difference. We also believe that taking the actual intensities of each pixel into account can result in even more precise reconstruction, though there is still a lot of work to be done before we are ready to prove this.

The object that our reconstruction method outputs will in general not be r-regular. We may, since the boundary of the reconstructed set consists of the join of finitely many curve segments, calculate the maximal curvature of a reconstructed set – but note that a maximal curvature or $\frac{1}{s}$ is not enough to ensure that our reconstructed set is s-regular. Thus we have left the question of regularity of the reconstruction out of this paper, though it is also be an interesting aspect of the reconstruction process.

B.9 Appendix: Proofs of the lemmas from Section B.3

We here include the proofs that were omitted in Section B.3. To lighten the notation, we will measure distances in units of d, so that each grid square has side length 1, and the assumption $r > d\sqrt{2}$ becomes $r > \sqrt{2}$. Note that if X is r-regular and $r > \sqrt{2}$, X is in particular $\sqrt{2}$-regular (cf. [1], Proposition A.2).

Proof of Lemma B.19. Let x and y be two points on a line of length $|l| < 2\sqrt{2}$ and let L be the line segment between them.

Since the distance from x to y is less that $2\sqrt{2}$, there must be a path $\pi(L)$ in ∂X between them, where π is the projection onto ∂X, see Section B.2. Since ∂X is a C^1-manifold and the projection is continuous and fixes the endpoints, there must be a point p on $\pi(L)$ such that the tangent to ∂X at p is horisontal. Let $p = (p_1, p_2)$. Since $p \in \partial X$ and X is an $\sqrt{2}$-regular set, there are balls $B_{\sqrt{2}}(x_b) \subseteq X$ and $B_{\sqrt{2}}(x_w) \subseteq X^c$ such that $\overline{B_{\sqrt{2}}(x_b)} \cap \overline{B_{\sqrt{2}}(x_w)} = \{p\}$, and since the tangent to ∂X at p is horisontal, the centres x_b and x_w must lie on the vertical line through p.

Note that $p \in \pi(L) \subseteq S(L, \sqrt{2})$. By Lemma B.14, the thickness of $S(L, \sqrt{2})$ is $\sqrt{2} - \sqrt{2 - \frac{L^2}{4}} \leq \sqrt{2} - \sqrt{2 - \frac{|l|^2}{4}}$. So $d(p, L) \leq \sqrt{2} - \sqrt{2 - \frac{|l|^2}{4}}$. Then

$$d(x_b, L) \leq d(x_b, p) + d(p, L) \leq 2\sqrt{2} - \sqrt{2 - \frac{|1|^2}{4}}$$

and

$$d(x_b, L) > d(p, x_b) - d(p, L) > \sqrt{2} - (\sqrt{2} - \sqrt{2 - \tfrac{|l|^2}{4}}) = \sqrt{2 - \tfrac{|l|^2}{4}}$$

If $|l| = 1$ this means that $d(x_b, L) \leq 1.51$ and $d(x_b, L) > 1$. So if we name the pixels as in Figure B.4, this means that x_b belongs to either A or D in this case – let us say D. Then D must be black. In fact, since the first and last inequalities are sharp, the common edge of B and C must be interior points of X, and hence it contains no intersection points. A symmetric argument for x_w shows that x_w must belong to A,

hence A must be white, and that the common edge of A and B cannot contain any points of ∂X.

If $l = 2$, then in $d(x_b, L) \leq 2\sqrt{2} - 1$ and $d(x_b, L) > 1$. Name the pixels as in Figure B.4. If $p \in B_1 \cup C_1$, then the centres c_b, c_w of the white and black balls must belong to A_1 and D_1, respectively, since they lie on a vertical line through p. Similarly if $p \in B_2 \cup C_2$, then the centres c_b, c_w of the white and black balls must belong to A_2 and D_2, respectively.

If ∂X is tangent to l at a point p', replacing p with p' in the above argument shows the result. □

Proof of Lemma B.20. Let us name the two grey pixels in the configuration B and C as in the right part of Figure B.5. Choose boundary points $x_C \in C$ and $x_D \in D$. Both of these points are contained in a ball $B_{\sqrt{5}/2}(p)$, where p is the midpoint of the common edge e of pixel B and C. By Corollary B.16 and Lemma B.15 applied to the projection π instead of ρ, there is a path γ in ∂X from x_C to x_D contained in $B_{\sqrt{5}/2}(p)$. This path must pass the line containing e, and since it cannot do so if passing this line means entering a black pixel, it must in fact pass the edge e. The endpoints of e are both black, hence if ∂X passes e once, it must also pass e a second time, as ∂X separates black points from white ones.

But then by Lemma B.19 A must be black and D must be white (it cannot be the other way around, because then a black and a white pixel would share a corner, meaning that ∂X passes through that corner – which is against our assumptions). □

Proof of Lemma B.21. Let c be the centre point of the grey pixel C. Assume $c \in X$ (the other case is similar). Then c belongs to a black ball of radius $\sqrt{2}$ by Proposition B.8, hence the centre of this black ball belongs to $B_{\sqrt{2}}(c)$ and thus to either C or one of its neighbours. Since the pixel containing the centre of the black ball must be entirely contained in the black ball, said pixel must be black. Hence one of the neighbours of C must be black. □

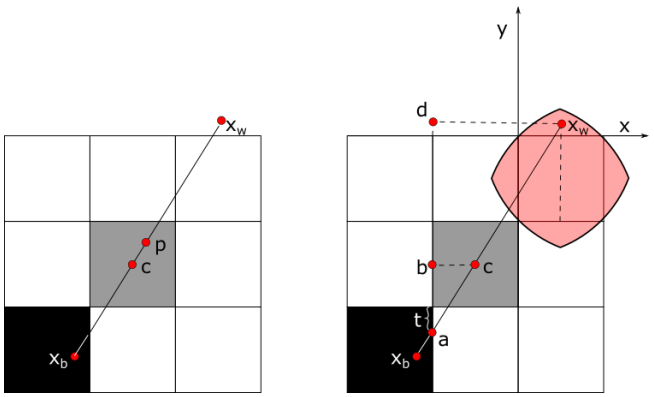

Figure B.33: We aim to show that the centre of the white ball tangent to ∂X at p belongs to the red set Y.

Proof of Lemma B.22. Place the configuration in a coordinate system as in the figure, such that the pixels have side length 1. The aim will be to show that x_w lies so close to the upper right pixel that the white ball $B_r(x_w)$ contains the pixel.

Note first that the line l through x_b and c passes an edge of the black pixel, say the right edge. Let a be this intersection point, see Figure B.33. To study the limit case, we will first assume that $x_b = a$.

Since $d(a,c) < r$, then by rotating the line segment from a to c about c with an angle π one sees that the line segment of length $2r$ from a through c has an endpoint $x_w = (x_1, x_2)$ with $x_1 \geq 0$.

Let b be a point directly above a such that $\angle abc = \frac{\pi}{2}$, and let d be a point directly above a such that $\angle adx_w = \frac{\pi}{2}$, see Figure B.6. Finally, let $t = d(a,b) - \frac{1}{2} \geq 0$.

Now, $\tan(\angle bac) = \frac{d(b,c)}{d(a,b)} = \frac{1/2}{1/2+t} \leq 1$, so $\angle bac \leq \frac{\pi}{4}$. Thus we have that $\frac{d(d,x_w)}{2\sqrt{2}} = \sin(\angle bac) \leq sin\left(\frac{\pi}{4}\right) = \frac{1}{\sqrt{2}}$, so $x_1 = d(d,x_w) - 1 \leq 1$. So $0 \leq x_1 \leq 1$. Also, by rotational symmetry and since $d(a,c) \leq r$, we must have $x_2 \geq -1 + t$.

Let Y be the intersection of the four r-balls with centres $(0,0)$, $(1,0)$, $(0,-1)$ and $(1,-1)$ (the corners of the upper right pixel) – this is the red set in Figure B.34. Then Y is a convex set containing $(0,0)$, $(1,0)$, $(0,-1)$ and $(1,-1)$, and hence the entire upper right pixel. Any point in Y is closer than r to all the points $(0,0)$, $(1,0)$, $(0,-1)$ and $(1,-1)$, so an r-ball with centre in Y contains all of the upper right pixel. Hence we aim to show that $x_w \in Y$.

Notice that the two triangles abc and adx_w are equiangular. Hence

$$\frac{1+x_1}{2\sqrt{2}} = \frac{\frac{1}{2}}{d(a,c)} = \frac{\frac{1}{2}}{\sqrt{(t+\frac{1}{2})^2 + \frac{1}{4}}} \Rightarrow t = \sqrt{\frac{2}{(x_1+1)^2} - \frac{1}{4}} - \frac{1}{2}.$$

Furthermore, we have that

$$8 = (2 + t + x_2)^2 + (1 + x_1)^2,$$

so

$$x_2 = \sqrt{8 - (1+x_1)^2} - 2 - t = \sqrt{8 - (1+x_1)^2} - \frac{3}{2} - \sqrt{\frac{2}{(x_1+1)^2} - \frac{1}{4}}$$

So we may express x_2 as a function of x_1. Since $0 \leq x_1 \leq 1$ and $x_2 \geq -1$, we need only check that x_w lies under the upper border of Y on the interval $[0,1]$, i.e. we must check that $x_2(x_1)$ lies under the function

$$\tilde{f}(x_1) = \begin{cases} \sqrt{2 - (x_1 - 1)^2} - 1 & x_1 \leq \frac{1}{2}, \\ \sqrt{2 - x_1^2} - 1 & x_1 \geq \frac{1}{2}, \end{cases}$$

on $[0,1]$. However, it turns out to be easier to check that $x_2(x_1)$ lies under the graph of the function

$$f(x_1) = \begin{cases} (\sqrt{7} - \frac{1}{2})x_1 & 0 \leq x_1 \leq \frac{1}{2}, \\ -(\sqrt{7} - \frac{1}{2})x_1 + (\sqrt{7} - \frac{1}{2}) & \frac{1}{2} \leq x_1 \leq 1. \end{cases}$$

Note that $f([0,1]) \subseteq Y$, since the image of f is just the union of two line segments, both of which have endpoints in the convex set Y.

To show that x_2 lies somewhere below f, note first that

$$\begin{aligned}
\frac{d^2}{dx_1^2}x_2 = & -\sqrt{8-(x_1+1)^2} - \frac{(x_1+1)^2}{\sqrt{8-(x_1+1)^2}^3} \\
& + \frac{4}{\sqrt{2(x_1+1)^2 - \frac{1}{4}(x_1+1)^4}^3} - \frac{6}{\sqrt{2(x_1+1)^6 - \frac{1}{4}(x_1+1)^8}} \\
\leq & \frac{4}{\sqrt{2(x_1+1)^2 - \frac{1}{4}(x_1+1)^4}^3} - \frac{6}{\sqrt{2(x_1+1)^6 - \frac{1}{4}(x_1+1)^8}} \\
= & \frac{1}{2(x_1+1)^3}\left(\frac{3x_1^2+6x_1-13}{\sqrt{2(x_1+1)^2 - \frac{1}{4}(x_1+1)^4}^3}\right) \\
\leq & 0,
\end{aligned}$$

where the first inequality comes from the fact that the first two terms of the derivative is negative, and the last inequality comes from observing that $3x_1^2+6x_1-13 \leq 0$ on $[0,1]$.

Now, we want to show that $f - x_2 \geq 0$. Note that since f is (piecewise) linear, we get that

$$\frac{d^2}{dx_1^2}(f-x_2) = \frac{d^2}{dx_1^2}(-x_2) \geq 0$$

on $[0,1/2]$ and $[1/2,1]$, so $\frac{d}{dx_1}(f-x_2)$ is increasing. Now,

$$\frac{d}{dx_1}(x_2) = -\frac{1+x_1}{\sqrt{8-(1+x_1)^2}} + \frac{2}{\sqrt{\frac{2}{(1+x_1)^2} - \frac{1}{4}}}\frac{1}{(1+x_1)^3},$$

so on $[0,1/2]$

$$\begin{aligned}
\frac{d}{dx_1}(f-x_2) &= \sqrt{7} - \frac{1}{2} + \frac{1+x_1}{\sqrt{8-(1+x_1)^2}} - \frac{2}{\sqrt{\frac{2}{(1+x_1)^2} - \frac{1}{4}}}\frac{1}{(1+x_1)^3} \\
&\geq \frac{d}{dx_1}(f-x_2)|_{x_1=0} \\
&= \sqrt{7} - \frac{1}{2} + \frac{1}{\sqrt{7}} - \frac{4}{\sqrt{7}} \\
&> 0,
\end{aligned}$$

and on $[1/2,1]$,

$$\begin{aligned}
\frac{d}{dx_1}(f-x_2) &= -\sqrt{7} + \frac{1}{2} + \frac{1+x_1}{\sqrt{8-(1+x_1)^2}} - \frac{2}{\sqrt{\frac{2}{(1+x_1)^2} - \frac{1}{4}}}\frac{1}{(1+x_1)^3} \\
&\leq \frac{d}{dx_1}(f-x_2)|_{x_1=1} \\
&= -\sqrt{7} + \frac{1}{2} + 1 - \frac{1}{2} \\
&< 0.
\end{aligned}$$

So $f - x_2$ is increasing on $[0, 1/2]$ and decreasing on $[1/2, 1]$. Hence, on $[0, 1/2]$

$$(f - x_2)(x_1) \geq (f - x_2)(0) = -\frac{\sqrt{7}}{2} + \frac{3}{2} > 0$$

and similarly, on $[1/2, 1]$

$$(f - x_2)(x_1) \geq (f - x_2)(1) = 0.$$

Putting the last two equations together we see that $f(x_1) - x_2(x_1) \geq 0$ everywhere on $[0, 1]$, so $x_2 \leq f$ as claimed. So if $x_b = a$, then x_w belongs to the set Y.

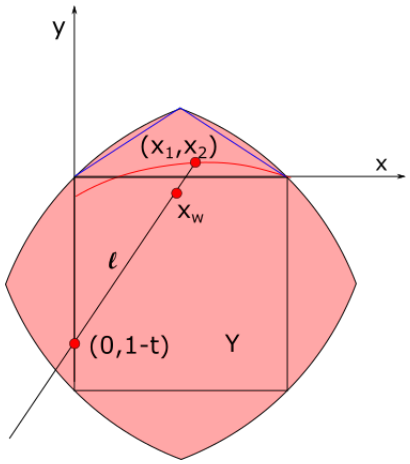

Figure B.34: Close-up on the upper right pixel. The red graph is the graph of $x_2(x_1)$, and the blue graph is the graph of $f(x_1)$. The point (x_1, x_2) on l is chosen such that $d((x_1, x_2), a) = 2r$, and hence x_b lies closer to c than (x_1, x_2) does.

Suppose now that x_b is just any point in the lower left pixel that is closer than $\sqrt{2}$ to c, and suppose that the line l through x_b and c leaves the lower left pixel in a point a on the right pixel edge. Then $(0, 1 - t)$ lies on l and inside Y. By what we just showed, the point (x_1, x_2), $x_1 \geq 0$, on l that is at a distance $2r$ from a is also in Y, hence the entire line segment from $(0, 1 - t)$ to (x_1, x_2) is in Y, since Y was convex, see Figure B.34. But noticing that $r \geq d(a, c) = d(c, (0, 1 - t))$, we get that

$$d(x_b, (0, 1 - t)) = d(x_b, c) + d(a, c) \leq 2r$$

and

$$d(x_b, (x_1, x_2)) = d(x_b, a) + d(a, x_w) \geq d(a, x_w) = 2r.$$

Combining these equations, we see that $d(x_b, (0, 1 - t)) \leq d(x_b, x_w) \leq d(x_b, (x_1, x_2))$. Hence x_w belongs to the line segment between $(0, 1 - t)$ and (x_1, x_2) which was contained in Y, so $x_w \in Y$. □

Proof of Lemma B.24. Let us show (i). Let x and y be corner points of the two pixels as in Figure B.8(a), and let L denote the line between them.

If there are points of X^C in L, then ∂X must either be tangent to X or intersect L in several points (since the endpoints of L clearly all belong to X). By Lemma B.19 this means that either the pixel above C or the pixel below pixel B is white. Both of these pixels share a corner with a black pixel. By the proof of Lemma B.19, the black

corner point must be an interior point of X^C and hence white – a contradiction. So $L \subseteq \mathrm{Int}(X)$.

If B is not black, pick white points $b \in \mathrm{Int}(B)$ and $c \in \mathrm{Int}(C)$. Let L_{bc} denote the line between them. Then there is a path $\rho_{X^C}(L_{bc})$ in $X^C \cup \partial X$ connecting b and c, and this path belongs to all balls of radius less than r that contains both b and c, (cf. Section B.2). In particular, $\rho_{X^C}(L_{bc}) \subseteq B_{\sqrt{2}}(x)$, since this ball contains all of B and all of C.

Let γ be the piecewise linear path from z through x and y to w. Then γ is contained in $\mathrm{Int}(X)$ and separates B from C inside $B_{\sqrt{2}}(x)$. Hence $\rho_{X^C}(L_{bc})$ must intersect γ somewhere, but this is impossible, since $\gamma \subseteq \mathrm{Int}(X)$ and $\rho_{X^C}(L_{bc}) \subseteq X^C \cup \partial X$. So B cannot contain any white points, and hence it must be black.

A similar reasoning can be applied to A: If A is not black, pick a white point $a \in A$, and let L_{ac} denote the line between a and c (where $c \in C$ is the point we chose earlier). Then there is a path $\rho_{X^C}(L_{ac})$ in $X^C \cup \partial X$ connecting a and c, and this path must belong to the ball $B_{\sqrt{2}}(x)$. But since γ also separates A from C inside $B_{\sqrt{2}}(x)$, $\rho_{X^C}(L_{ac})$ must intersect γ somewhere. However, this is impossible, since $\gamma \subseteq \mathrm{Int}(X)$ and $\rho_{X^C}(L_{ac}) \subseteq X^C \cup \partial X$ as before. So A cannot contain any white points, and hence it must also be black.

The second part of this proof also proves (ii). To prove (iii), we apply Lemma B.22 to argue that one of the pixels A_1, A_2, A_3, B_1, B_2, B_3 is black.

Indeed, suppose none of the pixels A_1, A_2, A_3, B_1, B_2, B_3 were black. Then A_1, A_3, B_1 and B_3 would have to be grey, since black and white pixels cannot be neighbours by assumption. But then by Remark B.23, either A_2 or B_2 would have to be black – a contradiction. So at least one of the pixels A_1, A_2, A_3, B_1, B_2, B_3 has to be black. If A_1, A_3, B_1 or B_3 is black, we are in situation (i) and may use this proof to complete the proof of (iii). If A_2 is black, and neither A_1 nor A_3 is black, Lemma B.20 shows that both B_1 and B_3 is black, and we are again in the situation of case (i). If A_2 and either A_1 or A_3 is black, we are in the situation of case (i). The proof works equivalently if B_2 is black. This proves (iii). □

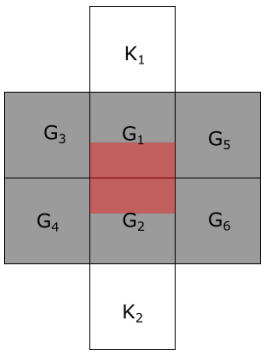

(a) We consider 2×3 grey pixels and wish to show that $\partial X \cap (G_1 \cup G_2)$ belongs to the red set in the figure, and that one of the pixels K_1, K_2 must be black, the other one white.

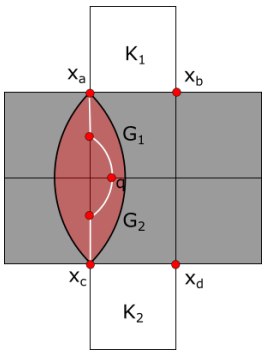

(b) If both K_1 and K_2 were white, then points x_a and x_c would be joined by a path in $X^C \cup \partial X$, and so would points x_b, x_d.

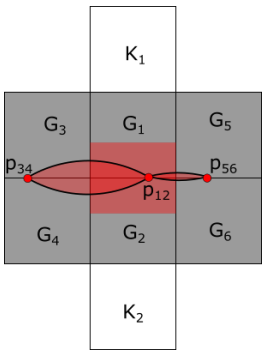

(c) The projection π yields a path γ in ∂X from p_{34} through p_{12} to p_{56}, and this path lives inside the spindles between points p_{34} and p_{12}, and points p_{12} and p_{56}.

Proof of Lemma B.25. Let us start by discussing (i).

Consider G_1 as in Figure B.35(b), and look at the configuration of 3×3 pixels with G_1 as the centre pixel. Then all but the three upper d-neighbours of G_1 are grey. By Remark B.23, the upper d-neighbour K_1 of G_1 cannot be grey, hence it must be either black or white. By the same reasoning, K_2 must be either black or white.

It remains to prove that K_1 and K_2 cannot have the same colour, so suppose that K_1, K_2 are both white. Let x_a, x_b be the lower corners of K_1 and x_c, x_d the upper corners of K_2, as in Figure B.35(b). Note that these points are all elements of $X^C \cup \partial X$.

Let L_{ac} be the line segment between x_a and x_c, and let L_{bd} be the line segment between x_b and x_d. Since $d(x_a, x_c) = d(x_b, x_d) = 2 < 2\sqrt{2}$, the map ρ maps these line segments to continuous paths in $X^C \cup \partial X$ by projecting points of $\mathrm{Int}(X)$ to ∂X and fixing all other points.

Now, L_{ac} and L_{bd} cannot both be contained entirely in $\overline{X^C}$, since this would imply that ρ_{X^C} kept them fixed. But since G_1, G_2 were grey, they must contain a point of $\mathrm{Int}(X)$ which in turn would belong to some black r-ball $B_r(x) \subseteq X$. However, an interior point of such an r-ball would have to intersect the boundary of $G_1 \cup G_2$, which hence cannot be a subset of $X^C \cup \partial X$.

So assume that ρ_{X^C} does not fix L_{ac}. Then there is a point q on L_{ac} that belongs to $\mathrm{Int}(X)$, hence since x_a, $x_c \in X^C$, there must be a point in ∂X on the line segment between x_a and q, and another point in ∂X on the line segment between q and x_c. But then ∂X intersects L_{ac} twice, so by Lemma B.19, either pixel G_5 or G_6 is not grey – a contradiction. Therefore K_1 and K_2 cannot have the same colour, completing the proof of (i).

For (iii), let N be the line separating the upper three grey pixels from the lower three grey pixels. We wish to prove that ∂X intersects N on the common edge of G_i and G_{i+1}, for $i = 1, 3, 5$.

Let again L_{ac} be the vertical line separating G_3 and G_4 from the other grey pixels, and similarly, let L_{bd} be the vertical line separating G_5 and G_6 from the others. Pick a boundary point x_i in each of the grey pixels G_i, $i = 1, \ldots, 6$, and let L_{ij} be the line segment joining x_i and x_j, $i, j = 1, \ldots, 6$.

Using the projection $\pi : N_r \to \partial X$, we know that there is a path $\pi(L_{12})$ in ∂X from x_1 to x_2, and this path must necessarily cross N somewhere. If it passes L_{ac} on the way, it must do so at least twice. By Lemma B.19, this would imply that either G_5 or G_6 would not be grey, which yields a contradiction. Hence $\pi(L_{12})$ does not intersect L_{ac}, and by a symmetric argument, it does not intersect L_{bd} either. So it must intersect N at a point p_{12} on the common edge of G_1 and G_2.

A similar argument shows that the line segments $\pi(L_{34})$ must intersect N in a point p_{34} on the common edge of G_3 and G_4, and that $\pi(L_{56})$ intersects N in a point p_{56} on the common edge of G_5 and G_6, respectively. This proves (iii).

For (ii), note that we have three points p_{12}, p_{34} and p_{56} of ∂X on N. Using the projection on the line segments between them, we get a path γ in ∂X from p_{34} through p_{12} to p_{56}, and this path must live inside the spindles $S(p_{12}, p_{34}, \sqrt{2})$, and $S(p_{12}, p_{56}, \sqrt{2})$, see Figure B.35(c).

Since the maximum height of such a spindle is $\sqrt{2} - 1$, then γ must belong to the red part of the pixels $G_1 \cup G_2$. Note that there cannot be any other elements of ∂X in $G_1 \cup G_2$ than those of γ, because ∂X can only intersect each of the lines L_{ac} and L_{bd} once by Lemma B.19, and these two points of intersection must be exactly

the ones on γ.

So since the path γ belongs to the red part of $G_1 \cup G_2$, the proof is complete. □

Proof of Lemma B.26. Suppose this configuration did occur, and look at the 3×3-configuration that also includes the three pixels to the right of it (see Figure B.10, right). Not all of the red pixels can be grey, since this would violate Lemma B.22 and Lemma B.21. Hence one of them must be another colour, say black.

If the upper red pixel were black, Lemma B.20 would require the bottom grey pixel to be white – a contradiction.

If the middle red pixel were black, then by the first part of Lemma B.24 one of the grey ones in the middle column of the configuration would be so, too – a contradiction again.

If the bottom red pixel were black, then by the third part of Lemma B.24 one of the grey ones in the middle column of the configuration would be so, too – yet another contradiction.

Hence there can be no legal way to colour the red pixels, so this configuration cannot occur. □

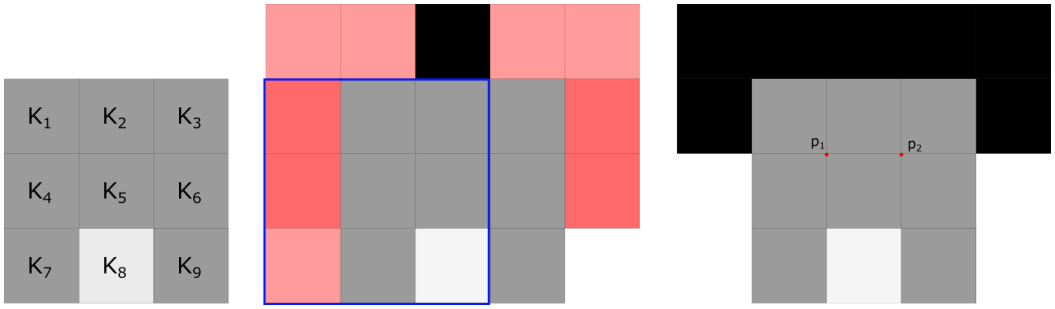

Figure B.36: The configuration to the left in this figure cannot occur in the image of an r-regular object with $d\sqrt{2} < r$. As a first part of the proof, we aim to show that the configuration is part of a larger configuration looking like the one on the right.

Proof of Lemma B.27. Before we go on to the proof, we will state and prove the following lemma for later use:

Lemma B.59. *Let $v_1, \dots v_n \in \mathbb{R}^2$ and let $A = \operatorname{conv}(v_1, \dots, v_n)$. Let $r > 0$. Then $\bigcap_{x \in A} B_r(x) = \bigcap_{i=1}^n B_r(v_i)$.*

Proof. It is clear that $\bigcap_{x \in A} B_r(x) \subset \bigcap_{i=1}^n B_r(v_i)$, since $v_i \in A$ for all i. Hence we need to show the other inclusion.

Let $p \in \bigcap_{i=1}^n B_r(v_i)$, and $x \in A$. We aim to show that $p \in B_r(x)$. Since $x \in A$, we may write x as $x = \sum_{i=1}^n \alpha_i v_i$ for a set of scalars $\alpha_i \geq 0$ satisfying $\sum_{i=1}^n \alpha_i = 1$. Then

$$\|x - p\| = \left\|\sum_{i=1}^n \alpha_i v_i - p\right\| = \left\|\sum_{i=1}^n \alpha_i v_i - \sum_{i=1}^n \alpha_i p\right\| \leq \sum_{i=1}^n \alpha_i \|v_i - p\| \leq \sum_{i=1}^n \alpha_i r = r,$$

since $p \in B_r(v_i)$ for all i. This shows that $p \in B_r(x)$ for arbitrary $x \in A$, hence $p \in \bigcap_{x \in A} B_r(x)$. ■

Now we turn to the proof of Lemma B.27.

Suppose the configuration did occur. Let us first argue that then it must be a part of a larger configuration looking like the one in Figure B.36, right. Let us name the pixels as in Figure B.36, left.

Since the top 2×3 pixels $K_1 - K_6$ are grey and K_8 is white, the upper d-neighbour of K_2 must be black by Lemma B.25, as indicated in Figure B.36 centre.

Similarly, look at the 3×3 configuration centred at K_4 (this is the one with the blue frame in Figure B.36, middle). This configuration has a grey centre and a white corner pixel. Combining Remark B.23 and Lemma B.24, this means that either left d-neighbour of K_1 or the left d-neighbour of K_4 (the two darker red pixels in the figure) must also be black. The equivalent is true for the 3×3 configuration centred at K_6. By Lemma B.24 (i) or (iii), if one of the two dark red pixels to the left is black, then the upper dark red pixels must be black, and so must the 4 red pixels in the top row in Figure B.36, middle, too. So if the configuration did occur in a digital image, it would have to sit in a configuration like the one in Figure B.36, right.

Now, consider the two red points p_1 and p_2 at the top corners of the centre pixel K_5 in Figure B.36 right. These cannot be black: If they were, then ∂X must intersect one of the edges of K_1 and K_3 at least twice, which would violate Lemma B.19. So they must both be white.

Now, since all corners of the centre pixel K_5 are white and the pixel itself is grey, the boundary ∂X must intersect at least one edge of K_5 at least twice. It cannot be the bottom edge, and it cannot be either of the two vertical edges either by Lemma B.19, so ∂X must intersect the line between p_1 and p_2 at least twice. We now aim to show that this line is in fact contained in the set of white points, so that it cannot contain any points of ∂X, giving us a contradiction.

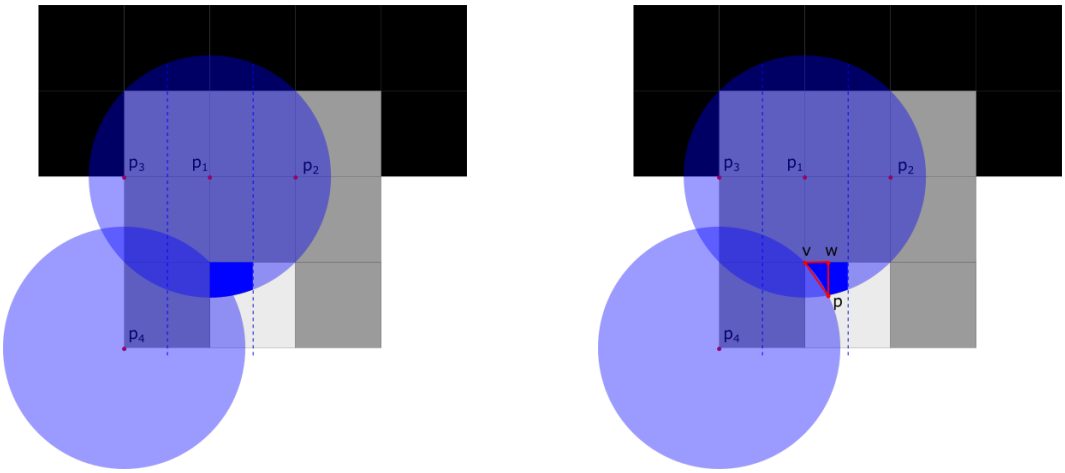

Figure B.37: Left: Since p_1 is white, it must lie in a white $\sqrt{2}$-ball B centred somewhere inside $B_{\sqrt{2}}(p_1)$ (the blue circle). Since B contains neither p_2 nor p_3, the centre of B must lie between the two dashed lines. Right: A point in the left part of the blue set T' must belong to the triangle with vertices p, v and w.

Since p_1 is white, it is contained in some white $\sqrt{2}$-ball B. The centre of B lies somewhere inside $B_{\sqrt{2}}(p_1)$. Since B cannot contain the black corner p_3 of K_1 (see Figure B.37 left), its center must lie closer to p_1 than to p_2, hence it must lie to the right of the vertical line midway between the two points. Likewise, B cannot contain

both p_1 and p_2 without also containing the entire line between them, so the centre of B must also lie closer to p_1 than to p_2, that is, to the left of the vertical line midway between the two points.

Finally, the centre of B can only belong to a white pixel. Hence it must belong to the bright blue part of the white pixel in Figure B.37, left. Let us call this set T.

Next, consider the grey pixel K_7, and let p_4 be its lower left corner. Since T is a part of the upper left quarter of K_8, a point in T is further from p_4 than from any of the other three corners of K_7. Hence if the white ball B contained p_4, it would contain all of K_7 which would then not be grey. So the centre of B must lie further away from p_4 than $\sqrt{2}$, hence outside the ball $B_{\sqrt{2}}(p_4)$. Let $T' = T \setminus B_{\sqrt{2}}(p_4)$, the blue set in Figure B.37, right.

By calculating the intersection p between the boundaries of $B_{\sqrt{2}}(p_1)$ and $B_{\sqrt{2}}(p_4)$ inside the white pixel K_8, we find that they intersect in a point that is a distance $\frac{1}{10}(2\sqrt{15} - 5) \approx 0.27$ from the left edge K_8 and a distance $\sqrt{3/20} \approx 0.39$ from the top edge of K_8.

Let m be the midpoint of the line between p_1 and p_2. A calculation shows that $d(p, m) < \sqrt{2}$, so $m \in B_{\sqrt{2}}(p)$. Any point of T' to the right of p is closer to m than p is, so any ball centred here must also contain m.

Consider a point in T' left of p. Such a point must be contained in the triangle with corners p, v and w as seen in Figure B.37, right. Here v is the upper left vertex of K_8, and w is the point on the edge K_8 that is directly above p. A calculation shows that $m \in B_{\sqrt{2}}(p) \cap B_{\sqrt{2}}(v) \cap B_{\sqrt{2}}(w)$, which by Lemma B.59 means that m belongs to $B_{\sqrt{2}}(x)$ for any x in the left part of T'. Since the same was true for any point right of p, m belongs to $B_{\sqrt{2}}(x)$ for any $x \in T'$. But since p_1 also belongs to $B_{\sqrt{2}}(x)$ for any x in T', any white ball containing p_1 also contains m, and hence the line segment from p_1 to m.

Repeating this argument for p_2, any white ball containing p_2 also contains m, and hence it contains the entire line segment from m to p_2.

But then each point on the line segment from p_1 to p_2 is contained in a white ball – a contradiction. □

Proof of Theorem B.28. Combining Lemmas B.24, B.19, B.20, B.21, B.22, B.26 and B.27, we get the result with the exception of the configuration located at $(23, 17)$ in Figure B.3. But this configuration is also impossible: Let C be the grey centre pixel. C must contain some boundary point $p \in \partial X$, so there would have to be a white ball of radius r tangent to ∂X at p. But such a ball would have to contain points of one of the black pixels around C – a contradiction. □

Proof of Lemma B.29. Look at the centre point c of the 4×4 pixels. Suppose it is white (the case where it is black is symmetric). Then one of the grey pixels having c as a vertex has only white vertices (in the figure, it would be the lower left pixel). Call this pixel A.

Since A s grey, the boundary ∂X must intersect one of its edges, and since all of its corners are white, an edge intersected by ∂X must be intersected at least twice. Note that only the edges of A that are shared with another grey pixel can be intersected by ∂X. But then by Lemma B.19, one of the grey pixels in the figure would have to be non-grey – a contradiction. So this configuration cannot occur. □

Proof of Lemma B.30. The proof follows from Lemma B.25: Look at the two pixels in the column to the right of the configuration (the red ones in Figure B.15, right). These cannot both be grey, since that would violate Theorem B.25, so at least one of them must have another colour. Say that one of them is black (the other case is symmetric). Depending on which one of the red pixels is black, some part of Lemma B.24 tells us that the 2×4 configuration in Figure B.15 must have more black pixels than what is the case – a contradiction. So the configuration cannot occur. □

Proof of Lemma B.31. Let C denote the 2×2 configuration of grey pixels. By Lemma B.19, if any edge of C is intersected by ∂X multiple times, then one of the pixels in C would not be grey – a contradiction. So if ∂X intersects all edges of C, it only intersects each edge once. Hence C has two black vertices on one diagonal and two white vertices on the other. Let L be the line connecting the black vertices and M the line connecting the white vertices.

There is a black path $\rho_X(L)$ in X connecting the two black corners of the pixel. By Corollary B.16 and Lemma B.15, this path must belong to $B_{\sqrt{2}}(p)$, where p is the centre of C.

Similarly, there is a path $\rho_{X^C}(M)$ in $X^C \cup \partial X$ connecting the two white vertices and contained in $B_{\sqrt{2}}(p)$. If $\rho_{X^C}(M)$ contains points of ∂X, we may push these points a little along the normal vector field of ∂X to get a path $\tilde{\rho}$ in X^C connecting the white vertices of C. This alteration can be made in the interior of $B_{\sqrt{2}}(p)$ since the endpoints of M are not boundary points, hence $\tilde{\rho}$ is also contained in C.

But then we have a black path in $B_{\sqrt{2}}(p)$ separating the white vertices of C, and a white path in $B_{\sqrt{2}}(p)$ connecting them. This means that the two paths must necessarily intersect each other in a point that must be both black and white – a contradiction. So ∂X cannot intersect all four edges of C. □

Proof of Theorem B.32. Combining Lemmas B.29, B.30 and B.31 yields most of the result. The only configuration remaining is the one centred at $(45, 22)$ in Figure B.13. But this is also not possible: If it where, the middle grey pixels would contain some boundary point $p \in \partial X$. Then there would be a white $\sqrt{2}$-ball with p in its boundary, and such a ball would either be centred inside the 4×4 pixels of the configuration, or in one of the pixels neighbouring the configuration. Since the pixel containing the centre of the white ball is white itself, the white ball cannot be centred inside the configuration. But it also cannot be centred in one of the pixels neighbouring the configuration, since this would mean that a white pixel and a black one were sharing boundary points, which is against our assumption. □

References

[1] Sabrina Tang Christensen. *Reconstruction of topology and geometry from digitisations.* PhD thesis, Aarhus University, 2016.

[2] Pedro Duarte and Maria Joana Torres. Smoothness of boundaries of regular sets. *J. Math. Imaging Vis.*, 48(1):106–113, January 2014. ISSN 0924-9907. doi: 10.1007/s10851-012-0397-0. URL http://dx.doi.org/10.1007/s10851-012-0397-0.

[3] L.J. Latecki, C Conrad, and A Gross. Preserving topology by a digitization process. *Journal of Mathematical Imaging and Vision*, 8, 01 1998.

[4] T. Pavlidis. *Algorithms for graphics and image processing*. Digital system design series. Computer Science Press, 1982. ISBN 9780914894650.

[5] Jean Serra. *Image Analysis and Mathematical Morphology*. Academic Press, Inc., Orlando, FL, USA, 1983. ISBN 0126372403.

[6] P. Stelldinger, L. J. Latecki, and M. Siqueira. Topological equivalence between a 3d object and the reconstruction of its digital image. *IEEE Transactions on Pattern Analysis and Machine Intelligence*, 29(1):126–140, Jan 2007. ISSN 0162-8828. doi: 10.1109/TPAMI.2007.250604.

[7] Peer Stelldinger and Ullrich Köthe. Shape preservation during digitization: Tight bounds based on the morphing distance. In Bernd Michaelis and Gerald Krell, editors, *Pattern Recognition*, pages 108–115, Berlin, Heidelberg, 2003. Springer Berlin Heidelberg. ISBN 978-3-540-45243-0.

[8] Peer Stelldinger and Ullrich Köthe. Towards a general sampling theory for shape preservation. *Image Vision Comput.*, 23(2):237–248, February 2005. ISSN 0262-8856. doi: 10.1016/j.imavis.2004.06.003. URL http://dx.doi.org/10.1016/j.imavis.2004.06.003.

Supplement B

A Stronger Result on the Similarity between An r-regular Object and Its Reconstruction from a Trinary Image

By Helene Svane

BB.1 Introduction

This section was written after the drafted paper in Chapter B, and is intended to be read as a continuation of that paper. Indeed, its main result is a strengthening of the result in Chapter B, and we use the same framework and a portion of lemmas from that chapter.

In their paper *Shape Preservation during Digitisation: Tight Bounds Based on Morphing Distance*, Stelldinger and Köthe discuss how to define a similarity criterion for sets, that capture human perception of set similarity. They come up with two notions, one of which is the weak s-similarity that we already discussed in Chapter B. The other one is called *strong s-similarity*:

Definition BB.1. Let $A, B \subseteq \mathbb{R}^2$ and $s > 0$. The sets A and B are called *strongly s-similar* if there exists a homeomorphism $f : \mathbb{R}^2 \to \mathbb{R}^2$ such that $f(A) = B$ and for all $x \in \partial A$ we have $\|f(x) - x\| < s$.

It is clear from this definition that two strongly s-similar sets are in particular weakly s-similar, hence strong s-similarity is a stronger notion than weak s-similarity.

This chapter will continue to consider trinary images as defined in B.3, of r-regular sets satisfying the convention B.4. Furthermore, we will reconstruct a set Γ from a trinary image in the same way as we did in Section B.4, but we will fix the bump function φ to be

$$\varphi(x) = \begin{cases} \frac{1}{1+exp(\frac{6|L|}{7x} - \frac{6|L|}{7(|L|-x)})} & \text{for } 0 < x < |L| \\ 0 & \text{for } x = 0 \\ 1 & \text{for } x = |L| \end{cases}$$

The aim of this paper will be to prove the following:

Theorem BB.2. *Let Γ be the set reconstructed from the digital image of an r-regular object X, where the pixel side length d of the pixels of the digital image satisfy $d\sqrt{2} < r$. Then Γ and X are strongly $\frac{d}{\sqrt{2}}$-similar.*

The main idea in this proof will be to write the grey pixels as a disjoint union of line segments. Let us define

Definition BB.3. Let $A \subseteq \mathbb{R}^2$ be a bounded set. A *line covering* of A is a partition of A into disjoint line segments with endpoints on the boundary of A.

We will now aim to construct a line covering on the set of grey pixels and show that we may push ∂X to γ along the lines of this line covering in a continuous way. This is only possible after a slight modification of ∂X, as we will elaborate on in a later section.

Before we get to defining the line covering, we need to establish some more basics about pixel configurations in trinary images of r-regular sets.

BB.2 Possible configurations of 4×4 pixels with 2×2 grey centre pixels

The aim of this section is to improve the result in Theorem B.32 on possible 4×4 pixel configurations with 2×2 grey pixels in the middle. This will allow us to divide the remaining 4×4 configurations with 2×2 grey pixels in the middle into categories, such that configurations in the same category share some similar features. We will also prove some small results on pixel configurations in general, which will turn out to be important later.

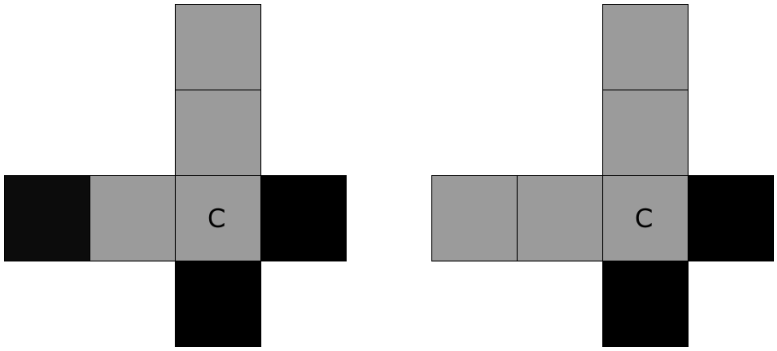

Figure BB.1: The upper left corner of a pixel C sitting in a configuration as the one above must always be white.

Lemma BB.4. *Consider a pixel C sitting in one of the configurations in Figure BB.1, mid or right. Its upper left corner must be white.*

Proof. Consider such a pixel C. If its upper left corner was black, the boundary ∂X would intersect one of the edges of C multiple times: it must intersect the boundary of C in order for C to be grey, and it must intersect each edge of C an even number

of times in order for all of the corners of C to be black. But this is impossible by Lemma B.19. □

Convention BB.5. Unless otherwise stated, we name pixels in a 3×3 or 4×4 configuration as in Figure BB.2.

K_1	K_2	K_3
K_4	K_5	K_6
K_7	K_8	K_9

K_1	K_2	K_3	K_4
K_5	K_6	K_7	K_8
K_9	K_{10}	K_{11}	K_{12}
K_{13}	K_{14}	K_{15}	K_{16}

Figure BB.2: Unless otherwise stated, we name pixels in a 3×3 or a 4×4 configuration as in this figure.

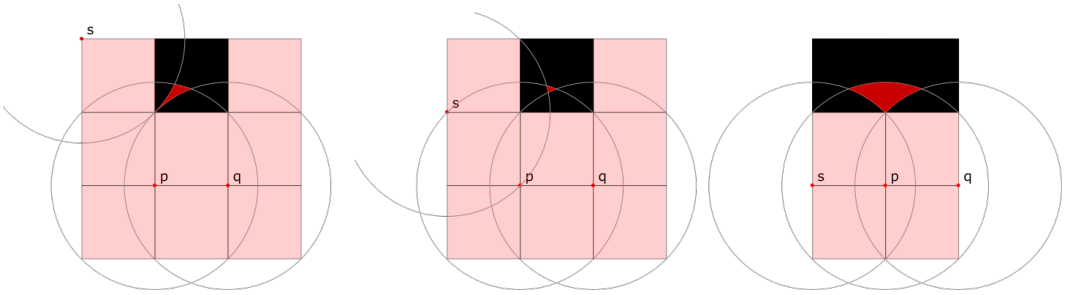

Figure BB.3: For each of these configurations, we aim to find the vertices of a polygon containing the red part of the black pixel

Lemma BB.6. *Consider configurations like in Figure BB.3, where we have a point $p = (0, 0)$ at the origin, and let $q = (d, 0)$. Let K_2 be the black pixel $K_2 := [0, d] \times [d, 2d]$ in Figure BB.3.*

i) For $s = (-d, 2d)$, the set $A_1 := K_2 \cap (B_{\sqrt{2}d}(p)) \setminus (B_{\sqrt{2}d}(s) \cup B_{\sqrt{2}d}(q)))$ is contained in the convex hull of the points $v_1 = (0, d)$, $v_2 = \left(\frac{d}{2}, d\sqrt{2 - \frac{1}{4}}\right)$, $v_3 = \left(\frac{d}{2}, \frac{\sqrt{15}d+10d}{10}\right)$ and $v_4 = \left(\frac{2d\sqrt{15}-5d}{10}, \frac{\sqrt{15}d+10d}{10}\right)$.

ii) For $s = (-d, d)$, the set $A_2 := K_2 \cap (B_{\sqrt{2}d}(p)) \setminus (B_{\sqrt{2}d}(s) \cup B_{\sqrt{2}d}(q)))$ is contained in the convex hull of the points $w_1 = \left(\frac{\sqrt{3}d-d}{2}, \frac{\sqrt{3}d+d}{2}\right)$, $w_2 = \left(\frac{\sqrt{15}d}{10}, \frac{2d\sqrt{15}+5d}{10}\right)$, $w_3 = \left(\frac{d}{2}, d\sqrt{2 - \frac{1}{4}}\right)$ and $w_4 = \left(\frac{d}{2}, \frac{\sqrt{3}d+d}{2}\right)$.

iii) For $s = (-d, 0)$ and $K_1 := [-d, 0] \times [d, 2d]$, the set $A_3 := (K_1 \cup K_2) \cap (B_{\sqrt{2}d}(p) \setminus (B_{\sqrt{2}d}(s) \cup B_{\sqrt{2}d}(q)))$ is contained in the convex hull of the points

$u_1 = (0, d)$, $u_2 = \left(-\frac{d}{2}, d\sqrt{2 - \frac{1}{4}}\right)$, $u_3 = \left(-\frac{13d}{50}, \sqrt{2}d\right)$, $u_4 = \left(\frac{13d}{50}, \sqrt{2}d\right)$ *and* $u_5 = \left(\frac{d}{2}, d\sqrt{2 - \frac{1}{4}}\right)$.

Proof. We start by proving i). Note that a calculation shows that the points v_1, v_2 and v_4 are the intersection points of the three circles $\partial B_{\sqrt{2}d}(p)$, $\partial B_{\sqrt{2}d}(q)$ and $\partial B_{\sqrt{2}d}(s)$ in K_2. Since the line segment from v_1 to v_2 is a secant in $B_{\sqrt{2}d}(q)$, it does not belong to A_1. Similarly, the line from v_1 to v_4 is a secant in $B_{\sqrt{2}d}(s)$, hence it also lies outside A_1. Now v_3 is the point that makes a right angle with v_2 and v_4, which both lie on the boundary of A_1. The line segments from v_2 to v_3 and from v_3 to v_4 both lie outside $B_{\sqrt{2}d}(p)$ by a calculation, hence also outside A_1. So the boundary of the convex hull of v_1, v_2, v_3 and v_4 lies outside A_1. Since the line from v_2 to v_4 lies inside A_1, the convex hull of v_1, v_2, v_3 and v_4 must contain A_1, as claimed.

The proof of ii) is nearly identical to the proof of i). The points w_1, w_2 and w_3 are the intersection points between the three balls $\partial B_{\sqrt{2}d}(p)$, $\partial B_{\sqrt{2}d}(q)$ and $\partial B_{\sqrt{2}d}(s)$ in K_2, and the line segments from w_1 to w_2 and from w_2 to w_3 lie outside A_2. The point w_4 is the point that makes a right angle with w_1 and w_3, and the line segments from w_4 to x_3 and from w_1 to w_4 also lie outside all three balls by a calculation, hence outside A_2. The polygon with vertices w_1, w_2, w_3 and w_4 contains A_2, which proves the claim in this case.

For iii), notice that u_1, u_2 and u_5 are points where the circles intersect, and that u_3 and u_4 and the line between them both lie above any set contained in $B_{\sqrt{2}d}(p)$, so in particular outside A_3. The line segments from u_1 to u_2 and from u_5 to u_1 are also outside A_3, since these line segments are secants of $B_{\sqrt{2}d}(s)$ and $B_{\sqrt{2}d}(q)$, respectively. Furthermore, the angle of the line from u_2 to u_3 with the x-axis is greater than the angle of the tangent to $B_{\sqrt{2}d}(p)$ at u_2 with the x-axis, hence the line segment from u_2 to u_3 is outside A_3, and similarly with the line segment from u_4 to u_5. So A_3 must be contained in the set spanned by u_1, u_2, u_3, u_4 and u_5, as claimed. □

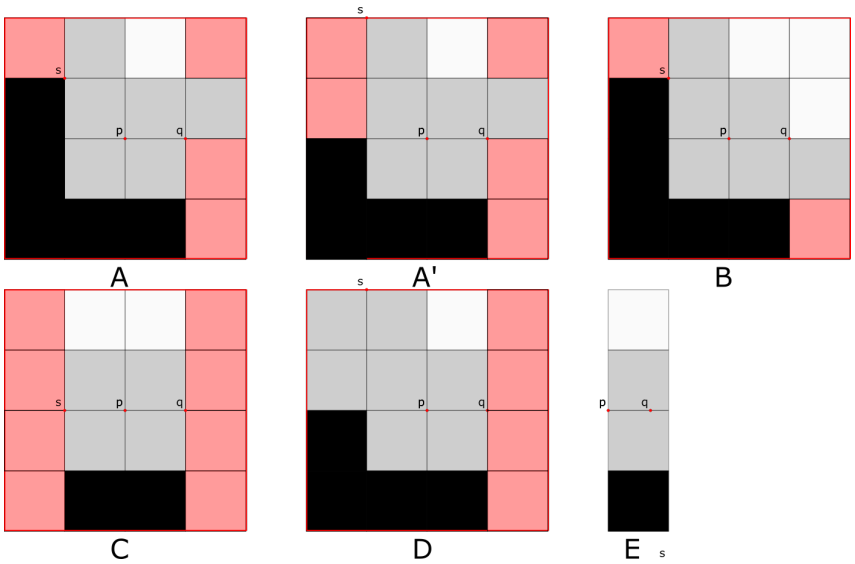

Figure BB.4: Consider the above configuration types. We aim to find a set containing the centre of a ball containing p.

Lemma BB.7. *Consider one of the configurations in Figure BB.4, placed in a coordinate system with p at the origin and with the colours of the red pixels unspecified. Let v_i, w_i and u_j be as in Lemma BB.6, $i = 1, 2, 3, 4$, $j = 1, 2, 3, 4, 5$.*

(i) *In configurations of type A from the figure, the set* $\operatorname{conv}(\bigcap_{i=1}^4 B_{\sqrt{2}d}(w_i), p)$ *is white. In configurations of type B, either the set* $\operatorname{conv}(\bigcap_{i=1}^4 B_{\sqrt{2}d}(w_i), p)$ *is white or the set* $\operatorname{conv}(\bigcap_{i=1}^4 B_{\sqrt{2}d}(w_i'), p)$ *is white, where* w_i' *is the reflection of* w_i *in the line* $y = x$.

(ii) *In configurations of type A′ and D, the set* $\operatorname{conv}(\bigcap_{i=1}^4 B_{\sqrt{2}d}(v_i), p)$ *is white.*

(iii) *Let p and q in configurations of type E be black points with* $d(p, q) = l < d$. *If a component of* ∂X *in the lower grey pixel has two endpoints on the line between p and q, the set* $\bigcap_{i=1}^3 B_{\sqrt{2}d}(t_i)$ *is white, where* $t_1 = (0, \sqrt{2}d)$, $t_2 = (l, \sqrt{2}d)$ *and* $t_2 = \left(\frac{l}{2}, d\sqrt{2 - \frac{l^2}{4}}\right)$.

(iv) *Consider a configuration of type C. If the line segment from the point q to some point* $(0, l)$ *is black for some* $l \in [0, d)$, *the set* $\bigcap_{i=1}^5 B_{\sqrt{2}d}(u_i) \cap \bigcap_{i=1}^3 B_{\sqrt{2}d}(t_i)$ *is white (where* $t_1 = (0, \sqrt{2}d)$, $t_2 = (l, \sqrt{2}d)$ *and* $t_2 = \left(\frac{l}{2}, d\sqrt{2 - \frac{l^2}{4}}\right)$*)*

Proof. Name the pixels according to the convention. Let us start with (i):

Consider first a configuration of type A in Figure BB.4. By Lemma BB.4 applied to the grey pixel K_{10}, p must be white. Hence there is a white $\sqrt{2}d$-ball $B_{\sqrt{2}d}(c_w)$ containing p, whose centre c_w must belong to $B_{\sqrt{2}d}(p)$. The pixel containing c_w must be white since $B_{\sqrt{2}d}(c_w)$ contains the entire pixel containing its centre, therefore c_w can only belong to the white pixel K_3 in configuration A (since K_{11} cannot be white without a white and black pixel sharing a corner, which is against our assumption). When c_w belongs to K_3, it contains the two lower vertices of K_3 along with p. Hence it cannot contain the point q too, for if it did, it would contain all corners of the grey pixel K_7, and hence all of K_7, which would then not be grey. Thus $c_w \notin B_{\sqrt{2}d}(q)$. Furthermore, since s is a black point, we must have $s \notin B_{\sqrt{2}d}(c_w)$ or, equivalently, $c_w \notin B_{\sqrt{2}d}(s)$. So, in short, c_w belongs to $K_3 \cap (B_{\sqrt{2}d}(p) \setminus (B_{\sqrt{2}d}(q) \cup B_{\sqrt{2}d}(s)))$. By Lemma BB.6, this set is contained in $\operatorname{conv}(w_1, w_2, w_3, w_4)$, so by Lemma B.59,, since $c_w \in \operatorname{conv}(w_1, w_2, w_3, w_4)$, the set $\bigcap_{i=1}^4 B_{\sqrt{2}d}(w_i)$ is contained in $B_{\sqrt{2}d}(c_w)$, and is thus white. Since $B_{\sqrt{2}d}(c_w)$ also contains p, it must in fact contain the entire set $\operatorname{conv}(\bigcap_{i=1}^4 B_{\sqrt{2}d}(w_i), p)$, which is thus white.

Similarly, in configurations of type B the point p must be white and hence contained in a white ball $B_{\sqrt{2}d}(c_w)$ whose centre $c_w \in B_{\sqrt{2}d}(p)$ must be contained in a white pixel. Hence c_w can only belong to the white pixels K_3 or K_8. We may as well assume that c_w belongs to K_3, because the argument for the other case corresponds to reflecting the entire configuration in the line $y = x$. As with the case for configuration A, if $c_w \in B_{\sqrt{2}d}(q)$ then $B_{\sqrt{2}d}(c_w)$ would contain the entire grey pixel K_7 which would then not be grey, and since s is a black point, we must also have $c_w \notin B_{\sqrt{2}d}(s)$. So c_w belongs to $K_3 \cap (B_{\sqrt{2}d}(p) \setminus (B_{\sqrt{2}d}(q) \cup B_{\sqrt{2}d}(s)))$, which by Lemma BB.6 ii) is contained in $\operatorname{conv}(w_1, w_2, w_3, w_4)$. By Lemma B.59, this means that the set $\bigcap_{i=1}^4 B_{\sqrt{2}d}(w_i)$ is contained in the white set $B_{\sqrt{2}d}(c_w)$. Again, since $B_{\sqrt{2}d}(c_w)$ also contains p, it must contain $\operatorname{conv}(\bigcap_{i=1}^4 B_{\sqrt{2}d}(w_i), p)$, which is then white.

Now, let us look at (ii): In both configuration A' and D, the point p is white by Lemma BB.4 applied to K_{10}, hence there is a white ball $B_{\sqrt{2}d}(c_w)$ containing p, meaning $c_w \in B_{\sqrt{2}d}(p)$. Since the pixel containing c_w is white, c_w must belong to the only white pixel intersecting $B_{\sqrt{2}d}(p)$ in configuration A, namely K_3.

In configuration D, c_w can belong to either the white pixel K_3 in the configuration, or to K_8 (but not to K_7, since a black and a white pixel would then be sharing a corner). If $c_w \in K_8$, then $B_{\sqrt{2}d}(c_w)$ would contain the left and lower edge of the grey pixel K_7, hence the only non-white edge of K_7 would be the left vertical edge. But then ∂X would have to intersect that edge at least twice in order for K_7 to be grey - a contradiction by Lemma B.19. So c_w must belong to K_3 in both configuration A' and D.

If $B_{\sqrt{2}d}(c_w)$ contained q in either configuration A' or D, it would contain all corners of, and hence all of the grey pixel K_7, meaning that K_7 would not be grey. So $c_w \notin B_{\sqrt{2}d}(q)$ in both cases.

Since c_w belongs to K_3 and to $B_{\sqrt{2}d}(p)$, but not to $B_{\sqrt{2}d}(q)$, it must belong to the lower left quarter $\{(x,y) \in \mathbb{R}^2 \mid 0 \leq x \leq \frac{d}{2}, d \leq y \leq \frac{3d}{2}\}$ of K_3. Hence c_w is further from the point s than it is from any other corner of K_2. Thus, if $B_{\sqrt{2}d}(c_w)$ contained s, it would also contain all the other corners of K_2, and hence it would contain the entire grey pixel K_2 – a contradiction. So $c_w \notin B_{\sqrt{2}d}(s)$. In short, the point c_w in configurations A' or D is contained in the white pixel K_2 and in $B_{\sqrt{2}d}(p) \setminus (B_{\sqrt{2}d}(q) \cup B_{\sqrt{2}d}(s))$, and by Lemma BB.6 i), this set is contained in $\mathrm{conv}(v_1, v_2, v_3, v_4)$. By Lemma B.59 again, this implies that the set $\bigcap_{i=1}^4 B_{\sqrt{2}d}(v_i) \subseteq B_{\sqrt{2}d}(c_w)$, meaning that this set is white. Since $p \in B_{\sqrt{2}d}(c_w)$ as well, the entire set $\mathrm{conv}(\bigcap_{i=1}^4 B_{\sqrt{2}d}(v_i), p)$.

For (iii), look at configuration E in Figure BB.4 and assume that p, q are black points, and that a component of ∂X in the lower grey pixel has two endpoints on the line from p to q. Then the part of ∂X in the lower grey pixel must be contained in $S(p, q, \sqrt{2}d)$, and there must be a point a in ∂X in the lower grey pixel where ∂X has a horisontal tangent. This means that there must be a white ball $B_{\sqrt{2}d}(c_w)$ osculating ∂X at a, and its centre c_w must lie in $[0, l] \times [d, \sqrt{2}d]$ since it must belong to a white pixel and it can be no further than $d\sqrt{2}$ from the lower grey pixel. Furthermore, since p and q were black, we must have $p, q \notin B_{\sqrt{2}d}(c_w)$ or equivalently $c_w \notin B_{\sqrt{2}d}(p) \cup B_{\sqrt{2}d}(q)$. With t_1, t_2 and t_3 as in the formulation of the lemma, this means that c_w must lie somewhere underneath the line between t_1 and t_2. Since the line from t_1 to t_3 and the line from t_2 to t_3 are contained in $B_{\sqrt{2}d}(p) \cup B_{\sqrt{2}d}(q)$, we must also have that c_w lies above these lines. This proves that c_w lies in the triangle spanned by t_1, t_2 and t_3. Consequently, the set $B_{\sqrt{2}d}(t_1) \cap B_{\sqrt{2}d}(t_2) \cap B_{\sqrt{2}d}(t_3)$ is contained in $B_{\sqrt{2}d}(c_w)$ by Lemma B.59, hence $B_{\sqrt{2}d}(t_1) \cap B_{\sqrt{2}d}(t_2) \cap B_{\sqrt{2}d}(t_3)$ is a white set.

For (iv), assume first that p is a white point. Again, this means that there is a white ball $B_{\sqrt{2}d}(c_w)$ whose centre $c_w \in B_{\sqrt{2}d}(p)$ is contained in a white pixel. Hence c_w is either contained in one of the white pixels K_2, K_3 in the figure, or in one of the red pixels K_5, and K_8. Suppose c_w belonged to K_5. Then $B_{\sqrt{2}d}(c_w)$ would contain p, s and $s + (0, d)$, hence it would contain the left and lower edge of grey pixel K_6 in the figure. Since K_6 also has a white upper edge, ∂X would have to enter and leave K_6 through its right edge – a contradiction by Lemma B.19. So $c_w \notin K_5$, and by a symmetric argument $c_w \notin K_8$. So c_w must belong to $K_2 \cup K_3$.

If $B_{\sqrt{2}d}(c_w)$ contained s, it would contain the entire grey pixel K_6, since c_w is closer to the upper corners of K_6 than to the lower ones, and $B_{\sqrt{2}d}(c_w)$ contains p. But K_6 cannot be contained in $B_{\sqrt{2}d}(c_w)$ since K_6 is grey, hence $c_w \notin B_{\sqrt{2}d}(s)$. Furthermore, $c_w \notin B_{\sqrt{2}d}(q)$ by a symmetrical argument. Hence c_w is contained $(K_2 \cup K_3) \cap (B_{\sqrt{2}d}(p) \setminus (B_{\sqrt{2}d}(s) \cup B_{\sqrt{2}d}(q)))$. By Lemma BB.6, this means that $c_w \in \text{conv}(u_1, u_2, u_3, u_4, u_5)$, implying that $\bigcap_{i=1}^{5} B_{\sqrt{2}d}(u_i)$ is contained in the white set $B_{\sqrt{2}d}(c_w)$ in this case.

Assume instead that p is a black point. Then, all corners of K_{11} are black, hence ∂X must intersect any edge of K_{11} an even number of times. It cannot intersect the left or right edge of K_{11} twice by Lemma B.19, and since there must be a segment of ∂X in K_{11}, ∂X must intersect the line from p to q at least twice. If the line segment from q to $(l, 0)$ is black, ∂X must intersect the line segment between p and $(l, 0)$ at least twice. But then, by point (iii), the set $\bigcap_{i=1}^{3} B_{\sqrt{2}d}(t_i)$ is white.

Since we do not know whether p is black or white, we can only say for sure that $\bigcap_{i=1}^{5} B_{\sqrt{2}d}(u_i) \cap \bigcap_{i=1}^{3} B_{\sqrt{2}d}(t_i)$ is white, since this set is white in both cases. □

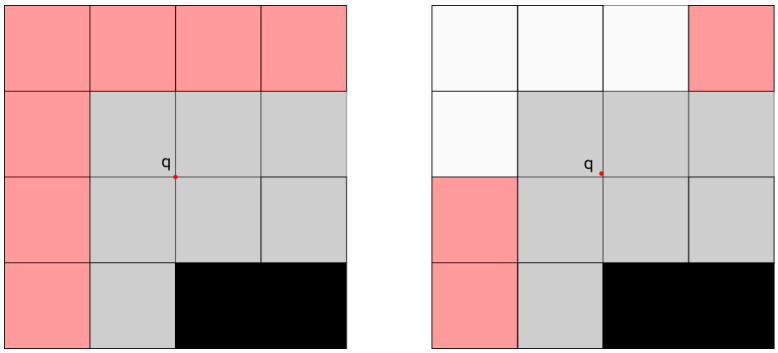

Figure BB.5: Consider a configuration as the one on the left, where the colours of the red pixels are unspecified. Such a configuration must sit in a configuration as the one on the right, and the point q must be black.

Lemma BB.8. *Consider a configuration as the one on in Figure BB.5 left, where the colours of the red pixels are unspecified. Such a configuration must sit in a configuration as the one on the right, and the point q must be black.*

Proof. Name the pixels according to convention, and suppose as in the figure that K_{15} is white. Then by Lemma B.25, (i) K_3 must be white.

Any configuration of 3×3 pixels with K_{10} as the centre must have a white pixel at either K_5 or K_9 - just consider all cases, see Theorem B.28. In any case, Lemma B.24 tells us that the pixels K_1, K_2 and K_5 must be white, hence the configuration must look like the one in Figure BB.5, right. By Lemma BB.4, q must be a black point. □

Theorem BB.9. *None of the 4×4 configurations displayed in Figure BB.6 can occur in the digital image of an r-regular object by a lattice $d\mathbb{Z}^2$ with $d\sqrt{2} < r$.*

Proof. Let us start by looking at the left configuration in Figure BB.6. Place the configuration in a coordinate system with the midpoint p of the configuration at the origin. Then p sits in a configuration of type B from Lemma BB.7, from which it

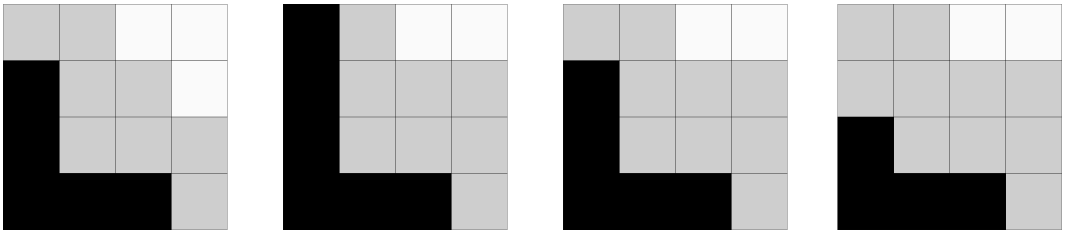

Figure BB.6: None of the 4×4 pixel configurations above can occur in the image of an r-regular object by a lattice $d\mathbb{Z}^2$ with $d\sqrt{2} < r$.

then follows that the set $H = \text{conv}(\bigcap_{i=1}^{4} B_{\sqrt{2}d}(w_i), p)$ is white, where w_1, w_2, w_3 and w_4 are as in Lemma BB.6, ii).

A calculation shows that H contains p, the upper corners of pixel K_7, and the point $(0.72d, 0)$. Hence the upper, left and right edge of K_7 are white, and so is the line segment from p to $(0.72d, 0)$. Since K_7 is grey, any component of ∂X in K_7 must have endpoints on somewhere on the line L between the points $(0.72d, 0)$ and $(d, 0)$. So by Lemma BB.7 (iii) applied to K_7, K_{11} and the points $(0.72d)$ and $(d, 0)$, the set $\bigcap_{i=1}^{3} B_{\sqrt{2}d}(t_i')$ is black (where the t_i' are the reflections of the t_i from the lemma in the line $x = \frac{d}{2}$). But a calculation shows that the grey pixel K_{16} is contained in the black set $\bigcap_{i=1}^{3} B_{\sqrt{2}d}(t_i')$ – a contradiction. So this configuration is impossible.

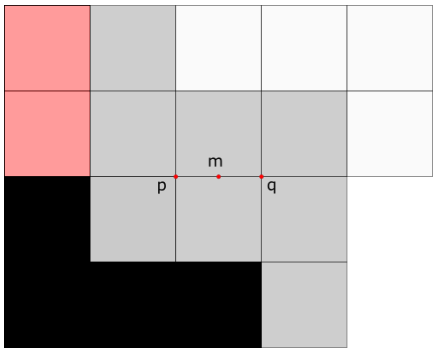

Figure BB.7: Both of the middle configurations in Figure BB.6 mid must sit in a larger configuration such as the above.

Let us show that the second, third and fourth configuration of Figure BB.6 does not occur. When naming the pixels according to convention, notice that the only difference between the three are the colours of pixels K_3 and K_4. Since we will not use information about the colour of these pixels in our proof, it follows that the proof will work for all three configurations.

The second, third and fourth configuration in Figure BB.7 must all sit in a configuration as the one in Figure BB.7 by Lemma BB.8. Placing the configuration in a coordinate system with p at the origin, we see that p sits in a configuration of type A' from Lemma BB.7. Thus by (ii) of that lemma, the set $S := \text{conv}(\bigcap_{i=1}^{3} B_{\sqrt{2}d}(v_i), p)$ is black. A calculation shows that the midpoint $m = (0, \frac{d}{2})$ on the line between p and q is contained in S.

Now, q is also placed in a configuration of type A' from Lemma BB.7, hence by a symmetrical argument, there is a white set $H := \text{conv}(\bigcap_{i=1}^{3} B_{\sqrt{2}d}(v_i'), q)$ containing m (where the v_i' are the image of the v_i under the suitable isometry). But then m

belongs to both a black and a white set – a contradiction. Thus the second, third and fourth configuration of Figure BB.6 cannot occur.

□

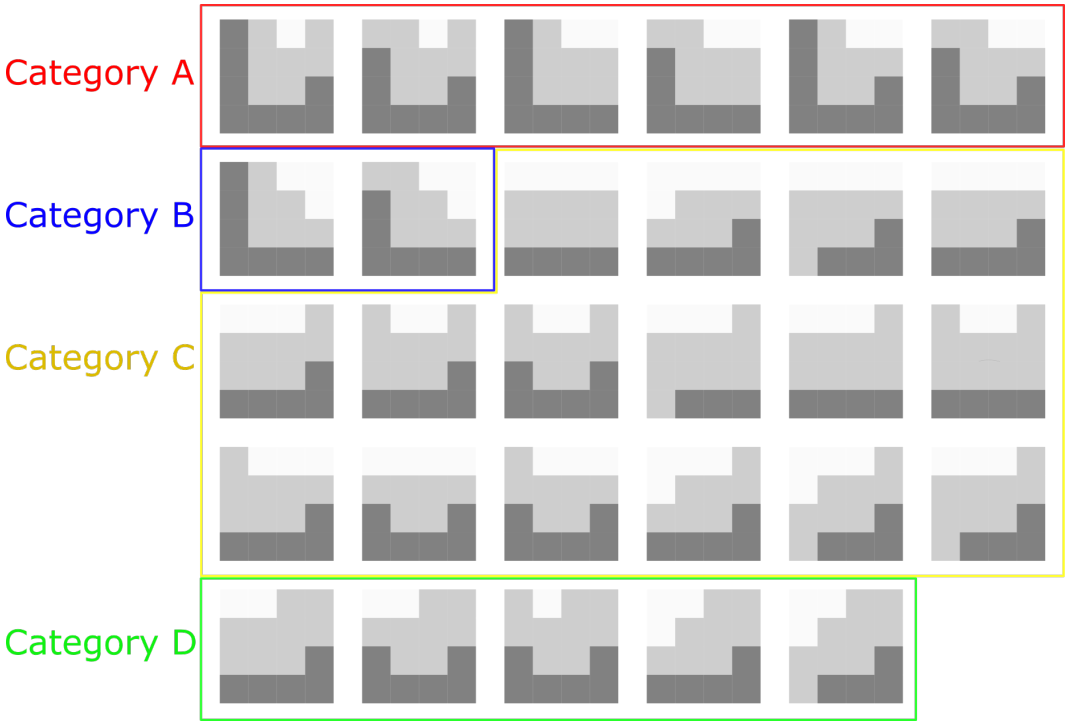

Figure BB.8: These are the only possible configurations of 4×4 pixels with 2×2 grey pixels in the middle that can occur in the digital image of an r-regular object by a grid $d\mathbb{Z}^2$ with $d\sqrt{2} < r$.

Corollary BB.10. *The only possible configurations of* 4×4 *pixels with* 2×2 *grey pixels in the middle are the ones in Figure BB.8.*

Proof. This follows from Theorem B.32 and Theorem BB.9. □

We now divide the configurations of Corollary BB.10 into four categories, as indicated by the boxes in Figure BB.8. As shown, the first category A will consist of the 6 configurations in the top row, the second category B will consist of the two configurations on the left side of second row, the third category C will consist of the remaining configurations in second row plus the configurations in the third and fourth row, and the final category D will consist of the configurations in the last row. Notice that the categories are related to the configurations from Lemma BB.7: The midpoint of a configuration in Category A sits in a configuration of type A and A' from the lemma, the midpoint of a configuration in Category B sits in a configuration of type B from the lemma, the midpoint of a configuration in Category C sits in a configuration of type C from the lemma and the midpoint of a configuration in Category D sits in a configuration of type D from the lemma.

Theorem BB.11. *Consider a configuration as the one in Figure BB.9. It is always possible to determine what colour the corners* a *and* b *are.*

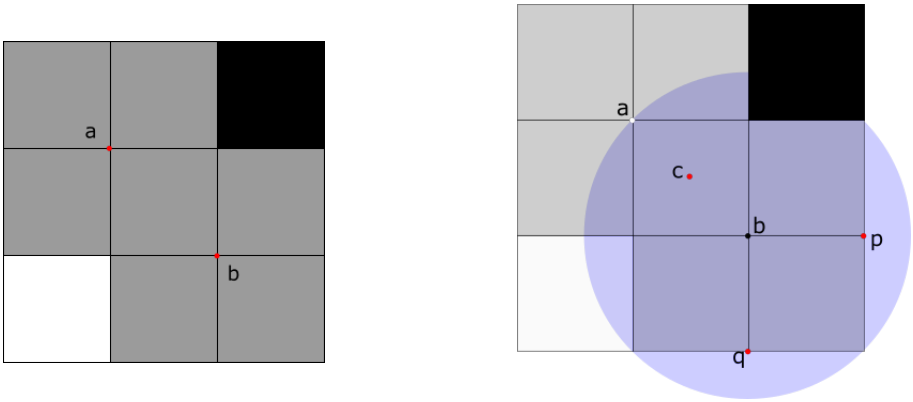

Figure BB.9: In a pixel configuration as the one on the left, it is always possible to determine the colours of the points a and b.

Proof. Let us start by arguing that the two points a and b cannot have different colours. Indeed, suppose they did, and that a were white and b were black.

If b is black, the common edge e of K_5 and K_6 would belong to the interior of X – if it contained any points of intersection with ∂X, it would either contain one such point with vertical tangent, or it would contain several such points since the endpoints of e are black. In both cases, Lemma B.19 would yield a contradiction. Therefore e is contained in $\mathrm{Int}(X)$.

Place the configuration in a coordinate system with b at the origin, so that K_5 and K_6 are the pixels to the upper left and upper right of b, respectively (see Figure BB.9, left). Since both K_5 and K_6 are grey, they contain points $x \in K_5 \cap \partial X$ and $x' \in K_6 \cap \partial X$. Let L be the line between x and x'. Then $\pi(L)$ is a path in ∂X from x to x'. This path is contained in any ball of radius less than $\sqrt{2}d$ containing x and x', so in particular it is contained in $B_{\sqrt{5}d/2}(0, \frac{d}{2})$, since this ball contains all of K_5 and all of K_6, and hence also x and x'. Hence $\pi(L)$ must pass the y-axis in a point where $\frac{d-d\sqrt{5}}{2} < y < \frac{d+d\sqrt{5}}{2}$, and since it cannot cross the black part of this line, it must in fact cross the line segment between b and q. By a similar argument, ∂X must pass the x-axis in a point between b and p.

Since b were black, there is be a black ball $B_{\sqrt{2}d}(c_b)$ of radius $\sqrt{2}d$ containing b, and it is centred somewhere in $B_{\sqrt{2}d}(b)$. It cannot contain q, for if it did, it would contain the entire line segment from b to q, contradicting the fact that there is a path in ∂X intersecting this line segment. Similarly, it cannot contain p, for if it did, it would contain the entire line segment from b to p, and hence also the point of ∂X on this line segment.

Since c_b can only belong to a black pixel because the pixel containing c_b is contained in the black ball $B_{\sqrt{2}d}(c_b)$, we must have that $c_b \in K_3 \cap B_{\sqrt{2}d}(b)$. Since a is white, $c_b \notin B_{\sqrt{2}d}(a)$. Putting all these together, we have that $c_b \in K_3 \cap B_{\sqrt{2}d}(b) \setminus (B_{\sqrt{2}d}(a) \cup B_{\sqrt{2}d}(p))$. By Lemma BB.6 this means that $c_b \in \mathrm{conv}(w_1, w_2, w_3, w_4)$, where the w_i's are as in the lemma.

Repeating this argument for the white point a, we find that there is a white ball $B_{\sqrt{2}d}(c_w)$ with $c_w \in \mathrm{conv}(w_1', w_2', w_3', w_4')$, where w_i' is the point w_i rotated an angle π about the centre c of pixel K_5.

But for all i, both the points w_i and the points w_i' are contained in $B_{\sqrt{2}d}(c)$,

hence c belongs to both $B_{\sqrt{2}d}(c_b)$ (which was black) and to $B_{\sqrt{2}d}(c_w)$ (which was white) by Lemma B.59 – a contradiction. So the two points a and b must always have the same colour.

Using Lemma BB.4 and considering all the cases in Figure BB.8 containing the configuration from figure BB.9, we see that it is always possible to determine the colour of a or b. □

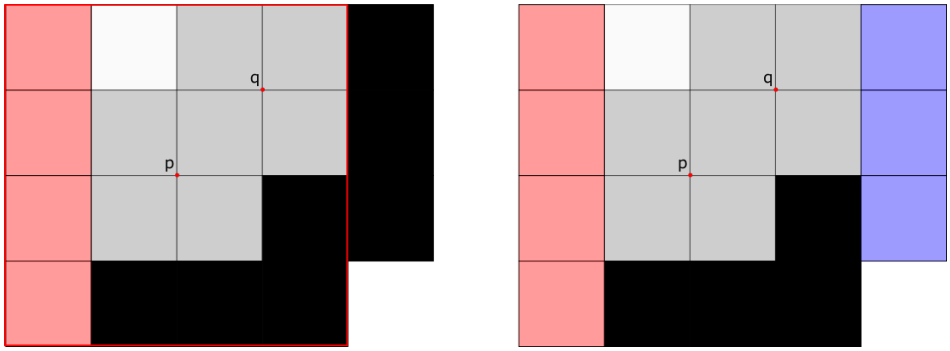

Figure BB.10: Left: A configuration from category D must sit in a larger configuration like the one on the left. Right: We consider a configuration within category D. The colours of the four left pixels (red) of such a configuration may vary, therefore we make no assumptions about those. We aim to determine which colours the blue pixels can have.

Lemma BB.12. *A configuration from category D must sit in a larger configuration such as the one in Figure BB.10, left.*

Proof. While the colour of the leftmost four pixels differ within category D, all configurations in category D share the colours of the rightmost 12 pixels. We aim to determine the colours of the blue pixels neighbouring such a configuration, see Figure BB.10, right.

Assume as in the figure that the configuration from category D has more black pixels than white (the opposite case is symmetric). Then by Theorem BB.11 and Lemma BB.4, the centres p, q of both 2×2 configurations of grey pixels in the 4×4-configuration from category D must be white.

Now, look at the 4×4 configuration centred around q. This configuration must also belong to category D, and it must be one of the configurations of category D with more black pixels than white, otherwise q would be black by Lemma BB.4 and Theorem BB.11. Looking at all possible configurations satisfying these two criteria, we see that they all have black pixels where the blue pixels in Figure BB.10, right, are. Hence the proof follows. □

BB.3 Area containing ∂X

This section is devoted to determining restrictions on, where the boundary ∂X can lie in 2×2 grey pixels.

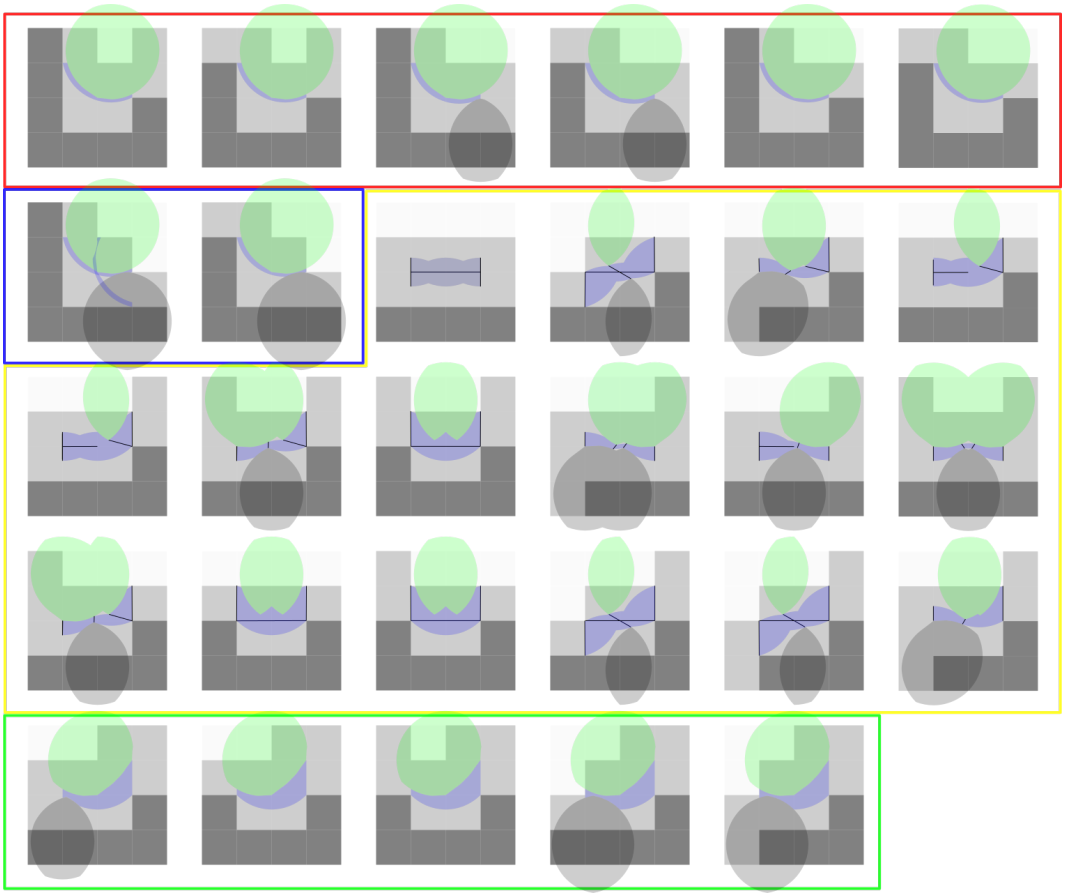

Figure BB.11: Any point of ∂X in the centre four pixels in any of the above configurations is contained in the blue set in that configuration

Theorem BB.13. *In any of the pixel configurations in Figure BB.11, the part of ∂X in the centre 2×2 pixels is contained in the blue set in the figure. The green sets in the figure are contained in X^C, and the dark grey sets are contained in X.*

Proof. We start by explaining how the green and grey sets are found. Place all 4×4 configurations in a coordinate system with the configuration centre at the origin.

Consider a configuration from category A in Figure BB.8. The centre point p belongs to a configuration of type A from Lemma BB.7, and in some cases also to a configuration of type A' from the same lemma. Hence by (i) the set $H := \mathrm{conv}(\bigcap_{i=1}^{4} B_{\sqrt{2}d}(w_i), p)$ is white, and therefore does not contain any points of ∂X. These are the green sets in the configurations of category A in Figure BB.11.

In the third and fourth configurations in category A, the pixel K_{12} is grey. Let q be the upper right corner of K_{12}. Then q is the centre of a pixel in a configuration of type C from Lemma BB.7, and a calculation shows that the point $(0.72d, 0)$ belongs to H along with p, and so the line segment from p to $(0.72d, 0)$ is white. Thus, by Lemma BB.7, (iv), the set $\bigcap_{i=1}^{5} B_{\sqrt{2}d}(u_i) \cap \bigcap_{i=1}^{3} B_{\sqrt{2}d}(t_i)$ is black - this is the black set in the configurations of category A where K_{12} is grey.

For a configuration from category B, the set $H := \mathrm{conv}(\bigcap_{i=1}^{4} B_{\sqrt{2}d}(w_i'), p)$ is again white (possibly after a reflection of the configuration in the line $y = x$) by Lemma BB.7, (i). A component of $\partial X \cap K_7$ must have endpoints on the part of

the edge between p and $(0, d)$ that is outside H, which (by a calculation) means between the points $(0.72d, 0)$ and $(0, d)$. By Lemma BB.7, (iii) this means that the set $S := \bigcap_{i=1}^{3} B_{\sqrt{2}d}(t_i')$ is black (where $l = 0.28d$ and the t_i' have been translated to fit the lemma). This is the black set in the figure. Note that the set S contains K_{16}, and so the second configuration in category D has in fact *not* been reflected in the line $y = x$, – if it had, K_{16} would not have been grey. The first configuration from category B may still have been reflected.

Consider a configuration from category C. Many of these contain a configuration like the one from Lemma BB.8, hence a point corresponding to the point q in Lemma BB.8 sits in a configuration of type A' from Lemma BB.7B By (ii) of Lemma BB.7, this means that the set $H := \text{conv}(\bigcap_{i=1}^{4} B_{\sqrt{2}d}(v_i'), p)$ has the same colour as q, (where the v_i' are the v_i under a suitable isometry). So whenever such a configuration occurs, we have coloured the corresponding set in the appropriate colour - green sets belong to X^C, black sets to X.

Furthermore, we have applied Lemma BB.6 (iv) where possible to obtain more sets that are either contained in X or X^C. This provides us with the remaining green and black areas in the configurations of category C in Figure BB.11.

Finally, consider a configuration in category D. By Lemma BB.7, (ii) applied to the configuration centre, the set $H_1 := \text{conv}(\bigcap_{i=1}^{4} B_{\sqrt{2}d}(v_i'), p)$ is white, where the v_i' are the reflections of the v_i in the y-axis. By a symmetric argument applied to the lower left corner q of pixel K_3 (and using Lemma BB.12), the set $H_2 = \text{conv}(\bigcap_{i=1}^{4} B_{\sqrt{2}d}(v_i''), q)$ is also white, where the v_i'' are the reflections of the v_i' in the line $y = 1-x$. Combining these, we get that $H = H_1 \cup H_2$ is contained in X^C - In Figure BB.11, H is the green set in the configurations of category D.

In the first configuration in category D, the point $q = p - (d, 0)$ is the centre in a configuration of type C from Lemma BB.7 since the point p is white, and the line segment from p to $p - (0.54d)$ is contained in H and thus white. Hence by (iv) of that lemma, the set $S := \bigcap_{i=1}^{5} B_{\sqrt{2}d}(u_i') \cap \bigcap_{i=1}^{3} B_{\sqrt{2}d}(t_i')$ is white, (where the u_i' and the t_i' are the image of the u_i and t_i under a suitable isometry that makes the considered configuration match the one from Lemma BB.7). S is the black set in the first configuration from category D. Similarly, in the latter two configurations from category D, a component of $\partial X \cap K_6$ must have endpoints somewhere on the line segment between the points $(d, 0)$ and $(0.54d, 0)$, since all other points on the boundary of K_6 are either contained in the white set H or in a white pixel. Thus by Lemma BB.7, (iii), the set $S := \bigcap_{i=1}^{3} B_{\sqrt{2}d}(t_i')$ is black, where the t_i' are the t_i under a suitable isometry applied to make the configuration match the one from the lemma.

These considerations explain how the green and grey sets in Figure BB.11 are found.

Now, we only need to explain how we find the blue sets in the figure.

Let Θ denote the four grey centre pixels in any configuration, and let p be the midpoint of Θ. We note that Θ can only contain one segment of ∂X: Indeed, if α, β were distinct components of $\Theta \cap \partial X$, they would have four endpoints a_1, a_2, b_1, b_2 on the boundary of Θ. But by Lemma B.31, these four cannot all belong to different edges of Θ, and by Lemma B.19, two of them cannot belong to the same edge of Θ either, so there cannot be four points in $\partial X \cap \partial\Theta$. Therefore Θ can only contain one component of ∂X. Let a_1, a_2 denote the two points of $\partial X \cap \partial\Theta$.

We remark also that if L is the line between a_1 and a_2, then $\pi(L) \subseteq \Theta$: If this were not the case, then $\pi(L) \subseteq \Theta^C$ except at the endpoints, since $\partial X \cap \Theta$ only contains one component of ∂X. But then the composition of $\partial X \cap \Theta$ and $\pi(L)$ would be a closed path in $\partial X \cap B_{\sqrt{2}d}(p)$, which is impossible, since such a path cannot contain a black or white r-ball, and therefore it cannot be the boundary of some component of X or X^C. So $\pi(L) \subseteq \Theta$.

This means that any point of $\partial X \cap \Theta$ belongs to $\pi(L)$, and therefore to $S(L, d\sqrt{2})$.

In a configuration from category A or B, all points of $\partial\Theta$ are contained in a white or black set except the ones on the line segment L_1 between $(-d, d)$ and $(-0.86d, d)$, and the line segment L_2 between the points $(d, 0.11d)$ and $(d, -0.03d)$, and since L_1 and L_2 both have one endpoint in a white set and one endpoint in a black set, they must each contain a point of ∂X - say $a_1 \in L_1$ and $a_2 \in L_2$.

Now every point of ∂X in Θ must belong to $\pi(L)$, which in turn must belong to $S(L, d\sqrt{2})$. Since a calculation shows that $L_1, L_2 \subseteq B_{\sqrt{2}d}(q)$ where $q = (0.39d, 1.24d)$, we must in particular have that every point of $\partial X \cap \Theta$ belongs to $S(L, d\sqrt{2}) \subseteq B_{\sqrt{2}d}(q)$. Remember that points on ∂X also cannot belong to neither the green sets H nor the black sets S in the figure, meaning that in a configuration from category A or category B, all points of $\partial X \cap \Theta$ must belong to $(B_{\sqrt{2}d}(q) \cap \Theta) \setminus (H \cup S)$ - these are the blue sets in category A or category B in the figure. Note that since the first configuration in Category B may have been reflected in the line $y = x$, the blue set may have been reflected too – therefore we have drawn two blue sets in the figure, to illustrate that we cannot determine to which of the two ∂X belongs.

Likewise if Θ is the four centre pixels in a configuration from Category D: The line segment L_1 between $(d, 0)$ and (d, d) has a black and a white corner, and therefore L_1 contains at least one of the points a_1 of $\partial X \cap \partial\Theta$. Similarly, a calculation shows that the line segment L_2 between the points $(-d, -0.05d)$ and $(-d, 0.18d)$ has a black and a white endpoint in any configuration from category D, hence the other point a_2 of $\partial X \cap \partial\Theta$ must belong to L_2. Since $L_1, L_2 \subseteq B_{\sqrt{2}d}(q')$ for $q' = (-0.24d, 0.97d)$, we must have $\partial X \cap \Theta \subseteq \pi(L) \subseteq B_{\sqrt{2}d}(q')$, and since points of ∂X cannot belong to neither a black set S or a white set H, we must in fact have that $\partial X \cap \Theta \subseteq B_{\sqrt{2}d}(q') \setminus (S \cup H)$. In some of the configurations in Category D, pixel K_9 is black, so we may even replace L_2 with the line segment between $(-d, 0)$ and $(-d, 0.18d)$, and in these cases conclude that $\partial X \cap \Theta \subseteq B_{\sqrt{2}d}(0, d) \setminus (S \cup H)$ by a similar calculation. These sets are the blue ones in the configurations from category D in Figure BB.11.

Finally, consider a configuration from category C. We remark the following:

Observation: Let a_1 and a_2 be the points in $\partial X \cap \partial\Theta$. If $L' \subseteq \Theta$ is a line segment whose endpoints have different colours, there must be a point $a_3 \in \partial X \cap L' \subseteq \partial X \cap \Theta$. Let L_{ij} be the line segment from a_i to a_j for $i, j = 1, 2, 3$. Then the composition of $\pi(L_{13})$ and $\pi(L_{32})$ is a path in ∂X connecting a_1 to a_2 and containing a point $a_3 \in \Theta$, hence it is equal to $\pi(L_{12})$. So $\pi(L_{12})$ is in fact contained in $S(L_{13}, d\sqrt{2}) \cup S(L_{32}, d\sqrt{2})$, which is a smaller set than $S(L_{12}, d\sqrt{2})$.

If a_1 belongs to some line segment L_1 and a_2 belongs to some line segment L_2, then $\partial X \cap \Theta$ belongs to

$$\left(\bigcap_{x : L_1, L' \subseteq B_{\sqrt{2}d}(x)} B_{\sqrt{2}d}(x) \right) \cup \left(\bigcap_{x : L_2, L' \subseteq B_{\sqrt{2}d}(x)} B_{\sqrt{2}d}(x) \right).$$

If we had another line segment $L'' \subseteq \Theta$ with the same properties as L', we would by the same reasoning have that $\partial X \cap \Theta$ belongs to

$$\left(\bigcap_{x:L_1,L'\subseteq B_{\sqrt{2}d}(x)} B_{\sqrt{2}d}(x)\right) \cup \left(\bigcap_{x:L',L''\subseteq B_{\sqrt{2}d}(x)} B_{\sqrt{2}d}(x)\right) \cup \left(\bigcap_{x:L_2,L''\subseteq B_{\sqrt{2}d}(x)} B_{\sqrt{2}d}(x)\right),$$

and so on for additional line segments. We may thus find the blue sets containing ∂X by finding intersections of $d\sqrt{2}$-balls containing line segments with different endpoints.

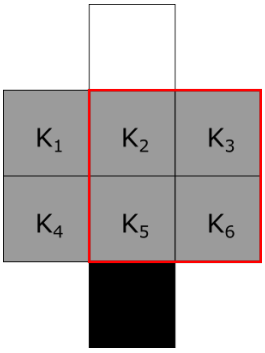

Figure BB.12: If Θ (bounded by the red line) is a part of 2×3 grey pixels, then ∂X must intersect the left edge of Θ no further than $0.3693d$ from the common corner of K_1 and K_5.

The next thing to note is the following: Suppose Θ is a part of a configuration of 2×3 grey pixels such as in Figure BB.12, where Θ is the set bounded by the red curve, and the pixels are named as in the figure. Then, by Lemma B.25, ∂X intersects the line between the upper and lower 3 grey pixels three times: once in a point x_1 on the common edge of K_1 and K_4, once in a point x_2 on the common edge of K_2 and K_5, and once in a point x_3 on the common edge of K_3 and K_6. Let L_{12} be the line segment between x_1 and x_2. Then $\pi(L_{12})$ is a path in ∂X connecting x_1 and x_2, and hence it must intersect $\partial\Theta$ in a point $a_1 \in S(L_{12}, d\sqrt{2}) \subseteq S(L, d\sqrt{2})$, where L is the line segment separating $K_1 \cup K_2$ from $K_4 \cup K_5$. By Lemma B.25, a_1 must be closer than $\sqrt{2}d - d$ to the common corner of K_1 and K_5. So the line segment L_1 containing a_1 is the vertical line segment of length $2\sqrt{2} - 2d$ centred at the common corner of K_1 and K_5.

Note that in a configuration of category C, ∂X can intersect no vertical edge of a pixel in Θ twice by Lemma B.19, and so ∂X must always intersect the horisontal edge between two pixels in Θ at least once. We may use these edges when determining the blue set. When Θ is part of a 2×3 configuration of grey pixels as in Figure BB.12, ∂X intersects the line between the upper and lower grey pixels three times, and so we may also apply Lemma B.25 in this case.

The blue sets are now found in the following way: We determine two line segments on $\partial\Theta$ containing a_1 and a_2 using the remarks above. We then choose one or more line segments in Θ whose endpoints have different colours (we often choose the line determining the shortest distance between the green and black sets in a configuration, and/or a horisontal edge between two pixels in Θ), and then we apply the observation above by finding intersections of balls containing each consecutive pair of line segments. This gives us the blue sets in the figure. The line segments that were used have been drawn. □

BB.4 Line covering on the grey pixels

This section is devoted to defining the line covering on the set of grey pixels, but first, we will prove the following:

Lemma BB.14. *Place a configuration from category B in a coordinate system with the configuration midpoint at the origin. Then the top left square* $\mathcal{Q} = [\frac{d}{4}, d] \times [\frac{d}{4}, d]$ *of pixel* K_7 *is white, and it contains no points of* γ*, the boundary of the reconstructed set* Γ*.*

Proof. The centre p of a configuration from category B sits in a configuration of type B from Lemma BB.7, hence by (i) of that lemma, the set $H = \mathrm{conv}(\bigcap_{i=1}^{4} B_{\sqrt{2}d}(w_i), p)$ is white, where the w_i's are as defined in Lemma BB.6. A calculation shows that H contains the corners of $\mathcal{Q}$, and hence all of $\mathcal{Q}$. Thus $\mathcal{Q}$ is white.

To see that $\mathcal{Q}$ contains no points of γ, just look at all possible circle arcs through auxiliary points. Since $\mathcal{Q}$ contains none of these circle arcs, it cannot contain any point between such two, and therefore it contains no points of γ. □

With this result, we might as well consider the top left square of a grey pixel like in Lemma BB.14 to be non-grey, so we will do this from now on.

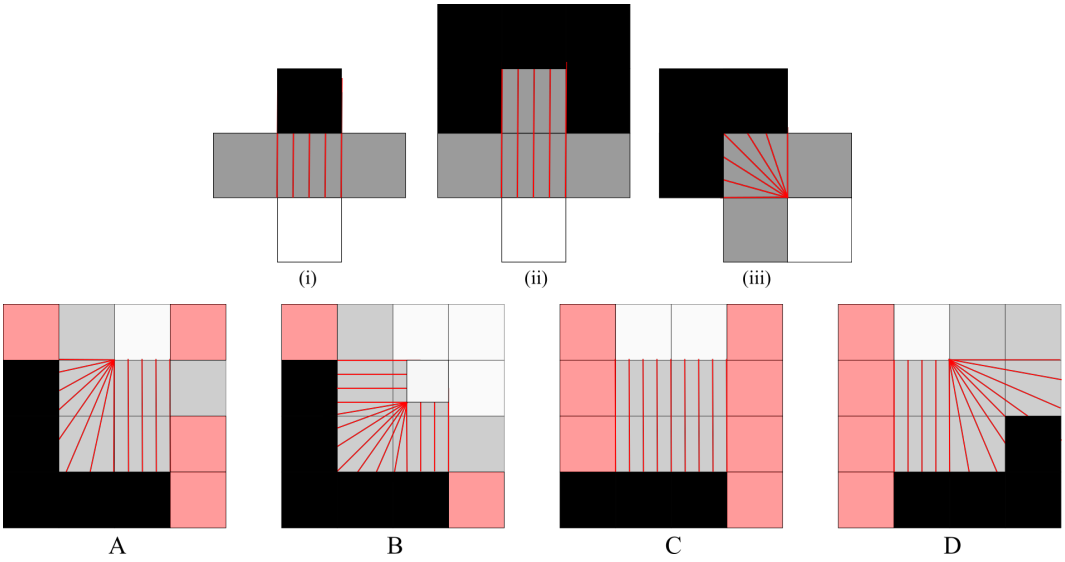

Figure BB.13: We put a line covering on the set of grey pixels as shown in this figure. We make no assumptions as to the colour of the red pixels.

We now put a line covering on the grey pixels as shown in Figure BB.13: In configurations of type (i) and (ii), the lines in the covering are all parallel and they are orthogonal to the lower pixel edge. In a configuration of type (iii), the line covering consists of lines pointing radially out from the corner of the white pixel.

For complex pixels, the line covering for configurations of category *A*-*D* look as in the lower row of Figure BB.13. Using Lemma BB.14, we have coloured the upper left quarter of pixel K_7 white in a configuration from category B, and we do not define the line covering on this part of the pixel. The lines of this line covering always point either radially away from a corner, or are orthogonal to a pixel edge. There are a few thing to note about this line covering:

- The line covering is defined on all grey pixels (except for the corner $\mathcal{Q}$ of pixels in configurations of category B), since it is defined on all possible configurations for both simple and complex pixels,
- The line covering is well-defined: Indeed, it is constructed in such a way that whenever two of the configurations in Figure BB.13 overlap, the lines of the line covering match on the overlap (even when this overlap is only a pixel boundary edge). Lemma BB.12 plays an important role in seeing this.
- The lines of the line covering do not intersect, (hence it is indeed a line covering)

The idea is now to show that we can push ∂X along the lines of this line covering through homeomorphisms. This is not immediately possible, so we need to start by straightening ∂X out a bit. Then we push the straightened ∂X to γ, and result of this process will be a homotopy of $\mathbb{R}^2$ through homeomorphisms, taking ∂X to γ and displacing each point of ∂X no more than $\frac{d}{\sqrt{2}}$.

To construct such a pushing map, we must show that the boundary γ of the reconstructed set Γ intersects all lines of the line covering in exactly one point. When this is proven, it implies that the set of grey pixels is homeomorphic to $\gamma \times [-1, 1]$. Hence if we straighten ∂X out to a curve $H(\partial X)$ that also intersects all lines of the line covering in exactly one point, $H(\partial X)$ is a continuous graph over γ, and therefore pushing $H(\partial X)$ towards γ is a continuous operation.

BB.5 Intersections with the lines of the line covering

We would like to show that ∂X only hits each line in the line covering once. Unfortunately, this turns out not to be entirely true, as it may fail in pixel configurations of type (*iii*) from Figure BB.13. However, in this case we do a little trick to avoid problems – but we will get back to this later. For now, we will just show for the remaining configurations of Figure BB.13 – one by one – that the boundary ∂X only hits each line of the line covering once in these configurations.

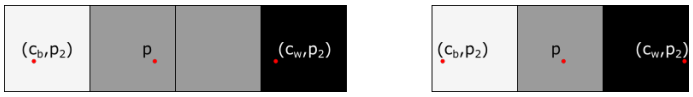

Figure BB.14: If ∂X has a vertical tangent at a point p in a pixel C, then C sits in one of the above configurations.

Lemma BB.15. *Suppose that ∂X has a vertical tangent at some point p in a grey pixel C. Then C sit in one of the configurations in Figure BB.14*

Proof. Let $C = [0, d]^2$ in a coordinate system, and let $p = (p_1, p_2) \in C$. Then $p_1, p_2 \in [0, d]$, but by symmetry, we may as well assume $p_1 \in [\frac{d}{2}, d]$.

Now, since ∂X has a vertical tangent at p, there must be two balls $B_{\sqrt{2}d}((c_b, p_2))$, $B_{\sqrt{2}d}((c_w, p_2))$ osculating at p, and their centres both lie on the horisontal line $y = p_2$ through p. Let us say that the centre (c_w, p_2) of the white ball lies to the left of p. Since $d((c_w, p_2), p) = \sqrt{2}d$, this implies $c_w \in [\frac{d}{2} - d\sqrt{2}, d - d\sqrt{2}] \subseteq [-d, 0]$, hence the centre of the white ball belongs to the left horisontal neighbour of C, meaning that this neighbour pixel must be white.

Since $d((c_b, p_2), (c_w, p_2)) = 2d\sqrt{2}$, we must then have $c_b \in [-d + 2d\sqrt{2}, 2d\sqrt{2}] \subseteq [d, 3d]$. But then C sits in a configuration like either the left one in Figure BB.14 (if $c_b \in [2d, 3d]$ and the right neighbour of C is also grey), or the right one in Figure BB.15 (if either $c_b \in [d, 2d]$ or $c_b \in [2d, 3d]$ and the left neighbour of C is black). □

Theorem BB.16. *Each line of the line covering intersects ∂X exactly once in each simple pixel C of type (i) or (ii) in Figure BB.13.*

Proof. Since each line of the line covering in such a simple pixel C has one black and one white endpoint, and since ∂X separates the black pixels from the white, each line of the line covering must intersect ∂X in at least one point. Suppose a line of the line covering intersected ∂X twice, say in points x and y. Let L be the (vertical) line between x and y. Then there would be a path $\pi(L)$ in $\partial X \cap S(L, \sqrt{2}d)$ from x to y, and since the lines of the line covering are all vertical in this case, then by Rolle's theorem, there would be a point q on this path that had vertical tangent. As q must belong to a $S(L, d\sqrt{2})$, it must belong to either C or to the left or right neighbour pixel of C. But neither C nor its two horisontally neighbouring pixels belong to a configuration like the one in Lemma BB.15 – a contradiction. Hence ∂X cannot intersect a line of the line covering in simple pixels of type (i) or (ii) twice. □

Theorem BB.17. *Each line of the proposed line covering intersects ∂X exactly once in each complex configuration of category A,B C or D.*

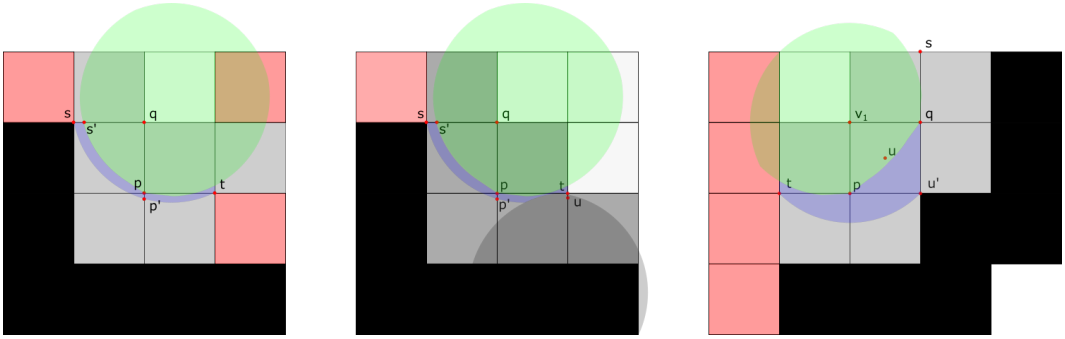

Figure BB.15: A configuration from category A (left), B (middle), or D (right) must sit in a configuration like the above.

Proof. Since the line covering cover all of the grey pixels and ∂X belongs to the set of grey pixels, every point on ∂X belongs to some line of the line covering. Furthermore, since every line in the line covering has a black and a white end point, there must be a point of ∂X on every line. Hence the claim follows if we can show that ∂X does not hit any line more than once.

Let Θ be the four grey pixels in the centre of a configuration of category A, B or C. Then $\partial X \cap \Theta$ can only consist of one connected component since $\partial X \cap \partial\Theta$ cannot contain more than three points by Lemma B.31 and Lemma B.19. Similarly, if Ψ it the 3×3 pixels centred at a point u in a configuration from category D (See Figure BB.15, right), then $\Psi \cap \partial X$ can only have one connected component, because

Ψ sits in a larger configuration as in Figure BB.15, right, meaning that ∂X can only intersect the upper and right edge of Ψ, and it can only intersect each of these edges once by Lemma B.19.

We now aim to show that the component of ∂X in Θ (or in Ψ in a configuration from Category D) can only intersect a line from the line covering once.

Observe the following: Suppose the boundary ∂X intersected a line a of the line covering at least twice, say in points p_1 and p_2. Let L be the line between p_1 and p_2. Then there is a C^1 path $\pi(L)$ in ∂X from p_1 to p_2 belonging to $S(L, \sqrt{2}d)$, and this means that there must be a point of ∂X in $S(L, \sqrt{2}d)$ that has a tangent parallel to a. Furthermore, $\pi(L) \subseteq \Theta$, because if not, then the union of $\pi(L)$ and $\partial X \cap \Theta$ would be a closed curve contained in a ball of radius $d\sqrt{2}$ centred at the centre of Θ, but such a curve cannot be the boundary of a component of X, since it cannot contain a ball of radius $d\sqrt{2}$.

Thus, if $a \subseteq \Theta$ and the component $\Theta \cap \partial X$ of ∂X does not have a tangent parallel to a, it cannot intersect a twice, and therefore ∂X cannot intersect a twice, see Figure BB.16.

Similarly, if $a \subseteq \Psi$ and ∂X crosses a twice, there is a point on $\partial X \cap \Psi$ where the tangent of ∂X is parallel to a. Let a_1, a_2 be the endpoints of $\partial X \cap \Psi$ – then one of them lies on the vertical line through t and the other on the horisontal line through s. Picking a third point $a_3 \in \partial X$ on the line segment between u and u' and letting L_{ij} be the line segment between a_i and a_j, we see that $\partial X \cap \Psi$ must be equal to $\pi(L_{13}) \cup \pi(L_{23})$, because $\partial X \cap \Psi$ only contains one component. Thus, in this case it suffices to show that the paths $\pi(L_{13})$ and $\pi(L_{23})$ do not have a tangent that is parallel to any line of the line covering that they intersect.

We are now ready to prove the theorem, one configuration at a time. We place each configuration in a coordinate system with the configuration centre at the origin. When we measure the angle between the x-axis and a line, we measure it in degrees, and we give a number in the interval $(-90°, 90°]$ that is positive if the slope of the line is positive, and negative if the slope of the line is negative.

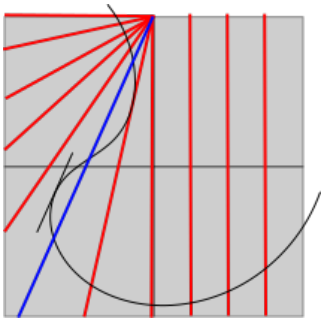

Figure BB.16: If ∂X (black curve) intersected a line $a \subseteq \Theta$ twice (blue line), there would be a point on the path $\partial X \cap \Theta$ where the tangent to ∂X was parallel to a.

Category A: Consider a configuration from Category A, as shown in Figure BB.15, left (all configurations in category A have black, grey and white pixels as shown in the figure – only the intensities of the red pixels vary within Category A). Place the configuration in a coordinate system with the configuration centre p at the origin, and

let q, s and t be the pixel corners as shown in the figure. By Lemma BB.7, (i) the set $H = \mathrm{conv}(\bigcap_{i=1}^{4} B_{\sqrt{2}d}(w_i), p)$ is white, where w_1, w_2, w_3, w_4 are as in Lemma BB.6.

Notice that the point $s' = (-\frac{86d}{100}, d) \in H$, and hence is white. Since the point s is black, there must be a point $x_1 \in \partial X$ on the line segment between s and s'.

Furthermore, since the horisontal line through p has endpoints of different colours, ∂X must intersect it somewhere at a point x_3, and by Theorem BB.13, x_3 must belong to the line segment between the points p and $p' := (0, -0.12d)$.

So we have a point x_1 on the line segment between s and s', and a point x_3 on the line segment between p and p'. The distance $d(x_1, x_3)$ is smaller than $1.502d$. The spindle angle v of the spindle $S(x_1, x_3, \sqrt{2}d)$ is thus smaller than $\sin^{-1}\left(\frac{1.502d}{2\sqrt{2}d}\right) < 32.1°$, see Figure BB.17.

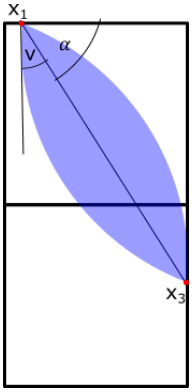

Figure BB.17: We aim to compare the possible angles in $[-\alpha - v, -\alpha + v]$ to the angles between lines of the line covering and the x-axis.

The angle α between the line segment from x_1 to x_3 and the x-axis must also satisfy $-53° < \alpha < -45°$. Let T be the tangent to a point on the path in $\partial X \cap S(x_1, x_3, \sqrt{2}d)$ from x_1 to x_3. By Proposition A.58, the angle between T and the x-axis must belong to the interval $[\alpha - v, \alpha + v] \subseteq [-53° - 32.1°; -45° + 32.1°] = [-85.1°; -12.9°]$. On the other hand, the angle between any line of the line covering in $K_6 \cup K_{10}$ and the x-axis belongs to the interval $[0°; 90°]$. Thus no tangent to ∂X on the path in $\partial X \cap S(x_1, x_3, \sqrt{2}d)$ from x_1 to x_3 has the same angle with the x-axis as the lines of the line covering, and thus the path in $\partial X \cap S(x_1, x_3, \sqrt{2}d)$ from x_1 to x_3 must intersect each line exactly once.

It remains to show that ∂X cannot intersect any line of the line in $K_7 \cup K_{11}$ twice. This follows by a similar calculation: The boundary ∂X intersects the vertical line through the point t in a point x_2. Then $d(x_3, x_2) < 1.502d$, hence the spindle angle of $S(x_2, x_3, \sqrt{2}d)$ is less than $\sin^{-1}\left(\frac{1.502d}{2\sqrt{2}d}\right) < 32.1°$. Furthermore, the angle between the line segment from x_2 to x_3 and the x-axis lies in the interval $[-45°, 48.2°]$, so a point on the part of ∂X that connects x_2 and x_3 inside the spindle $S(x_2, x_3, \sqrt{2}d)$ has a tangent whose angle with the x-axis belongs to $[-45° - 32.1°; 48.2° + 32.1°] = [-77.1°, 80.3°]$. Meanwhile, the angle between the lines of the line covering in these two pixels and the x-axis is always $90°$, hence the result follows.

Category B: This category only contains two configurations, and these two have the non-red pixel of Figure BB.15, middle in common. Let us place the configura-

tion in a coordinate system with p at the origin. By Lemma BB.7, either the set $\operatorname{conv}(\bigcap_{i=1}^4 B_{\sqrt{2}d}(w_i), p)$ or the set $\operatorname{conv}(\bigcap_{i=1}^4 B_{\sqrt{2}d}(w_i'), p)$ is white, where w_1, w_2, w_3 and w_4 are the points from Lemma BB.6, and w_i' is the reflection of w_i in the line $y = x$, for $i = 1, 2, 3, 4$. We may assume that $\operatorname{conv}(\bigcap_{i=1}^4 B_{\sqrt{2}d}(w_i), p)$ is white: By Theorem BB.13, if $\operatorname{conv}(\bigcap_{i=1}^4 B_{\sqrt{2}d}(w_i'), p)$ is white in a configuration from category B, then the pixel K_1 is contained in a black set. Thus, if the red pixel K_1 in Figure BB.15 is black, we may reflect the entire configuration in the line $y = x$ if necessary to ensure that $\operatorname{conv}(\bigcap_{i=1}^4 B_{\sqrt{2}d}(w_i), p)$ is white, and if K_1 is grey, then $\operatorname{conv}(\bigcap_{i=1}^4 B_{\sqrt{2}d}(w_i'), p)$ cannot be white, meaning that $\operatorname{conv}(\bigcap_{i=1}^4 B_{\sqrt{2}d}(w_i), p)$ is white.

By Theorem BB.13, the set $S := \bigcap_{i=1}^3 B_{\sqrt{2}d}(t_i)$ is then black, where $t_1 = (\frac{72d}{100}, -\sqrt{2}d)$, $t_2 = (d, -\sqrt{2}d)$ and $t_3 = (\frac{86d}{100}, -d\sqrt{2 - \left(\frac{14d}{100}\right)^2})$. A calculation shows that $u := (d, -0.028d) \in S$, hence u is a black point.

As for configurations from category A, there is a point $x_1 \in \partial X$ on the line segment between s and s', and there is another point $x_3 \in \partial X$ on the line segment between p and $p' = (0, -0.12d)$, since both segments have endpoints of different colours.

Now, by the calculation from before, the angle between the x-axis and a tangent at any point on the path in $\partial X \cap S(x_1, x_3, \sqrt{2}d)$ from x_1 to x_3 must lie in the interval $[-85.1°; -12.9°]$. The angle between the x-axis and any line of the line covering is however always contained in $[0°, 90°]$, hence by the observation above, the path in $\partial X \cap S(x_1, x_3, \sqrt{2}d)$ from x_1 to x_3 intersects no line of the line covering more than once.

Let t be the pixel corner as shown in Figure BB.15, middle. The points u and t also have different colours, hence there is a point $x_2 \in \partial X$ on the line segment between them. Then there exists a path in $\partial X \cap S(x_2, x_3, \sqrt{2}d)$ between x_2 and x_3. Since $d(x_2, x_3) < 1.01d$, the spindle angle v of $S(x_2, x_3, \sqrt{2}d)$ is less than $\sin^{-1}\left(\frac{1.01}{2\sqrt{2}}\right) < 21°$. The angle between the line segment from x_2 to x_3 and the x-axis lies in $[-7°, 7°]$, hence angle between the x-axis and the tangent of ∂X at any point on the path in $\partial X \cap S(x_2, x_3, \sqrt{2}d)$ from x_2 to x_3 belongs to $[-28°, 28°]$.

Now, $S(x_2, x_3, \sqrt{2}d)$ must belong to the set $[0, d] \times [-d, 0.1d]$. Any line of the line covering that hits this set has an angle with the x-axis that belongs to the interval $[38.7°, 90°]$. Hence no point on the path from x_2 to x_3 has a tangent that is parallel to a line that hits the path, and therefore the path must intersect each line of the line covering exactly once.

Category C: Consider a configuration in category C, and suppose that ∂X intersects a line a of the line covering twice. This would mean that there were a point $p \in \partial X \cap S(a, \sqrt{2}d)$ on the path in ∂X connecting these two intersection points where ∂X had a vertical tangent. Since $p \in S(a, d\sqrt{2})$, the point p must lie somewhere inside the 8 pixels $K_5 - K_{12}$. Furthermore, since ∂X has a vertical tangent at p, by Lemma BB.15 this would imply that the pixel containing p sat in a configuration like either of the ones in Figure BB.14. But this is not the case for any of the pixels $K_5 - K_{12}$ in any of the configuration from category C, hence ∂X cannot intersect a line of the line covering in a configuration of category C twice.

Configuration D: Consider a configuration in category D instead. The configuration must sit in a larger configuration as the one in Figure BB.15, right by Lemma BB.12. Let us name the 16 leftmost pixels of this configuration according to the convention. Now place the configuration in a coordinate system with p at the origin, and name the points as in Figure BB.15, right. By Theorem BB.13, the set $H = \operatorname{conv}(\bigcap_{i=1}^{4} B_{\sqrt{2}d}(v_i'), p) \cup \operatorname{conv}(\bigcap_{i=1}^{4} B_{\sqrt{2}d}(v_i''), q)$ is white, where v_i' is the reflection in the y-axis of the point v_i from Lemma BB.6, and v_i'' is the reflection of v_i' in the line $y = d - x$, for $i = 1, 2, 3, 4$. A calculation shows that H contains the triangle with vertices p, q and v_1', hence this triangle is white.

Now ∂X must intersect the line segment between t and p in a point x_1; a component of $\partial X \cap K_6$ cannot have two endpoints on the left edge of K_6 by Lemma B.19, and it cannot have any endpoints at the upper white edge or the white edge between p and v_1. Hence it must have at least one endpoint x_1 on the line segment between t and p. Similarly, ∂X must intersect the line segment between the points q and s in a point x_2.

Then there is a path in $\partial X \cap S(x_1, x_2, \sqrt{2}d) \subseteq \partial X \cap B_{\sqrt{2}d}(v_1')$ from x_1 to x_2. This path must intersect the line segment between u and $u' := (d, -d)$ in a point x_3, since u and u' have different colours.

Now, since x_1 and x_3 lie on the line segments between t and p and between u and u', respectively, we must have $d(x_1, x_3) \leq 2d$, hence the spindle angle v of the spindle $S(x_1, x_3, \sqrt{2}d)$ must be smaller than $\sin^{-1}\left(\frac{1}{\sqrt{2}}\right) = 45°$. Furthermore, the angle α between the line segment from x_1 to x_3 and the x-axis lies in the interval $(0, 45°)$.

But then the angle between the x-axis and the tangent of ∂X at a point on the path in ∂X from x_1 to x_3 in $S(x_1, x_3, \sqrt{2})$ must belong to the interval $(\alpha - v, \alpha + v) \subseteq (0° - 45°; 45° + 45°) = (-45°, 90°)$.

Meanwhile, the angle between the x-axis and a line of the line covering right of the vertical line through t and left of the line through u and u' belong to the set $(-90°; -45°] \cup \{90°\}$. A symmetric argument shows that the same is true for lines of the line covering in Category D that do not lie between the line through u, u' and the vertical line through t. Hence no tangent to ∂X in a configuration of category D is parallel to a line of the line covering, so each line intersects ∂X exactly once between x_1 and x_3. □

We now know that in all but one of the configurations in Figure BB.13, the boundary ∂X can only intersect each line of the line covering once. As mentioned earlier, this is unfortunately not necessarily the case in pixels of type (iii) (a counterexample is shown in Figure BB.18. We therefore need to pertube ∂X a little so that it only intersects each line in the line covering once in this case, too. Note that we need to make sure that this small pertubation does not move points of ∂X too far:

Lemma BB.18. *Consider a simple pixel of type (iii) in Figure BB.13. There is a homeomorphism $H : \mathbb{R}^2 \to \mathbb{R}^2$, fixed on points of ∂X outside pixels of type (iii), taking ∂X to a set $H(\partial X)$ that only hit each line of the line covering once. This mapping moves points of ∂X no more than $d\sqrt{2} - d\sqrt{2 - \frac{1}{2}}$.*

Proof. Let C be a simple pixel of type (iii), see Figure BB.15. We only need to move a part of ∂X if there is a line a of the line covering in C that ∂X intersect more than once, and by Theorem BB.16 and Theorem BB.17, this is only possible for lines

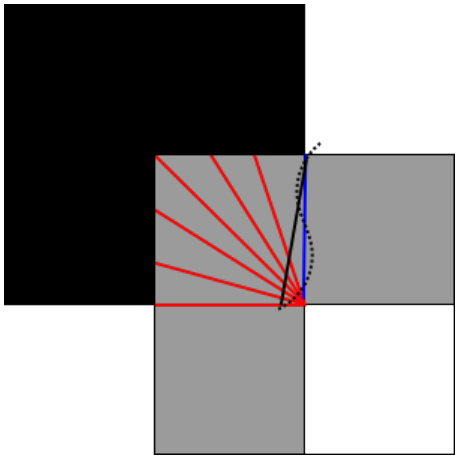

Figure BB.18: The only cases where ∂X (dashed line) can intersect lines of the line covering more than once are cases like the above.

of the line covering inside a pixel of type (*iii*). Suppose therefore that ∂X intersects a line a in C twice. Let $x \in \partial X$ be a point on one of the edges of C and $y \in \partial X$ a point on another edge of C. Let L be the line between x and y.

There is a path $\pi(L)$ in ∂X contained in $S(x, y, \sqrt{2}d)$, and this path must also be contained in the interior of the ball $B_{|L|/2}(\frac{x+y}{2})$ centred at the midpoint of L and containing x and y in its boundary. If $B_{|L|/2}(\frac{x+y}{2})$ contained any point p of ∂X not in $\pi(L)$, then $d(p, x) \leq |L| < d\sqrt{2}$, so the projection π of the line segment from x to p would give a curve in ∂X contained in $B_{|L|/2}(\frac{x+y}{2})$, and likewise the projection π of the line segment from y to p would give a curve in ∂X, contained in $B_{|L|/2}(\frac{x+y}{2})$. Then the composition of these two paths with $\pi(L)$ would give a closed curve in ∂X, contained in a ball of radius $\frac{|L|}{2}$. Such a curve could not be the boundary of a component of X, since it cannot contain a ball of radius $d\sqrt{2}$ – a contradiction. Thus $B_{|L|/2}(\frac{x+y}{2}) \cap \partial X = \pi(L)$.

By Addendum A.35, orthogonal projection $\Pi : S(L, \sqrt{2}d) \to L$ of $\pi(L)$ onto L is a homeomorphism. We can extend it to a homeomorphism $\bar{H}$ of $B_frac|L|2(\frac{x+y}{2})$ that is fixed on the boundary: for $p \in \pi(L)$, we map each line $\Pi^{-1}(p) \cap B_frac|L|2(\frac{x+y}{2})$ to itself by the piecewise linear mapping taking p to $\Pi(p)$. This map displaces the point $p \in \pi(L)$ no more than the spindle height, which is largest when $d(x, y) = |L| = \sqrt{2}d$, in which case the spindle height is $d\sqrt{2} - d\sqrt{2 - \frac{1}{2}} \approx 0.19d$.

The homoeomorphism $\bar{H}$ does not move any other points of ∂X than those in $B_{|L|/2}(\frac{x+y}{2})$, which by the argument above are only the points on $\pi(L)$. The result of $\bar{H}$ is that we have moved a segment of ∂X that may have intersected a line of the line covering more than once to a straight line in C between two grey edges, and such a line certainly cannot intersect a line of the line covering in C more than once. Extending the map $\bar{H}$ by the identity to all of $\mathbb{R}^2$ and applying it to all simple pixels of type (*iii*), we get a homeomorphism $H : \mathbb{R}^2 \to \mathbb{R}^2$ taking ∂X to a set that intersects each line of the line covering only once, and displacing points on ∂X no more than $d\sqrt{2} - d\sqrt{2 - \frac{1}{2}}$.

Now, after applying this homeomorphism, the moved boundary $H(\partial X)$ is equal to ∂X in pixels not of type (*iii*) from Figure BB.13, and in pixels of type (*iii*), it is

equal to a line segment from a point on one grey edge of the pixel to a point on the other grey edge. Hence $H(\partial X)$ only intersects each line of the line covering once. □

This proof completes the argument for showing that ∂X (after some small modification) only intersects each line of the line covering once. However, we need to establish the corresponding result for the boundary of the reconstructed set γ:

Theorem BB.19. *The curve γ intersects each line of the line covering in exactly one point.*

Proof. By Theorem B.42, the curve γ separates black pixels from white in the sense that any path from a black to a white pixel must intersect γ somewhere. Since all lines of the line covering has one endpoint in a black pixel and one endpoint in a white pixel, this in particular means that γ must intersect each line of the line covering at least once. We aim to show that it cannot intersect any line more than once.

Note that a line of the line covering cannot intersect two different segments γ_C, $\gamma_{C'}$ (where C and C' are pixels): Indeed, no line of the line covering intersects two pixels with two auxiliary points on their boundary, so when $\gamma_C \subseteq C$ and $\gamma_{C'} \subseteq C'$, no line of the line covering can intersect both. If γ_C was not contained in C, it would belong to either $K_7 \cup K_{11}$ in a configuration of Category A, or to $K_6 \cup K_{10}$ in a configuration of Category D. Since no line of the line covering leaves $K_7 \cup K_{11}$ in a configuration of Category A, and similarly no line of the line covering leaves $K_6 \cup K_{10}$ in a configuration of Category D (See Figure BB.13), no line of the line covering can intersect two distinct segments γ_C and $\gamma_{C'}$. Thus it suffices to show that no segment γ_C can intersect a line of the line covering twice.

Let C be a pixel with 2 auxiliary points on its boundary, and let L be the line between these. If a line of the line covering intersects a point in C, it also intersects L – just look at all possible configurations. Hence if $\gamma_C \subseteq C$, any line of the line covering that intersect γ_C must also intersect L. If $\gamma_C \nsubseteq C$, the same is still true – again by considering all possible cases. Therefore it is sufficient to check that a line of the line covering that hits L is not intersected twice by γ_C.

By the construction of γ in Section B.4, each segment γ_C of γ is a graph over the line segment L connecting the endpoints of γ_C. If γ_C intersected a line a of the line covering twice, it would contain a point where the tangent of γ_C was parallel to a. We aim to show that this cannot be the case.

Let us start by considering the simple pixels of type (i), (ii) in Figure BB.13. A simple pixel C of type (i) or (ii) has an auxiliary point on the midpoint of each of its vertical edges, hence γ_C is a graph over the horisontal line connecting these two auxiliary points. Such a graph cannot have a vertical tangent, hence γ_C cannot cross a vertical line of the line covering more than once.

Consider now a pixel C whose auxiliary points are sitting in one of the configurations in Figure BB.19. Let L be the line between the auxiliary points on the boundary of C, and let us give L the orientation indicated by the arrow in the figure. Identify L with the line segment from $(0,0)$ to $(|L|,0)$ in $\mathbb{R}^2$ and think of γ_C as a graph over L with this orientation, i.e. $\gamma_C : L \to \mathbb{R}^2$. We find the maximal and minimal derivative of γ_C, which we can then translate to the maximal and minimal angle between L and a tangent line of γ_C. Let us calculate the angle in degrees, and

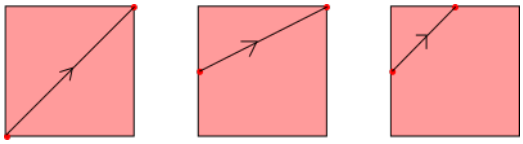

Figure BB.19: Two auxiliary points on the boundary of a complex pixel C may sit in a configuration as in the above figure left or middle. The auxiliary points on a simple pixel of type (iii) sit in a configuration as the right one. Considering γ_C to be a graph over the line L between these points, we may find the maximal and minimal derivative of γ_C, which can then be translated to the maximal and minimal angle between L and a tangent line of γ_C.

let it be given by a number in $(-90°, 90°]$ such that the degree is positive when the derivatives are positve, and negative when the derivatives are negative.

γ_C'	$\frac{\sqrt{5}d}{2}$	$\frac{\sqrt{130}d}{4}$	∞
$\frac{\sqrt{5}d}{2}$	$[-\frac{1}{3}, \frac{1}{3}]$	$[-\frac{1}{3}, 0.129]$	$[-\frac{1}{3}, 0.154]$
$\frac{\sqrt{130}d}{4}$	$[-0.129, \frac{1}{3}]$	$[-\frac{1}{8}, \frac{1}{8}]$	$[-\frac{1}{8}, 0.059]$
∞	$[-0.154, \frac{1}{3}]$	$[-0.059, \frac{1}{8}]$	$\{0\}$

Table BB.1: For each choice of radius of γ_1 and γ_2, we may calculate an interval containing γ_C'.

Look at a simple pixel C of type (iii), see Figure BB.13. Let L be the line between the auxiliary points on its boundary, and identify L with the line segment from $(0, 0)$ to $(\frac{\sqrt{2}d}{2}, 0)$, with the orientation specified in Figure BB.19, right. Then the angle between L and a line of the line covering hitting L belongs to $(-90°, -45°] \cup [45°, 90°]$ since all such lines point out radially from the point $\left(\frac{d}{2\sqrt{2}d}, \frac{d}{2\sqrt{2}d}\right)$. On the other hand, γ_C is composed of the two curves γ_1 and γ_2, and there are three possibilities for each of these. For each possible pair of γ_1 and γ_2 we may calculate the derivative of γ_C – this is done in Table BB.1. We see that for any possible γ_1, γ_2, we have $\gamma_C' \in [-\frac{1}{3}, \frac{1}{3}]$, meaning that the angle between L and a tangent of γ_C belongs to $[\tan^{-1}(-\frac{1}{3}), \tan^{-1}(\frac{1}{3})] \subseteq [-18.44°, 18.44°]$. Hence no tangent of γ_C is parallel to a line of the line covering hitting L, so γ_C cannot intersect any line more than once.

Now, consider a complex pixel C of the left type in Figure BB.19. Such pixels only appear in configurations of category D, and by Lemma BB.12, configurations of category D always appear in a configuration like the one in Figure BB.10. Let L be the line segment between the two auxiliary points on the boundary of C. Identify L with the line segment from $(0, 0)$ to $(d\sqrt{2}, 0)$ in $\mathbb{R}^2$ and assume that the lines of the line covering that hit L all point out radially from the point $p := \left(\frac{\sqrt{2}d}{2}, \frac{\sqrt{2}d}{2}\right)$. Then the angle between a line of the line covering hitting L and L itself belongs to $(-90°, -45°] \cup [45°, 90°]$.

The curve γ_C is a merge of two circle arcs γ_1 and γ_2, and going through all cases, we see that there are only three possibilities for γ_1, and three possibilities for γ_2 (once we have fixed p and remember Lemma BB.12). For each possible radius of γ_1 and each possible radius of γ_2 we may calculate an interval that the derivative γ_C' of $\gamma_C = \varphi\gamma_1 + (1 - \varphi)\gamma_2$ belongs to – this is done in Table BB.2. Looking at this

γ_C'	$\frac{\sqrt{170}d}{12}$	$\frac{\sqrt{10}d}{2}$	$\frac{5\sqrt{10}d}{4}$
$\frac{\sqrt{170}d}{12}$	$[-\frac{6}{7}, \frac{6}{7}]$	$[-\frac{1}{2}; \frac{6}{7}]$	$[-0.305; \frac{6}{7}]$
$\frac{\sqrt{10}d}{2}$	$[-\frac{6}{7}; \frac{1}{2}]$	$[-\frac{1}{2}, \frac{1}{2}]$	$[-0.187, \frac{6}{7}]$
$\frac{5\sqrt{10}d}{4}$	$[-\frac{6}{7}; 0.305]$	$[-\frac{6}{7}, 0.187]$	$[-\frac{2}{11}, \frac{2}{11}]$

Table BB.2: For each possible radius of γ_1 and each possible radius of γ_2, we may calculate the interval that the derivative of $\gamma_C = \varphi\gamma_1 + (1-\varphi)\gamma_2$ belongs to.

table, we see that $\gamma_C' \in [-\frac{6d}{7}, \frac{6d}{7}]$ no matter which curves are used for γ_1 and γ_2. But this means that the angle between L and a tangent to γ_C belongs to the interval $[-\tan^{-1}(\frac{6}{7}), \tan^{-1}(\frac{6}{7})] \subseteq [-41°, 41°]$. So the angle between a tangent of ∂X and L is nowhere as great as the angle between a line of the line covering and L. Hence γ_C cannot intersect a line of the line covering more than once.

Now, look at a complex pixel sitting in position K_6 in either a configuration of category A or B, see Figure BB.8. The corresponding part γ_{K_6} of γ is contained in K_6, and the auxiliary points on the boundary of K_6 sit in a configuration like the one in Figure BB.19, middle. Let L_6 be the line between these auxiliary points, and identify it with the line segment from $(0,0)$ to $(\sqrt{\frac{5}{4}}d, 0)$ in a coordinate system. In configurations of Category A, the lines of the line covering hitting K_6 point out radially from the point $(\frac{\sqrt{5}d}{10}, \frac{\sqrt{5}d}{5})$, hence the angle between a line of the line covering and the line L_6 belongs to the interval $[63.4°, 90°] \cup [-90°, -26.5°]$. In a configuration from category B, the lines of the line covering hitting L_6 are either parallel to the pixel boundary, hence at angle of 63.4° with L_6, or pointing out radially from the point $(\frac{9\sqrt{5}d}{20}, \frac{3\sqrt{5}d}{20})$. Hence the angle between L_6 and a line of the line covering hitting L_6 in a configuration from category B belongs to the set $[63.4°, 90°] \cup [-90°, -70°]$.

γ_{K_6}	$\frac{\sqrt{85}d}{4}$	$\frac{\sqrt{130}d}{4}$	∞
$\frac{\sqrt{10}d}{4}$	$[-0.334, 1]$	$[-0.455, 1]$	$[-0.389, 1]$
$\frac{\sqrt{65}d}{8}$	$[-\frac{1}{4}, \frac{2}{3}]$	$[-0.353, \frac{2}{3}]$	$[-0.286, \frac{2}{3}]$
$\frac{5\sqrt{2}d}{4}$	$[-\frac{1}{4}, \frac{1}{3}]$	$[-0.226, \frac{1}{3}]$	$[-0.155, \frac{1}{3}]$

Table BB.3: For each possible radius of γ_1 and each possible radius of γ_2, we may calculate the interval that the derivative of $\gamma_{K_6} = \varphi\gamma_1 + (1-\varphi)\gamma_2$ belongs to. Note that a radius of ∞ means the case where the circle arc is not an actual arc, but a line. The above are the possibilities for K_6 in category A or B.

On the other hand, look at the circle arcs γ_1 and γ_2 merging into γ_{K_6}. There are three possibilities for γ_1, and three possibilities for γ_2 (two possibilities for category A, one for category B). Like before, we may calculate the maximum and minimum derivatives for the composition of such curve segments. This has been done in Table BB.3. We can see from the table that for any two choices of γ_1 and γ_2, the derivative γ_{K_6}' of γ_{K_6} belongs to the interval $[-0.455, 1]$. This corresponds to saying that the angle between the tangent of γ_{K_6} in a point and L_6 lies in the interval $[\tan^{-1}(-0.455), \tan^{-1}(1)] \subseteq [-24.5°, 45°]$.

So no tangent of γ_{K_6} is parallel to a line of the line covering hitting L_6, thus γ_{K_6} can hit no such line twice. By symmetry, the above argument also means that in a configuration of Category B, the path $\gamma_{K_{11}}$ cannot intersect any lines of the line covering more than once. This proves the statement for configurations of Category B.

Suppose there is an auxiliary point on the midpoint of the edge between K_7 and K_8 in a configuration of category A, and let L_7 be the line between the two auxiliary points on the boundary of K_7, with the orientation specified in Figure BB.19. Then the path segment γ_{K_7} must be of the same type as the ones in Table BB.3, hence like before, the angle between the tangent to γ_{K_7} and L_7 belongs to $[\tan^{-1}(-0.286), \tan^{-1}(1)] \subseteq [-16°, 45°]$. On the other hand, the angle between L_7 and any line of the line covering hitting L_7 is $\tan^{-1}(2) \approx 63.4°$, so no tangent of γ_{K_7} is parallel to a line of the line covering hitting L_7, and hence γ_{K_7} does not hit any line twice.

Finally, if the two auxiliary points on the boundary of K_7 sit on a horisontal line, no point of γ_{K_7} can have a vertical tangent since γ_{K_7} is a graph over the line L_7. But then γ_{K_7} cannot hit any line of the line covering more than once, and by the above reasoning, this also means that any line of the line covering hitting γ_{K_7} in a point is only hit once by γ. This proves the result for configurations of category A.

Applying the same kind of reasoning, we see that if two auxiliary points on the boundary of a complex pixel K in category C sit on a horisontal line L, then no tangent of γ_K can be vertical since γ_K is a graph over L. Hence γ_K cannot intersect a line of the line covering twice in this case.

γ'_{K_6}	$\frac{\sqrt{85}d}{4}$	$\frac{\sqrt{130}d}{4}$	∞
$\frac{5}{4}$	$[-0.311, \frac{1}{2}]$	$[-\frac{1}{5}, \frac{1}{2}]$	$[-0.224, \frac{1}{2}]$
$\frac{\sqrt{85}}{4}$	$[-0.211, \frac{1}{4}]$	$[-\frac{1}{5}, \frac{1}{4}]$	$[-0.117, \frac{1}{4}]$
∞	$[-0.117, \frac{1}{4}]$	$[-\frac{1}{5}, 0.0942]$	$\{0\}$

Table BB.4: The interval containing γ'_{K_6} for different choices of radii of the curves γ_1 and γ_2.

Suppose instead that one of the centre pixels in a configuration of category C, say K_6, has two auxiliary points on its boundary, sitting like the ones in Figure BB.19, middle. Let L be the line connecting them. Then γ_{K_6} is composed of two circle arcs γ_1 and γ_2, and there are three possible choices for each of these curves. Identifying L with the line segment between the points $(0,0)$ and $\left(\frac{\sqrt{5}d}{2}, 0\right)$ in a coordinate system, we may, like before, calculate the minimal and maximal derivative of γ_{K_6} for each choice of γ_1 and γ_2. This is done in Table BB.4. We see that $\gamma'_{K_6} \in [-0.311, \frac{1}{2}]$ no matter which circle arcs γ_1 and γ_2 the curve γ_{K_6} is composed of. Hence the angle between L and a tangent line of γ_{K_6} belongs to the interval $[\tan^{-1}(-0.311), \tan^{-1}(\frac{1}{2})] \subseteq [-17.2°; 26.6°]$. On the other hand, the angle between L and each line of the line covering hitting L is $\tan^{-1}(-2) \approx -63.4°$, so no point of γ_{K_6} has a tangent parallel to a line of the line covering hitting L. Hence γ_{K_6} only hits lines of the line covering intersecting L once, so any line of the line covering intersecting γ_{K_6} is only intersected once by γ. Applying this argument to the remaining centre pixels of a configuration from category C, we get the result for pixels in category C.

Now, consider a configuration in category D as in Figure BB.8. We already

showed that γ_{K_7} does not intersect any line of the line covering twice. Thus we need to show that the same thing goes for γ_{K_6} or $\gamma_{K_{10}}$, depending on which of K_6 and K_{10} γ passes through.

Note first that if there are two auxiliary points on the boundary of K_6 sitting on a horisontal line, then γ_{K_6} cannot intersect a line of the line covering more than once, since γ_{K_6} is a graph over a horisontal line and hence cannot have a vertical tangent.

γ'_{K_6}	$\frac{\sqrt{85}d}{4}$	$\frac{\sqrt{130}d}{4}$	∞
$\frac{\sqrt{170}d}{12}$	$[-0.348, \frac{3}{5}]$	$[-0.22, \frac{3}{5}]$	$[-0.262, \frac{3}{5}]$

Table BB.5: Depending on the choice of γ_2, the derivative of γ_{K_6} lies in the above intervals when there is an auxiliary point on the midpoint of the edge between K_5 and K_6

$\gamma'_{K_{10}}$	$\frac{\sqrt{85}d}{4}$	$\frac{\sqrt{130}d}{4}$	∞
$\frac{5\sqrt{10}d}{4}$	$[-\frac{1}{4}, \frac{1}{7}]$	$[-0.146, \frac{1}{5}]$	$[-0.068, \frac{1}{7}]$

Table BB.6: Depending on the choice of γ_2, the derivative of $\gamma_{K_{10}}$ lies in the above intervals when there is an auxiliary point on the midpoint of the edge between K_9 and K_{10}

Suppose instead that there is an auxiliary point on the midpoint of the edge between K_5 and K_6, and let L_6 be the line between the auxiliary points on the boundary of K_6, with the orientation specified in Figure BB.19. Let us look at the possible tangents of γ_{K_6}. For this choice of auxiliary point, γ_1 is fixed, but there are three possible choices for γ_2. Depending on the choice of γ_2, the derivative of γ_{K_6} lies in the intervals in Table BB.5, hence for any choice of γ_2, we have $\gamma'_{K_6} \in [-0.348, \frac{3}{5}]$. Consequently, the angle between L_6 and a tangent of γ_{K_6} lies in $[\tan^{-1}(-0.348), \tan^{-1}(\frac{3}{5})] \subseteq [-19.19°, 30.97°]$. On the other hand, the angle between γ_{K_6} and a line of the line covering hitting L_6 is $\tan^{-1}(-2) \approx -63.43$, so no tangent of γ_{K_6} is parallel to a line of the line covering hitting γ_{K_6}, and hence γ cannot intersect such a line twice.

Likewise, if there is an auxiliary point on the midpoint of the edge between K_9 and K_{10}, let L_{10} be the line between the auxiliary points on the boundary of K_{10}, with the orientation specified in Figure BB.19. The arc γ_1 used for constructing $\gamma_{K_{10}}$ is fixed, but there are three possible choices for γ_2. Depending on the choice of γ_2, the derivative of $\gamma_{K_{10}}$ lies in the intervals in Table BB.6. Hence for any choice of γ_2, we have $\gamma'_{K_{10}} \in [-0.348, \frac{3}{5}]$ and consequently, the angle between L_{10} and a tangent of $\gamma_{K_{10}}$ lies in $[\tan^{-1}(-\frac{1}{4}), \tan^{-1}(\frac{1}{5})] \subseteq [-14.04°, 11.31°]$. On the other hand, the angle between $\gamma_{K_{10}}$ and a line of the line covering hitting L_{10} is $\tan^{-1}(2) \approx 63.43$, so no tangent of $\gamma_{K_{10}}$ is parallel to a line of the line covering hitting $\gamma_{K_{10}}$, and hence γ cannot intersect such a line twice. Thus γ cannot intersect a line of the line covering in a configuration of category D more than once. □

Now, since both γ and $H(\partial X)$ are continuous curves that intersect each line of this line covering exactly once, we may map $H(\partial X)$ to γ by projecting along the lines homeomorphically. This yields a homeomorphism from $H(\partial X)$ to γ that may be extended to a homeomorphism G supported on the grey pixels, mapping each

line of the line covering to itself piecewise linearly while also mapping the point of $H(\partial X)$ on each line to the point of γ on the same line. The composed map

$$F : \mathbb{R}^2 \to \mathbb{R}^2, \qquad F(p) = G(H(p))$$

is then a homeomorphism taking ∂X to γ, and hence also taking X to Γ, as we wanted. The only thing left to prove in order to get the main result, is that the map F displaces points of ∂X no more than $\frac{d}{\sqrt{2}}$.

Theorem BB.20. *The map F satisfies $\|p - F(p)\| \leq \frac{d}{\sqrt{2}}$ for all points in ∂X. Hence X and Γ are strongly $\frac{d}{\sqrt{2}}$-similar.*

Proof. The map H only displaces points of ∂X in simple pixels of the third type in Figure BB.13, so for points in any other types of pixels, we may as well ignore the map H) and just calculate the distance between points of ∂X and points of γ on each line of the line covering.

Note first that for simple pixels of the second type in Figure BB.13, the fact that the distance between a point of ∂X and a point of γ on the same line of the line covering is closer to each other than $\frac{d}{\sqrt{2}}$ follows by the proof of Theorem B.45 and Lemma B.50.

Consider now a simple pixel C of the first type in Figure BB.13, top left. Any circle arc used in building γ_C has a radius greater than $\frac{\sqrt{5}d}{2}$, hence is no further than $\frac{\sqrt{5}d-d}{2}$ from the top or bottom edge of C. γ_C cannot be further from the top or bottom of C than the circle arcs used for building γ_C. Hence since any point of ∂X lies either between the top of C and γ_C, or between the bottom of C and γ_C, any point of ∂X in C is also closer than $\frac{\sqrt{5}d-d}{2}$ to γ_C.

Let us instead look at a simple pixel C of the third kind in Figure BB.13. After applying the map H of Lemma BB.18, $H(\partial X)$ is a straight line from one grey edge of C to the other.

Let $(0, 0)$ be the point in C where the lines of the line covering originate from, and let the two grey edges of C be parallel to the x-axis and y-axis in a coordinate system. Then $H(\partial X) \cap C$ is a line from a point on the x-axis to a point on the y-axis, so it lies beneath the line $y = d - x$.

Now, suppose γ_C is composed of circle arcs γ_1 and γ_2. A calculation shows that no point of γ_1 is further than $\frac{\sqrt{5}d-\sqrt{2}d}{2}$ from $(0, 0)$. Thus, for any point b of $\partial X \cap C$ below the line $y = \frac{d}{2} - x$, the distance to a point of γ_C on the same line through $(0, 0)$ as b is less than $\frac{\sqrt{5}d-\sqrt{2}d}{2}$. Meanwhile, no matter the choice of γ_1, the curve γ_C lies between the lines $y = \frac{d}{2} - x$ and $y = d - x$. Writing these lines in polar coordinates, we see that γ_C lies between the lines $r_1(\theta) = \frac{d}{\cos(\theta)+\sin(\theta)}$ and $r_2(\theta) = \frac{d}{2(\cos(\theta)+\sin(\theta))}$, hence the distance along a line through (0,0) between points on these two curves is no greater than $\max_{\theta\in[0,\pi/2]}(r_1(\theta) - r_2(\theta)) = \frac{d}{2}$. Hence pushing a point of $H(\partial X)$ lying between these two lines towards γ_C along the lines of the line covering displaces the point no more than $\frac{d}{2}$. Since furthermore H only displaced points of ∂X at most $0.19d$, the composition of H and the push along the lines of the line covering can displace a point no more than $0.69d$, as claimed.

Category A: Consider a point $x \in \partial X$ sitting in one of the four grey centre pixels of a configuration from category A, see Figure BB.20. Name the four centre pixels A,

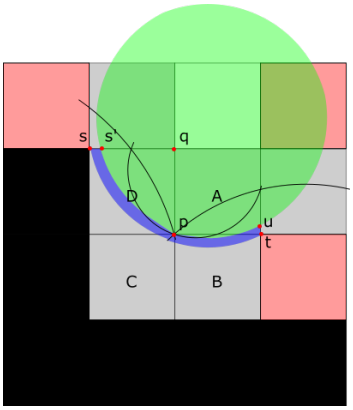

Figure BB.20: A configuration in Category A looks like the one above. Points of ∂X in the four grey centre pixels must belong to the blue set.

B, C and D as in the figure. Then x either belongs to $C \cup D$ or to $A \cup B$. Let us treat these two cases separately.

Suppose $x \in C \cup D$. By the proof of Theorem BB.13 for category A, the set $H := \mathrm{conv}(\bigcap_{i=1}^{4} B_{\sqrt{2}d}(w_i), p)$ is white, and ∂X intersects the upper edge of D in a point x_1 located between the points s and $s' = (-\frac{86d}{100}, d)$. ∂X also intersects the common edge of A and B in a point x_2, since ∂X must intersect ∂A twice, and it cannot intersect the left edge of A because this edge is contained in the white set H, nor can it intersect the right edge of A twice by Lemma B.19.

Let L_{12} be the line between x_1 and x_2. Then there is a path $\pi(L_{12})$ in $\partial X \cap S(L_{12}, d\sqrt{2}) \subseteq \partial X \cap S(s, t, \sqrt{2}d) \setminus H$ between them, where s and t are corners of pixel A and D, respectively (see Figure BB.20). Note that $S(s, t, \sqrt{2}d) \setminus H$ is contained in the ball $B_{\sqrt{2}d}(\frac{\sqrt{15}d}{10}, \frac{2\sqrt{15}d+5d}{15})$. Then $\pi(L_{12})$ intersect the line between $A \cup B$ and $C \cup D$ in $B_{\sqrt{2}d}(\frac{\sqrt{15}d}{10}, \frac{2\sqrt{15}d+5d}{15}) \setminus H$, so somewhere between the points p and $p' := (0, -0.086d)$. Call this point of intersection x_3 with ∂X, and let L_{13} be the line between x_1 and x_3. Then $\pi(L_{13}) \subseteq C \cup D$, since x_1 and x_3 are the only points from ∂X on the boundary of $C \cup D$ by Lemma B.19. Hence all points of ∂X in $C \cup D$ belong to $S(L_{13}, d\sqrt{2}) \cap (C \cup D) \subseteq B_R(q)$, where $q = (0, d)$ and $R = 1.086d$. Furthermore, $B_{R'}(q) \subseteq H$ for $R' = 0.409d$, so $\partial X \cap (C \cup D) \subseteq B_R(q) \setminus B_{R'}(q)$.

On the other hand, the part of boundary Γ of the reconstructed set in $C \cup D$ is γ_D, and γ_D is a merge between two circle arcs γ_1 and γ_2. Furthermore, γ_D belongs to the set bounded by γ_1 and γ_2. Any such two circle arcs γ_1, γ_2 are contained in the space between the circle arcs $\partial B_{\sqrt{10}d/2}((\frac{d}{4}, \frac{3d}{4}))$ and $\partial B_{\sqrt{130}d/4}((-\frac{11d}{4}, -\frac{3d}{4}))$ (just consider all cases). A calculation shows that for $R' = \frac{\sqrt{170}d - \sqrt{130}d}{4} \approx 0.409d$, the ball $B_{R'}(q)$ is disjoint from $\partial B_{\sqrt{130}d/4}((-\frac{11d}{4}, -\frac{3d}{4}))$. Since $\gamma_D \subseteq B_{\sqrt{130}d/4}\left(-\frac{11d}{4}, -\frac{3d}{4}\right)$, $B_{R'}(q)$ cannot contain any points of γ_D. Similarly, a calculation shows that the ball $B_R(q)$ contains any circle arcs γ_1, γ_2 through auxiliary points on the boundary of D, hence $\gamma_D \subseteq B_R(q)$.

In short, we have that $\gamma_D, \partial X \cap (C \cup D) \subseteq B_R(q) \setminus B_{R'}(q)$. Since the lines of the line covering hitting $C \cup D$ are pointing out radially from q, this means that on each line, the distance between the point of ∂X and the point of γ hitting that line is smaller than $R - R' \approx 0.677d < 0.7d$, as claimed.

Suppose in stead that $x \in A \cup B$. If $A \cup B$ are the middle pixels in a configuration of 2×3 grey pixels, we are done by item i) of the proof of Theorem B.45. Suppose therefore that they are not. Then the pixel K_{12} right of B must be black. Since $S(s,t,\sqrt{2}d)$ contains all points of ∂X in B, no point of ∂X in B can be further from the common edge of A and B than the southernmost point of the spindle, which is a distance $\sqrt{2}d - \frac{2d\sqrt{15}+5d}{10} \approx 0.1396d$ from the common edge of A and B. Points of ∂X in A must lie outside the white set H, thus must lie closer to the common edge of A and B than the point $u := (d, 0.102d)$ does. So any point of ∂X in $A \cup B$ is closer than $0.14d$ to the common edge of A and B.

Furthermore, notice that any point on the two circle arcs $\partial B_{\sqrt{10}d/2}((\frac{d}{4}, \frac{3d}{4}))$ and $\partial B_{\sqrt{130}d/4}((-\frac{11d}{4}, -\frac{3d}{4}))$ is closer than $\frac{d}{2}$ to the common edge of A and B. But then the same holds for a point of γ_A, since γ_A belongs to the set bounded by the two circle arcs. So since points of $\partial X \cap (A \cup B)$ are closer than $0.14d$ to the common edge of A and B, and points of γ_A are closer than $\frac{d}{2}$ to the common edge of A and B, the vertical distance between points of $\partial X \cap (A \cup B)$ and points of γ_A is smaller than $0.64d < 0.7d$ to each other, as claimed.

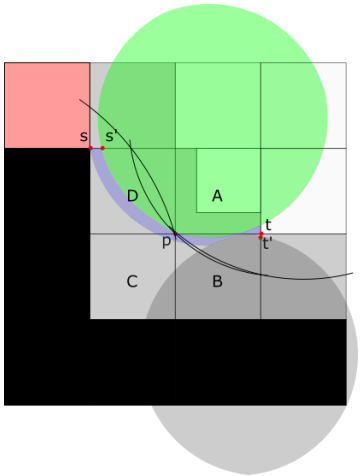

Figure BB.21: A configuration from category B looks like the above. ∂X belongs to the blue set in the figure.

Category B: Consider a configuration from category B. It has black, grey and white pixels as the configuration in Figure BB.21, and only the colour of the red pixel in the figure may vary within the category. Name the pixels and points as in the figure.

Place the configuration in a coordinate system with p at the origin. By Theorem BB.13, the set $H := \mathrm{conv}(\bigcap_{i=1}^{4} B_{\sqrt{2}d}(w_i), p)$ is white (possibly after reflecting the configuration in the line $y = x$), where the w_i are the ones from Lemma BB.6. By Theorem BB.13 again, points of ∂X in $A \cup B \cup C \cup D$ belong to $B_{\sqrt{2}d}(0.39d, 1.24d) \setminus H$.

Now the curve γ_D lies between the two circle arcs through the auxiliary points on the boundary of D, hence it certainly lies between the most extreme cases of such circle arcs, namely the minor arc of $\partial B_{\sqrt{130}d/4}((-\frac{11d}{4}, -\frac{3d}{4}))$ and the minor arc of $\partial B_{5\sqrt{2}d/4}(\frac{5d}{4}, \frac{5d}{4})$. Therefore $\gamma_D \in B_{\sqrt{130}d/4}((-\frac{11d}{4}, -\frac{3d}{4})) \cap B_{5\sqrt{2}d/4}(\frac{5d}{4}, \frac{5d}{4})$.

We may parametrise these arcs as $\gamma_1(y) = \sqrt{\frac{130d^2}{16} - \left(y + \frac{3d}{4}\right)^2} - \frac{11d}{4}$ and $\gamma_2(y) = -\sqrt{\frac{50d^2}{16} - \left(y - \frac{5d}{4}\right)^2} + \frac{5d}{4}$ for $0 \leq y \leq d$.

Since points of ∂X in D lie in $B_{\sqrt{2}d}(0.39d, 1.24d)$, they lie right of the circle arc describing its boundary, namely the curve $f_1(y) = -\sqrt{2 - (y - 1.24)^2}d + 0.39d$, $y \in [\frac{d}{4}, d]$. Since points of ∂X also lie left of H, they in particular lie left of γ_1, since $\gamma_1 \subseteq H$. Similarly, since γ_D lie right of γ_2, it in particular lies right of f_1, since $\gamma_2 \subseteq B_{\sqrt{2}d}(0.39d, 1.24d)$. So in short, both γ_D and ∂X lie between the curves γ_1 and f_1. The maximal horisontal distance between these curves is $\|f_1 - \gamma_1\|_\infty < 0.64d$. Hence when the lines of the line covering on a configuration as in Figure BB.21 are horisontal, then pushing γ to ∂X along the lines of the line covering displaces each point less than $0.7d$, as claimed.

Similarly, look at the part of the configuration where the lines of the line covering are vertical, that is, the set $[\frac{d}{4}, d] \times [-d, \frac{d}{4}]$. In this set, points of ∂X lies inside $B_{\sqrt{2}d}(0.39d, 1.24d)$, hence above the line $y = 1.24d - d\sqrt{2}$. Points of ∂X also lie under the line $y = 0.11d$, since points above this line belong to H.

Meanwhile, points of γ intersecting vertical lines of the line covering belong to γ_B and lie between the two circle arcs whose merge is γ_B. We know these two circle arcs precisely, because we know the auxiliary points that they pass through – these are the circle arcs in pixel B in Figure BB.21, and they are arcs of $\partial B_{5\sqrt{2}d/4}(\frac{5d}{4}, \frac{5d}{4})$ and $\partial B_{\sqrt{85}d/4}\left(\frac{3d}{2}, \frac{7d}{4}\right)$. Calculating γ_B, we see that it must lie between the two horisontal lines $y = -\frac{d}{2}$ and $y = 0$. In particular, both the points of γ and the points of ∂X that intersect a vertical line of the line covering lie between the lines $y = 0.11d$ and $y = -\frac{d}{2}$, hence the distance along a vertical line of the line covering between points of ∂X and points of γ is no greater than $0.61d$, as claimed.

It remains to show that points of ∂X and points of γ on a non-vertical, non-horisontal line of the line covering are closer than $0.7d$. Note therefore that the ball $B_{d/4}\left(\frac{d}{4}, \frac{d}{4}\right)$ lies outside $B_{\sqrt{130}d/4}(-\frac{11d}{4}, -\frac{3d}{4})$ and belongs to both $B_{5\sqrt{2}d/4}(\frac{5d}{4}, \frac{5d}{4})$ and $B_{\sqrt{85}d/4}\left(\frac{3d}{2}, \frac{7d}{4}\right)$. This means that the ball $B_{d/4}(\frac{d}{4}, \frac{d}{4})$ does not contain points of γ. Since $B_{d/4}(\frac{d}{4}, \frac{d}{4})$ also lies inside H, it does not contain any points of ∂X.

A calculation shows that points in the set $[-d, \frac{d}{4}]^2 \cap B_{\sqrt{2}d}(0.39d, 1.24d)$ lie inside the ball $B_{7d/8}(\frac{d}{4}, \frac{d}{4})$, hence any point of ∂X hitting a non-vertical, non-horisontal line of the line covering must belong to $B_{7d/8}(\frac{d}{4}, \frac{d}{4}) \setminus B_{d/4}(\frac{d}{4}, \frac{d}{4})$. Another calculation shows that the same is true for points of γ in this set (simply check that it holds for any circle arc that may be used in constructing γ_B and γ_D). So both points of γ and points of ∂X hitting a non-vertical, non-horisontal line of the line covering are contained in $B_{7d/8}(\frac{d}{4}, \frac{d}{4}) \setminus B_{d/4}(\frac{d}{4}, \frac{d}{4})$. Since the line covering points out radially from $(\frac{d}{4}, \frac{d}{4})$, this means that a point of ∂X and a point of γ on the same line of the line covering can be no further than $\frac{7d}{8} - \frac{d}{4} = \frac{5d}{8} < 0.7d$ apart, as claimed.

Category C: Consider a point $p \in \partial X$ located in one of the four grey centre pixels of a configuration from Category C. If p belongs to one of the two centre pixels of a 2×3 configuration of grey pixels, we are done by the proof of i) in Theorem B.45. Suppose therefore that p is not a centre pixel of a 2×3 configuration of grey pixels. Then p must belong to a grey pixel sitting in a configuration like A

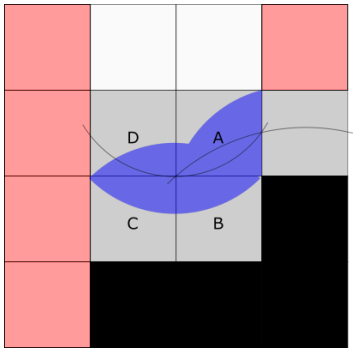

Figure BB.22: If p belongs to a configuration in category C, but does not belong to the two centre pixels of a configuration of 2×3 grey pixels, p must belong to a grey pixel sitting in a configuration like either A or B in this figure.

or B in Figure BB.22. Let us name the four grey centre pixels of this configuration according to the figure.

Now, ∂X must intersect the right edge of pixel A exactly once since the endpoints of this edge have different colours, and using Lemma B.19. Let us call the intersection point x_1. Furthermore, ∂X must intersect the edge between A and B at least once, since a component of $\partial X \cap B$ cannot cannot have both endpoints on the left edge edge of B by Lemma B.19. Let us name the intersection point x_2. Similarly, ∂X must intersect the common edge of pixels C and D at least once, either by the same reasoning (if pixel K_5 is white or pixel K_9 is black), or by Lemma B.25 (if both pixels K_5 and K_9 are grey. Let x_3 be the intersection between ∂X and the common edge of C and D.

Now, place the configuration in a coordinate system with the common vertex of pixels A, B, C and D at the origin. There is a path in ∂X connecting x_1 and x_2 and contained in $S(x_1, x_2, \sqrt{2}d)$, which is again contained in $B_{\sqrt{2}d}((\frac{\sqrt{3}d+d}{2}, -\frac{\sqrt{3}d-d}{2})) \cap B_{\sqrt{2}d}((\frac{d}{2}, d\sqrt{2-\frac{1}{4}}))$, since these balls contain both the lower and right edge of A. Furthermore, there is a path in ∂X from x_2 to x_3 contained in $S(x_2, x_3, \sqrt{2}d) \subseteq S(L, \sqrt{2}d)$, where L is the line segment separating $A \cup D$ from $B \cup C$. Composing these two paths, we get a path τ from x_1 through x_2 to x_3 which is contained in the part of $B_{\sqrt{2}d}((\frac{\sqrt{3}d+d}{2}, -\frac{\sqrt{3}d-d}{2})) \cup S(L, \sqrt{2}d)$ that belongs to grey pixels – this is the blue set in the figure. Note that the only points of ∂X in $A \cup B$ are the points on τ, since no edge of $A \cup B$ can have more than one intersection with ∂X by Lemma B.19. Hence $\partial X \cap (A \cup B) \subseteq (B_{\sqrt{2}d}((\frac{\sqrt{3}d+d}{2}, -\frac{\sqrt{3}d-d}{2})) \cup S(L, \sqrt{2})) \cap (A \cup B)$.

Now, look at the curve γ_A, which is the part of the reconstructed curve γ that is contained in $A \cup B$. By Lemma B.39, it is contained in the convex hull of two circle arcs γ_1 and γ_2. If we can show that any point in this convex hull may be pushed to ∂X via the lines of the line covering without pushing it further than $0.7d$, we are done.

It suffices to check the circle arcs of the circles $\partial B_{\sqrt{85}d/4}(\frac{3d}{2}, -\frac{7d}{4})$ and $\partial B_{5d/4}(0, \frac{5d}{4})$, since any other circle arc through auxiliary points lie between these two. We therefore need to maximise the distances between the functions $\gamma_1(x) = \sqrt{\frac{85d^2}{16} - (x - \frac{3d}{2})^2} - \frac{7d}{4}$, $\gamma_2(x) = -\sqrt{\frac{25d^2}{16} - x^2} + \frac{5d}{4}$ describing these two circle arcs, and the functions

$f_1(x) = -d\sqrt{2-x^2} + d$ and

$$f_2(x) = \begin{cases} d\sqrt{2-x^2} - 1 & \text{if } 0 < x < d\frac{(\sqrt{3}-9)\sqrt{13}+13\sqrt{3}+13}{52}, \\ d\sqrt{2-\left(x-\frac{\sqrt{3}+1}{2}\right)^2} - \frac{\sqrt{3}d-d}{2} & \text{if } d\frac{(\sqrt{3}-9)\sqrt{13}+13\sqrt{3}+13}{52} < x < d \end{cases}$$

that bounds the blue area of $A \cup B$ that may contain points of ∂X. Maximising these distances, we see that $\|\gamma_1 - f_1\|_\infty \approx 0.65d < 0.7d$, $\|\gamma_1 - f_2\|_\infty = \frac{d}{2} < 0.7d$, $\|\gamma_2 - f_1\|_\infty = \frac{d}{2} < 0.7d$ and $\|\gamma_2 - f_2\|_\infty \approx 0.67d < 0.7d$.

Now, since any two centre pixels in a configuration from category C either are the centre of 2×3 grey pixels or sit in a configuration as in Figure BB.22, this completes the proof in this case.

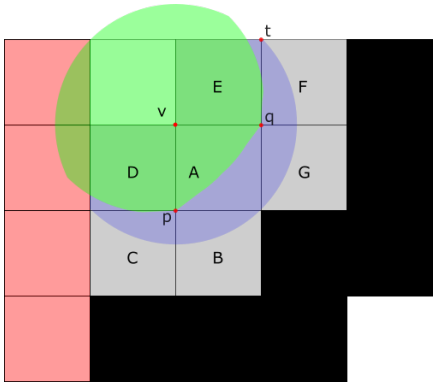

Figure BB.23: Points of $\partial X \cap (A \cup B \cup G)$ belongs to the part of the blue ball that lies outside the green set.

Category D: Consider a configuration from Category D. By Lemma BB.12, it must sit in a configuration like the one in Figure BB.10. Let us name the points and grey pixels as in this figure.

By Theorem BB.13, the set $H := \text{conv}(\bigcap_{i=1}^4 B_{\sqrt{2}d}(v_i'), p) \cup \text{conv}(\bigcap_{i=1}^4 B_{\sqrt{2}d}(v_i''), q)$ is white, where v_i' and v_i'' are as in the theorem. This is the green set in Figure BB.23.

The boundary ∂X must intersect the common edge of C and D: Indeed, a component of $\partial X \cap D$ must have two endpoints on the boundary of D, but since the upper and right edge of D are white, these endpoints can only lie on the lower or left edge of D. Since ∂X cannot intersect the left edge of D twice by Lemma B.19, one of these endpoints must belong to the lower edge of D, so ∂X intersects this edge at least once, say in a point x_1.

By a symmetrical argument, ∂X must intersect the common boundary of E and F in a point x_2. Let L_{12} be the line between x_1 and x_2. Then there is a path $\pi(L_{12})$ in $\partial X \cap S(x_1, x_2, \sqrt{2}d) \subseteq B_{\sqrt{2}d}(v) \setminus H$ connecting x_1 and x_2 which must necessarily pass through A, B and G. Since ∂X can only intersect the common edge of F and G once, and also intersect the common boundary of B and C at most once by Lemma B.19, the only points in $\partial X \cap (A \cup B \cup G)$ are the ones on the path from x_1 to x_2, which all belong to $B_{\sqrt{2}d}(v)$, where $v = (d, 0)$.

$B_{\sqrt{2}d/2}(v) \cap (A \cup B \cup G) \subseteq H$, so $B_{(\sqrt{2}d)/2}(v)$ contains no points of ∂X in $A \cup B \cup G$. Checking the possible circle arcs used in building γ_A, we can also conclude that γ_A belongs to $B_{\sqrt{2}d}(v) \setminus B_{(\sqrt{2}d)/2}(v)$. Since the lines of the line covering that hit

$A \cup B \cup G$ point out radially from v, this means that on each line, there is a point of ∂X and a point of γ_A that are no more than $\sqrt{2}d - \frac{\sqrt{2}d}{2} = \frac{d\sqrt{2}}{2}$ apart, as claimed. This proves the result for the pixels A, B and G. It remains to prove the result in pixels C and D (since E and F are symmetric to C and D).

If $C \cup D$ are the two centre pixels of a 2×3 configuration of grey pixels, we are done by part i) in the proof of Theorem B.45, so let us consider the case where the left d-neighbour of either C or D is not grey.

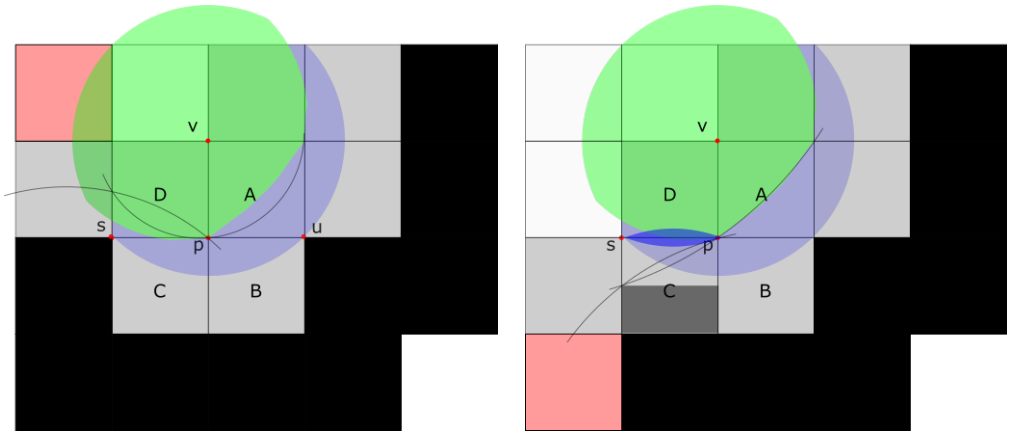

Figure BB.24: If pixels C and D are not the centre column of a configuration of 2×3 grey pixels, a configuration in Category D looks either like the one on the left, or like the one on the right (where we do not wish to specify the colours of the red pixels).

Suppose first that the left d-neighbour of C is black, and hence the left d-neighbour of D is grey, see Figure BB.24, left. Since ∂X must enter and leave $B \cup C$ through the edge between $s := (-d, 0)$ and $u := (d, 0)$, any point in $\partial X \cap C$ must belong to $S(s, u, d\sqrt{2}) \subseteq B_{\sqrt{2}d}(v)$. Furthermore, any point of ∂X in D must belong to $D \setminus H$.

Now, any circle arc used to build γ_D lies beneath the circle arc $\partial B_{\sqrt{85}d/4}(-\frac{3d}{2}, -\frac{7d}{4})$ (this is the upper circle arc in D in Figure BB.24, left). Furthermore, since this arc is contained in H, any point of ∂X in $C \cup D$ must also lie south of it. In short, any point of γ in $C \cup D$ and any point of ∂X in $C \cup D$ must lie between the circle arcs $\partial B_{\sqrt{85}d/4}(-\frac{3d}{2}, -\frac{7d}{4}) \cap D$ and $\partial B_{\sqrt{2}d}(v_i) \cap C$. Hence the maximum vertical distance between two such points is bounded by the maximum distance between these two circle arcs. We may parametrise these circle arcs by putting $f_1(x) = \sqrt{\frac{85d^2}{16} - (x - \frac{-3d}{2})^2} - \frac{7d}{4}$ and $f_2(x) = -d\sqrt{2 - x^2} + d$ for $-d \leq x \leq 0$. A calculation shows that $\|f_1 - f_2\|_\infty \approx 0.638d < 0.7d$. Hence the proof is true in this case.

Suppose now instead that the left d-neighbour of D is white, hence the left d-neighbour of C is grey, see Figure BB.24, right. Then by Theorem BB.13, there is a black set $S = B_{\sqrt{2}d}(t_1') \cap B_{\sqrt{2}d}(t_2') \cap B_{\sqrt{2}d}(t_3')$, where the t_i are as in the theorem. A calculation shows that S contains $G = \mathrm{conv}((-d, -d), (-d, -\frac{d}{2}), (0, -\frac{d}{2}), (0, -d))$, which is the entire lower half of pixel C (G is the dark grey part of C in Figure BB.24, right).

Now looking at all possible circle arcs used in constructing γ_C, we see that they all are contained in $C \setminus G$. The same goes for any point of ∂X in C. Any point of ∂X in D is no further than $\sqrt{2}d - d\sqrt{2 - \frac{1}{4}}$ from the common edge of C and D, because

this is the height of the spindle $S(s, p, \sqrt{2}d)$. So any point of γ and any point of ∂X in C is at most $\frac{d}{2}$ from the common edge of C and D, and any point of γ and any point of ∂X in D is at most $\sqrt{2}d - d\sqrt{2 - \frac{1}{4}}$ from the common edge of C and D. Hence any point of γ and any point of ∂X in $C \cup D$ is at most $\frac{d}{2} + d\sqrt{2} - d\sqrt{2 - \frac{1}{4}} \approx 0.59d$ apart vertically, proving the claim in this case.

□

Paper C

Reconstructing Objects from Noisy Images at Low Resolution

By Helene Svane and Aasa Feragen

This paper was published in the proceedings for the 12th International Workshop on Graph-based Representations in Pattern Recognition[1], which was held in Tours, France, in June 2019. It tries to accommodate the theory developed in the earlier papers to images that we may realistically encounter in the real world. The paper is included here in the printed version.

[1]Helene Svane and Aasa Feragen. Reconstructing objects from noisy images at low resolution. In *Graph-Based Representations in Pattern Recognition*, pages 204–214, Cham, 2019. Springer International Publishing. ISBN 978-3-030-20081-7.

Reconstructing objects from noisy images at low resolution*

Helene Svane[1][0000−0002−1171−7694] and Aasa Feragen[2][0000−0002−9945−981X]

[1] Aarhus University, Department of Mathematics, Denmark
helenesvane@math.au.dk
[2] University of Copenhagen, Department of Computer Science (DIKU), Denmark
aasa@di.ku.dk

Abstract. We study the problem of reconstructing small objects from their low-resolution images, by modelling them as r-regular objects. Previous work shows how the boundary constraints imposed by r-regularity allows bounds on estimation error for noise-free images. In this paper we present a graph-based framework for reconstructing noise-free images from noisy ones. We provide an optimal, but potentially computationally demanding algorithm, as well as a greedy heuristic for reconstructing noise-free images of r-regular objects from images with noise.

Keywords: Object reconstruction · r-regularity

1 Introduction

Whenever new imaging techniques enable us to improve image resolution, we find something smaller scale or further away that we would like to investigate. As a result, the ability to reconstruct objects whose size is on a similar scale as the resolution, is and remains a highly relevant problem, which finds applications in fields as diverse as microscopy and astronomy, see Figure 1, left. Reconstruction of such small objects is hampered by the fact that all information about the object is contained in just a few pixel intensities. In this paper we assume that the imaged object satisfies *r-regularity*, which reduces the possible complexity of the object and therefore enables inference with bounds on precision (see Section 2 for a precise definition of r-regularity).

Previous work by Du Plessis and Svane [8] studied ideal images of r-regular objects. By *ideal* images, we mean images of completely black objects placed on completely white backgrounds, taken with a perfect camera so that the intensity of each pixel is exactly equal to the fraction of the pixel that is covered by the original object. In real life, ideal images are rare, maybe even non-existent. Hence we would like to use our knowledge of ideal images to reconstruct r-regular objects from their noisy images. The strength of this approach is that there are

* This research was supported by Centre for Stochastic Geometry and Advanced Bioimaging, funded by a grant from the Villum Foundation. The authors thank François Lauze for valuable discussions.

relatively strict limitations on which configurations of black, grey and white pixels can occur in an ideal image of an r-regular object. Thus, by considering noisy images as distortions of the ideal one, we aim to use these limitations to deduce the most likely corresponding ideal image. From this idealised image, we apply techniques developed for ideal images to suggest a reconstruction of the original object.

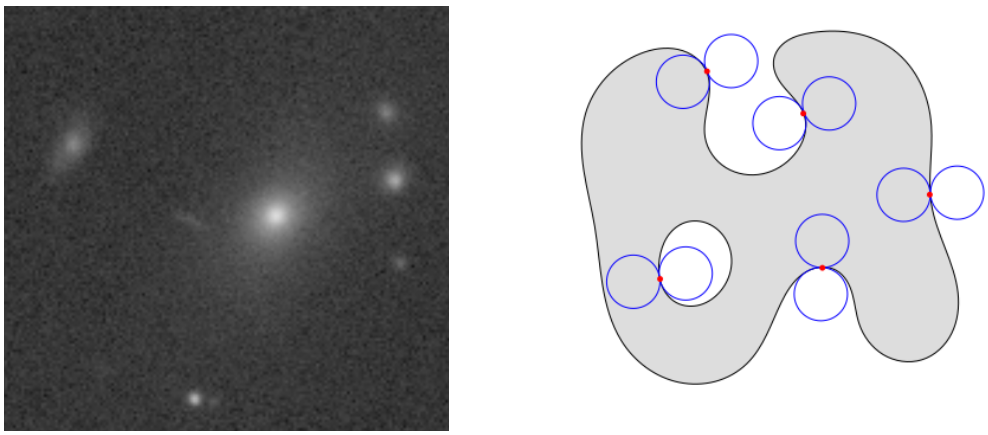

Fig. 1. *Left:* Noisy image of distant galaxies from [9]. Astronomers are interested in knowing the shape of such galaxies: Are they circular, ellipsoid or do they have spiral arms?
Right: An r-regular set with osculating r-balls shown.

We formulate the idealisation of a noisy image as a graph problem which can be solved using integer linear programming (ILP); this is explained in Section 3. As finding an optimal solution using ILP is NP-hard, we also suggest a less computationally demanding greedy algorithm, which makes stepwise locally optimal improvements starting from a trivial initialization.This algorithm generally produces a suboptimal output, but in practice it performs well when run multiple times.

2 Related Work

While "object reconstruction" aims to infer any geometric or topological property of the original object, the ultimate goal is to reconstruct the object itself, a task which largely coincides with image segmentation. Modern image segmentation algorithms such as deep convolutional neural networks [6] work as pixel classifiers which cannot possibly return the underlying object itself. At the very best, they return an ideal image of the object. Our proposed algorithm thus should not be viewed as an alternative to these segmentation tools, but rather

as a tool to be used together with them, estimating object boundaries from pixel classification output.

2.1 Related segmentation algorithms

A number of classical image segmentation algorithms aim to estimate object boundaries from images. For instance, variational segmentation algorithms aim to estimate either the object [7] or its boundary [1, 2, 5, 11] by optimizing a functional which measures the fit between the proposed object (boundary) and the image. In Active Shape Models [3], this is done with the additional information of a statistical object model. In [4], simulated annealing is used to reconstruct the entire object (and therefore, implicitly, its boundary) using a statistical image model based on thermodynamics.

As these methods are based on non-convex optimization, they are not guaranteed to find an optimal solution, and therefore work best when one has some initial idea about what object to find. In contrast, under the assumption of r-regularity, [8] obtain bounds on the error of the reconstructed object boundary, at least in the non-noisy case. We therefore propose estimating the optimal non-noisy image from a noisy one, as explained in Section 3. The object boundary can then be reconstructed from the non-noisy image with guarantees.

Note, additionally, that the assumption of r-regularity is a local restriction on the shape of the original object, and not a global assumption as the one that is needed in e.g. the Active Shape Model approach [3].

2.2 Reconstructing r-regular objects from ideal images

The strength of our approach is the assumption of r-regularity of the objects that we are looking for, since this puts restrictions on their possible ideal images. Let us introduce the concept of r-regularity:

Definition 1. *Let $r \in (0, \infty)$. A closed set $X \subseteq \mathbb{R}^n$ is said to be* r-regular *if, for any point $p \in \partial X$, there exist two balls $B_r(x_b) \subseteq X$ and $B_r(x_w) \subseteq X^c$ of radius r such that $\overline{B_r(x_b)} \cap \overline{B_r(x_w)} = \{p\}$, see Figure 1, right.*

In [8], du Plessis and S. studied digital images of r-regular objects constructed in the following way:

Definition 2. *Let $X \subseteq \mathbb{R}^2$ be a subset and $(d\mathbb{Z})^2 \subseteq \mathbb{R}^2$ a lattice. To each lattice square C, we assign an* intensity $\lambda \in [0, 1]$ *given by*

$$\lambda = \frac{Area(X \cap C)}{d^2} \in [0, 1].$$

The image of X (by $(d\mathbb{Z})^2$) is now the collection of pairs (C, λ) of lattice cubes and their corresponding intensities.

In this paper, we will consider noisy images. In a noisy image, the intensities are distorted, so it will most likely be hard to use intensities for reconstruction. Hence, we may as well restrict ourselves to only consider pixels as being either black, grey or white. We therefore introduce the following:

Definition 3. *Let I be an image. The* trinary *image J (of I) is the image I where all grey values are set to 0.5. If I is ideal, we call J the trinary ideal image.*

Theorem 1 (Proved in [8]). *Let J be a trinary ideal image of an r-regular object X by a lattice $(d\mathbb{Z})^2$, with $d\sqrt{2} < r$. Then we can construct an object Y from J such that $d_H(\partial X, \partial Y) < d$, where d_H denotes the Hausdorff distance. The running time for this reconstruction algorithm on an $n \times n$ image is $O(n^2)$.*

Empirical results suggest that we can improve the Hausdorff distance between object and reconstruction, but for now it will have to remain a conjecture.

In the process of proving this theorem, the following theorem popped up, and it will be essential later on:

Theorem 2 (Proved in [8]). *In the trinary ideal image of an r-regular object by a lattice $(d\mathbb{Z})^2$ with $d\sqrt{2} < r$, there are at most 562 different configurations of 3×3 pixels. These are the ones shown in Figure 2, along with their rotations, mirror images and interchanging of black and white colours.*

Furthermore, there are limits on which configurations can be combined with which in such an image.

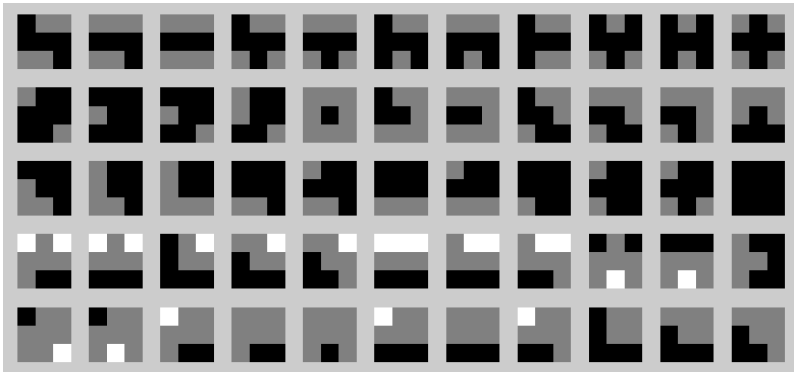

Fig. 2. Up to rotation, mirroring and interchanging of black and white pixels, these are the only 3×3 configurations of pixels we expect to see in the image of an r-regular object with $d\sqrt{2} < r$

3 Noisy images

Consider a noisy image I of an r-regular object X where $d\sqrt{2} < r$. We want to use our knowledge of trinary ideal images of r-regular objects to find the trinary ideal image of X from the noisy one. Henceforth, the only ideal images we will be working with will be trinary, so we will often omit the word 'trinary' for brevity. We will say that a noisy image I has an underlying (trinary) ideal image J that is not observed.

By Theorem 2 there is a collection $C = \{C_k\}_{k\in K}$ of ideal 3×3 pixel configurations that we may see in the image of an r-regular set when $d\sqrt{2} < r$. We use these to formulate the problem as a graph problem. Let $\mathcal{I}_{i,j}$ denote the 3×3 pixels centered at the (i, j)'th pixel of the noisy image I.

Over each configuration $\mathcal{I}_{i,j}$ in I, the ideal configurations in C are possible configurations in the same position of the underlying ideal image J. These ideal configurations form the vertices of a graph. An ideal configuration $C_k \in C$ sitting over the noisy configuration $\mathcal{I}_{i,j}$ is given a weight $p_k^{i,j}$ measuring the similarity between C_k and $\mathcal{I}_{i,j}$. Two ideal configurations are connected by an edge if they sit over neighbour configurations in I and match on their overlap, see Figure 3. By 'neighbour configurations' we here mean any two 3×3 configurations sharing 6 pixels.

The problem is now to choose an ideal configuration over each noisy configuration in I, such that the chosen configurations match their neighbours on the overlap, and the sum of their similarity weights are maximised. If this problem is solved, we may piece an ideal image together from the configurations chosen. This image is then optimal in the sense that the sum of its similarity weights is maximal among all ideal images.

The problem can be formulated as an integer linear programming problem in the following way: Let

$$c_k^{(i,j)} = \begin{cases} 1 & \text{if } k\text{'th configuration is chosen at position } (i,j) \\ 0 & \text{otherwise} \end{cases}.$$

The sum to be maximised is then

$$\sum_{i,j,k} c_k^{(i,j)} p_k^{(i,j)},$$

where

$$\sum_{k\in K} c_k^{(i,j)} = 1$$

for each (i, j), since we only choose one configuration over each configuration in the noisy image. Stacking $c_k^{(i,j)}$ to a vector c, let A be the adjacency matrix of the graph. Requiring that each chosen configuration is connected to its chosen neighbour configuration may be formulated as

$$Ac \geq Bc,$$

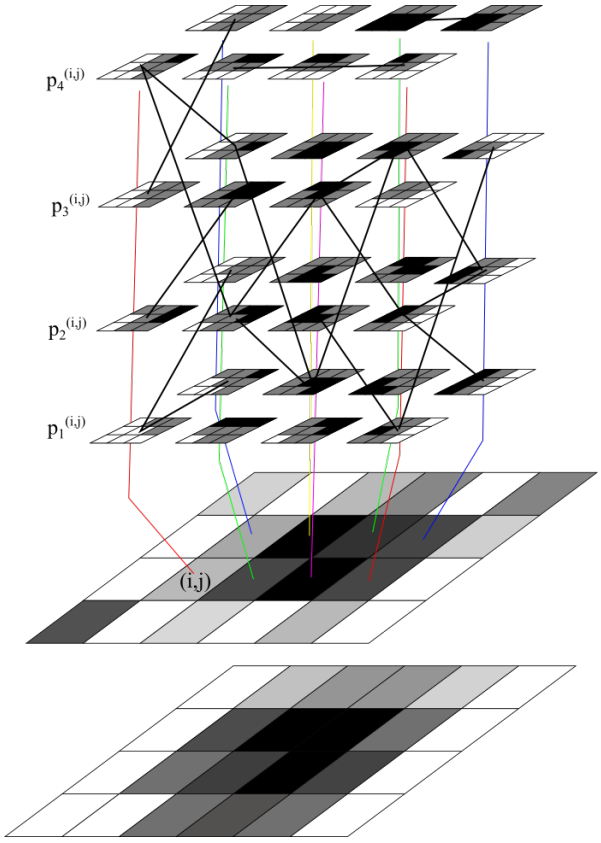

Fig. 3. Over each 3×3 configuration in a noisy image I, we have a set of possible configurations for the underlying image J. These configurations form the vertices of a graph and are given weights quantifying their deviation from the observed configuration. Two configurations are connected by an edge if they sit over neighbour configurations in I and match on their overlap.

Algorithm 1 Pseudo-code for the local algorithm

INPUT Noisy image I
$\hat{J}$ = Suggestion for I, initialised to an all white image.
$Weights$ =Matrix of weights of the configurations in current $\hat{J}$
$[XMin, YMin]$ =Position of minimal value of $Weights$
Update configuration at position $[XMin, YMin]$ in $\hat{J}$ to configuration with a black pixel in the middle, and greys around it.
Update $Weights$ to match this new $\hat{J}$
$NbList$ =Positions of horisontal/vertical neighbour configurations of altered ones.
$k = 0$
while k=0 **do**
  TempNbList=NbList;
  Find the entry (i, j) in $TempNbList$ where changing white pixels of corresponding configuration in $\hat{J}$ to greys and centre pixel to black would cause the largest increase in $Weights(i, j)$.
  if Such a configuration exists **then**
    Check if this update of $\hat{J}$ contains any illegal configurations
    if It does not **then**
      Update $\hat{J}$
      Update $Weights$
      Update $NbList$ by adding positions of neighbour configurations
    else
      Remove position (i, j) from $TempNbList$
    end if
  else
    $k = 1$
  end if
end while
if n connected component are expected in the image **then**
  Repeat the above n times
end if

where B is a diagonal matrix whose (l, l)'th element is the number b_l of neighbour configurations of configuration l.

Solving these equations is a well-known optimisation problem with a range of software options available, of which we used CPLEX [10].

4 A greedy local algorithm

As ILPs are generally NP-hard, the running time for the above algorithm quickly increases for large images. Therefore, we also tried another approach: We start with one solution to the graph problem and try to improve it.

Let I be a noisy image with underlying ideal image J. We suggest the greedy algorithm detailed in Algorithm 1, which was implemented in MatLab.

5 Similarity weights

In Section 3 we needed weights $p_k^{i,j}$ on ideal configurations C_k measuring their similarity to an observed noisy configuration $\mathcal{I}_{i,j}$. We propose to construct the weights as follows:

Let p_1 be a pixel from the noisy image and p_2 a trinary pixel from one of the ideal configurations. We measure the distance between p_1 and p_2 with a function $\hat{d}$ given by

$$\hat{d}(p_1, p_2) = \begin{cases} 0 & \text{if } p_2 = 0.5 \text{ and } 0 < p_1 < 1 \\ |p_1 - p_2| & \text{otherwise} \end{cases}$$

We can then define the weight $p_k^{i,j}$ as

$$p_k^{i,j} = \sqrt{\sum_{r,s=1}^{3} \hat{d}(\mathcal{I}_{i,j}(r,s), C_k(r,s))^2},$$

where $\mathcal{I}_{i,j}(r,s)$ denotes the (r,s)'th entry in $\mathcal{I}_{i,j}$.

6 Experiments

Results from both the ILP algorithm and the greedy local algorithm are shown in Table 1. The noisy images were obtained from ideal ones by adding Gaussian white noise with mean 0 and variance 0.1. The greedy algorithm was run several times with different starting points (s.p.), giving different outputs. The results using the three most likely starting points are shown in columns 3-5. In column 6 the minimum of 8 outputs of the greedy algorithm with different starting points is shown. Since the minimum image may contain configurations not in the list from Theorem 2, we may not use our reconstruction algorithm on it. Therefore we have used the ILP algorithm on it to remove illegal configurations, see column 7. Finally, in column 8 we have used the ILP algorithm directly on the noisy image. The yellow lines in the figures in column 3-5 and 7-8 are reconstructed boundaries from Theorem 1.

7 Discussion

The ILP algorithm reconstruction to the far right in Table 1 works well, although there are more grey pixels in the reconstructed image than in the original one. This may partly be due to boundary effects, since configurations near the boundary have fewer neighbour configurations they need to match.

The main problem with the ILP algorithm is that the NP-hardness makes it very time-consuming. Several tests indicate that for images only slightly bigger than those in this paper, the ILP algorithm is so slow that it is of no practical use.

The running time for the greedy algorithm is $O(n^4 \log_2 n)$ for an $n \times n$ image, but images with many white pixels are processed faster than images with many

Table 1. Reconstruction results for both the greedy algorithm with different starting points and the ILP algorithm.

black pixels. In practical cases, the greedy algorithm is much faster and therefore easier to work with. However, results from the greedy algorithm are generally not as nice as results from the ILP algorithm. The output quality depends greatly on the starting point and the algorithm is not good at finding large black areas or the right number of components. This is due to the construction of the algorithm, which may still be improved. The algorithm can also not reconstruct loops, since this requires addition of a configuration not in the list C.

All of these flaws are present in the outputs of the greedy algorithm in Table 1. However, the superposition is a good approximation of the object, and when the ILP and greedy algorithms are used together, we get a good suggestion for the reconstruction as seen in column 7 of the table. Empirical results seem to indicate that the running time of the ILP algorithm on the superposition of the outputs from the greedy algorithm is a bit shorter than the running time of the ILP algorithm used directly on the noisy image, but note that the ILP algorithm used with the greedy algorithm is still rather slow since the ILP is still solving an NP-hard problem.

To sum up, the ILP algorithm gives the best output, but its running time must be brought down if it is to be of practical relevance. The greedy algorithm is faster, but the quality of the output is less reliable. We are still working on improving running time and output for both algorithms.

References

1. Caselles, V., Kimmel, R., Sapiro, G.: Geodesic active contours **22**(1), 61–79 (1997)
2. Chan, T., Vese, L.: Active contours without edges. IEEE TIP **10**(2), 266–277 (2001)
3. Cootes, T.F., Taylor, C.J.: Active shape models – "smart snakes". In: BMVC (1992)
4. Geman, S., Geman, D.: Stochastic relaxation, Gibbs distributions, and the Bayesian restoration of images. TPAMI **6**(6), 721–741 (1984)
5. Kass, M., Witkin, A., Terzopoulos, D.: Snakes: Active Contour Models. IJCV **1**(4), 321–331 (1988)
6. Litjens, G.e.: A survey on deep learning in medical image analysis. MedIA **42**, 60 – 88 (2017)
7. Mumford, D., Shah, J.: Optimal approximations by piecewise smooth functions and associated variational problems. Comm. Pure Appl. Math. **42**, 577–684 (1989)
8. du Plessis, A., Svane, H.: Reconstruction of r-regular objects from trinary images, 2018. Available at `https://drive.google.com/drive/folders/1qxnDkmvXI3JQVlgTPCz2k4aPt_BUSv-u?usp=sharing`
9. SDSS, S.D.S.S.: `https://www.sdss.org`
10. V12.8.0, I.I.C.O.S.: `www.cplex.com`
11. Yezzi, A., Kichenassamy, S., Kumar, A., Olver, P., Tannenbaum, A.: A geometric snake model for segmentation of medical imagery. IEEE TMI **16**(2), 199–209 (1997)

Paper D

Preservation of Topology during Digitisation of a 3-dimensional r-regular Object

By Helene Svane and Andrew du Plessis

Abstract

We study what information is contained in the set of black voxels of a grey-scale image of an object $X \subseteq \mathbb{R}^3$. We have shown that under reasonable assumptions on the regularity of the object X and the resolution of the three-dimensional image, it is possible to construct an object from the black voxels that have the same topological features as the original object X.

D.1 Main Theorem

We study the following kind of digitisations of an object:

Definition D.1. Let $X \subseteq \mathbb{R}^n$ be a Lebesgue-measurable set and $d > 0$ a number. Then $d\mathbb{Z}^n$ is a lattice and to each point p of this lattice, there is a cube $C = C(p)$ of side length d whose centre lies at p. Let μ be the three-dimensional Lebesgue measure and $\varphi : [0,1] \to [0,1]$ a function such that $\varphi(x) = 1$ if and only if $x = 1$, and $\varphi(x) = 0$ if and only if $x = 0$. We associate an intensity

$$\lambda_C = \varphi\Big(\frac{\mu(C \cap X)}{d^n}\Big)$$

to each such cube that is a function of the fraction of the square that is covered by the object.

The *digital image* I of X by the lattice $d\mathbb{Z}^3$ is the collection of grid points and associated intensities, and may be thought of (or visualised as) the collection of lattice cubes $C(p)$, $p \in d\mathbb{Z}^n$, each coloured a shade of grey corresponding to the associated intensity so that cubes with intensity $\lambda_C = 1$ are black, cubes with intensity $\lambda_C = 0$ are white, and cubes of other intensities are a shade of grey.

Let $V(X)$ (or sometimes just V) denote the set of black voxels in this digital image. In correspondance with the terminology introduced in [5], we will sometimes refer to $V(X)$ as the inner Jordan digitisation of X (by a lattice $d\mathbb{Z}^3$).

Since we will work with the inner Jordan digitisations in this paper, it is not important how the exact intensities of the non-black voxels are calculated, as long as the only black voxels of the image are the ones inside the object.

In the following, we will consider r-regular objects:

Definition D.2. Let $r \in (0, \infty)$. A closed set $X \subseteq \mathbb{R}^3$ is said to be *r-regular* if, for any point $p \in \partial X$, there exists two balls $B_r(x_b) \subseteq X$ and $B_r(x_w) \subseteq X^c$ or radius r such that $\overline{B_r(x_b)} \cap \overline{B_r(x_w)} = \{p\}$.

An equivalent definition of r-regularity is to say that X is r-regular if and only if X and $\overline{X^C}$ are both unions of closed r-balls, see Theorem A.2.

To measure the similarity between an object and its reconstruction, we use the notion of *isotopy*:

Definition D.3. Let M, N be manifolds and I an interval. An *isotopy* from N to M is a smooth map $F : N \times I \to M$ such that for each $t \in I$ the map

$$F_t : N \to M, \qquad x \mapsto F(x, t)$$

is an embedding. When such a map exists, the maps F_0 and F_1 are called *isotopic*.

When $N = M$, the map F_t is a diffeomorphism for each $t \in I$ and $F_0 = \mathrm{Id}_M$, F is called an *ambient isotopy*. Two smooth embeddings $f_0, f_1 : N \to M$ are called *ambiently isotopic* if there exists an ambient isotopy $F : M \times I \to M$ such that $f_1 = F_1 \circ f_0$.

In this paper, the main theorem will be the following:

Theorem D.4. *Let X be an r-regular object and $d > 0$ a number satisfying $d\sqrt{3} < r$. Let $V(X)$ be the inner Jordan digitisation of X by a lattice $d\mathbb{Z}^3$.*

It is possible to construct a set Z from the inner Jordan digitisation $V(X)$ that is ambiently isotopic to X.

This theorem implies that we given a digital image I of an r-regular object X at a reasonable resolution can construct an object Z from the image such that Z has the same topological features (number of connected components, number of holes etc.) as X. Hence we can in a sense reconstruct the topology of X from its digital image.

There are two key assumptions in our main theorem: Firstly, we require X to be r-regular, and secondly, we require that $d\sqrt{3} < r$. The first assumption is to make sure that the set X is 'nice' enough to give us a chance of reconstructing it (see Figure D.1(a)), and the second assumption is to make sure that the resolution is good enough to distinguish key features of the object, see Figure D.1(b).

D.2 Tang Christensen's Work

In her Ph.D.-thesis [2], Tang Christensen considered a problem similar to the one that we are adressing. She also used a digitisation of an object to reconstruct the topology

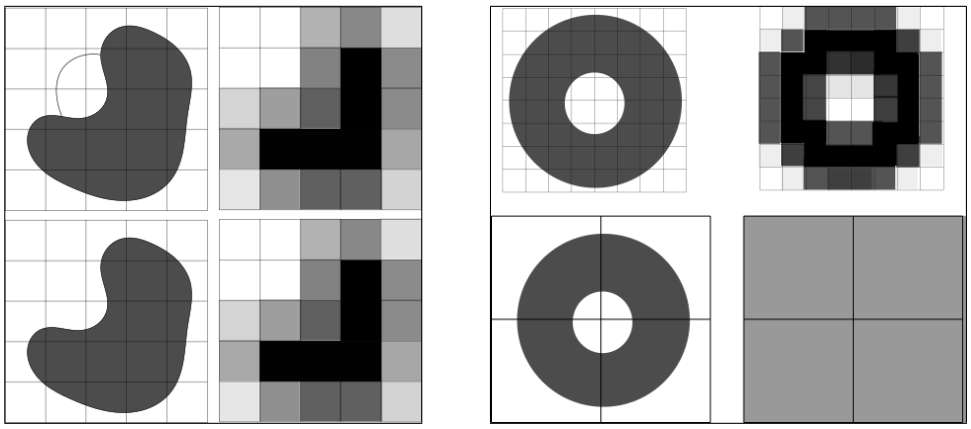

(a) **(b)**

Figure D.1: (a): A two-dimensional figure of the digitisation of a set X. The upper and lower X-sets (left) yield the same digital image (right), but their topology are quite different. So in this case, we cannot hope to recover an object from the image that has the same topology as the original one. However, the upper set is not r-regular for any $r > 0$. (b): If the resolution of our image is too small, we will not be able to reconstruct the topology of the original object. While the upper digital image is clearly a picture of a torus, the lower digital image cannot detect the hole in the middle of the torus.

of the object. However, she used another kind of digitisation than we do, known as Gauss Digitisation in [5], and considered sets with another regularity. Therefore we cannot apply her results directly. Instead, we modify her technique to prove our main theorem. Thus, it is appropriate to give a short overview of what she did in her thesis. She considered the following kind of digitisation:

Definition D.5. Let $d\mathbb{Z}^3$ be a cubic lattice and $A \subseteq \mathbb{R}^3$ an r-regular set with $\frac{d\sqrt{3}}{2} < r$. Let the set $A_0 = A \cap d\mathbb{Z}^3$ denote the digitisation of A, and let $V(A)$ denote the corresponding voxel reconstruction of A given by

$$V(A) = \cup_{l \in A_0} V(l),$$

where $V(l)$ is a $d \times d \times d$-cube with centre l.

The set $V(A)$ is sometimes denoted the *subset digitisation* or the *Gauss digitisation* in the literature, see [5]. Tang Christensen denotes it by *the voxel reconstruction.*

Her main result corresponds to ours:

Theorem D.6 (Tang Christensen's Main Result). *Let $d\mathbb{Z}^3$ be a cubic lattice and A an r-regular set with $0.95571d < r$. Then it is possible to construct an object Z from the Gauss digitisation $V(A)$ such that Z is ambiently isotopic to A, and hence contains the same topological information as the original object A.*

Tang Christensen proved the following, as a step towards her main result:

Theorem D.7. *There is a 1:1-correspondence between connected components of A and connected components of $V(A)$.*

For both her and our situations, the following holds:

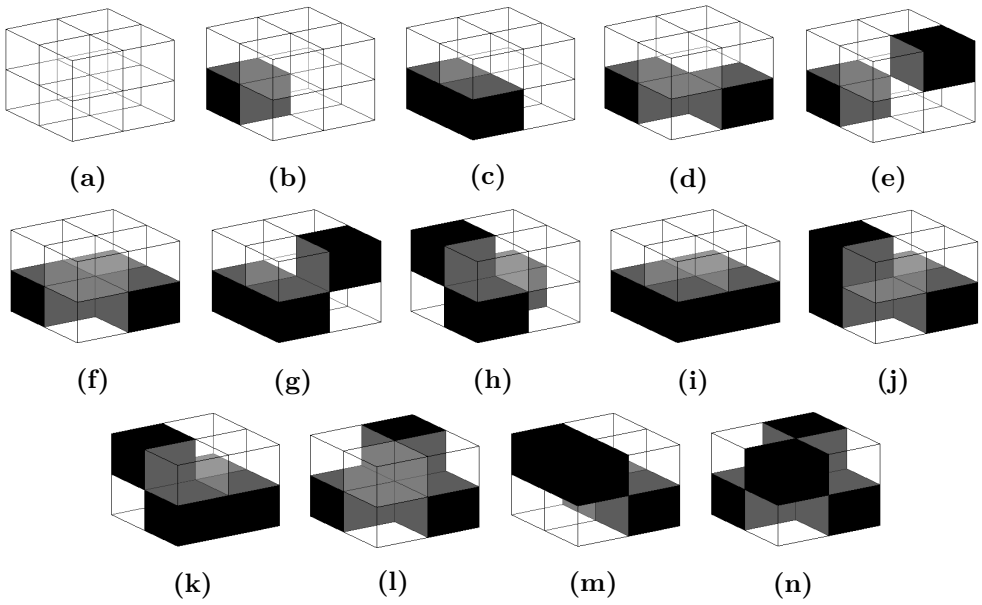

Figure D.2: Possible configurations of a $2 \times 2 \times 2$-cube with at most 4 black voxels. The remaining possible configurations correspond to (a)-(h) with the colours inverted.

Lemma D.8. *Up to rotation, reflection an inversion of the colours, there are 14 possible colour combinations of black and non-black voxels in each* $2 \times 2 \times 2$*-configuration, see Figure D.2.*

Proving this lemma is merely a question of doing combinatorics; for instance, if the $2 \times 2 \times 2$-cube contain exactly 2 black voxels, these two either share a face, an edge or a corner, and up to rotation and reflection, each of these can happen in exactly one way. If the $2 \times 2 \times 2$-cube contains 0,1,3 or 4 cubes, one can arrive at the possible configurations by similar reasoning, and if it contains 5,6,7 or 8 black voxels, then switching the colours of the black and non-black voxels one can use the arguments from the cases with 0-4 black voxels. We leave the details out.

Now, Tang Christensen introduced the following:

Definition D.9. A voxel reconstruction is a quasi-manifold (with boundary) if it satisfies:

(i) The only configurations of black voxels (up to rotational and reflectional symmetry) are (a)-(g), (i), (j) and (l) of Figure D.2, together with (a)-(g) with the colours inverted.

(ii) Configurations (d) and (g) are only allowed when paired with their own or each other's complement as illustrated in Figure D.3;

(iii) Any pair of black voxels in the same component of the voxel reconstruction is connected by a chain of face-adjacent black voxels.

Theorem D.10. *The black voxel reconstruction* $V(A)$ *of an* r*-regular set* A *by a lattice of side length* d*,* $0 < 0.95571d < r$*, is a quasi-manifold.*

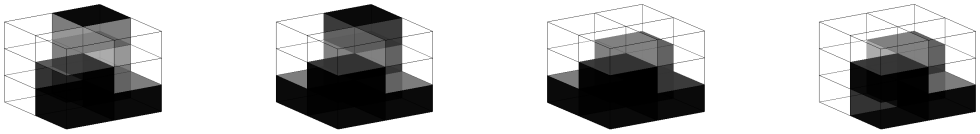

(a) (g) paired with its own inverse. **(b)** (g) paired with the inverse of (d). **(c)** (d) paired with its own inverse. **(d)** (d) paired with the inverse of (g).

Figure D.3: The only possible occurences of configurations (d) and (g) from Figure D.2. Note that the second and fourth configurations are each others inverses.

Theorem D.11. *Given a quasi-manifold V, it is possible to insert and remove wedges from V to obtain a topological manifold W. Furthermore, the edges and vertices of W may be smoothed in arbitrarily small neighbourhoods to obtain a smooth manifold Z.*

In her thesis [2], Appendix B, Tang Christensen thoroughly explains how the sets W and Z are constructed. She then proves the following:

Proposition D.12. *There is a set T diffeomorphic to $\partial A \times [-1,1]$, with boundaries $T_{-1} \simeq \partial A \times \{-1\}$, $T_1 \simeq \partial A \times \{1\}$, such that*

- *The intersections $\partial Z \cap T_{-1}$ and $\partial Z \cap T_1$ are empty,*
- *The boundary ∂Z of Z is a subset of $\mathrm{Int}(T) = f^{-1}((-d\sqrt{3}, d\sqrt{3}))$,*
- *The boundary ∂Z separates T in the sense that $T \setminus \partial Z$ consists of two connected components, one containing $T_{-1} \simeq A \times \{-1\}$, the other containing $T_1 \simeq A \times \{1\}$.*

The main idea to prove the main theorem D.6 is to use the following corollary of the Poincare-Hopf Theorem and the above theorem:

Proposition D.13. *[Proposition 2.20 in [2]] Let M, N be compact smooth n-manifolds without boundary, and let T be a set diffeomorphic to $M \times [-1,1]$. Let T_{-1}, T_1 be the subsets of T corresponding to $M \times \{-1\}$, $M \times \{1\}$, respectively, under this diffeomorphism. Suppose $N \subset T$ in such a way that N separates T, i.e. there are open sets $U \supset T_{-1}$ and $V \supset T_1$ such that $T \setminus N = U \amalg V$ is a disjoint union.*

Let v be a continuous, nowhere zero vector field on T and suppose v points inwards at T_{-1}, outwards on T_1 and is transverse to N. Then

$$\chi(M) = \chi(N),$$

where χ is the Euler characteristic.

Tang Christensen introduces a vector field satisfying the requirements of Proposition D.13 on the set T from Proposition D.12, which allows her to combine these above two results to get

Corollary D.14. $\chi(\partial Z) = \chi(\partial A)$. *In particular, ∂A and ∂Z are homeomorphic.*

This corollary is crucial, because it allows us to apply the following theorem to Tang Christensen's situation:

Theorem D.15 (Chazal and Cohen-Steiner, [1]). *Let $M, N \subseteq \mathbb{R}^3$ be two compact, orientable surfaces such that*

- *M is homeomorphic to N,*
- *N is included in a set T homeomorphic to $M \times [-1, 1]$,*
- *N separates the sides of T in the sense that $T \setminus N$ consists of two connected components, one containing $T_{-1} \simeq M \times \{-1\}$, the other containing $T_1 \simeq M \times \{1\}$.*

Then N and M are isotopic through an isotopy in T.

Applying this theorem to her situation and using isotopy extension on T, we get the following, which imply Tang Christensen's Main Theorem D.6:

Theorem D.16. *Let Z be the smoothed voxel reconstruction of an r-regular set A by a grid $d\mathbb{Z}^3$. Then ∂Z is ambiently isotopic to ∂A.*

These were the ideas that Tang Christensen used, at that we will copy.

Going through Tang Christensen's work, it turns out that she uses the symmetry between the white and the black voxels that is present in her digitisation model, so whenever she showed things for the black voxels, they would automatically hold for the white voxels as well. We are not quite as lucky, so we need to take extra care. Thus, diving into her approach, we see that in order to apply it to our digitisation model, we should reformulate Theorem D.7 as

Theorem (Reformulation of Tang Christensen's Theorem D.7). *There is a 1:1-correspondence between connected components of A and connected components of $V(A)$. Furthermore, there is a 1:1-correspondence between components of A^C and components of $V(A)^C$.*

We should also reformulate point iii) in the definition of a quasi-manifold, so the definition becomes the following

Definition (Reformulation of Definition D.9)**.** A voxel reconstruction is a quasi-manifold (with boundary) if it satisfies:

(i) The only configurations of black voxels (up to rotational and reflectional symmetry) are (a)–(g), (i), (j) and (l) of Figure D.2, together with (a)–(g) with the colours inverted.

(ii) Configurations (d) and (g) are only allowed when paired with their own or each other's complement as illustrated in Figure D.3;

(iii) Any pair of black voxels in the same component of the voxel reconstruction $V(X)$ is connected by a chain of face-adjacent black voxels. Furthermore, any pair of non-black voxels in the same component of the complement $V(X)^C$ of the voxel reconstruction is connected by a chain of face-adjacent non-black voxels.

In order to apply Tang Christensen's approach to our setup, we need to prove that those of Tang Christensen's theorems that are specific to her digitisation model also holds for our digitisation model. That means that we have to prove the following:

- There is a 1:1-correspondence between components of X and components of $V(X)$, and also between components of X^C and components $V(X)^C$.
- $V(X)$ is a quasi-manifold (in our reformulated sense),
- There is a set T satisfying the requirements of Proposition D.12.

The rest of the paper we will be dealing with these problems, one at a time.

D.3 Preliminaries

Before we start, we should mention some important facts about r-regular sets, which we will use excessively in the following.

Definition D.17. For $\delta > 0$, we denote the δ-tubular neighbourhood of ∂X in $\mathbb{R}^3$ by $N_\delta = \{x \in \mathbb{R}^3 \mid d(x, \partial X) < \delta\}$.

Proposition D.18 (Duarte & Torres, [4]). *Let $X \subseteq \mathbb{R}^n$ be an r-regular set. Then there is $\eta : \partial X \to \mathbb{R}^3$ such that*

- *η is a normal vector field along ∂X,*
- *$\|\eta(x)\| = r$ for every $x \in \partial X$,*
- *$\mathrm{Lip}(\eta) \leq 1$.*

Lemma D.19 (Duarte & Torres, [3]). *Let X be an r-regular set. For each $x \in N_r$ there is a unique point $\pi(x) \in \partial X$ such that $d(x, \partial X) = d(\pi(x), x)$. Hence there is a well-defined projection $\pi : N_r \to \partial X$, and this map is continuous.*

The corresponding theorems in Duarte and Torres [3, 4] only shows this theorem on $N_{r/2}$, However, the proof works just as well on N_r by Theorem A.13, (ii).

Theorem D.20 (Proven in A.13,(iii)). *Let $f : N_r \to \mathbb{R}$ be the function given by*

$$f(x) = \frac{1}{r}\langle x - \pi(x), \eta(\pi(x))\rangle.$$

Then f is C^1 and the zero set of f is $f^{-1}(\{0\}) = \partial X$.

In this last theorem, we have modified the function from Duarte and Torres' papers [3, 4] by a factor of $\frac{1}{r}$. However, this does not change the results.

With our definition f measures the (signed) distance between a point and the boundary of X, since $x - \pi(x)$ and $\eta(\pi(x))$ are parallel (cf. Remark A.10). The theorem implies the main result of Duarte and Torres' paper [3]:

Theorem D.21 (Duarte & Torres [3]). *Let $X \subseteq \mathbb{R}^n$ be an r-regular set. Then ∂X is a co-dimension one manifold of class C^1.*

One can come up with examples of r-regular sets that are C^1, but not C^2 (see [3]), so this is the best we can hope for in terms of smoothness of r-regular sets.

Proposition D.22 (Proven in A.27). *Let $-r < s_1 < s_2 < r$ and let f be the function from Theorem D.20. Then*

(i) $f^{-1}([s_1, s_2])$ *has manifold boundary* $f^{-1}(\{s_1\}) \cup f^{-1}(\{s_2\})$

(ii) $f^{-1}([s_1, s_2])$ *is diffeomorphic to* $\partial X \times [-1, 1]$.

Furthermore, we have a retraction $\rho : N \to X^C \cup \partial X$ from Definition A.28 defined by

$$\rho(x) = \begin{cases} x & \text{if } x \in X^C \cup \partial X \\ \pi(x) & \text{otherwise} \end{cases},$$

This retraction will be crucial in later arguments, since it has some nice properties:

Proposition D.23 (Stelldinger et al., [6]). *Let* $x, y \in X^C$ *with* $d(x, y) < 2r$ *and let* $L \subseteq \mathbb{R}^n$ *be the line segment between them. Then*

(i) The line segment L *is a subset of* $X^C \cup N_r$*, and* $\rho|_L$ *is injective,*

(ii) For $s < r$ *and* B_s *any* s*-ball containing* x *and* y*,* $\rho(L)$ *is a subset of* B_s*.*

Definition D.24. Let $L \subseteq \mathbb{R}^n$ be a closed line segment of length $|L| < 2r$. Then the r-spindle $S(L, r)$ is the intersection of all closed balls of radius r whose boundaries contain both endpoints of L.

Lemma D.25 (Proven in Addendum A.32). *Let* $L \subseteq \mathbb{R}^n$ *be a closed line segment of length* $|L| < 2r$*. Then the* r*-spindle* $S(L, r)$ *is the intersection of all closed balls of radius less than* r *that contain* L*.*

Corollary D.26 (Proven in Corollary A.33). *Let* $x, y \in X^C$ *with* $d(x, y) < 2r$ *and let* $L \subseteq \mathbb{R}^n$ *be the line segment between them. Then* $\rho(L)$ *is a subset of the* r*-spindle* $S(L, r)$*.*

When $x, y \in X^C$ are white points and L is the line between them, we will call the path $\rho(L)$ between them a *white path* (even though it may contain points in ∂X).

Another useful fact will be the following:

Theorem D.27 (Proven in A.38). *Let* x, y, z *be three non-collinear points in a closed* s*-ball* B_s*,* $s \in (0, r)$*, and let* T *be the triangle that they span. Write* L_i *for the edge of* T *opposite vertex* i*. Then there exists a continuous map* $\sigma : T \to B_s \cap (X^C \cup \partial X)$ *such that*

(i) *The image* $\sigma(T)$ *of* T *under* σ *is a subset of* B_s*,*

(ii) *The function* σ *is equal to the function* ρ *on* $L_x \cup L_y \cup L_z$*.*

D.4 Reconstructing topological features

D.4.1 Correspondence between components of X and $V(X)$

We now turn return to our setup, where X is an r-regular object and $V(X)$ is the inner Jordan digitisation of X by a lattice $d\mathbb{Z}^3$ with $d\sqrt{3} < r$.

As already explained, one of the ingredients needed to apply Tang Christensen's work to our situation is to show that there is a correspondence between components of X and $V(X)$, so that is what we will do in this section.

Theorem D.28. *There is a 1:1-correspondence between connected components of X and connected components of $V(X)$.*

This result is established through a series of results. First, we need to know that the reconstruction actually detects all components of X:

Lemma D.29. *Every connected component X' of X contains at least one black voxel in its digital reconstruction.*

Proof. Let X' be a connected component of X. Then X' is also r-regular, so in particular there is a ball $B_r(x) \subseteq X'$. Let $V(l)$ be the voxel containing x, centred at l. Since $\operatorname{diam} V(l) = d\sqrt{3} < r$, this means that $V(l) \subseteq B_r(x) \subseteq X$, and hence $V(l)$ must be black. □

Lemma D.30. *The reconstruction of a connected component of X is also connected.*

Proof. Consider two black cubes $V(l), V(l')$ in $V(X')$, the inner Jordan digitisation of X'. If $V(l)$ and $V(l')$ both contain elements y, y' of $X_\ominus = \{x \in X \mid d(x, \partial X) > d\sqrt{3}\}$, pick a path in $X_\ominus$ from y to y' – this is possible since $X_\ominus$ is connected. Then any voxel that this path enters must be black: a point in such a voxel can be no further away from $X_\ominus$ than $d\sqrt{3}$, whereas elements of X^C must be strictly further away than $d\sqrt{3}$. Hence the path from y to y' gives rise to a path of black voxels from $V(l)$ to $V(l')$.

On the other hand, if $V(l)$ does not contain a point of $X_\ominus$, then $\frac{d}{2} \leq d(l, \partial X) < d\sqrt{3} - \frac{d}{2}$. Let y denote the point $\pi(l) - \frac{d\sqrt{3}}{r}\eta(\pi(l))$. Then the point y lies on the line through l and normal to ∂X at $\pi(l)$, and $d(y, \partial X) = d\sqrt{3}$. Thus

$$d(y, l) = d(y, \partial X) - d(l, \partial X) \leq d\sqrt{3} - \frac{d}{2} < \frac{3d}{2}$$

so y must belong to a neighbouring voxel $V(m)$, since points not in a neighbouring voxel is at least a distance $\frac{3d}{2}$ away from l. And by our previous argument, since $y \in X'_\ominus$, $V(m)$ must be black. Since any black voxel is adjacent to a black voxel containing an element of $X'_\ominus$, and since any voxels containing elements of $X'_\ominus$ can be connected through a chain of black voxels, we must have that $V(X')$ is connected. □

The final lemma that we need in order to prove Theorem D.28 is the following:

Lemma D.31. *Let $\mathcal{X}$ denote the set of connected components of X. Then*

$$V(X) = \bigcup_{X' \in \mathcal{X}} V(X'),$$

and this union is disjoint.

Proof. It should be clear that $V(X) = \bigcup_{X' \in \mathcal{X}} V(X')$, so the only tricky part is to show that this union is disjoint. But this is clear, since for connected components X' and X'', $V(X') \subseteq X'$ and $V(X'') \subseteq X''$, which are disjoint. □

Proof of Theorem D.28. Let X' be a connected component of X. By Lemma D.29 X' contains a voxel, hence for each connected component of X, there is at least one black voxel in X'. By Lemma D.31, black voxels belonging to different connected components of X are not connected through a chain of black voxels, so for each component X', there is at least one connected component of $V(X)$. By Lemma D.30, there must in fact be exactly one connected component of $V(X)$ for every connected component of X. Since any voxel of $V(X)$ belong to some connected component of X, we get a 1:1-correspondence. □

A similar result is true for the complement:

Theorem D.32. *The connected components of X^C is in 1:1-correspondence with the connected components of $V(X)^C$.*

Proof of Theorem D.32. The proof of this is similar to what we just did. Let $V(X)^C$ denote the set of non-black voxels in the reconstruction of X.

Let Y' be a connected component of X^C. Then there is a white ball $B_r(x_w) \subseteq Y'$. The voxel $V(l)$ containing x_w must be contained in $B_r(x_w)$ and hence be white, so each component of X^C contains at least one non-black voxel.

Assume $V(l_1)$ and $V(l_2)$ are non-black voxels that each contain an element y_1, y_2 of Y'. Since Y' is connected, there is a path in Y' connecting y_1 and y_2. Each point of this path is contained in a white ball, hence each point of the path must belong to a non-black voxel. So the path gives rise to a path of non-black voxels connecting $V(l_1)$ and $V(l_2)$, showing that the set of non-black voxels containing points of a connected component Y' is connected. Thus any connected component of X^C gives rise to a connected component of $V(X)^C$. If we can show that these connected components are disjoint, we would have a 1:1-correspondence between components of X^C and components of $V(X)^C$.

Consider two connected components Y' and Y'' of $V(X)^C$ and two voxels $V(l_1)$ containing a point $y_1 \in Y'$ and $V(l_2)$ containing a point $y_2 \in Y''$. If $V(l_1)$ and $V(l_2)$ are adjacent, then $d(y_1, y_2) \leq 2d\sqrt{3} < 2r$. Let L denote the line between y_1 and y_2. By the previous section, there is a path $\rho(L)$ in $X^C \cup \partial X$ from y_1 to y_2, and since ∂X has a nice normal vector field, we can push this path a little along the normal vector field of ∂X to obtain a path in X^C from y_1 to y_2. But then y_1 and y_2 belong to the same connected component of $V(X)^C$, contradicting the assumptions. Hence two voxels containing points from two different connected components cannot be adjacent, so each connected component of X^C give rise to a distinct connected component of $V(X)^C$, as claimed. □

D.5 Configurations

The next thing that we need to prove in order to apply Tang Christensen's results is that the inner Jordan digitisation $V(X)$ is a quasi-manifold. This is a key point in the argument, and also something that requires some work. To do this, we need to consider which configurations cannot occur in the digital image of an r-regular object by a lattice $d\mathbb{Z}^3$ with $d\sqrt{3} < r$. This section is devoted to such considerations.

Now, the aim of this section will be to show the following two theorems:

Theorem D.33. *Assume $r > d\sqrt{3}$. In the inner Jordan digitisation $V(X)$ of an r-regular set X by a lattice $d\mathbb{Z}^3$, neither of the following configurations of black and non-black configurations can occur:*

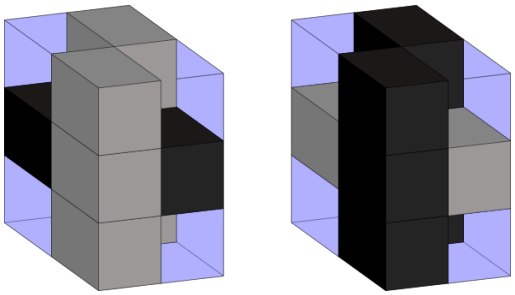

The grey cubes in these figures represents the non-black voxels, and the blue cubes represent voxels of unspecified colour.

Theorem D.34. *Assume $r > d\sqrt{3}$. In the inner Jordan digitisation $V(X)$ of an r-regular set X by a lattice $(d\mathbb{Z})^3$, neither of the following configurations of black and non-black configurations can occur, and nor can their inverses:*

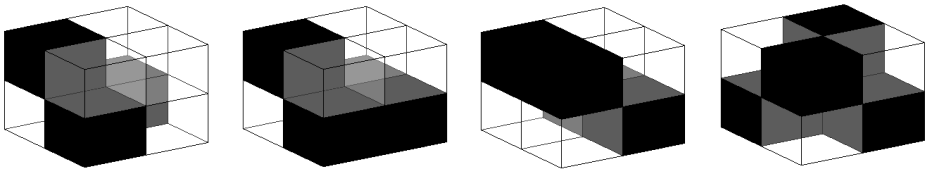

Furthermore, the following configuration cannot occur:

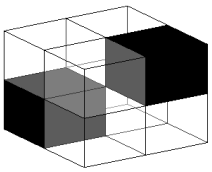

We remark that Theorem D.34 implies the first bullet point in the quasi-manifold definition, while the second bullet point in the quasi-manifold definition follows from Theorem D.33.

From now on, we will measure all lengths in units of d. We let X be an r-regular set with $d\sqrt{3} < r$. Tote that a set that is r-regular for some $r > \sqrt{3}$ in particular is $\sqrt{3}$-regular. Let $r' = d\sqrt{3}$ from now on.

In our arguments we will repeatedly need some basic facts, so we will go through these first. The following is perhaps the most important:

Lemma D.35. *Consider a configuration of 8 voxels in a $2 \times 2 \times 2$-cube centered at $x \in \mathbb{R}^3$ and suppose $A_1, \ldots, A_n$, $n \in \{3, 4\}$, are (some of the) non-black voxels in this configuration. Pick a white point x_i in the interior of each A_i and let $L_{i,j}$ denote the straight line segment from x_i to x_j. Suppose the configuration allows the following:*

- *There exists a simple black path $\gamma : [0, 1] \to \overline{B_{r'}(x)} \cap X$ from one boundary point of $B_{r'}(x)$ to another, such that $\gamma(0), \gamma(1) \in \partial B_{r'}(x)$ and $\gamma((0, 1)) \subseteq \mathrm{Int}(X)$, see Figure D.4,*

- *The composition of the paths $\rho(L_{i,i+1})$, $i = 1, 2, \ldots, n$ and $\rho(L_{1n})$ is linked with $\tilde{\gamma}$ in $B_{r'}(x)$, where $\tilde{\gamma}$ is the path obtained from γ by joining the endpoints of γ with an arc in $\partial B_{r'}(x)$.*

Then the configuration cannot occur in inner Jordan digitisation of an r-regular set, see Figure D.4.

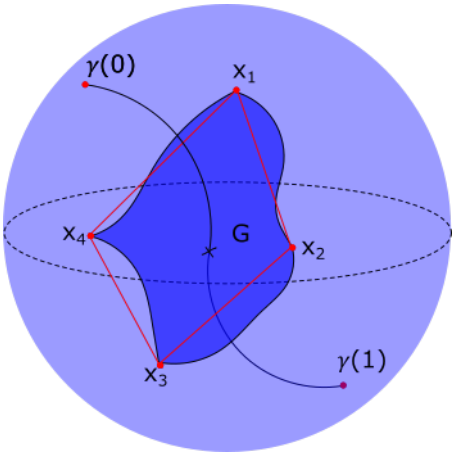

Figure D.4: It is impossible for the image of ρ on the boundary of a polygon spanned by four white points in a ball $B_{r'}(x)$ to be linked with a path $\gamma \in B_{r'}(x) \cap \mathrm{Int}(X)$.

Proof. Consider a configuration of voxels that allows the above conditions to be satisfied.

If $n = 3$, let G be the triangle with corners at the x_i's, and if $n = 4$, let G be the union of two edge-adjacent triangles with corners at the x_i's. Note that in both cases, the boundary of G will be line segments L_{ij}.

Let $H : D \to G$ be a homeomorphism, where D is a closed 2-disc. Note that (each of) the triangle(s) of G are mapped by σ to a subset of $B_{r'}(x)$ by Theorem D.27, since all x_i's are interior points of one of the voxels. Thus $\sigma(G) \subseteq B_{r'}(x) \cap (X^C \cup \partial X)$.

Define the map $F : \partial D \times [0, 1] \to \sigma(G) \subseteq B_{r'}(x) \cap (X^C \cup \partial X)$,

$$F(x, t) = \sigma(H(tx))$$

Then F is a continuous homotopy from $\sigma \circ H|_{\partial D} = \rho \circ H|_{\partial D}$ to a constant map $\sigma(H(0))$.

Now $\gamma((0, 1)) \subseteq \mathrm{Int}(X)$, so $\sigma(G) \cap \gamma((0, 1)) = \emptyset$, which means that $\rho \circ H|_{\partial D}$ is homotopic to a constant map in $B_{r'}(x) \setminus \gamma^*$.

On the other hand, $\rho(H(\partial D)) = \rho(\partial G)$ is the path formed by composing the $\rho(L_{i,i+1})$ and $\rho(L_{1,n})$ for $i = 1, 2, \ldots, n - 1$. Since it is linked with $\tilde{\gamma}$, the homology class of $\rho(\partial G)$ in $H_1((\gamma(0, 1))^C)$ is non-trivial, so the curve cannot be null-homotopic in $B_{r'}(x) \setminus \gamma((0, 1))$ – a contradiction. So a situation like the one in this lemma cannot occur in the reconstruction of an r-regular surface. □

Lemma D.36. *Let $A := [0, 1] \times [-1, 0] \times [0, 1]$ and $B := [-1, 0] \times [0, 1] \times [0, 1]$ be two grey voxels sharing an edge (see Figure D.5, left), and let $x_1 \in A$, $x_2 \in B$ be two white points. Let L be the line segment between x_1 and x_2. Then the path $\rho(L)$ must intersect the plane P containing $(1, 1, \pm 1)$ and $(-1, -1, \pm 1)$ inside a rectangle R with vertices $(1, 1, -1), (-1, -1, -1), (1, 1, 2)$ and $(-1, -1, 2)$.*

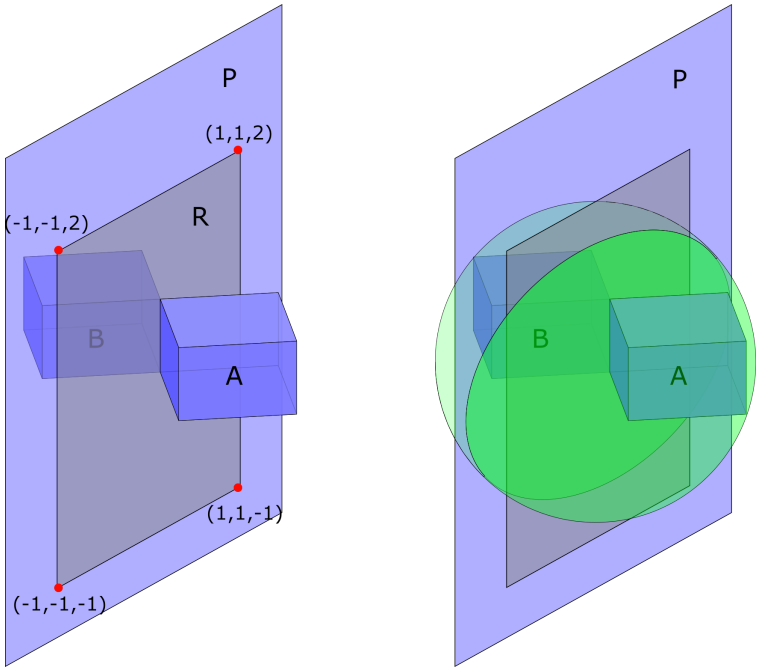

Figure D.5: Left: The path $\rho(L)$ between cubes A and B must intersect the blue plane P somewhere inside the black rectangle R. Right: The r-ball centered at the origin contains both A and B, and hence any spindle between two points in these cubes. It intersects the plane P somewhere beneath the level $z = 2$.

Proof. Let L be the line segment between x_1 and x_2 and note that $\rho(L) \subseteq S(L, r)$, which is the intersection of all closed balls of radius less than r containing L. It might therefore be a good idea to look at smartly chosen balls.

Note that the ball $B_{r'}(0, 0, 0)$ contains both A and B, and hence any spindle between them, see Figure D.5, right. The maximum z-coordinate value for a point in this sphere is $\sqrt{3}$, so any r-spindle between A and B must intersect P somewhere beneath the plane $z = \sqrt{3} < 2$.

Similarly, the ball $B_{r'}(0, 0, 1)$ also contains all of A and all of B, but does not contain any points with a z-coordinate less than $1 - \sqrt{3} > -1$. So any r-spindle between A and B must intersect P somewhere above the plane $z = -1$.

Now let $c_1 = (-\frac{1}{2}, -\frac{1}{2}, \frac{1}{2})$ and consider the ball $B_{r'}(c_1)$. It contains all of A and all of B. The maximum x-coordinate for a point in $P \cap B_{r'}(c_1)$ is $x = \frac{\sqrt{6}-1}{2} < 1$. So any r-spindle between A and B must intersect P in a point (x, x, z) where $x < 1$.

A similar argument with $c_2 = (\frac{1}{2}, \frac{1}{2}, \frac{1}{2})$ and the ball $B_{r'}(c_2)$ shows that an r-spindle between A and B must intersect P in a point (x, x, z) where $x > -1$, see Figure D.6.

Thus the white path $\rho(L)$ must pass the plane P somewhere inside the interior of the rectangle with vertices $(1, 1, -1), (-1, -1, -1), (1, 1, 2)$ and $(-1, -1, 2)$. □

Lemma D.37. *Let $n \geq 2$ and consider the two stacks of black voxels $C := [1, 2] \times [0, 1] \times [0, n]$ and $D := [0, 1] \times [1, 2] \times [0, n]$, see Figure D.7. Then the interior points of the rectangle R spanned by the corners $(2, 0, 0)$, $(2, 0, n)$, $(0, 2, 0)$ and $(0, 2, n)$ all belong to the interior of X.*

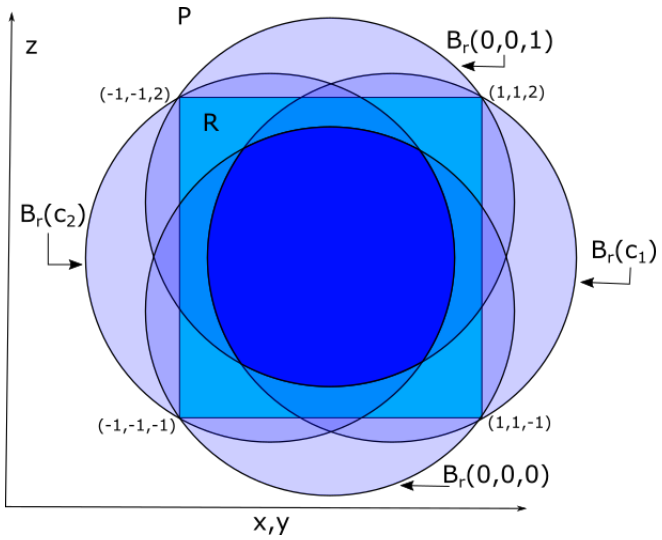

Figure D.6: The plane P. The intersection (dark blue area) of the plane P with the four balls is contained in the rectangle (bright blue) in P with vertices $(1,1,-1),(-1,-1,-1),(1,1,2)$ and $(-1,-1,2)$.

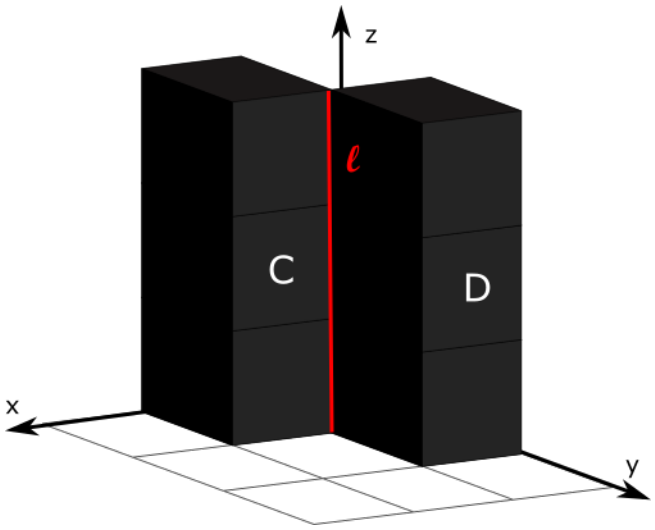

Figure D.7: The situation in Lemma D.37, in the case where $n = 2$ The hard part is to show that elements on the red line l cannot belong to ∂X

.

Proof. The statement is clear for all points in $R \setminus \partial R$ that does not belong to the open line segment l between $(1, 1, 0)$ and $(1, 1, n)$, since such points belong to the interior of black cubes and hence the interior of X. So we only need to consider the points of l.

But if $(1, 1, p) \in l$ was in fact a boundary point of X, for some $p \in (0, n)$, then there would exist a white r'-ball tangent to X at $(0, 0, p)$. However, such a ball would have non-empty intersection with either C or D, contradicting the fact that C and D are both black.

□

Lemma D.38. *Let $A := [0, 1] \times [0, 1] \times [0, 1]$ and $B := [0, 1] \times [0, 1] \times [-1, 0]$ be two grey voxels sharing a face as in Figure D.8, and let $x_1 \in \mathrm{Int}(A)$, $x_2 \in \mathrm{Int}(B)$ be two white points. Let L be the line segment between x_1 and x_2. If the path $\rho(L)$ intersects the plane P containing $(1, 0, \pm 1)$ and $(0, 1, \pm 1)$, then it does so inside the rectangle R with vertices $(1, 0, \pm 1)$ and $(0, 1, \pm 1)$.*

Proof. Note that $\rho(L)$ is contained in the r-spindle $S(L, r)$ which in turn is contained in every closed ball of radius less than r containing L, and hence also in every open ball of radius less than r containing L. Consider the open ball $B_{r'}(0, 0, 0)$. This ball contains both $\mathrm{Int}(A)$ and $\mathrm{Int}(B)$. In particular it contains both x_1 and x_2, and therefore $S(L, r)$. Now $\partial B_{r'}(0, 0, 0) \cap P$ is a circle centered at the origin and with radius 1, see Figure D.8, and such a circle is contained in the rectangle R with vertices $(1, 0, -1)$, $(1, 0, 1)$, $(0, 1, -1)$ and $(0, 1, 1)$.

Since $B_{r'}(0, 0, 0)$ was open, points in $B_{r'}(0, 0, 0)$ intersects P somewhere in the interior of R.

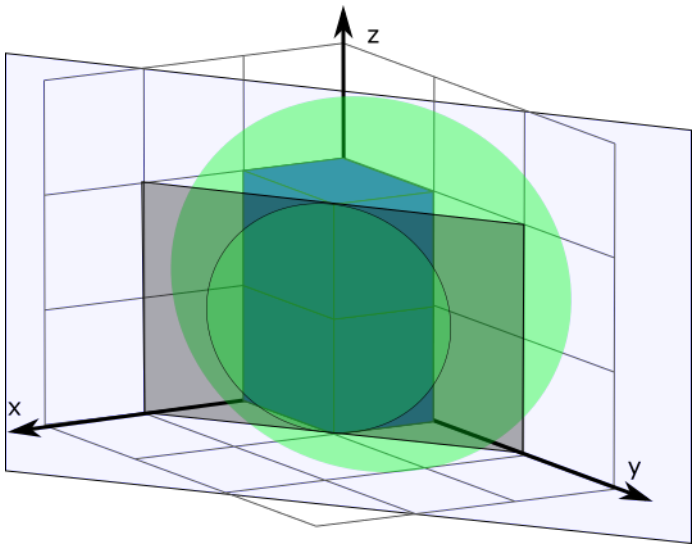

Figure D.8: The ball $B_{r'}(1, -1, 0)$ contains A and B and intersects the plane P in a circle of radius 1 centered at the origin

So if the path $\rho(L)$ intersects the plane P, it does so somewhere in the interior of R. □

We are now ready to prove Theorem D.33. Let us treat the cases one at a time.

D.5.1 Left configuration from Theorem D.33

Consider the configuration in Figure D.9.

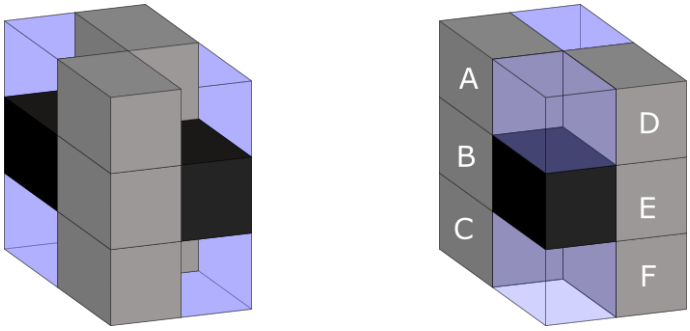

Figure D.9: The configuration that we are now considering, seen from two different angles. We do not wish to assume anything about the colour of the blue voxels in the figure.

Let us as usual start by naming the grey cubes as in the figure:

$$
\begin{aligned}
A &:= [0,1] \times [0,1] \times [1,2] \\
B &:= [0,1]^3 \\
C &:= [0,1] \times [0,1] \times [-1,0] \\
D &:= [-1,0] \times [-1,0] \times [1,2] \\
E &:= [-1,0] \times [-1,0] \times [0,1] \\
F &:= [-1,0]^3
\end{aligned}
$$

Remember that by Lemma D.36, the path $\rho(L)$ between any two white points in B and E, respectively, intersects the plane P containing the points $(\pm 1, \mp 1, 0)$ and $(\pm 1, \mp 1, 1)$ somewhere inside the rectangle R with corners $(1,-1,-1)$, $(1,-1,2)$, $(-1,1,-1)$ and $(-1,1,2)$. Notice that in our setup, the middle part $Q := \{(x,y,z) \in R \mid z \in [0,1]\}$ of that rectangle is black since it is contained in black voxels, so in fact such a path can only pass P somewhere above the level $z = 1$ or somewhere below $z = 0$.

Lemma D.39. *In the configuration in Figure D.9, there exists a ball $B_{r'}(x)$, a closed white path $\mathcal{L} \in B_{r'}(x)$ and a simple black path $\gamma \in B_{r'}(x)$ with end points in $\partial B_{r'}(x)$ such that $\mathcal{L}$ is linked with γ inside $B_{r'}(x)$.*

Proof. Choose white points $x_A \in \mathrm{Int}(A)$, $x_B \in \mathrm{Int}(B)$, $x_C \in \mathrm{Int}(C)$, $x_D \in \mathrm{Int}(D)$, $x_E \in \mathrm{Int}(E)$ and $x_F \in \mathrm{Int}(F)$, and let L_{ij} denote the line segment between x_i and x_j.

Consider the path a consisting of the join of the three path segments $\rho(L_{BA})$, $\rho(L_{AD})$ and $\rho(L_{DE})$. It is a path joining x_B to x_E that cannot pass P under the level $z = 0$ by Lemma D.38 and Lemma D.36, and hence it has to pass P somewhere above $z = 0$. Let us orient the path such that it starts at x_B and ends at x_E. This path must pass the plane P somewhere inside R, because this is true for each of the path segments $\rho(L_{BA})$, $\rho(L_{AD})$ and $\rho(L_{DE})$.

Similarly, the path b consisting of the path segments $\rho(L_{BC})$, $\rho(L_{CF})$ and $\rho(L_{EF})$ is a path joining x_B and x_E, and must intersect P somewhere below $z = 0$ for the

same reasons. Let us orient this path such that it starts at x_E and ends at x_B. Again, this path must pass the plane P somewhere inside R, because this is true for each of the path segments $\rho(L_{BC})$, $\rho(L_{CF})$ and $\rho(L_{EF})$.

Consider any path γ in Q, the black part of P, that run from one side $\{(1,-1,t) \mid t \in [0,1]\}$ of Q to the other $\{(-1,1,t) \mid t \in [0,1]\}$. Extending this path by adding a sufficiently large arc connecting the end points, we get a closed curve $\tilde{\gamma}$ that is linked with ab, since ab intersect P somewhere inside the rectangle R, see Figure D.10.

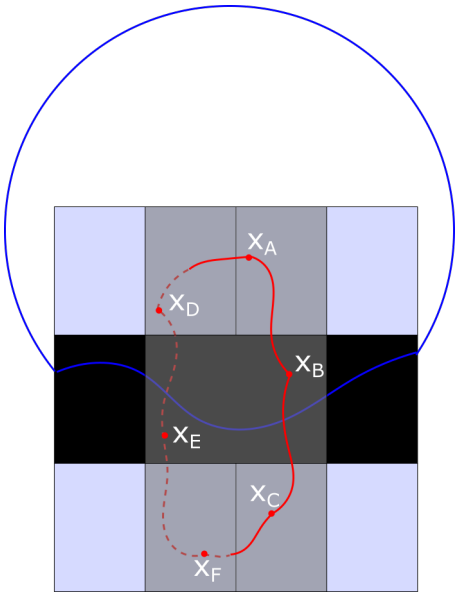

Figure D.10: The situation that we are considering. The figure shows the configuration, projected onto the plane P. The red path is the path ab, connecting the six white points. Any path γ (such as the blue path in this figure) inside Q (the black part of the rectangle) that has an endpoint on each side of Q can be connected with an arc in P that is so big that the composition of γ and the arch is linked with ab.

Put $c = \rho(L_{BE})$, oriented so that it starts at x_B and ends at x_E. Then, if $\text{link}(g,h)$ denotes the linking number of two path g and h,

$$1 = \text{link}(ab,\tilde{\gamma}) = \text{link}(a\bar{c}cb,\tilde{\gamma}) = \text{link}(a\bar{c},\tilde{\gamma}) + \text{link}(cb,\tilde{\gamma}),$$

showing that either $a\bar{c}$ or cb has non-trivial linking number with $\tilde{\gamma}$. Let us say that cb is linked with γ. Because cb is the composition of the path segments $\rho(L_{BC})$, $\rho(L_{CF})$, $\rho(L_{EF})$ and $\rho(L_{BE})$ that all belong to spindles of line segments of points in $B_{r'}(0,0,0)$, so must cb. Since cb is linked with γ for any path γ in Q that connects the sides of Q, we can in particular choose Q to be the piecewise linear path from $(1,-1,1)$ through $(0,0,\frac{1}{2})$ to $(-1,1,1)$. Then the end points of γ will belong to $\partial B_{r'}(0,0,0)$, which was what we wanted.

□

This lemma has now brought us in the situation of Lemma D.35, so we may now conclude that the configuration in Figure D.9 cannot occur.

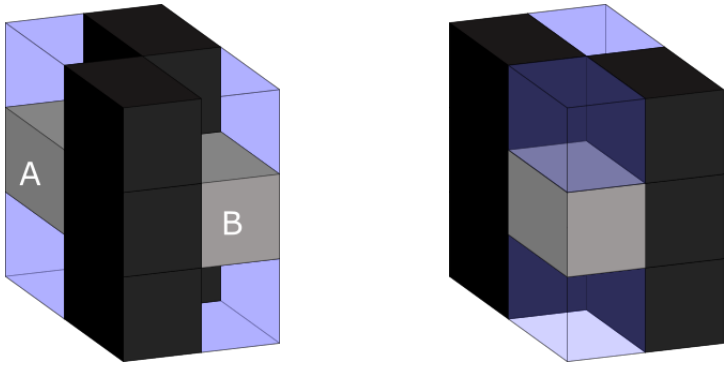

Figure D.11: The configuration of black and grey voxels that we consider, shown from two different angles. We do not wish to assume anything about the colour of the blue voxels in the figure.

D.5.2 Right configuration from Theorem D.33

Consider the configuration in Figure D.11. We wish to prove that this cannot occur.

For this pick a white point $x_1 \in A := [0,1] \times [-1,0] \times [0,1]$ and a white point $x_2 \in B := [-1,0] \times [0,1] \times [0,1]$, and let L be the straight line between them. Then $d(x_1, x_2) < 2r$, so there is a white path $\rho(L)$ between them that is contained in the r-spindle $S(L,r)$.

Consider the plane P through the points $(1,1,\pm 1)$, $(-1,-1,\pm 1)$. By Lemma D.36, the path $\rho(L)$ passes P somewhere inside the rectangle R with vertices $(1,1,2)$, $(1,1,-1)$, $(-1,-1,2)$ and $(-1,-1,-1)$. The interior of R is black since it is contained in black voxels (see Figure D.12) and cannot contain any boundary points of X by Lemma D.37, so $\rho(L)$ cannot pass P here – a contradiction. Thus the configuration in Figure D.11 cannot occur.

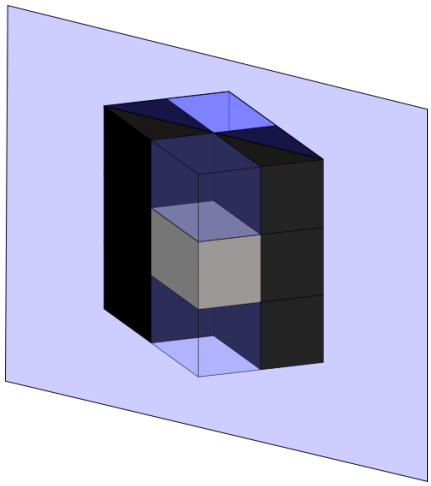

Figure D.12: We argue that the path $\rho(L)$ between a point in A and a point in B (the grey cube behind the plane) must pass the plane P somewhere inside the black part of P.

Now, combining the results of Subsections D.5.2 and D.5.1, we get Theorem D.33.

We now proceed to the proof of Theorem D.34. We consider the configurations

one at a time:

D.5.3 Third configuration three from Theorem D.34

Consider the configuration in Figure D.13. Once again, we wish to rule out the possibility of this occurring in a digitisation of an object.

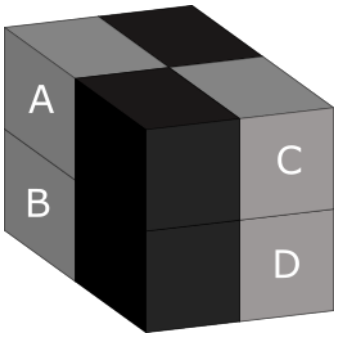

Figure D.13: The configuration we will show cannot occur. The voxel hidden behind the figure is also black, so that this configuration consists of four grey and four black voxels. The grey voxels have been named for later use.

We can start by naming the four grey voxels as in the figure, such that

$$\begin{aligned} A &:= [0,1] \times [-1,0] \times [0,1], \\ B &:= [0,1] \times [-1,0] \times [-1,0], \\ C &:= [-1,0] \times [-1,0] \times [0,1], \\ D &:= [-1,0] \times [0,1] \times [-1,0]. \end{aligned}$$

The aim will now be to apply Lemma D.35. To this end we will prove the following:

Lemma D.40. *Consider the configuration in Figure D.13. There is a white path* $\mathcal{L} \subseteq B_{r'}(0,0,0)$ *that runs once around a simple black piecewise linear path* γ *with endpoints* $(1,1,1)$, $(-1,-1,1)$.

Proof. Pick white points x_A, x_B, x_C, x_D, one in the interior of each of the four grey voxels A, B, C, and D. Each of these will be closer than $2r'$ to any one of the others. Let γ be the piecewise linear path from $(1,1,1)$ through $(0,0,1-\varepsilon)$ to $(-1,-1,1)$ for some small ε. Let L_{ij} be the straight line between x_i and x_j. We would like $\mathcal{L}$ to be a composition of white path segments $\rho(L_{ij})$, so we need to look at how these behave.

Let P be the plane through $(1,1,\pm 1)$, $(-1,-1,\pm 1)$, see Figure D.14 – this plane contains γ. By Lemma D.36, $\rho(L_{AC})$ has to pass P somewhere inside the rectangle R with corners $(1,1,-1)$, $(1,1,2)$, $(-1,-1,-1)$ and $(-1,-1,2)$, and since the lower half of this rectangle is black and does not contain any boundary points of X by Lemma D.37, $\rho(L_{AC})$ must in fact pass P in a point (x,x,z) where $z \in [1,2]$, as in the figure. So $\rho(L_{AC})$ passes P somewhere above γ.

Similarly, the white path $\rho(L_{BD})$ must pass P somewhere inside the non-black part of the rectangle with corners $(1,1,-2), (1,1,-1), (-1,-1,-2)$ and $(-1,-1,-1)$. So $\rho(L_{BD})$ passes P somewhere below γ.

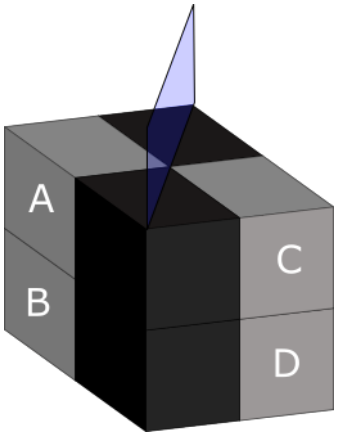

Figure D.14: The path $\rho(L_{AC})$ intersects the plane P somewhere inside the blue rectangle R. Since most of this rectangle is black, the path must intersect R somewhere above the plane $z = 1$.

By Lemma D.38, if $\rho(L_{AB})$ passes P, it does so somewhere in the interior of the rectangle with vertices $(1, 1, -1), (-1, -1, -1), (1, 1, 1)$ and $(-1, -1, 1)$. But this rectangle is black, and contains no boundary points of X in the interior by Lemma D.37, so $\rho(L_{AB})$ cannot pass P. By a similar argument, $\rho(L_{CD})$ cannot pass P either.

Composing the paths $\rho(L_{AB})$, $\rho(L_{BD})$, $\rho(L_{DC})$ and $\rho(L_{CA})$ we thus get a closed path that winds once around γ, and hence is also linked with γ. Note that this path is contained i $B_{r'}(0, 0, 0)$, since all points x_1, x_2, x_3 and x_4 are contained in this ball. □

Now we are in the situation of Lemma D.35, so we conclude that this configuration cannot occur.

D.5.4 First, second and fourth configuration from Theorem D.34

Consider the configuration in Figure D.15. We will not assume anything on the colours of the blue voxels, as we wish to prove that this configuration cannot occur regardless of what colours they may have. If we can show this, it follows that neither of the configurations (h), (k) or (n) from Figure D.2 can occur, and nor can their inverses.

Assume that x_A is a white point in the interior of $A := [0, 1]^3$ and that x_B is a white point in the interior of $B := [-1, 0] \times [-1, 0] \times [0, 1]$, and look at the line L_{AB} between them. Then $\rho(L_{AB})$ is a path in $X^C \cup \partial X$ between the two points, since $d(x_A, x_B) < 2r'$.

Consider the plane P containing the vertices $(1, -1, \pm 1), (-1, 1, \pm 1)$. We wish to determine where the white path $\rho(L_{AB})$ intersects this plane for the first time, starting from x_A. By Lemma D.36, $\rho(L_{AB})$ must intersect P somewhere inside the rectangle R with vertices $(1, -1, -1)$, $(1, -1, 2)$, $(-1, 1, -1)$, $(-1, 1, 2)$, see Figure D.16.

Notice that the middle part of the rectangle is black, so the white path cannot intersect P in this part of the rectangle. We wish to show the following:

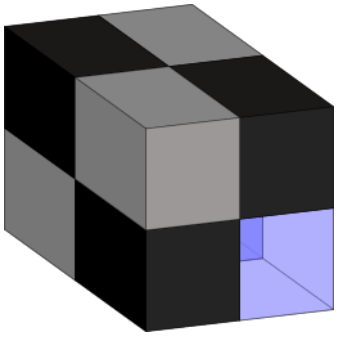

Figure D.15: The configuration we are considering. The voxel that is hidden is also blue, and we do not assume anything about the colour of the two blue voxels.

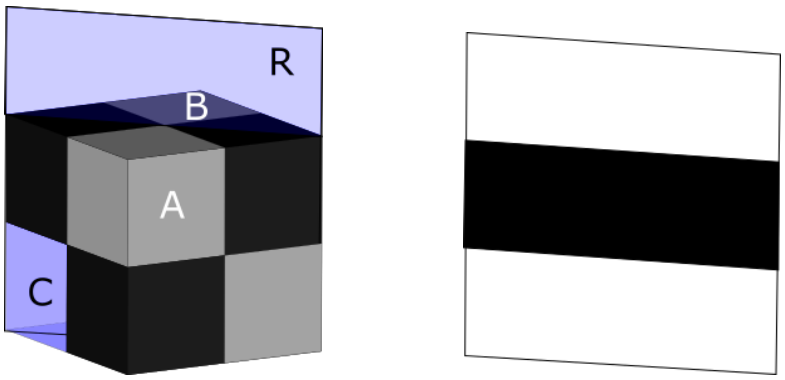

Figure D.16: The intersection between P and any r-spindle between a point in A and a point in B lies inside the rectangle R. Thus, the white path between x_A and x_B also intersects this rectangle. To the left, both the rectangle R and the configuration we consider are shown, and to the right the rectangle is shown on its own. In the latter figure, the middle part of the rectangle is coloured black, since we know that this part of the rectangle is contained in black voxels, and hence it is contained in X.

Lemma D.41. *The path $\rho(L_{AB})$ must intersect the plane P for the first time somewhere above the plane $z = 1$.*

Proof. Assume that this is not the case. Then the path intersects P for the first time somewhere beneath the black rectangle. Suppose $\rho(L_{AB})$ passes P for the first time somewhere in the voxel $C := [0, 1] \times [-1, 0] \times [-1, 0]$, see Figure D.16. Then $\rho(L_{AB}$ must also enter C for the first time (coming from A somewhere on the same side of the plane P as A. We investigate through which face(s) of C the path $\rho(L_{AB})$ can enter C for the first time when coming from A.

It cannot enter through one of the black faces of C, since $\rho(L_{AB})$ is a white path. It also cannot enter through one of the blue faces in the Figure D.17, since these faces lie on the opposite side of P, and $\rho(L_{AB})$ has not passed P yet by assumption. This leaves two faces.

Now $\rho(L_{AB})$ belongs to $S(L_{AB}, r')$, and thus to any ball of radius less than r' containing L_{AB}. If we let $c = (\frac{-1}{2}, \frac{1}{2}, \frac{1}{\sqrt{2}})$, then $B_{r'}(c)$ contains all of $\mathrm{Int}(A)$ and $\mathrm{Int}(B)$, and thus all spindles between them.

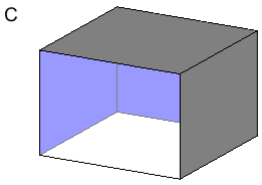

Figure D.17: We assume that the white path $\rho(L_{AB})$ enters the cube C. It cannot happen at the two black faces of C since the path is white, and it cannot happen through the blue faces, since they are on the wrong side of P.

The ball $B_{r'}(c)$ does not intersect the two remaining sides of the cube C, since

$$\begin{aligned} d(c,(1,y,z)) &= \sqrt{\left(-\frac{1}{2}-1\right)^2+\left(\frac{1}{2}-y\right)^2+\left(\frac{1}{\sqrt{2}}-z\right)^2} \\ &\geq \sqrt{\left(\frac{3}{2}\right)^2+\left(\frac{1}{2}\right)^2+\left(\frac{1}{\sqrt{2}}\right)^2} = \sqrt{3} = r' \end{aligned}$$

when $-1 \leq y, z \leq 0$, and similarly on the face $\{(x,y,-1) \mid 0 \leq x \leq 1, -1 \leq y \leq 0\}$, see Figure D.18. Since $\rho(L_{AB})$ belongs to $B_r(c)$, it cannot enter the cube C through either of the two white faces of C, and hence it cannot enter C before passing through P the first time.

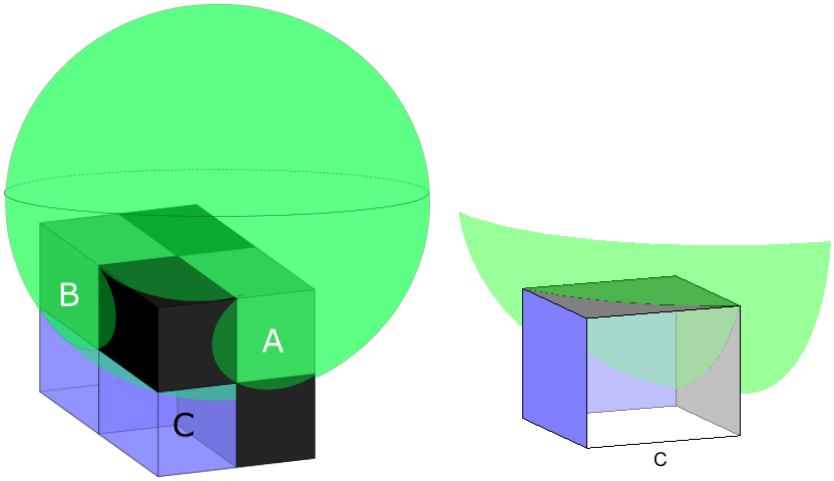

Figure D.18: The green ball contains A and B, but does not intersect C in a non-black face on the same side of P as x_A. The right hand picture shows only C and the sphere. Notice that the figures have been rotated to give a better picture of what is happening.

So $\rho(L)$ has to pass P somewhere above the black rectangle the first time. (In fact our argument shows that if $\rho(L)$ ever enters C, it must do so in the part of $\mathbb{R}^3 \setminus P$ containing x_B, and it must also leave C in this part of $\mathbb{R}^3$). So $\rho(L)$ is not wound around the black rectangle. □

In short, we have a white path $\rho(L_{AB})$ that passes over the black piecewise linear path γ through $(-1,1,1)$, $(0,0,\frac{1}{2})$ and $(1,-1,1)$. The aim will now be to use Lemma D.35. We will start by proving the following:

Lemma D.42. *There exists a white path $\mathcal{L}$ in $B_{r'}(0,0,0)$ that runs once around the piecewise linear path γ from $(-1,1,1)$ through $(0,0,\frac{1}{2})$ to $(1,-1,1)$.*

Proof. We already have a white path $\rho(L_{AB})$ that passes over the black piecewise linear path γ. We now wish to show that neither the path $\rho(L_{BD})$ from x_B to x_D, nor the path $\rho(L_{AD})$ from x_A to x_D, pass over γ, because then the result will follow from composing the three paths $\rho(L_{AB})$, $\rho(L_{BD})$ and $\rho(L_{AD})$.

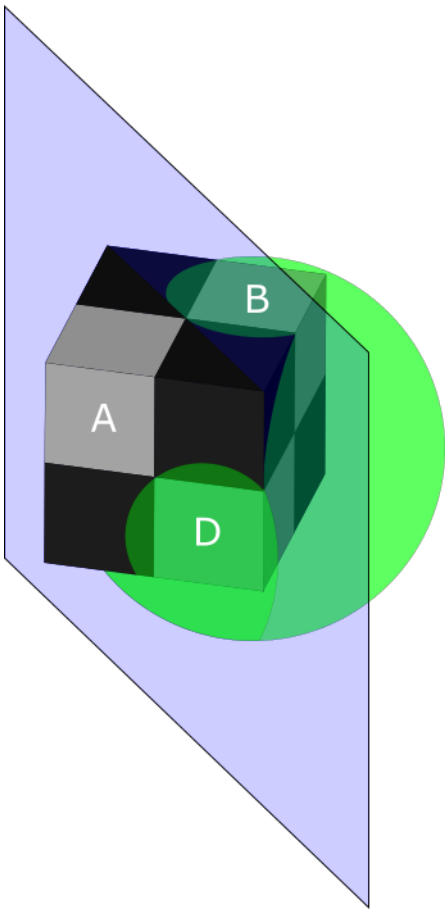

Figure D.19: The green sphere $B_{r'}((-\frac{1}{2},-\frac{1}{2},-\sqrt{\frac{5}{2}}+1))$ contains both B and D (the two rightmost grey cubes), but $\rho(L_{BD})$ must intersect the plane P (light blue) in a point that is not in the interior of X, so somewhere under γ

Consider the ball $B_{r'}((-\frac{1}{2},-\frac{1}{2},-\sqrt{\frac{5}{2}}+1))$. A computation shows that this ball contains all of B and all of D,(see Figure D.19) and thus any r-spindle between these two cubes. It also intersects P under the path γ: If $(x,-x,z) \in P \cap B_{r'}((-\frac{1}{2},-\frac{1}{2},-\sqrt{\frac{5}{2}}+1))$, then $z \leq 1$. Hence if the path from x_B to x_D, $\rho(L_{BD})$, passes through P, then it does so somewhere under the level $z=1$. But since $\rho(L_{BD})$ is non-black, it must in fact pass P somewhere under the level $z=0$, since the rectangle R is black in the part where $0 \leq z \leq 1$. So if the path $\rho(L_{BD})$ passes through P somewhere under the level $z=1$, it must also pass P somewhere under γ.

A similar argument shows that if $\rho(L_{AD})$ passes P, it also does so somewhere beneath γ.

So what we end up with now is a white path $\rho(L_{AB})$ from x_A to x_B that passes P somewhere over γ, and a white path $\rho(L_{BD}) \cup \rho(L_{AD})$ from x_A to x_B passing P somewhere under γ. Putting all three paths together, this yields a white path $\mathcal{L}$ in the ball $B_{r'}(0,0,0)$ that winds once around γ. □

Having established this result, we can now apply Lemma D.35 to conclude that the configurations in Figure D.15 cannot occur in the digital reconstruction of an r-regular set.

D.5.5 Configuration of two black voxels sharing just one corner

Consider the configuration of voxels in Figure D.20. We wish to show that this cannot occur.

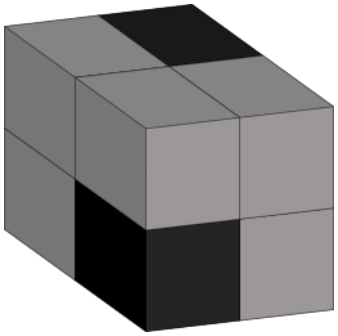

Figure D.20: The configuration that we are considering. The voxel hidden on the backside of the cube is also grey.

The origin o in this configuration is black and cannot belong to ∂X: If it did, there would be a white ball tangent to the origin, which is impossible since any such ball would contain a part of one of the black voxels.

Let $p \in \partial X$ be the boundary point closest to o, i. e. $p = \pi(o)$. Then there are two cases: Either the line from o to p passes through a black voxel, or it does not. We treat these two cases separately.

Lemma D.43. *Assume that the line through o and p does not pass through one of the black voxels. Then the configuration in Figure D.20 cannot occur.*

Proof. Let θ be the smallest angle between the position vector of p and the axes, say the z-axis.

Since p is a boundary point, there exists two balls $B_{r'}(x_b) \subseteq X$ and $B_{r'}(x_w) \subseteq X^C$ such that $\overline{B_{r'}(x_b)} \cap \overline{B_{r'}(x_w)} = \{p\}$. As p is the closest boundary pointto o, the tangent plane to ∂X at p is orthogonal to the position vector of p, and thus the centres x_b, x_w of the balls both lie on the line through p and o. The aim will be to show that the centre x_b of the black ball lies inside a grey voxel, for if this is the case, the voxel would be black, which gives a contradiction.

Let us look at the plane containing p and the z-axis, see Figure D.21.

Now, p was the nearest boundary point to o, meaning that it can be no further away from o than $r' = \sqrt{3}$. Hence one of the centres of the balls x_b or x_w must lie on the opposite site of o from p, and since the ball with this centre must contain o which was black, we must in fact have that x_b lies on the opposite site of o than p.

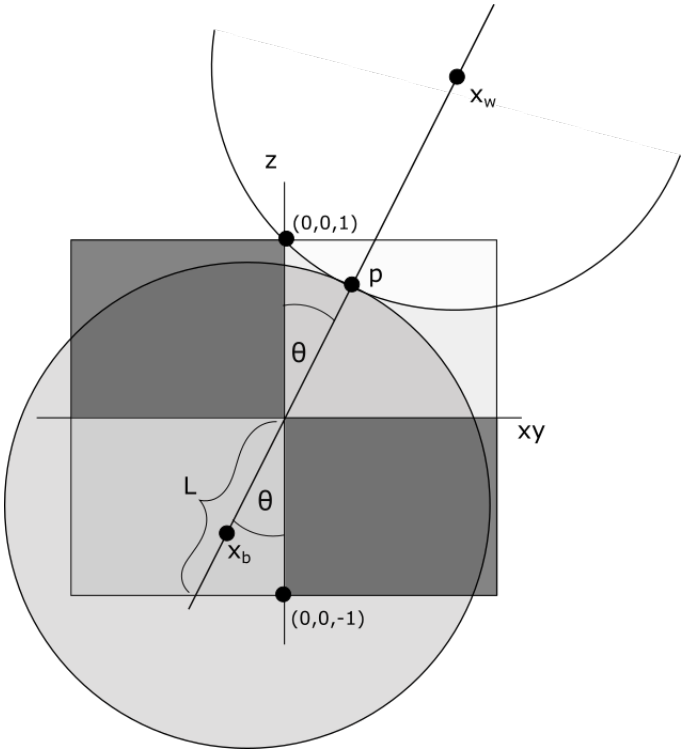

Figure D.21: The situation viewed in the plane containing the z-axis and p.

Since x_b lies on the line through p, in a distance r' to p, it is furthest from the origo when p is as close as possible to the origo. So we need a limit on how close p can be to the origo.

The white ball $B_r(x_w)$ is tangent to ∂X at p, and the point $(0,0,1)$ is black, so p cannot be so close to o that this white ball contains $(0,0,1)$. Thus p can get no closer to o than in the situation on the drawing, where $(0,0,1)$ is a boundary point of $B_r(x_w)$.

Let L be the length of the part of the line through p and o that is contained in the other non-black voxel, see Figure D.21. Then

$$L = \frac{1}{\cos\theta},$$

and using the law of cosines on the triangle with corners $(0,0,1)$, o and x_w and the fact that the circle has radius $r' = \sqrt{3}$, we have

$$\cos\theta = \frac{\|x_w\|^2 + 1 - 3}{2\|x_w\|}.$$

This equation may be rewritten as a quadratic equation in $\|x_w\|$ having the (non-negative) solution

$$\|x_w\| = \cos\theta + \sqrt{\cos^2\theta + 2}.$$

Putting these two together we get that

$$\|p\| + L = \|x_w\| - \sqrt{3} + L = \frac{1}{\cos\theta} + \cos\theta + \sqrt{\cos^2\theta + 2} - \sqrt{3}.$$

Since θ was the smallest angle between the position vector of p and one of the axes, we must have $\theta \leq \frac{\pi}{2}$. A computation now shows that the minimum value of $\|p\| + L$ is greater than r', which means that x_b lies inside the grey voxel.

So the centre of the black sphere would lie inside a grey voxel in this case, which would force the grey voxel to be black – a contradiction. □

Thus we only need to consider the case where the line from o to p passes through a black voxel.

Lemma D.44. *Assume that the line between o and the nearest boundary point p of ∂X passes through one of the black voxels. Then the configuration in Figure D.20 cannot occur.*

Proof. Assume that the line from p to o passes through a black voxel. Continuing along the line from p past o we would then enter the other black voxel. As before, somewhere on the line between o and p we would have two points x_b, x_w such that $B_{r'}(x_w) \subseteq X^c$, $B_{r'}(x_b) \subseteq X$ and $\overline{B_{r'}(x_w)} \cap \overline{B_{r'}(x_b)} = \{p\}$. Our aim will now be to show that $B_{r'}(x_b)$ contains one of the grey voxels, which would force the grey voxel to be black and thereby give us a contradiction. In order to do this, we need to know how far the centre of an r-ball containing a voxel V can be be from that voxel.

Concider a voxel V as in Figure D.22, with the vertices named as in the figure. Let $q = (\frac{1}{2}, \frac{1}{2}, \frac{3}{2})$. Then $q \in B_{r'}(a_i)$ and $q \in B_{r'}(b_i)$ for all i. Since the same thing

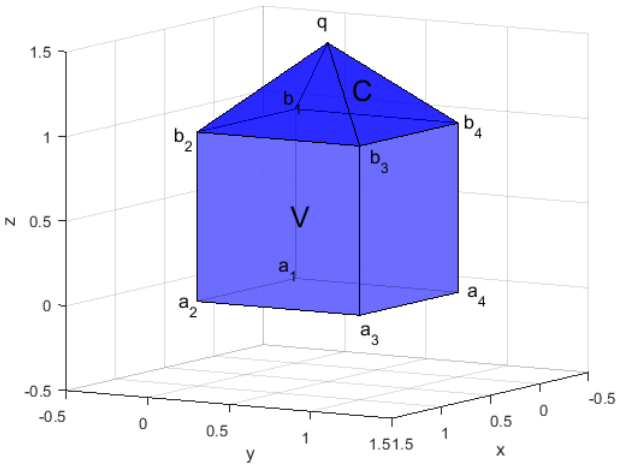

Figure D.22: We are considering a voxel V as the bright blue one. A sphere of radius $\sqrt{3}$ centered in the blue pyramid C on top of V will contain all of V.

holds for each corner, i.e. $a_i, b_i \in B_{r'}(a_j)$ and $a_i, b_i \in B_{r'}(b_j)$ for all i, j, and since all of these spheres are convex, the convex hull C of the b_i's and q must also lie in all these spheres. So an r'-ball centered in C must contain all a_i's and b_i's, and hence all of C. We will call C a pyramid attached to V.

Now the aim is to show that x_b belongs to one of the pyramids of the grey voxels, since this would force the corresponding voxel to be black, which would be a contradiction, see Figure D.23.

First of all, note that $\sqrt{3} \geq d(p, o) \geq 1$, since p cannot lie inside the black voxel that the line between the two points pass through. We now want to find the minimal

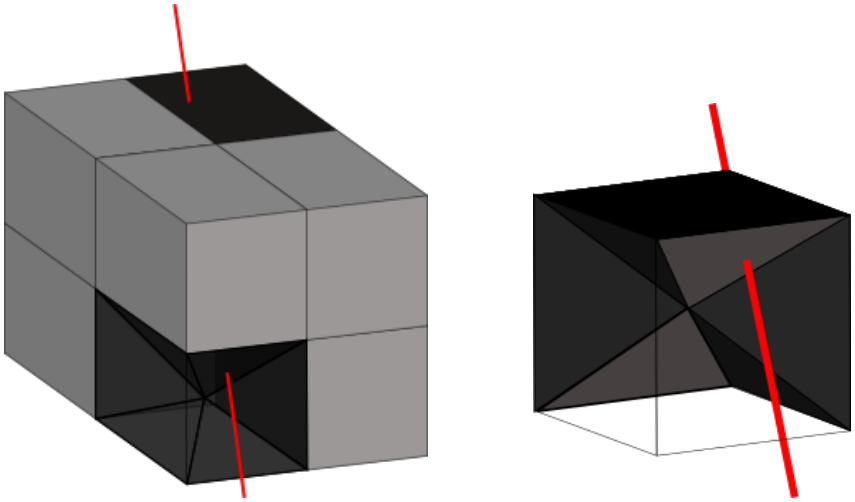

Figure D.23: Left: The center x_b of the black ball must lie on the line through o and p (red) in a distance of $\sqrt{3}$ from p. We show that in this case, x_b must lie in one of the pyramids attached to the lower grey voxels. Right: Close-up of the lower black voxel and the three pyramids attached to the neighbouring grey voxels

distance between o and the place c where the line leaves one of the pyramids attached to the grey voxels, see Figure D.23.

The line through p enters one of the pyramids at o, and must thereafter exit that pyramid in a point c on a face opposite of o. So we must find the smallest distance between a corner of a pyramid and a point on one of the faces opposite that corner.

Consider just a single pyramid as the one in Figure D.24, and suppose that our line enters it at o and leaves at one of its far faces, for instance the far face where $1-x \leq y \leq x$. The coordinate for a point on this face is of the form $(1-t, s, t)$ where $t \in [0, \frac{1}{2}]$ and $t \leq s \leq 1-t$. Thus

$$d((0,0,0),(1-t,s,t))^2 = (1-t)^2 + s^2 + t^2 \geq (1-t)^2 + 2t^2 \geq \frac{2}{3},$$

so that $d((0,0,0),c) \geq \sqrt{\frac{2}{3}}$ everywhere. But then

$$d(p,c) = d(p,o) + d(o,c) \geq 1 + \sqrt{\frac{2}{3}} > \sqrt{3}.$$

So since $d(p,x_b) = \sqrt{3} < d(p,c)$, x_b must belong to one of the pyramids, which would force one of the grey voxels to be black – a contradiction. □

These two lemmas put together show that the configuration in Figure D.20 cannot occur.

Now, combining the results of Subsections D.5.3, D.5.4 and D.5.5, and noting that the configurations in Theorem D.34 are all treated in these subsections, along with the inverses of the first four configurations, we have proved Theorem D.34.

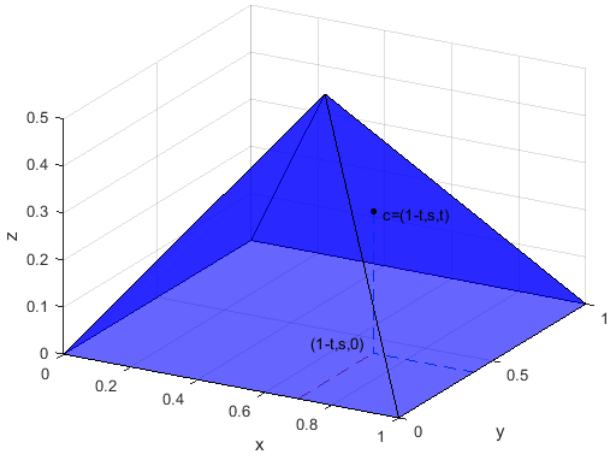

Figure D.24: A pyramid. We imagine a line that enters the pyramid at o and leaves at one of the opposite faces

D.6 Quasi-manifold property

This section is devoted to show that $V(X)$ satisfy the quasi-manifold requirements in our reformulated sense. Let us show that point (iii) of the quasi-manifold definition is satisfied by our digitisation.

Theorem D.45. *Let X' be a connected component of X. Then any two voxels in $V(X')$ are connected through a chain of face-adjacent voxels.*

Proof. Consider a connected component X' of X and two black cubes $\mathcal{V}(l), \mathcal{V}(l')$ in $V(X')$. By Theorem D.28 they belong to the same connected component, so there is a chain Γ of black voxels connecting them. We thus only need to show that we can replace Γ by a chain Γ' of face-adjacent black voxels.

Since the last of the configurations in Theorem D.34 cannot occur, then whenever two black voxels in Γ are vertex-adjacent, one of them must share a face and the other an edge with a third black voxel that we may then add to Γ. Similarly, whenever two black voxels are edge-adjacent, then they either both share a face with a third black voxel (which we may then add to the chain), or Theorem D.33 tells us that they must both share an edge with a third black voxel. If this is the case, then going through the possibilities for the neighbouring voxels and using Theorem D.34 they must be connected through a chain of face-adjacent black voxels. Hence in both cases there will be black voxels that we can add to Γ to obtain a chain of face-adjacent black voxels. □

Again, a similar result holds for X^C, but the proof is a bit different:

Theorem D.46. *Any two voxels containing points from the same connected component of X^C are connected through a chain of face-adjacent voxels.*

Proof. By the proof of Theorem D.32, there is a chain of voxels connecting any two non-black voxels $V(l_1)$ and $V(l_2)$. If two voxels $V(l)$ and $V(l')$ in this chain are adjacent, then the same proof shows that there is a white path γ connecting two white points $y_1 \in V(l)$ and $y_2 \in V(l')$. Each point on this path is white and

hence contained in the interior of a white ball, so each voxel containing a point of γ must be non-black. Hence if $V(l)$ and $V(l')$ are not face-adjacent, we may add voxels containing points of γ to get a path of face-adjacent non-black voxels from $V(l)$ to $V(l')$, as we wanted. □

Using Tang Christensen's definition of a quasi-manifold, we now have

Theorem D.47. *The black voxel reconstruction of an r-regular set by a lattice of side length d, $0 < d\sqrt{3} < r$, is a quasi-manifold.*

Proof. Remember that we have to check that $V(X)$ satisfies the following three requirements:

(i) The only configurations of black voxels (up to rotational and reflectional symmetry) are (a)–(g), (i), (j) and (l) of Figure D.2, together with (a)–(g) with the colours inverted.

(ii) Configurations (d) and (g) are only allowed when paired with their own or each other's complement as illustrated in Figure D.3;

(iii) Any pair of black voxels in the same component of the voxel reconstruction $V(X)$ is connected by a chain of face-adjacent black voxels. Furthermore, any pair of non-black voxels in the same component of the complement $V(X)^C$ of the voxel reconstruction is connected by a chain of face-adjacent non-black voxels.

Requirement (i) is satisfied if we can rule out the possibility of configurations (h), (k), (m) and (n) from Figure D.2. But this follows from Theorem D.34

For requirement (ii), let us start by considering which configurations of four voxels is allowed underneath a configuration of type (d). Since the configuration in Figure D.9 was ruled by Theorem D.33, at least one of the voxels under the non-black voxels in the bottom of (d) has to be black. If this is the case, both of the voxels under the black voxels in (d) must also be black, since we otherwise would get one of the forbidden configurations of Theorem D.34. Thus either all or all but one of the voxels under configuration (d) must be black, and in this case we end up in the scenario of Figure D.3(c) or D.3(d), respectively. Applying the same kind of argumentation to configuration (g), we get that (g) can only occur in the configurations on Figure D.3(a) or D.3(b).

Requirement (iii) is satisfied by Theorem D.45 and Theorem D.46, which concludes the proof. □

We can now insert wedges in $V(X)$ in exactly the same way that Tang Christensen did in Section 2.3.2 and B.2 of her thesis [2], since this process is done independently of the choice of r or the type of reconstruction, but only uses the possible configurations of voxels. We thus obtain the wedged reconstruction $W(X)$ of X. The insertion and removal of wedges from $V(X)$ is done in such a way that it does not split any component of $V(X)$ or $V(X)^C$ in two, implying that there still is a 1:1-correspondence between components of X and components of $W(X)$, and also between components of X^C and components of $W(X)^C$. This implies the following:

Corollary D.48. *The connected components of ∂X are in 1:1-correspondence with the connected components of $\partial W(X)$.*

Proof. As mentioned, the wedging is done in such a way that there is a 1:1-correspondence between components of X and components of $W(X)$, and also between components of X^C and components of $W(X)^C$. This implies the following:

Suppose ∂X has k components. By a corollary to the Jordan-Brouwer Separation Theorem, this means that ∂X separates $\mathbb{R}^3$ in $k+1$ connected components, and each component is either a subset of X or a subset of X^C. Hence

$$\begin{aligned} k+1 &= \#\{\textit{components of } X\} + \#\{\textit{components of } X^C\} \\ &= \#\{\textit{components of } W(X)\} + \#\{\textit{components of } W(X)^C\} \end{aligned}$$

Since $\partial W(X)$ divides $\mathbb{R}^3$ into $l+1$ components, where l is the number of connected components of $\partial W(X)$, and since each component of $\mathbb{R}^3 \setminus \partial W(X)$ is either a connected component of $W(X)$ or of $W(X)^C$, then $l = k$. Hence ∂X and $\partial W(X)$ have the same number of connected components. □

D.7 Finding a set T with the required properties

If we could apply Proposition D.13 to $M = \partial X$ and $N = \partial W(X)$, they would have the same Euler characteristic and hence be homeomorphic, since they are 2-manifolds. But in order to apply this theorem, we need a set T diffeomorphic to $\partial X \times [-1,1]$ containing $\partial W(X)$ as in the proposition, a non-zero vector field v on T satisfying the requirements, and a way to get around the problem of $\partial W(X)$ not being a smooth manifold.

To address the last issue first, Tang Christensen replaced $W(X)$ by a smoothed version of $W(X)$ that we will denote by Z. The smoothening procedure is described in [2], Section B.2 and it may be done such that $W(X)$ is only altered arbitrarily little. Let $d\sqrt{3} < s < r$ and let Z be a smoothing of $W(X)$ that has been made in so small a neighbourhood that $d_H(V(X), Z) < \varepsilon$, where $\varepsilon = r - s$ and d_H denotes the Hausdorff distance.

Tang Christensen provides us with a suggestion for the set T and a vector field on T with the required properties, so if we can just show that T satisfies the requirements of Proposition D.13 in our situation as well, we can use her suggestion for v, Z and T to prove that ∂Z and ∂X are homeomorphic using Proposition D.13. We make a suggestion for T similar to the one that Tang Christensen made:

Definition D.49. Put $T = f^{-1}([-s, s])$, where f is the function from Theorem D.20. By Proposition A.27, T is diffeomorphic to $\partial X \times [-1,1]$, and its boundary is $\partial T = f^{-1}(\{-s, s\})$.

With this definition, the set T consists of points $x \in \mathbb{R}^3$ that is closer than $s > d\sqrt{3}$ to ∂X.

We need to check that T satisfies the requirements of the Proposition D.12:

Proposition D.50. *Let T be as above, and let T_{-1}, T_1 be the two boundary components of T. Let Z be the smoothened version of $W(X)$ as described in [2]. Then*

- *The intersection $\partial Z \cap T_{-1}$ and $\partial Z \cap T_1$ are empty,*
- *The boundary ∂Z of Z is a subset of* $\mathrm{Int}(T) = f^{-1}((-s, s))$,

- *The boundary ∂Z separates T.*

Proof. Let $\tilde{T} = f^{-1}([-d\sqrt{3}, d\sqrt{3}]) \subseteq T$, and let $\tilde{T}_1$, $\tilde{T}_{-1}$ be the two boundary components of $\tilde{T}$. Note that $\tilde{T} \subset T$.

Consider a point $x \in \partial V(X)$, the inner Jordan digitisation of X. Since x is a boundary point, it must belong to a non-black voxel $V(l)$. Such a non-black voxel must contain a white point $p \in X^C$, and since X^C is open, we may assume that p is an interior point of this voxel. Since $V(X) \subseteq X$, x is a black point and thus

$$d(x, \partial X) \leq d(x, p) < d\sqrt{3}.$$

Since an element y of $\tilde{T}_{-1} \cup \tilde{T}_1$ satisfies $d(y, \partial X) = d\sqrt{3} > d(x, \partial X)$ and $x \in \partial V(X)$ was arbitrary, we must have $\partial V(X) \cap (\tilde{T}_{-1} \cup \tilde{T}_1) = \emptyset$, and $\partial V(X) \subseteq \mathrm{Int}(T)$, since $\mathrm{Int}(T)$ consists of the points that are closer than $d\sqrt{3}$ to ∂X. But since Z was $\varepsilon = r - s$ close to $V(X)$, this in particular means that $Z \subseteq \mathrm{Int}(T)$, and $\partial Z \cap (T_{-1} \cup T_1) = \emptyset$.

Furthermore, $\partial V(X)$ separates the sides of $\tilde{T}$: Any point $y \in \tilde{T}_{-1}$ satisfies $d(y, \partial X) = d\sqrt{3}$ by the above, hence the voxel containing y must be black, and thus $y \in V(X)$. Similarly, a point $y' \in \tilde{T}_1$ satisfies $d(y', \partial X) = d\sqrt{3}$, so the voxel containing y' must be non-black. Thus any path from a point in $\tilde{T}_{-1}$ to a point in $\tilde{T}_1$ must pass from a black to a non-black pixel somewhere, implying that $\partial V(X)$ separates the sides of $\tilde{T}$. Since Z was ε close to $V(X)$, it must also separate the sides of the slightly larger set T.

□

Since we have proved all the necessary items listed in Section D.2, we get the following theorems for free. The first one follows from Proposition D.13, used on T and ∂Z and the vector field defined in [2].

Theorem D.51. *The set ∂Z is homeomorphic to ∂X.*

The second theorem comes from the above, together with Theorem D.15 used on the manifolds ∂Z, ∂X, and the isotopy extension theorem:

Theorem D.52. *The set Z is ambiently isotopic to X.*

So, as the last theorem tells us, given the voxel reconstruction $V(X)$ of of an r-regular set X by a lattice $(d\mathbb{Z})^3$, $d\sqrt{3} < r$, it is possible to construct an object Z that is ambiently isotopic to X.

References

[1] Frédéric Chazal and David Cohen-Steiner. A condition for isotopic approximation. *Graphical Models*, 67(5):390–404, 2005. doi: 10.1016/j.gmod.2005.01.005. URL https://doi.org/10.1016/j.gmod.2005.01.005.

[2] Sabrina Tang Christensen. *Reconstruction of topology and geometry from digitisations.* PhD thesis, Aarhus University, 2016.

[3] Pedro Duarte and Maria Joana Torres. Smoothness of boundaries of regular sets. *J. Math. Imaging Vis.*, 48(1):106–113, January 2014. ISSN 0924-9907. doi: 10.1007/s10851-012-0397-0. URL http://dx.doi.org/10.1007/s10851-012-0397-0.

[4] Pedro Duarte and Maria Joana Torres. r-regularity. *Journal of Mathematical Imaging and Vision*, 51(3):451–464, Mar 2015. ISSN 1573-7683. doi: 10.1007/s10851-014-0535-y. URL https://doi.org/10.1007/s10851-014-0535-y.

[5] Reinhard Klette and Azriel Rosenfeld. *Digital Geometry: Geometric Methods for Digital Picture Analysis*. Morgan Kaufmann Publishers Inc., San Francisco, CA, USA, 2004. ISBN 1558608613.

[6] P. Stelldinger, L. J. Latecki, and M. Siqueira. Topological equivalence between a 3d object and the reconstruction of its digital image. *IEEE Transactions on Pattern Analysis and Machine Intelligence*, 29(1):126–140, Jan 2007. ISSN 0162-8828. doi: 10.1109/TPAMI.2007.250604.